Quantitative Analogue Experimental Sequence Stratigraphy

Modelling landscape evolution and sequence stratigraphy of river-shelf sedimentary systems by quantitative analogue experiments

Kwantitatieve Analoge Experimentele Sequentie Stratigrafie

Modelleren van landschapsontwikkeling en sequentie stratigrafie van rivier-shelf sedimentaire systemen met kwantitatieve analoge experimenten

(met een samenvatting in het Nederlands)

Proefschrift
ter verkrijging van de graad van doctor
aan de Universiteit Utrecht
op gezag van de Rector Magnificus, Prof. Dr. H.O. Voorma,
ingevolge het besluit van het College voor Promoties
in het openbaar te verdedigen
op maandag 27 november 2000 des namiddags te 4.15 uur

door
Maximiliaan Wilhelmus Ignatius Maria van Heijst
geboren op 17 juni 1971
te Breda

Promotor:

Prof. Dr. P.L. de Boer
Faculty of Earth Sciences, Utrecht University
Utrecht, The Netherlands

Co-Promotor:

Dr. G. Postma
Faculty of Earth Sciences, Utrecht University
Utrecht, The Netherlands

Aan mijn ouders

Members of the dissertation committee:

Dr. H.J.A. Berendsen
Faculty of Geographical Sciences, Utrecht University
Utrecht, The Netherlands

Prof. Dr. P.A. Burrough
Faculty of Geographical Sciences, Utrecht University
Utrecht, The Netherlands

Prof. Dr. S.B. Kroonenberg
Faculty of Applied Earth Sciences, Delft University of Technology
Delft, The Netherlands

Prof. Dr. J.E. Meulenkamp
Faculty of Earth Sciences, Utrecht University
Utrecht, The Netherlands

Prof. Dr. W. Schlager,
Faculty of Earth Sciences, Free University
Amsterdam, The Netherlands

The project was funded by Shell International Exploration and Production, Rijswijk, The Netherlands under contract wc/56809

The research was carried out under supervision of Dr. G. Postma at the Sedimentology Division, Faculty of Earth Sciences, Utrecht University.

Visiting address:
Budapestlaan 4
PO Box 80021
3508 TA Utrecht
The Netherlands

Internet site: www.geo.uu.nl/Research/Sedimentology

Contents

Biblography / Postscriptum		2
Chapter 1:	Introduction, Scope and Summary	9
Chapter 2:	Quantitative analogue flume-model study of the Late Quaternary Colorado river-delta evolution	19
Chapter 3:	Fluvial response to sea-level changes: a quantitative, analogue experimental approach	51
Chapter 4:	Control of syn-depositional faulting on systems tract evolution across growth-faulted shelf margins: an analogue experimental model of the Miocene Imo River Field, Nigeria	85
Appendix	Grain properties and sediment transport	122
References		126
Samenvatting voor de leek	*(Simplified summary in Dutch based on Chapter 1)*	136
Acknowledgements		142
Curriculum Vitae		144

Bibliography

Chapter 2
Van Heijst, M. W. I. M., G. Postma, X. Meijer, J. B. Anderson, and J. N. Snow, (2001) Quantitative analogue flume-model study of river shelf systems: principles and verification exemplified by the Late Quaternary Colorado river-delta evolution: **Basin Research, v. 13, p. 243-268.**

Chapter 3
Van Heijst, M. W. I. M., and G. Postma, (2001) Fluvial response to sea-level changes: a quantitative, analogue experimental approach: **Basin Research, v. 13, p. 269-292.**

Chapter 4
Van Heijst, M. W. I. M., G. Postma, W. P. Kesteren, and R. G. De Jongh, (2002) Control of Syn-Depositional Faulting on Systems Tract Evolution across Growth-Faulted Shelf Margins: An Analog Experimental Model of the Miocene Imo River Field, Nigeria: **American Association of Petroleum Geologists Bulletin, v 86, p. 1335-1366.**

Postscriptum

Since the thesis defence, chapters 2, 3 and 4 have been published in scientific journals. The copyright of those chapters has been transferred to the respective journals.

Max van Heijst

August 27th 2002

Cover illustration—Top: An outcrop of Pliocene deltaic sediments at Ponte Capodarso, Sicily, Italy. The offlapping delta sediments are truncated by horizontal beds. Bottom: A similar deltaic succession with offlapping sediments truncated by horizontal beds was formed in the analogue experiments of this study.

Omslag illustratie—Boven: Delta afzettingen uit het Plioceen ontsloten bij Ponte Capodarso, Sicilië, Italië. De hellende lagen van de uitbouwende delta worden aan de top afgesneden door horizontale lagen. Onder: Delta afzettingen zoals die zijn gevormd tijdens de analoge experimenten van deze studie vertonen een vergelijkbaar patroon.

ISBN: 90-5744-055-5

Chapter 1

Introduction, Scope and Summary

General

In the long run, sedimentary systems are governed by three main allocyclic controls: sea-level change, tectonics and climate. The key issue for geologists, sedimentologists, and for stratigraphers in particular is to unravel the relative contributions of each of these parameters from the eventual stratigraphy preserved in the fossil sedimentary system. However, such a reconstruction is hindered by incompleteness of information, since the stratigraphic record is often not fully accessible and contains hiatuses.

Similarly, the sedimentary records of river deltas on passive continental margins reflect a complex history of sea level, climate and tectonic interactions of unknown proportions. Conceptual geologic models such as the sequence-stratigraphic concept have improved our knowledge of the effects of allocyclic controls on the marine shelf and slope environment. Unfortunately, the fluvial system has been mainly overlooked in these models even though it is the main sediment feeder of the entire marine system. Even today, the sequence-stratigraphic concept for fluvial stratigraphy still lags behind that for shelves, possibly because of insufficient data of complete river-shelf systems and the complexity of the fluvial system.

Aim of this research is to assess the control of sea-level change, tectonics and climate on integral siliciclastic river-shelf systems by use of analogue flume experiments. The approach is directed towards systematic, experimental investigation of the effects of each allocyclic control on the morphological and volumetrical evolution of the river-shelf system. The scope of the study will be presented in more detail after a brief introduction on river-shelf depositional systems and a short review of sequence stratigraphy, an often-applied geological concept to unravel the sedimentary record. The chapters have been written as three research articles with a particular focus each. Chapter 2: testing of the experimental method and scaling strategy for quantitative analogue modelling. Chapter 3: investigating the fluvial response to sea-level changes. Chapter 4: modelling the impact of local growth faulting and sea-level changes on shelf-margin-delta evolution. This introductory chapter includes a summary of the thesis, followed by some concluding remarks.

River-shelf systems

Schumm (1977) divided the sediment transport path from mountain to sink into 3 zones (Fig. 1.1a). 1 the production zone (drainage basin); 2 the transfer zone (fluvial valley) and 3 the deposition zone (piedmont or coastal zone). The deposition zone for coastal systems extends from the river's estuary or delta towards the shelf and slope.
The overall geometry of the river-shelf depositional system can be illustrated by the world's hypsometric curve (Fig. 1.2). The horizontal axis of the hypsometric curve indicates the total percentage of the earth's surface above a given altitude. The land

surface accounts for 29% of the present earth's surface area. A sea-level lowstand at 120 m below present-day level, which is common for Quaternary glacio-eustatic lowstands, will make the shoreline retreat to the shelf break and will enlarge the continents up to 37%. Under lowstand conditions, rivers extend over the shelf and the fluvial profile has to adjust to the lower sea level. As a result the fluvial gradient increases.

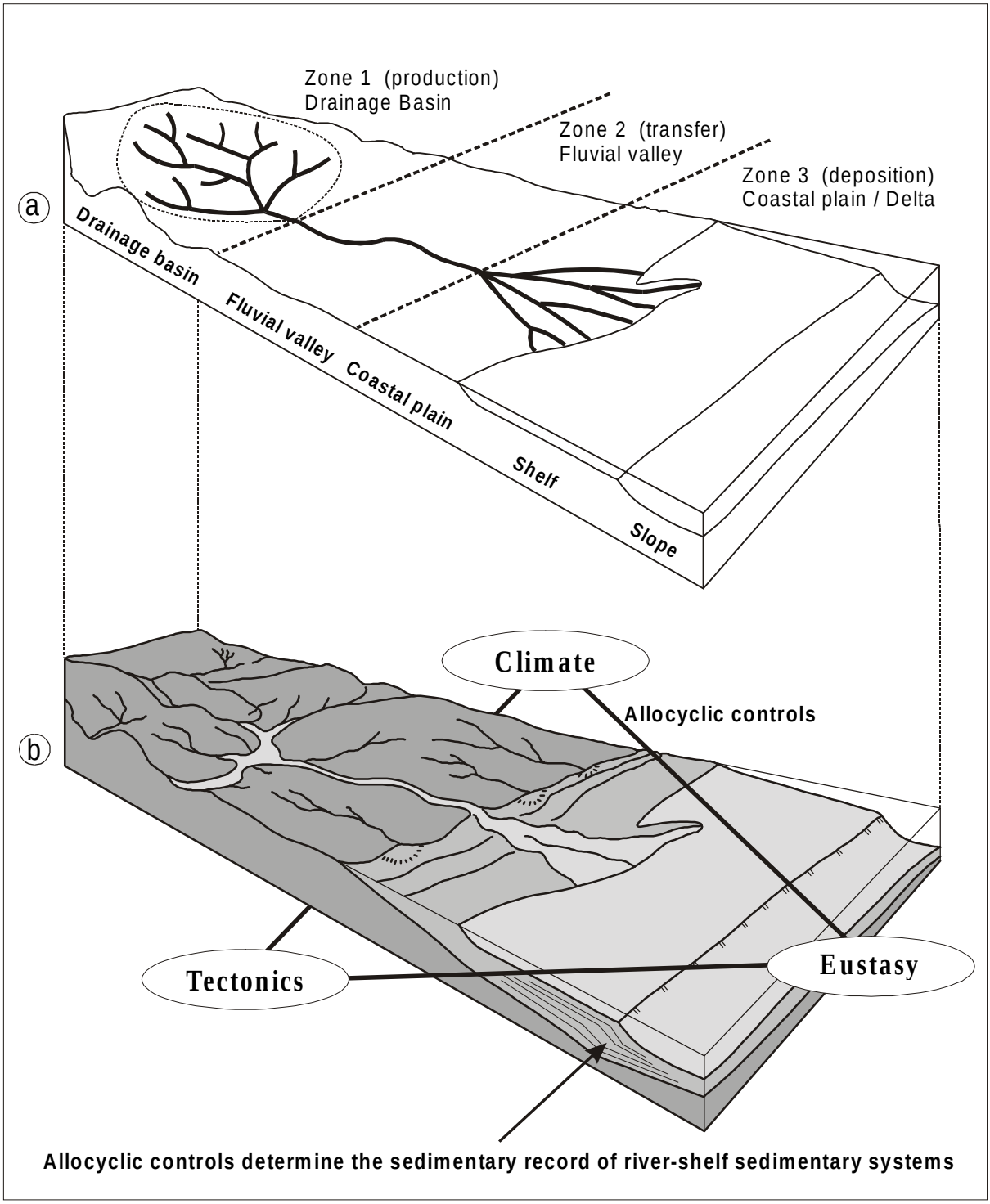

Fig. 1.1—(a) Components of the fluvial system according to Schumm (1977). (b) Illustration of a river-shelf sedimentary system and its main allocyclic controls on deposition and erosion.

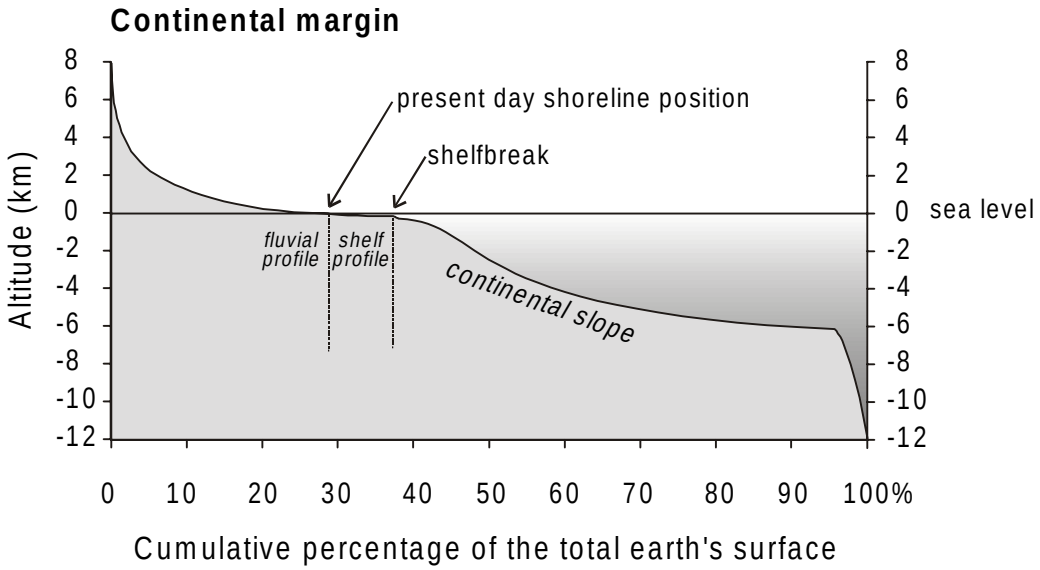

Fig. 1.2—Hypsometric curve of the earth. The horizontal axis indicates the total percentage of the earth's surface above a given altitude. The break in slope of the hypsometric curve reflects the shelfbreak. Modified after Allen (1997).

Not only sea-level changes are recorded in the sedimentary succession, variations in climate and tectonics play an important role in the deposition of sediments on the shelf and slope as well (Fig. 1.1b). Climate changes play a role by affecting the river's discharge and the sediment load. Tectonics and climate in the drainage basin determine the rate of denudation. Vertical tectonic motions and eustatic sea-level changes determine the amount of accommodation space that is available for preservation of the sediments in the deposition zone. A complicating factor is that deposits that are preserved on the alluvial plain and shelf can become progressively reworked during a following sea-level cycle. To understand the factors that control the stratigraphy of fluvial and shelfal successions it is important to distinguish between fluvial load from the drainage basin and reworking of sediments within the system.
Base level is defined as the level above which deposition is temporary and erosion occurs. Sea level is regarded as ultimate base level. It pinpoints the end of the fluvial profile that is defined by an infinite sequence of adjacent local base levels together forming the base profile (Quirk, 1996). The shoreline position plays a crucial double role in a river shelf setting. It acts as reference point to which both the fluvial and shelf profiles grade (Fig. 1.2). Integration of the fluvial system into the study of shelf and slope systems is a prerequisite for the study of ancient continental shelf deposits because the fluvial system is intrinsically related to the graded shelf profile. Therefore, it was decided to model both the downstream fluvial reach and the shelf in one analogue flume set-up.

Background of sequence stratigraphy

Technical developments in marine geology during the 1950's and 60's (e.g. coring techniques, side-scan-sonar imaging, seismics) led to the first concepts that described coastal sediments in terms of packages (sequences) related to sea-level changes and sediment supply (Curray, 1964; Ludwick, 1964). The availability of large-scale seismic surveys along the world's continental shelves and slopes during the 1960's stimulated the first basin-wide stratigraphic studies and raised the need for a general interpretation technique of seismic sections. This led to the first publications on seismic sequence stratigraphy by Vail *et al*. (1977). An important step forward was the recognition of regional unconformities and conformities on seismic sections, which can be used to delineate sequences of genetically related strata. These basic ideas were applied to interpret the rock record of passive margins all around the world, resulting in further improvement of the initial Vail *et al*. (1977) concept. It became further expanded by the recognition of parasequences (Van Wagoner *et al*., 1988) and the simulation of sequence building in forward numerical models (Jervey, 1988). Meanwhile, the name seismic sequence stratigraphy changed into sequence stratigraphy. Owing to the common data gab between marine and continental seismics, the concept focused mainly on the passive margin and not on the main source of the sediment, the fluvial system and drainage basin. A first attempt to include some aspects of the fluvial system was done by Posamentier & Vail (1988). At the same time, the global correlation of shelfal successions pointed out sea level (eustasy) as the main control on the formation of the seismic sequences (Haq *et al*. 1988). Undesirably, sequence stratigraphy evolved from a general interpretation methodology to a concept stigmatised by global eustasy.

Attributing stages of the sea-level curve to depositional geometries works fairly well on Quaternary shelves (e.g. Suter & Berryhill, 1985; Morton & Price, 1987; Tesson *et al*., 1990; Hernandez-Molina *et al*., 1994). However, from an increasing amount of studies (e.g. Nummedal & Swift, 1987; Boyd *et al*., 1989; Embry, 1990) it was realised that the sequence-stratigraphic model is stimulating but too simple. Apart from proposing changes to the sequence-stratigraphic methodology (Galloway, 1989; Thorne & Swift, 1991), the international scientific community started to dispute the overruling signature of eustatic changes and re-introduced the two other allocyclic controls: climate (supply) and tectonics into the debate (Miall, 1991; Miall, 1992; Posamentier & Allen, 1993; Posamentier & James, 1993; Schlager, 1993). The increased interest in incised valley fills (Zaitlin *et al*., 1994) and continental successions (Shanley & McCabe, 1993) demanded a sequence-stratigraphic framework that incorporates the sediment production and transfer in the fluvial realm. Hence, the debate extended towards the fluvial system (Schumm, 1993; Shanley & McCabe, 1994) and it was realised that geomorphic thresholds and stream dynamics introduce spatial and temporal complexity that must be accounted for in sequence-stratigraphic models (Wescott, 1993; Thorne, 1994). From this perspective it is better to assume that the stratigraphic record is governed by a combination of two or more allocyclic controls that acted in concert rather than having a single parameter with dominant control. However, such is hard to extract from the ancient stratigraphy alone (Blum & Price, 1998). Analogue models can contribute to sensitivity analyses by

isolating allocyclic controls. Model results may lead to modifications of general concepts that in turn can be tested against geological data (Ethridge *et al*., 1998).

Scope

The aim of this research is to investigate the effect of changes in sea level, sediment supply and tectonics on sedimentary geometries in a siliciclastic river-shelf depositional system by means of quantitative analogue flume experiments. The approach is inspired by analogue experiments conducted at the Colorado State University (Wood *et al*., 1993; Wood *et al*., 1993; Koss *et al*., 1994) that successfully modelled river-shelf evolution during a single sea-level cycle. The model studies proved to be valuable for testing geological concepts for river-shelf systems in a qualitative way. It showed for instance that the concept of sequence stratigraphy is scale independent (Koss *et al*., 1994). The Colorado State University models were conducted as experimental analogues rather than true-scaled models. The results were not compared with real world examples. Neither was the resultant stratigraphy analysed or the results tested on reproducibility. This study aims to add quantitative aspects to the analogue modelling approach.

Early 1995, Shell sponsored a pilot study at Utrecht University to explore the technical possibilities to measure the topography of sedimentary geometries produced by analogue model experiments of the river-shelf environment. Four experiments were conducted to study the effect of sea-level changes on a river-shelf sedimentary system as part of the author's M.Sc. thesis. A prototype, half-automated bed profiler was developed to quantify the amount of erosion and deposition per time step of an experiment. The modelling results were promising, although it was recognised that the setup needed further development to obtain sufficient accuracy with respect to the quantification of sediment flux, and to make the measurements less time consuming. The scientific collaboration with Shell was prolonged in the form of a sponsored Ph.D. project to improve the experimental method, and to collect data of series of experiments.

The first objective of the research was to develop a high-resolution bed profiler that digitises fully automatically the topography of the sand bed. Hence, the accuracy had to be improved and the scanning had to be done overnight to leave more time to conduct experiments. Scanning of the topography by laser has been an important innovation enabling us to obtain a large quantitative data set on bulk sediment transport and deposition in a series of experiments. Such an experimental data set permits systematic investigation of the impact of each imposed control on the model. However, the quantitative treatment of analogue models requires a satisfactory scaling rationale for calibration of bulk sediment volumes (sediment budgets) of model and prototype. Consequently, the development of a scaling strategy for analogue modelling of large-scale sedimentary system makes up a vital part of the thesis. The applied scaling strategy needs to be adequately explored and checked by quantitative comparison of model results with real-world prototypes. The model results are valuable on a common level for identification of strength and flaws in geological concepts for river-shelf systems such as sequence stratigraphy (Fig 1.3).

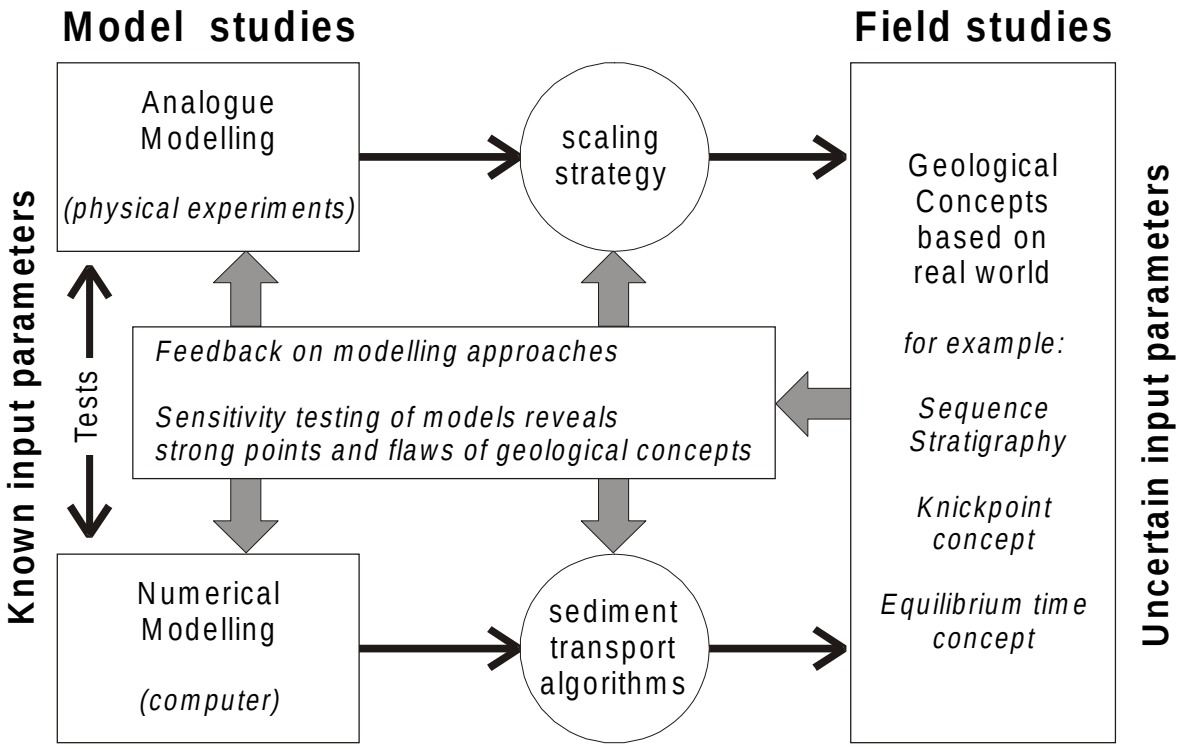

Fig. 1.3—Role of analogue models in the research of sedimentary systems.

Summary of the Thesis

Chapter 2 demonstrates the experimental method and applied scaling strategy of the analogue experiments using a real-world prototype of a river-shelf system. The chapter starts with an introduction on the scaling issues of analogue experiments by reviewing the various scaling methodologies of physical models. An inventory is made of the important parameters that need to be considered for modelling landscape evolution and sequence stratigraphy of river-shelf sedimentary systems on geological time scales. A best possible scaling strategy is proposed for the analogue modelling of river-shelf systems, which is subsequently exemplified and tested using the Quaternary Colorado river-delta evolution as a prototype. We modelled the bulk sediment transport of a real world sedimentary system by bed-load transport of a uniformly grained material in our laboratory by honouring the following scaling constraints:

1. maintaining realistic hydraulic conditions to ensure constancy in bed-load transport rate;
2. maintaining geometric similarity between model and prototype;
3. maintaining a similar basin response factor for model and prototype, which is the ratio of the total time span under consideration (here the duration of a sea-level cycle) over the equilibrium time of the sedimentary system;
4. applying the scaling factors for spatial dimension and time for quantitative comparison of the time averaged sediment transport rate in model and prototype, and
5. checking the relationship between sedimentation rate and the rate of change in accommodation space in model and prototype by a basin fill factor.

Although no hydraulic scaling was applied, the hydraulic conditions are kept at realistic values for river transport. Grain size was not scaled, the bed load is merely an isotropic medium used to model sediment displacements in real-world systems. We chose unimodal medium sand, but we could have taken any type of grains as long as the hydraulic boundary conditions are maintained and the effect of the grain properties on the sediment transport rate (diffusivity) is accounted for in the calculation of the equilibrium time of the system.

Analogue experiments aid in qualitative and quantitative understanding of erosion and deposition of a real-world river-shelf system if sufficient credit is given to the scaling factors. The modelled river-shelf evolution for one sea-level cycle compares well with the Colorado river-delta evolution over the last glacio-eustatic cycle. Quantitative comparison of sediment budgets on the shelf between model and prototype shows a similar peak in deposition rate during lowstand. The experimental results illustrate how such a peak results from sea-level-fall-induced erosion on the shelf and coastal plain which significantly influences the timing and amount of sediment supply to the shelf.

Chapter 3 investigates the fluvial response to imposed sea-level changes by a set of 18 analogue experiments with sea-level change as the only independent variable. The scaling strategy of Chapter 2 was followed, but now the focus was on the time-scaling aspect by application of the proposed basin response factor. The range of experiments was set to explore the fluvial response to a sea-level change with shorter, equal and longer duration than the model's specific equilibrium time (of approximately ten hours). The experimental results proved to be reproducible and produced statistically significant quantitative data. They support the general notion that neither a fall nor a rise in sea level does instantly affect the upstream fluvial reaches. All experiments show a time lag between emergence of the shelf as a result of a sea-level fall and the onset of erosion in the fluvial realm. This time lag was termed connection delay; the time required to connect initial incisions on the just emerged shelf with the fluvial valley. All experiments showed continuation of highstand aggradation in the fluvial valley during the first phases of sea-level fall before connection occurred. This is very counter-intuitive to the sequence-stratigraphic concept that assumes rivers to respond instantly to a sea-level fall by stream rejuvenation and river incision. We quantified the time lag in fluvial response to sea-level fall more generally by defining the connection rate, which is the ratio between shelf width and the connection delay. The connection rate is a function of the rate of headward erosion induced by the sea-level fall. It determines the relative timing of the onset of erosion in the fluvial domain relative to the sea-level cycle and has therefore strong implications for fluvial and shelfal stratigraphy when looking at: 1) the amount and duration of continued fluvial aggradation during sea-level fall; 2) the percentage of fluvial sediment versus eroded shelf material in the lowstand delta; 3) the volume of the lowstand delta; 4) the volume of the transgressive systems tract; 5) the amount of diachroneity along the sequence boundary.

Chapter 4 is a case study of Imo River Field, Nigeria, where deltaic sediments have been dissected by a listric growth fault during deposition. It is the first time that an analogue flume experiment was used to study the combined effect of growth faulting and sea-level change on the depositional architecture of shelf margin deltas. The usual problems with stratigraphic correlation of sedimentary sequences over a growth fault in such field settings can be avoided by using tracer grains as time lines during experimental sequence development. The model results are presented in the form of a conceptual sequence model for growth-faulted shelf-margin deltas that focuses on the systems tract distribution on either side of the fault. The hangingwall receives sediments from falling stage to early transgression. The footwall succession, in contrast, displays a lower preservation potential and is characterised by late-transgressive, incised-valley fill and highstand deposits. On the one hand, the stratigraphy of the model emphasises a strong control of the rate of local subsidence on depositional architecture of the hangingwall. On the other hand, sea-level-fall-induced cannibalism on the stable footwall block causes a basinward sediment flux that preserves the eustatic signal in the hangingwall succession, even in cases where the rate of local subsidence outpaced the rate of sea-level fall. Stratigraphic features of the model are compared with other growth-faulted settings, extensional synrift tectonic settings and are finally discussed in terms of hydrocarbon potential.

Concluding Remarks

Analogue flume models are useful for qualitative studies of the drainage evolution of sedimentary systems in three dimensions. This study adds quantitative aspects to the analogue modelling approach by quantification of erosion and deposition during experiments. Our scaling strategy obeyed a realistic flow regime, geometric similarity and response time of the modelled sedimentary system.

This study shows that analogue flume models generate reproducible and deterministic results. The results of the series of experiments reveal that the basin response factor, the ratio of the duration of a period of change over the equilibrium time of a sedimentary system, is a vital parameter to model the response of sedimentary systems and to compare them on different temporal scales. The quantitative analogue models aid in understanding of time-averaged bulk sediment displacements that are induced by sea-level changes. Quantification of these fluxes is only possible by doing basin-wide studies that investigate both source and sink. This type of model studies exemplifies the need for volumetric data of real-world systems in the form of isopach maps with dated bounding surfaces. Unfortunately, at present such data are scarce and volumetric numbers are hard to compile. A tentative reconstruction for the Colorado river-shelf system was included in this study to indicate the type of data that is required.

The model results support the notion that the basic principles of sequence stratigraphy are scale-independent. Those basic principles are also embedded in the basin-fill factor that is introduced as a geological scaling tool to compare the evolution of sedimentary systems in terms of sedimentation rate and change in accommodation space. It is a useful dimensionless number to compare sedimentary systems, both in real world and model examples. The model results support the general applicability of sequence-stratigraphic concepts for the shelf and slope. However, the model shows at the same time that the application of the sequence-stratigraphic concept to the upper shelf and continental successions must be done with caution. Instead of direct incision and stream rejuvenation as assumed in the sequence-stratigraphic concept, the model result shows that the fluvial system does not respond instantly to a sea-level fall. The time lag in fluvial response is related to the time required to connect initial incision on the emerged shelf with the fluvial valley by the process of headward erosion. This implies that sequence boundaries have the tendency to become increasingly younger in the landward direction and can be strongly diachronous. Consequently, fluvial erosion and deposition can be out of phase with the sea-level curve. This makes it inappropriate to designate system tracts to fluvial strata, even within the upstream limit of sea-level-fall-induced erosion (i.e., knickpoint). Under such conditions, correlation between sediment body and relative position on the sea-level cycle becomes speculative, despite the very suggestive names that are used in the systems-tract terminology.

The various types of analogue experiments described in this thesis support the strong impact of sea-level changes on river-shelf sedimentary systems. Sea-level lowering induces fluvial and continental degradation cycles (river and shelf cannibalism) that deliberate significant volumes of sediment that add to the hinterland supply to the basin. These fluxes are responsible for a strong imprint of the eustatic signal in shelfal successions. Such a lowstand-supply signal preserves the eustatic signal even in growth-fault or syn-rift settings where local subsidence on the shelf compensates the effect of an eustatic sea-level fall.

This study has primarily focussed on the modelling of the effects of sea-level changes and local subsidence on river-shelf sedimentary systems. The drainage basin or source area was not included in the setup. It was replaced by a sediment feeder and a tap with adjustable discharge. Pilot studies revealed that the fluvial valley was capable to accommodate imposed changes in sediment supply at the feeder up to a factor two. Changes in discharge regime would be required to effect a substantial increase in fluvial supply during an experiment. This is only possible to a limited degree because of the hydraulic scaling constraints of the model. Despite the limited degree of freedom to choose input values for sediment supply and discharge, it would be interesting to explore their thresholds and further expand the experimental data set by modelling glacio-eustatic sea-level-climatic interactions. For this purpose it might be useful to envisage a hybrid modelling approach combining analogue and computer modelling studies.

It is impossible to include all dynamics of sediment transport and deposition in a computer model because the non-linear dynamics of depositional systems put severe theoretical limits on this deterministic approach (Schlager, 2000). The strong point of analogue flume models is that they are three-dimensional and incorporate real, albeit simplified analogues of sedimentary systems (Paola, 2000). They are potentially useful in illustrating how only a single allocyclic control can produce complexity in the final stratigraphy. Series of analogue experiments, systematically varying one variable at the time, allow sensitivity analysis and testing of hypothesis and geological concepts (Fig. 1.3). This is more adequate in generating feedback on geological concepts and modelling approach than a single calibration exercise of a model to match a particular prototype. In contrast to computer models, once the analogue model runs and all variables have been chosen, the operator can hardly influence the outcome. In addition, analogue flume experiments can give a firmer base to 3D computer modelling when applied as a test case of a small sedimentary system where, in contrast with a field example, all input parameters are known. Analogue experimental results include data of process rates, hierarchy and sensitivity of a small-scale sedimentary system that can be used to calibrate the sediment transport algorithms of numerical models.

Chapter 2

Quantitative analogue flume-model study of the Late Quaternary Colorado river-delta evolution

Max W.I.M. van Heijst[1], George Postma[1], Xander D. Meijer[1],
Jennifer N. Snow[2] & John B. Anderson[2]

1) Faculty of Earth Sciences, Utrecht University, PO Box 80021, 3508 TA, Utrecht, The Netherlands.
2) Dept. of Geology & Geophysics, Rice University, PO Box 1892, Houston, Texas, 77005, USA.

Abstract

Physical modelling of clastic sedimentary systems over geological time spans has to resort to analogue modelling since full scaling can not be achieved. Such models are suitable for systematic investigation of the system's sensitivity to allocyclic changes by isolating governing parameters. In this paper we present a qualitative and quantitative comparison of analogue flume experiments and seismic-stratigraphic studies of the east Texas shelf.

The model's dimensions are proportionally scaled except for a vertical exaggeration. Time is scaled using a Basin Response factor to maintain a similar ratio between the period of change and the system's equilibrium time for model and prototype. A Basin Fill factor was used to compare the ratio between the time-averaged sedimentation rate and the rate of change in accommodation space of model and prototype.

The flume-model results are in the form of sediment budgets that are related to shelf cannibalism and fluvial supply. They are compared with the ancestral Colorado river-delta evolution of the last 40 kyr. Model and prototype have similarities in delta evolution in response to one cycle of sea-level change. With sea-level change as the isolated variable, the flume model generates a significant supply pulse caused by headward erosion of the shelf in response to the sea-level fall. This pulse adds to the yield of the hinterland. The sea-level-change-induced supply persists during the early rise, although its rate declines. A similar trend is observed on the east Texas shelf. Based on our experimental results we argue that shelfal and fluvial degradation cycles induced by sea-level changes can significantly influence the timing and amount of sediment supply to basins and must therefore be taken into consideration.

On a common level, our attempt to use quantitative flume-model results to understand shelf-stratigraphy demonstrates a general problem of insufficient quantitative field data on river-shelf domains that can be used to calibrate and to verify experimental studies.

(Submitted for publication in Basin Research)

Introduction

Physical scale models of sedimentary systems are based on similarity theory, which produces a series of non-dimensional parameters that fully characterise fluid flow (Bruun, 1966; Yalin, 1971; De Vries, 1983; Peakall *et al*., 1996). In the ideal case, every variable occurring in nature is perfectly scaled (Hubbert, 1937). However, many modellers need to apply time scaling, which introduces distortion to their model results (Wang & Kron, 1991). The further the model departs from 1:1 hydraulic scaling, the more the scaling of dimensionless flow Reynolds and Froude numbers must be released (e.g. Leddy *et al*., 1993), up to a point that hydrodynamic scaling is no longer the case (Peakall *et al*., 1996; Paola, 2000). It means that entire sedimentary systems with prototype dimensions from tens to hundreds of kilometres that evolve over geological time spans can only be modelled as analogue flume models and not as true-scaled hydraulic models (Zhang *et al*., 1997).

Examples of analogue models are sandbox models used to study tectonic deformation (McClay *et al*., 1998). Flume-type models are also used as analogues for landscape evolution of siliciclastic systems. They proved to be valuable for understanding, for instance, delta evolution (Jopling, 1963; Endo *et al*., 1996), channel patterns (Schumm & Khan, 1972; Schumm, 1977; Germanowski & Schumm, 1993; Ashworth *et al*., 1994), processes of thalweg avulsion (Bryant *et al*., 1995), process of knick point migration (Holland & Pickup, 1976; Schumm *et al*., 1987; Bryan, 1990, and references cited herein), and base-level induced erosion and deposition (Posamentier *et al*., 1992; Wood *et al*., 1993; Koss *et al*., 1994; Milana, 1998). These analogue studies were predominantly qualitative in nature and based on the "similarity of process" principle (Hooke, 1968) in which gross scaling relationships must be met, but where the flow regime remains unscaled.

Since analogue models are not true-scaled physical models, it is necessary to calibrate the models using data of real world prototypes. We have chosen the Late Quaternary ancestral Colorado fluvial-deltaic system as a prototype for various reasons, but most importantly, because it has been relatively well covered by seismic profiling and core data, and because its drainage basin has been studied well (see further below). The analogue modelling programme in Utrecht aimed to systematically collect a quantitative data set that must reveal the effect of sea-level changes on river-shelf evolution. The approach differs from previous analogue river-shelf experiments in that volumes of erosion and deposition are quantified per interval of the experiment. Quantification of bulk sediment transport allows quantification of the large-scale behaviour of a sedimentary system relative to changes in base level. The quantitative results of three identical experiments are compared with the prototype by use of the here proposed scaling methodology.

The purpose of this paper is to demonstrate how quantitative, analogue flume modelling can aid in understanding landscape evolution and stratigraphy of clastic sedimentary systems. By landscape evolution we mean here the study of large-scale features formed by erosion and deposition controlled by tectonics, climate and sea-level change (Fig. 2.1). With stratigraphy we study depositional patterns caused by changes in landscape through time, the changes being mostly dependent on the rate of change in sediment supply and accommodation space (Schlager, 1993). Since base

level plays a central role in landscape evolution and preservation (stratigraphy), we focus our demonstration on the base-level controlled mass balance.

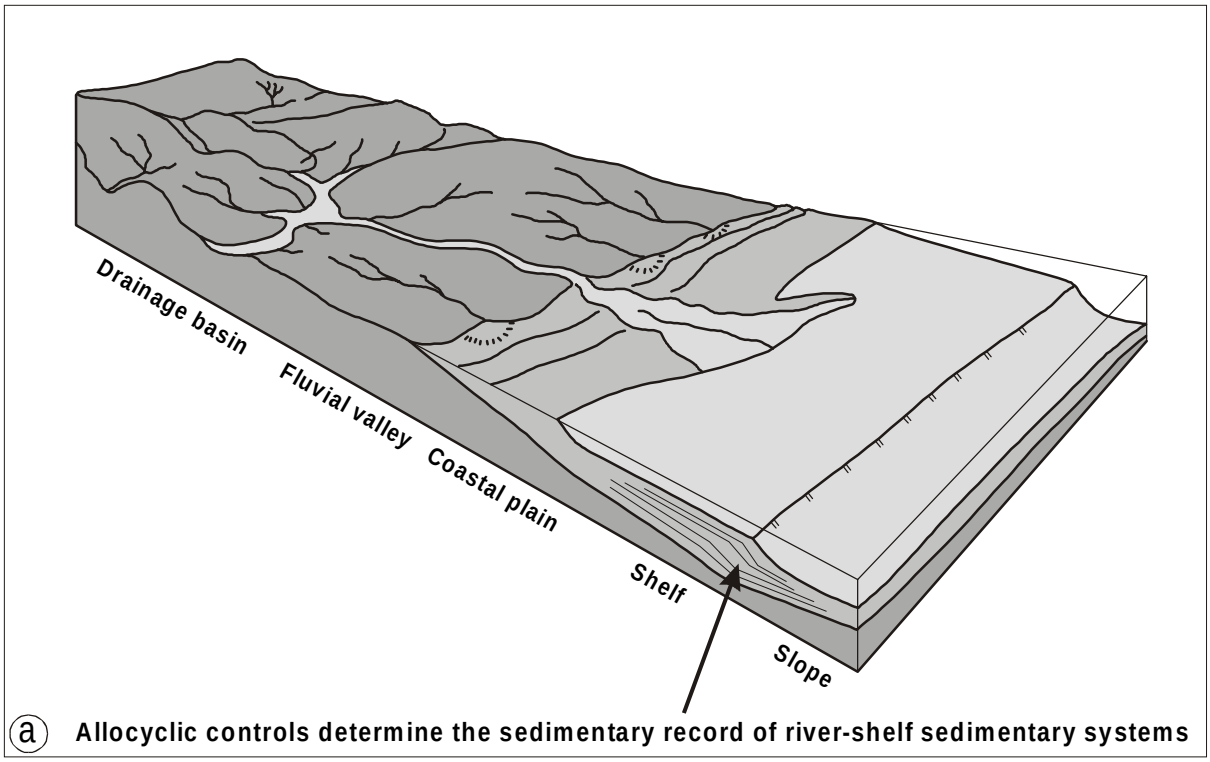

Fig. 2.1—(a) General representation of a river-shelf sedimentary system. (b) Schematic sketch of relevant parameters for modelling river-shelf sedimentary systems.

Choice of parameters

Most fundamental to our understanding of the dynamics of sedimentary systems is their response in terms of sediment production and transport to the main controlling allocyclic variables tectonics, climate (represented by discharge and sediment yield) and sea-level change (Posamentier & Allen, 1993; Ethridge *et al*., 1998). Hence, quantification of the evolution of sedimentary systems means in the first place quantification of erosion and deposition.

Quantitative modelling of the mass balance of sedimentary systems grounds on the most fundamental physical concept invoked in mathematical modelling of landscapes, that of mass conservation (e.g. Paola *et al*., 1992). In this context, mass is that portion of earth material that extends above a reference datum and is of varying mineralogical composition, density and volume (e.g. Lawrence, 1996). The continuum hypothesis is imposed to most theoretical models, while it is implicitly present in physical models. It implies a natural spatial scale at which denudation, itself being controlled by environmental features (general physiography defined by climate), tectonics and sea-level change, influences landscape evolution. In order to create a model that aids in unravelling the cause and effect relations of allocyclic controls acting on a sedimentary system, it is extremely important to consider the scale of the system and the time span involved (Paola *et al*., 1992; Paola, 2000). The maximum scale that can be considered is the length of the entire sedimentary system. The smallest suitable scale in our case is the point at which the hydraulic effects of individual river channels start to be recognised as the controlling factor on sediment deposition and erosion instead of the underlying allocyclic controls. Hence, a choice must be made at what scale we wish to consider the landscape and whether we wish to consider only components of the system or the system as a whole (cf. Schumm & Lichty, 1965). A similar dilemma has led to different approaches in numerical modelling of landscape change and sequence stratigraphy. A purely hydraulic ("grain by grain") modelling approach is very suitable for modelling short time spans, where hydraulic processes of sediment transport must be taken into account (e.g. SEDSIM model see, Martinez & Harbaugh, 1993). On a longer, geological scale of observation, a diffusion or streampower approach is more appropriate (e.g. Willgoose *et al*., 1990; Paola *et al*., 1992; Niedoroda *et al*., 1995).

Schumm & Lichty (1965) classified the morphologic variables that influence erosion, runoff and sediment yield in drainage basins in hierarchical order of dependence in relation to different time spans. Table 2.1 shows that the number of dependent variables (i.e., variables an experimenter does not need to control) increases with increasing time-span. Cyclic time (1 Ma-5 kyr) refers to the long-term landscape evolution, for example, one uplift-denudation cycle. Graded time (thousands of years) represents a short span of cyclic time during which dynamic equilibrium is maintained. Steady time (hundreds of years) is a very short time span of geomorphic stability. Schumm & Lichty (1965) did not include eustatic sea-level change as an independent variable. For each basin, however, tectonics and eustatic sea level can be considered independent variables that perturb the alluvial system by changing its base level. Climate governs both discharge and sediment yield and thus the gradient of the alluvial profile. The geology of the study area is another important independent variable to be considered for long time spans, because it controls the erodability of the

substrate. Vegetation, relief and drainage dynamics are variables that depend on climate, tectonics and sea level if landscape development is considered over long time spans. Hence, landscape modelling over long time spans can ignore the effects of channel hydraulics and geomorphic thresholds (e.g. Schumm & Lichty, 1965; Bull, 1979). In contrast, landscape evolution over increasingly shorter time periods makes the suite of variables change from dependent to independent and from independent to not relevant (Table 2.1).

Based on the above philosophical reasoning, we presume that mass transfer within a river-shelf sedimentary system as shown in Fig. 2.1 is governed mainly by the five independent variables for cyclic time. These variables define the large-scale dynamics of both sedimentary systems and landscape evolution. If we wish to validate our experimental results, the mass balances for both real-world prototypes and model studies must be compared. Hence, we quantify landscape evolution and stratigraphy by measuring time-averaged sediment transport.

Table 2.1. Listing of variables and their control on different time scales (modified from Schumm & Lichty, 1965).

	Drainage basin variables	Status of variables during designated time spans		
		Cyclic time *(1 Ma - 5 ka)*	**Graded time** *(5 - 1 ka)*	**Steady time** *(last 1000 years)*
1.	Time	Independent	Not relevant	Not relevant
2.	Tectonics	Independent	Not relevant	Not relevant
3.	Eustatic sea level	Independent	Not relevant	Not relevant
4.	Climate	Independent	Independent	Independent
5.	Geology (lithology, structure)	Independent	Independent	Independent
6.	Vegetation (type and density)	Dependent	Independent	Independent
7.	Relief (volume above base level)	Dependent	Independent	Independent
8.	Hydrology	Dependent	Independent	Independent
9.	Drainage morphology	Dependent	Dependent	Independent
10.	Hillslope morphology	Dependent	Dependent	Independent
11.	Hydrology	Dependent	Dependent	Dependent

Scaling of analogue experimental models

Modelling clastic sedimentary systems over geologic time scales by analogue experiments implies that the hydraulic scaling conditions are released. However, it does not mean that the hydraulic conditions can be ignored. Lower flow regime (Froude number < 1) was preferred because it is representative for fluvial transport and it excludes side effects like bedform formation.

Geometric scaling is crucial for any model that aims to understand sediment delivery at the continental margin (shelf-edge) through time (cf. Wetzel, 1993; Mulder & Syvitski, 1996), since it determines the relative dimensions of potential sediment storage rooms and sediment sources. The geometric similarity satisfies the first demand of the similarity of process approach that gross scaling relationships should be met (Hooke, 1968). In the ideal case full geometric similarity is maintained by keeping similar scaling factors for the x, y and z dimension. However, in the practice of

analogue modelling, inevitably the vertical scale needs to be exaggerated to maintain realistic hydraulic conditions ($\lambda_x = \lambda_y > \lambda_z$).

The most important aspect of time scaling is that the response time of a sedimentary system must be taken into account. The response time referred to here is the equilibrium time T_{eq} that was defined by Paola *et al.* (1992). They stressed the importance of the ratio between the period of change of a variable, T and the systems equilibrium time, T_{eq}. The equilibrium time in relation to the duration of one cycle of allocyclic change must be of the same proportion in both model and prototype. Hence, we define a Basin Response factor (Br):

$$Br = \frac{T_{(rw)}}{T_{eq(rw)}} = \frac{T_{(\exp)}}{T_{eq(\exp)}} \qquad [-] \qquad (2.1)$$

Where T is the duration of one period of allocyclic change (e.g. duration of one sea-level cycle) and T_{eq} the response time of the sedimentary system in the real world (rw) and experiment (exp). The formulae that exist to estimate the equilibrium time of a sedimentary system are derived from non-dimensional analysis of diffusion equations that are in use by landscape modellers (De Vries, 1975; Howard, 1982; Paola *et al.*, 1992), which give a first order approximation of T_{eq} by:

$$T_{eq} = \frac{L^2}{k} \qquad [T] \qquad (2.2)$$

Where L is the basin length and *k* is the sediment transport diffusivity. Basins with different length L and/or different values for *k* will have different equilibrium times, and thus a different response time to imposed changes. The value of T_{eq} varies with sea level change and type of alluvial system. For instance, a sea-level fall will expose significant shelf areas, changing both the L and *k* values of the fluvial system. Spatial variation in sediment diffusivity is defined by relief (e.g. created by tectonics), characteristics of the substrate (bank stability, roughness, density, erodability, etc.) and discharge. We applied above-mentioned diffusion approaches to verify the T_{eq} of our model. These equations give realistic approximations of the model's T_{eq} as shown in Chapter 3. Alternatively, it has been proposed that for river transport T_{eq} is linearly related to length scale and discharge (Kooi & Beaumont, 1996; Paola, 2000).

Quantification of bulk sediment transport will allow quantification of the large-scale behaviour of a sedimentary system. Since the size of the model does not allow strict Froude scaling, there is a need for an alternative for 1:1 scaling of sediment transport to compare sediment fluxes in the model with a prototype. Since we are interested in modelling basin fills over long periods of time, we use the time-averaged sediment transport rate. By time averaging over sufficiently long time spans (i.e., graded time) this number includes both the "normal" and the catastrophic events. The time-averaged sediment transport rates in model and prototype can be compared by:

$$Q_s = \frac{\Delta V_{(rw)}}{\Delta T_{(rw)}} = \frac{\Delta V_{(\exp)} \cdot \left(\lambda_x \cdot \lambda_y \cdot \lambda_z\right)}{\Delta T_{(\exp)} \cdot \left(\lambda_t\right)} \qquad [L^3/T] \qquad (2.3)$$

Where Q_s is the time-averaged volumetric sediment transport rate, ΔV is the displaced sediment volume and ΔT is the time period over which the amount of displaced volume is determined. The subscripts rw and exp denote real world and experiment, respectively. The scaling factors λ operate on the spatial dimensions (x-y-z) and time (t). In a perfect model, the upscaled time-averaged sediment flux observed in the experiment equals the value of the prototype. However, the time-averaged sediment flux in model and real world are expected to deviate owing to differences in substrate erodability and transport efficiency as will be discussed.

In practice, for the purpose of geological modelling of sedimentary systems we want to compare the vertical stacking of depositional environments in model and prototype. This can be done by considering the time-averaged sedimentation rate per unit area (R_s) which is obtained by dividing the time-averaged sediment deposition ($\Delta Q_s \geq 0$) by the total area of deposition (A):

$$R_s = \frac{\Delta Q_s}{A} \qquad [L/T] \qquad (2.4)$$

Analogous to the concept of Curray (1964), we use the Basin Fill factor (Bf), a non-dimensional parameter that describes the time-averaged sedimentation rate in relation to the rate of increase in accommodation space:

$$Bf = \frac{R_{s(rw)}}{R_{acc(rw)}} = \frac{R_{s(\exp)}}{R_{acc(\exp)}} \qquad [-] \qquad (2.5)$$

Where R_{acc} accounts for the rate of change in accommodation space per unit area for both the fluvial and marine realm in real world (rw) and experiment (exp). Note that R_s and R_{acc} should be both time-averaged over the same time span ΔT.

Since sediment transport is being modelled by bed load only, we must be aware that bed-load dominated systems exhibit quite different transport processes compared to suspension dominated systems (Postma, 1990). The predominant bed-load transport results in Gilbert-type deltas with steeply inclined (±33°) foreset beds formed by slip face avalanches. Delta clinoforms do not develop under these circumstances (cf. Driscoll & Karner, 1999), and mass flow transport into lowstand fans can not be modelled dynamically in a bed-load transport model. It is, therefore, important to realise that sediment volumes that reach the slope and basin (i.e., bypasses the shelf) are quantified here, which is the total amount that is preserved in the lowstand Gilbert-type delta. As for this aspect, we have to accept any geometrical discrepancy between model and prototype.

It must be clear at this point that in studying evolutionary trends in sedimentary systems by experiment we scale volumetric changes in the various sedimentary systems of the basin over relatively long time spans (i.e., cyclic time of Schumm & Lichty, 1965). The changes we observe and quantify by means of volume measurements can be related to the allocyclic controls we impose.

Experimental Modelling

The above scaling strategy for analogue models of large-scale sedimentary systems requires testing by a model-prototype comparison on a qualitative and quantitative basis. In this paper, we focus our modelling study on the effects of sea-level change induced erosion and deposition in the river-shelf realm (Fig. 2.1). We compare our model results with the Colorado system of the Gulf of Mexico, of which the stratigraphy of the last glacial cycle has been studied in detail (e.g. Suter & Berryhill, 1985; Berryhill, 1987; Anderson *et al.*, 1996).

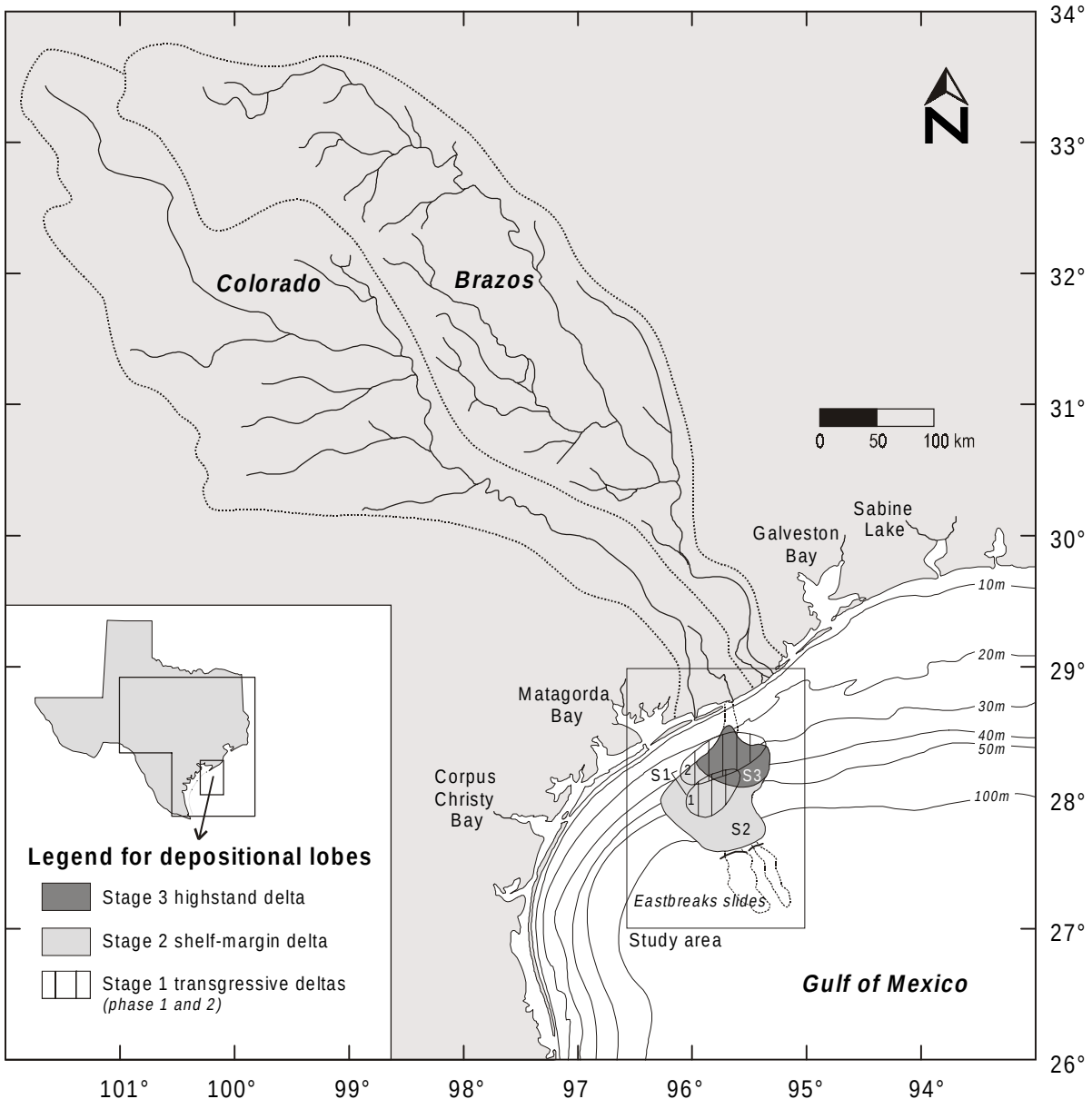

Fig. 2.2—Map of the Colorado river-shelf system over the last 40 kyr. Depositional geometries on the shelf include the isotope stage-3 highstand delta (40-23 ka), the stage-2 shelf-margin delta (23-11.5 ka) and two transgressive delta lobes of stage-1 (11.5-5 ka). (Map compiled from Morton & Price, 1987; Blum & Valastro, 1994; Anderson *et al.*, 1996).

The late Quaternary Colorado data base

The Colorado River is fed by a drainage basin of 110000 km^2 (Fig. 2.2). It is a bed-load dominated, high supply system that extended over the shelf during periods of sea-level lowstand feeding shelf and shelf-margin deltas (Anderson *et al*., 1996). In order to make a quantitative comparison between the Colorado Shelf and our model, we need to make gross volume approximations from the seismic studies of the shelf. Such have been made using isopach maps of the depositional sediment bodies related to oxygen isotope stage-3, 2 and 1 that have been compiled from Morton & Price (1987) and Snow (1998). The volumes are listed in Table 2.2. Oxygen isotope stage-3 starts at 58 ka with the Mid-Wisconsin highstand. Regional correlation along the Texas inner shelf (Rodriguez *et al*., 2000) suggests a shoreline position of 15 ± 2 m below present sea level for the stage-3 highstand. A similar estimate of 20 m for the stage-3 transgression is reported by Suter *et al.* (1987). As illustrated in Fig. 2.3, these values are much shallower in comparison with the commonly used oxygen isotope curves.

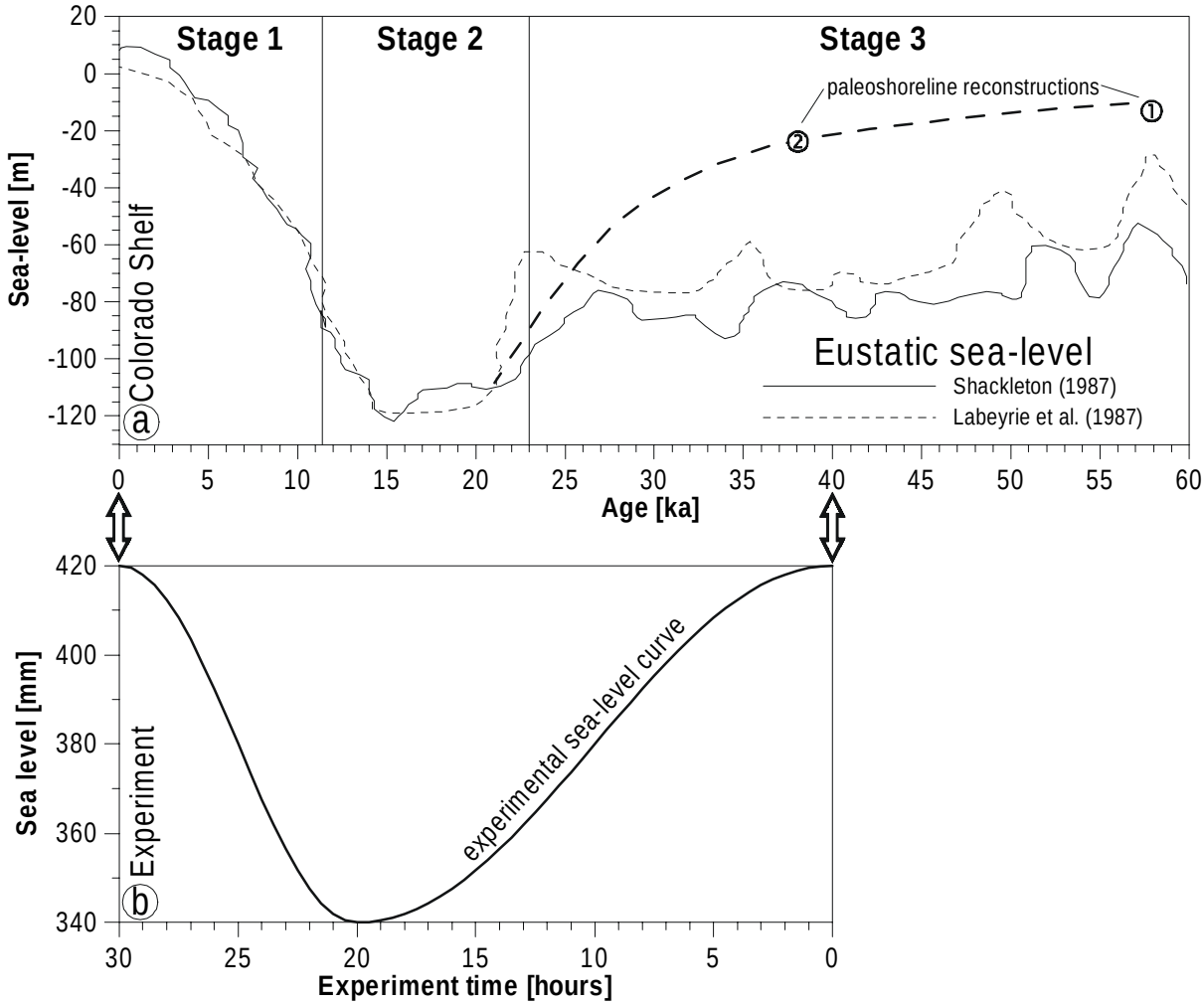

Fig. 2.3—(a) Oxygen isotope curves from Shackleton (1987) and Labeyrie *et al.* (1987) as a proxy for sea level. Both curves suggest much lesser height during stage-3 than is evident from regional paleoshoreline reconstructions of (1) Rodriguez *et al.* (2000) and (2) Snow (1998). Based on the regional data, we infer a conceptual sea-level curve (dashed line) for the regression. (b) The experimental sea-level curve approximates the shape of the conceptual curve.

Geological data from over the world and models support that sea-levels during the last interglacial were much higher than predicted by the isotopic curve owing to variation in isotopic composition of ice sheets, temperature variations in the deep sea and the effect of bioturbation in degrading the isotopic record (Mix & Ruddiman, 1984; Skene *et al*., 1998). We decided to use the paleo-shoreline constraints to select our experimental sea-level curve, because these are based on chrono-stratigraphic correlation supported by radiometric datings within the area. The first part of stage-3 represents a phase of maximum flooding, which is accompanied by deposition of prodelta muds on the inner shelf (Snow, 1998). As sea level started to fall at middle stage-3, a sandy highstand delta prograded on top of the prodelta clays on the inner shelf (Fig. 2.4). Bivalves in sediments of the up-dip portion of the stage-3 delta directly above the prodelta clays yielded radiocarbon ages of 38,850 ± 1380 and 39,320 ± 480 years BP (Rodriguez *et al*., 2000) and relate to a depositional depth of 26 m below present sea level (Snow, 1998). Hence, we assume 40 ka as the time of onset of the stage-3 highstand delta progradation (Fig. 2.3). The isopach map of the stage-3 delta yields a sand volume of 11.5 km^3 (Fig. 2.4), which is a minimum value because the top of the delta was truncated during the stage-2 sea-level lowstand. The missing volume of presumably sandy delta top sediments that were excavated during the last lowstand is estimated to be 9.5 km^3 through calculation of the space occupied by the incised valleys of the lowstand topography (Fig. 2.5). Hence we assume an original total sand volume of the stage-3 delta of 21 km^3.

The stage-2 sea-level lowstand incised the shelf, including sediments of stage-5 and stage-3 highstand deltas. The redeposited shelf sediments contributed to the total river load that was diverted to the shelf margin forming a large, shelf-edge delta (Suter & Berryhill, 1985, their Delta A). The contour map for combined coarse and fine sediments of the stage-2 shelf-margin delta was compiled after Morton & Price (1987). However, the base of their stage-2 deposits is not well dated and we suspect that the map may also include some late stage-3 deposits. The total volume enclosed by the stage-3 and -2 isopach maps is 89 km^3 (Fig. 2.4). Subtracting the preserved sand volume of the stage-3 highstand delta (11.5 km^3) from the total volume gives an approximation for the volume of stage-2. This yields a total volume of 77.5 km^3 for the stage-2 deposits on the shelf. The sand content is unknown, but a tentative sand volume estimate of 50% for the stage-2 shelf-margin delta can be based on cores of the shelf-margin delta (Morton & Price, 1987). This is much higher than the 37% of sand that makes up the Louisiana shelf (Coleman & Roberts, 1990). The Holocene sea-level rise resulted in two phases of transgressive backstepping of delta lobes on the shelf during stage-1 (Fig. 2.6). Phase 1 (11.5 to 9.5 ka) resulted in three fluvially dominated delta lobes with a sand volume of 6.3 km^3. A wave-dominated elongated lobe that contains 4.5 km^3 of sand was formed during phase 2 (9.5 to 5 ka).

Mass wasting processes that formed the East Breaks slides on the continental slope (Lehner, 1969; Hardin, 1987) are not accounted for in our volume estimates. Although the slides cover a large area on the slope (see Fig. 2.2) and encompass a large volume of sediments (Woodbury *et al*., 1978), the gliding predominantly affected the slope sediments between 200 m and 1350 m water depth (Rothwell *et al*., 1991) and probably not the shelf margin delta itself. We only considered the sediment volume that was received by the shelf and upper slope.

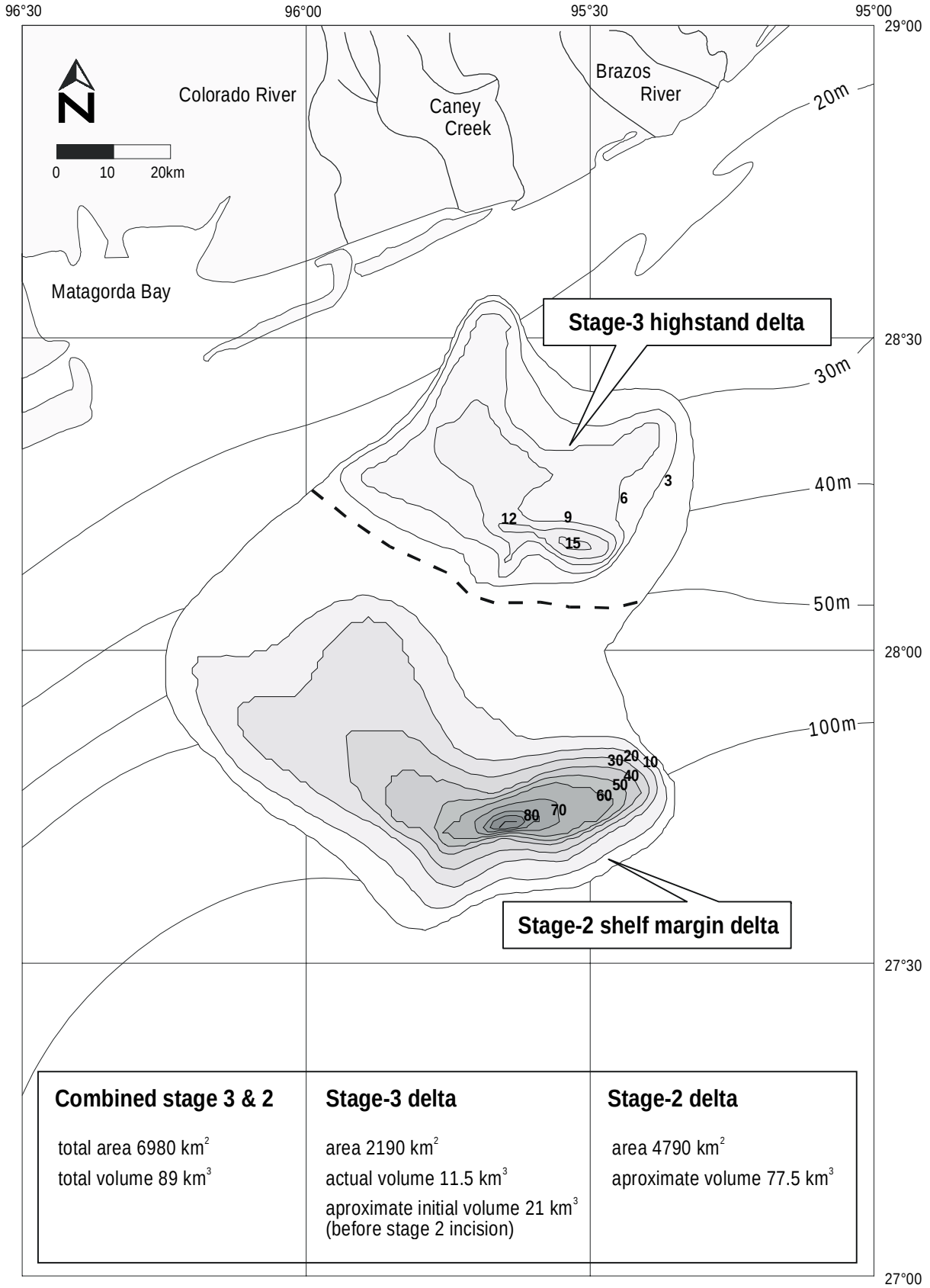

Fig. 2.4—Isopach maps (sediment thickness contours in metres) of the stage-3 shelf delta (from Snow, 1998) and the stage-2 shelf margin delta (from Morton & Price, 1987). The volumes of the successive depositional systems are depicted in the box and discussed in the text.

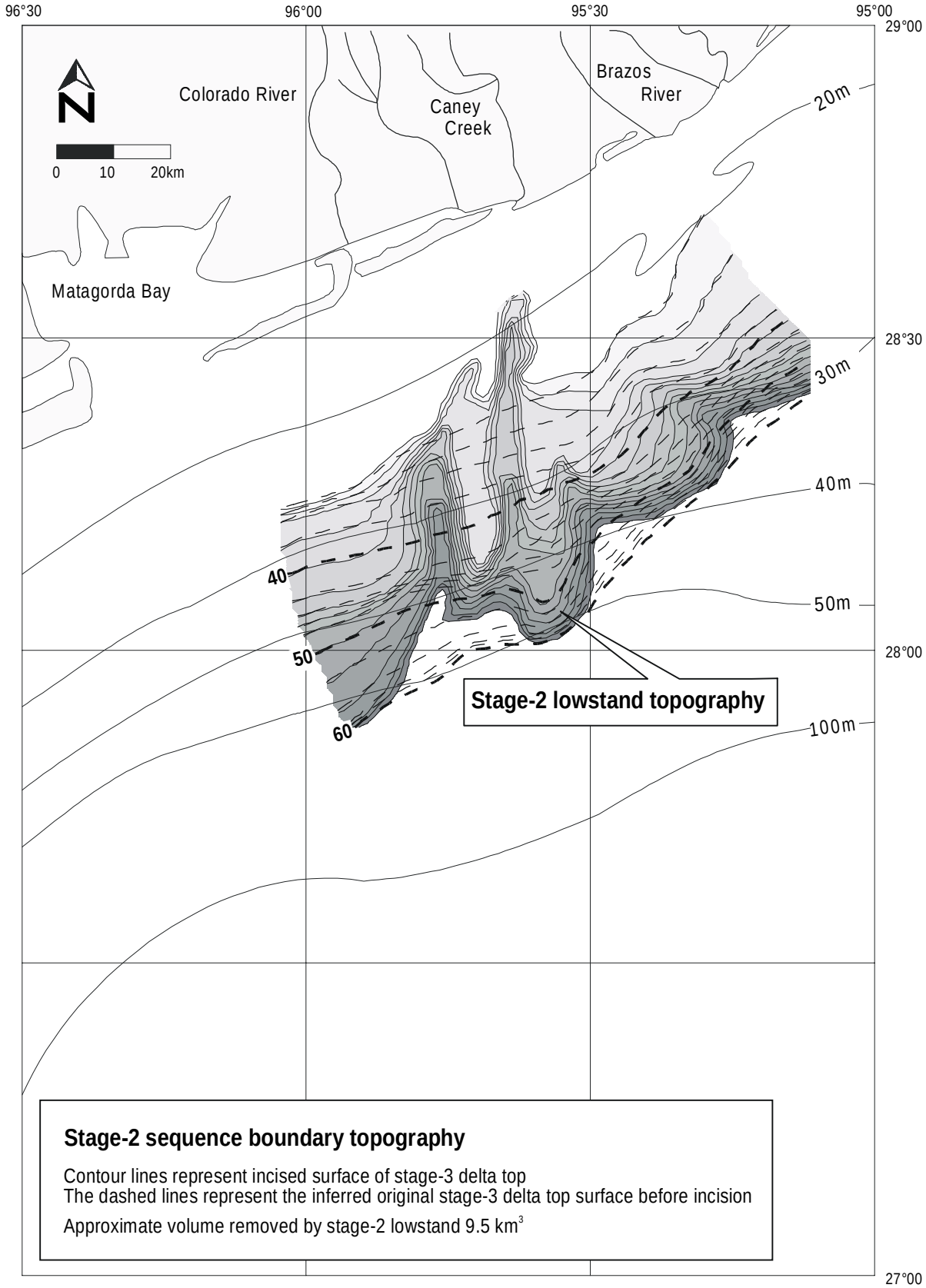

Fig. 2.5—Structural contour map (depth contours in metres) of the stage-2 sequence boundary. It displays the extensive excavation of the highstand delta by a number of incised valleys that seem to merge updip into a single feeder system. The dashed lines show the reconstruction of the original top surface of the stage-3 delta before it was incised during the stage-2 lowstand. The volume of stage-3 deposits that were cannibalised during stage-2 is approximately 9.5 km^3.

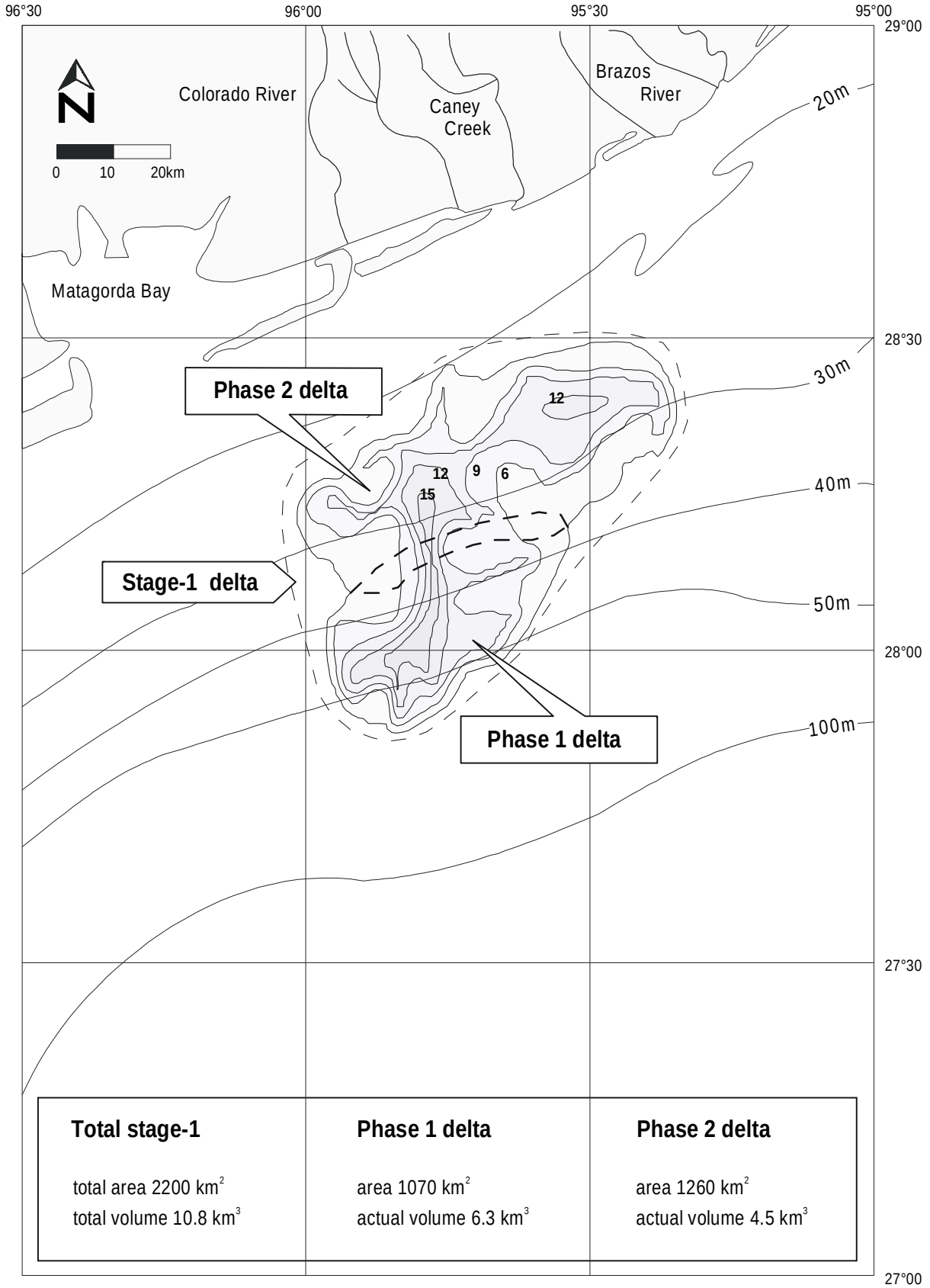

Fig. 2.6—Isopach map (sediment thickness contours in metres) of the stage-1 delta (from Snow, 1998). The map shows two distinct backstepping lobes: A phase 1 delta (11.5 ka to 9.5 ka) and further coastward a phase 2 delta (9.5 ka to 5 ka). The volumes and areas of the phase 1 and 2 delta lobes are included in the box.

Table 2.2. Volume approximations for depositional systems on the Colorado Shelf based on Figs 2.4 to 2.6. The second column shows the period over which the sediment flux was averaged.

Isotope stage	Period, ΔT (ka)	Volume deposited, ΔV (km^3)	Deposition rate, Q_s (km^3/kyr)	Area of deposition, A (km^2)	Sedimentation rate, R_s (m/kyr)	Rate of sea-level change, R_{acc} (m/kyr)	Basin Fill factor, Bf (-)
Late stage-3	40 – 23	21.0 (11.5+9.5)	1.24	2190	0.56	-3.80	-0.15
Stage-2	23 – 11.5	77.5	6.74	4790	1.41	0.83	1.70
Stage-1 Phase 1	11.5 – 9.5	6.3	3.15	1070	2.95	12.2	0.24
Stage-1 Phase 2	9.5 – 5.0	4.5	1.00	1260	0.79	8.94	0.09

Table 2.3. Facts on the set-up and the experimental method.

Experimental set-up	Properties
Dimensions	Main tank: 4 x 4 x 1 m, table with shelf-slope configuration 3x3.4 m Fluvial valley, Duct: 4 x 0.5 x 0.11 m
Co-ordinate system	x, y and z axes with values in mm (Fig. 2.7)
Measurements	Main tank: automated bed profiler, accuracy of x, y and z data within 0.4 mm. Applied data-point spacing 20 mm. Fluvial valley: manual stream profile measurement with rulers spaced 100 mm apart (accuracy 2 mm).
Discharge	400 dm^3/h
Sediment supply	1 dm^3/h (~1.85 kg of dry sediment per hour)
Sediment properties	Unimodal medium sand used as uniform substrate (bed material) and as supply for the fluvial valley. D_{50}; median grain diameter = 250 μm D_{90}; ninety percentile grain diameter = 700 μm And 40 μm < D < 1000 μm to avoid cohesion problems with clays and to exclude partitional sortening effects of large grains.
Hydraulic conditions	h = 6-10 mm (channel depth) $\overline{u}$ = 0.18 m/s (average flow velocity in the fluvial valley) Fr = 0.77 (Froude number in the fluvial valley) Re = 886 (Reynolds number in the fluvial valley)

Experimental set-up

The set-up consists of a 4 x 4 x 1 m main tank, which is connected to a rectangular duct of 4 x 0.11 x 0.5 m (Fig. 2.7 and Table 2.3). A water pump circulates water from the main tank to the upstream end of the duct. The discharge is controlled by a flow meter. A sediment feeder at the upstream end of the duct consists of an adjustable funnel above a conveyor belt, allowing regular supply of a given quantity of sediment.

The discharge and sediment feeder replace the drainage basin, supplying sediment load through the fluvial valley at a constant rate (Table 2.3). The water level in the tank is controlled by a manually adjustable overflow. A table of 3 x 3.4 m in the main tank supports a sand cover that forms the coastal plain-shelf-slope topography.

Essential for the quantitative evaluation of the analogue model results is the use of an automated x-y positioning system equipped with a Dynavision SPR-2 laser sensor that enables high resolution measurements of the bed elevation with an accuracy of 0.4 mm in x, y, and z directions (Fig. 2.7b). With a default grid spacing of 2 cm, it took 15 hours to complete a digital elevation map (DEM) of the shelf-slope configuration in the main tank. Subtraction of the data sets of subsequent scans results in contour maps displaying the net amount of sediment erosion and deposition. Changes of the fluvial valley's stream profile were measured by means of rulers that were attached to the valleys glass wall at 10 cm spacing.

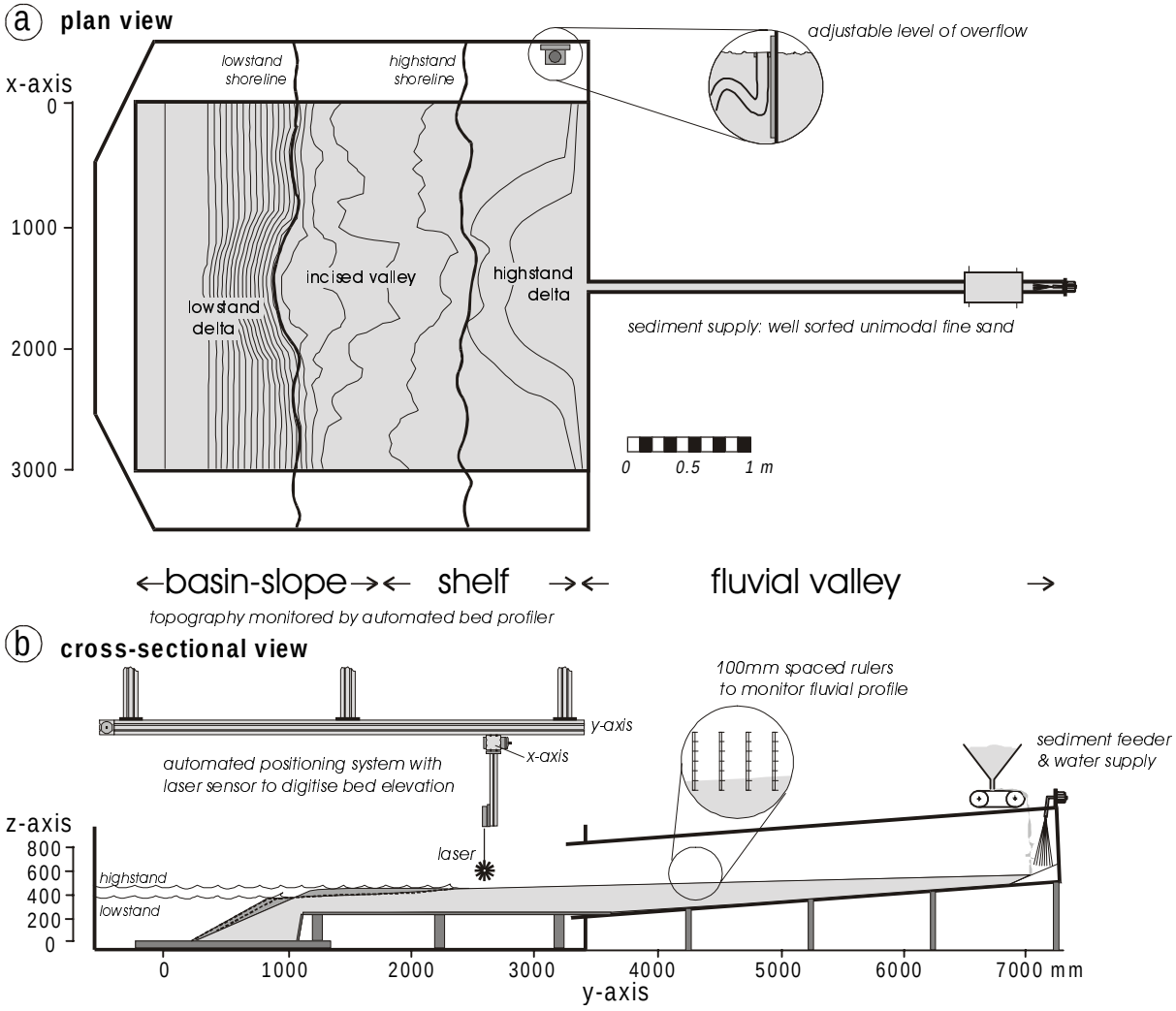

Fig. 2.7—Experimental set-up in plan view (a) and cross-sectional view (b). The shelf-slope setting is moulded on a table in the main tank. A duct with discharge and sediment feeder at its upstream end replicates the drainage basin. A laser sensor carried by a positioning system enables detailed measurement of the topography within the main tank. The fluvial valley's profile was measured using rulers spaced 10 cm apart.

Application of the scaling strategy for analogue experiments

We modelled the bulk sediment transport of a real world sedimentary system by bed-load transport of a uniformly grained material. Although sediment transport was modelled over too long time spans so that hydraulic scaling conditions must be relaxed, Froude numbers were kept below unity, which is realistic for steady fluvial transport (Table 2.3). Thus we applied conditions of lower flow regime to avoid bedform formation in the flume that would affect the apparent bed roughness, but maintained sufficiently high discharges to ensure a constant bed-load transport rate in the fluvial valley. The grain size fraction smaller than 40 μm was removed to avoid undesirable cohesion effects. By sieving all grains larger than 1000 μm out, the ratio of the ninety percentile grain diameter over water depth was approximately 7-10, which kept partial sorting of coarse size grades to a minimum (e.g. Middleton & Southard, 1984). Testing of the model for various discharge regimes supports that the observed bed-load transport rates in the model are steady and realistic for the applied conditions (see Appendix). It must be clear that grain size itself was not scaled. Here, sand is merely an isotropic medium used to model sediment displacements in real world systems. The sediment properties (grain size, roundness, etc.) define the diffusivity and herewith equilibrium time. In fact, we could have taken any type of grains as long as the hydraulic boundary conditions are maintained and the effect of the grain properties on the sediment transport rate (diffusivity) is accounted for in the calculation of the equilibrium time of the system. We used unimodal medium sand for practical reasons, which gave the desired match between the time-averaged sediment transport rate in model and prototype (see further Appendix and discussion).

Since the relative sizes and gradients of each of the landscape components play an important role in the landscape evolution and resulting basin fill architecture, we based the dimensional scaling of the model (Table 2.4) on those of the prototype (e.g. Blum & Price, 1998, their fig. 4). The horizontal dimensions of the Colorado river-shelf system have been scaled by a factor $6x10^4$ (Table 2.4a). The vertical scaling factor is $1.5x10^3$ (Table 2.4b) which means that the gradients are, unavoidably, distorted with respect to the prototype. The model gradients are steeper in the model because they depend on the applied discharge (applied shear stress along the bottom) and sediment supply rate (Table 2.4c). The initial geometry of the sand bed in the model, however, is common for Quaternary passive margins, with the downstream fluvial profile steeper than the coastal plain profile but less steep than the shelf gradient (e.g. Miall, 1991; Nummedal *et al.*, 1993).

For a proper time scaling the Basin Response factor must be similar for model and prototype. We applied an experiment duration of one cycle of sea-level change such that Br ~ 4. This is comparable to the prototype's Br-value, since the equilibrium time of the Colorado system is about 10 kyr if a diffusivity of 0.1 km^3/yr is assumed (Paola *et al.*, 1992) and the period of our sea level "cycle" T is ~40 kyr (Fig. 2.3). The T_{eq} for our model is 5 to 10 hours, depending on the emerged shelf width. The theoretical values are in agreement with the observed experimental values of 6 to 10 hours as will be shown in Chapter 3 (Table 3.4). Thus, modelling river-shelf evolution over one glacio-eustatic sea-level change brings the duration of one glacio-eustatic sea-level cycle down to about 30 hours for a flume experiment. This means that time is scaled by a factor $1.168x10^7$ (Table 2.4d). The time-averaged sediment-transport rate

in the experiment can be compared with the prototype by applying the values for the scaling factors (λ) from Table 2.4a-d. The calculation in Table 2.4f shows that the upscaled value for time-averaged sediment transport is comparable to the contemporary estimate for the sediment transport rate of the Colorado River from Burgess & Hovius (1998).

The sea-level curve has been chosen in agreement with the geometric scaling of the shelf physiography of the prototype. The shape of the experimental curve reproduces the overall trend of the glacio-eustatic cycle with a slow sea-level fall and a rapid rise (Fig. 2.3). However, it starts and ends at a similar highstand level for reasons of generalisation. In fact, we did a range of experiments with equal shelf slope configuration, but which differ in the rate of sea-level fall. The results of the whole range of experiments have been described in Chapter 3. Here we present the experiment that fits most closely to the rate of sea-level change for the prototype. We repeated the experiment two times to have a check on its reproducibility.

Table 2.4. Characteristics of the prototype and the model over the modelled period.

a) Horizontal scaling / dimensions $\lambda_x \sim \lambda_y \sim 60000$	**Colorado**	**Model**
Downstream river length	250 km	4 m
Length of coastal plain	60 km	1 m
Initial shelf width	75 km	1.2 m
Unit width of modelled area	180 km	3 m
b) Vertical scaling $\lambda_z \sim 1500$	**Colorado**	**Model**
Amplitude of eustatic sea-level changes	120 m	0.08 m
c) Slopes $\lambda_s = \lambda_y / \lambda_z \sim 40$	**Colorado**	**Model**
Downstream river gradient	S=0.0004 (~0.022°)	S=0.025 (~1.5°)
Coastal plain gradient	S=0.0003 (~0.017°)	S=0.02 (~1.1°)
Shelf gradient	S=0.0008 (~0.046°)	S=0.03 (~1.7°)
Slope gradient	S=0.01 (~0.57°)	S=0.42 (~22°)
d) Time scaling $\lambda_t = 1.168 \times 10^7$	**Colorado**	**Model**
40 ka – recent (oxygen-isotope stages 3, 2 and 1)	40 kyr	30 hours
e) Sediment supply and discharge	**Present Colorado**	**Model**
Total load of the fluvial system	6.50 km^3/kyr (Burgess & Hovius, 1998)	5.0×10^{-4} kg/s (=1.80 kg/h ~1 dm^3/h)
Q_s, Sediment transport rate	$Qs_{(rw)} = 0.21$ m^3/s	$Qs_{(exp)} = 2.77 \times 10^{-7}$ m^3/s
f) Time-averaged sediment transport (Eq. 2.3)	**Colorado**	**Model**
$Qs = \frac{\Delta V_{(rw)}}{\Delta T_{(rw)}} = \frac{\Delta V_{(\exp)} \cdot (\lambda_x \cdot \lambda_y \cdot \lambda_z)}{\Delta T_{(\exp)} \cdot (\lambda_t)}$	$Qs_{(rw)}$	$Qs_{(\exp)} \cdot \frac{(\lambda_x \cdot \lambda_y \cdot \lambda_z)}{(\lambda_t)}$
The upscaled time-averaged sediment transport rate of the experiment is about half the present day prototype value.	= 0.21 m^3/s	= 0.13 m^3/s

Run procedures

Preparations for each experiment include levelling of the sand according to a fixed initial topography, which was defined by a marker line on the fluvial valley and sidewalls along the table in the main tank. The sand bed was submerged two times to improve the packing. Each experiment started at highstand level with a 15 hours run to establish a stable graded fluvial stream profile as uniform starting condition. The sea-level change is imposed by adjustment of the level of overflow in the main tank at ten minutes interval. Every hour, both discharge and sediment supply were checked and the stream profile in the fluvial valley was measured by reading the rulers on the valley's glass wall. At a five hour interval the topography in the main tank was measured by use of the automated bed profiler, which has to be done subaerially. For each scan the experiment was paused and the tank was drained carefully to avoid disturbances in the sediment bed.

Results

Observations

Observations include time-lapse video recordings, photographs (Fig. 2.8) and scans taken at 5 hour intervals (Fig. 2.9). Volume changes (net sediment erosion and deposition) are listed in Table 2.5. During the 15 hour highstand preparation run, the apex of the highstand delta is located near the outlet of the fluvial valley. The delta plain aggrades and the entire delta front progrades steadily through frequent channel avulsion in the upper delta plain.

In response to the sea-level fall, the shoreline shifts basinward and downward following the gradient of the shelf. As a result, the toe of the highstand delta is progressively incised (Fig. 2.8a) and small, elongated delta lobes (extensions) form on the middle shelf and build out further seaward, fed by leveed channels. As the sea-level fall proceeds towards the fall inflection point numerous incipient valleys incise the newly emerged shelf break. These small, V-shaped shelf valleys feed small, shelf edge deltas that form along the upper slope (Figs 2.8a and 2.9a). The leveed channels that develop on the middle shelf alternately feed several of these cross-shelf valleys through continuing avulsion process on the upper highstand delta plain. Meanwhile, aggradation in the fluvial valley continues in harmony with continued aggradation on the delta, although its rate is decreasing. The process of headward erosion of the cross-shelf valleys proceeds by retreat of knickpoints. These are the small limbs at the head of the incisions that mark the upstream limit of erosion (Figs 2.8a and 2.9a).

At early lowstand one of the shelf valleys has eroded headward towards the toe of the former highstand delta. As its knickpoint approaches the former highstand delta plain, that valley captures most of the discharge from the fluvial valley, cutting off the other leveed channels on the exposed shelf (Figs 2.8b and 2.9b). At that time, most valleys on the shelf become abandoned due to insufficient discharge. One dominating valley that progressively captures all discharge from the fluvial valley evolves into a mature U-shaped canyon by deepening and widening. It makes full drainage connection with the fluvial valley before lowstand, between 15 and 17 hours runtime. The knickpoint retreat in the dominating valley is shown in Fig. 2.10b, a star marks the drainage connection. As a result of drainage connection, the top of the former

highstand delta becomes incised, which means that all avulsion processes on the former delta plain stops. All sediment from the fluvial valley and drainage basin is now fed straight onto the only remaining active lowstand shelf-margin delta. The stream profile of the main valley continues to adjust towards lowstand base level and the shelf-margin delta further increases in size (Figs 2.8c and 2.9c). Thus, the sediment of the shelf-margin delta has three sources: 1) the drainage basin, 2) the river valley floor and 3) the shelf. At lowstand, the shelf-edge delta aggrades (Figs 2.9c-d), but after the first significant sea-level rise shoreline retreat forces backstepping of the delta front. During early rise, the basinward part of the main cross-shelf bypass valley becomes filled with small, backstepping delta lobes instead of one cross-valley delta front (Figs 2.8d). At late rise, a transgressive backstepping delta restores the topography left by the valley incision on the inner shelf and coastal plain (Fig. 2.9e). Near the final highstand, the fluvial valley re-establishes its initial, equilibrium profile. The observed sediment supply to the highstand delta is lower than the supply rate from the feeder (Fig. 2.10c), which must be attributed to aggradation in the fluvial valley during highstand. The above description of the shelf evolution is representative for the full range of experiments, although the timing of the depositional and erosional events depends on the rate sea-level fall (see further Chapter 3). The experiment was repeated two times with almost identical results (Fig. 2.10).

Table 2.5. Volume changes as measured from the isopach maps of experiment 240 in Fig. 2.9. The right column shows the Basin Fill factor (Eq. 2.5) that enables comparison with the prototype values for the Colorado Shelf (Fig. 2.11).

Experiment Run	Period, ΔT (h)	Volume deposited, ΔV (dm^3)	Rate of deposition, Q_s (dm^3/h)	Area of deposition, A (m^2)	Sedimentation rate, R_s (m/h)	Rate of sea-level change, R_{acc} (m/h)	Basin Fill factor, Bf (-)
241	0 – 5	3.5	0.7	0.67	0.0010	-0.0024	-0.44
242	5 – 10	3.7	0.7	0.30	0.0025	-0.0056	-0.44
243	10 – 15	15.7	3.1	1.60	0.0020	-0.0056	-0.35
244	15 – 20	15.4	3.1	1.90	0.0016	-0.0024	-0.67
245	20 – 25	5.5	1.1	1.05	0.0011	0.0080	0.13
246	25 – 30	4.1	0.8	0.97	0.0008	0.0080	0.10

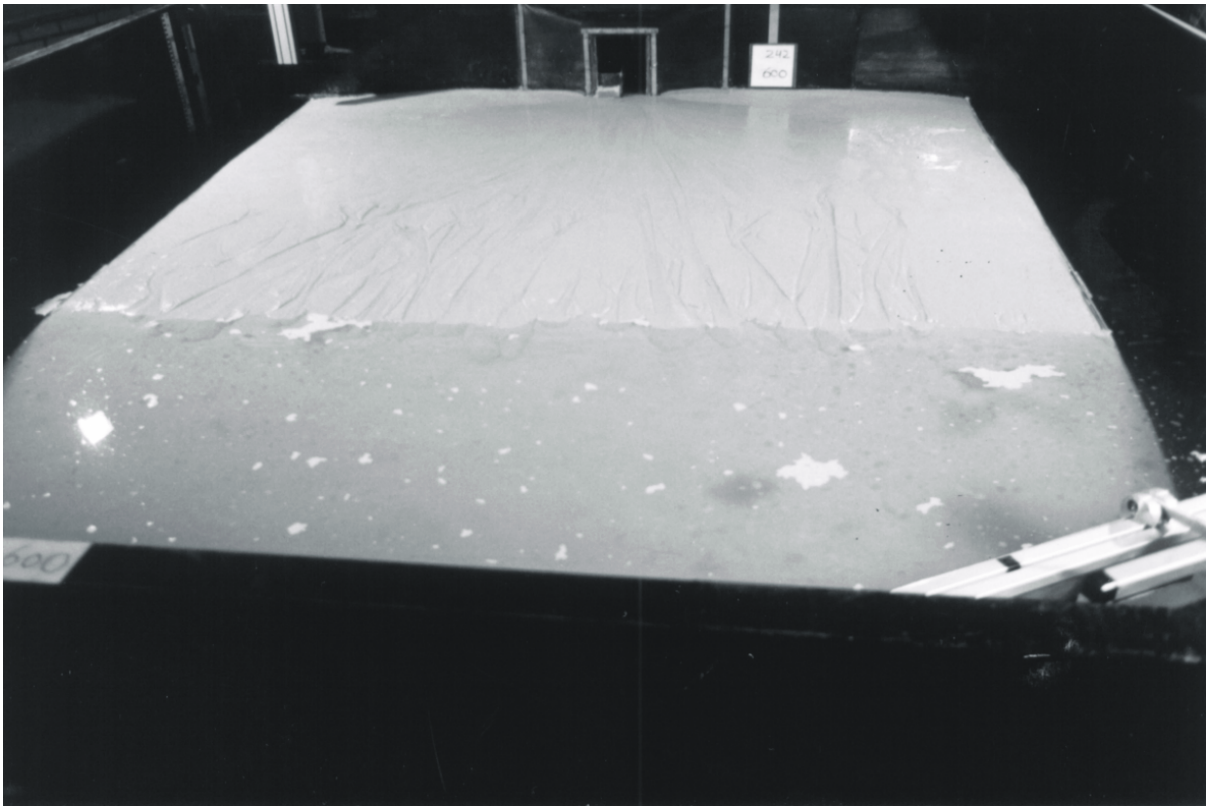

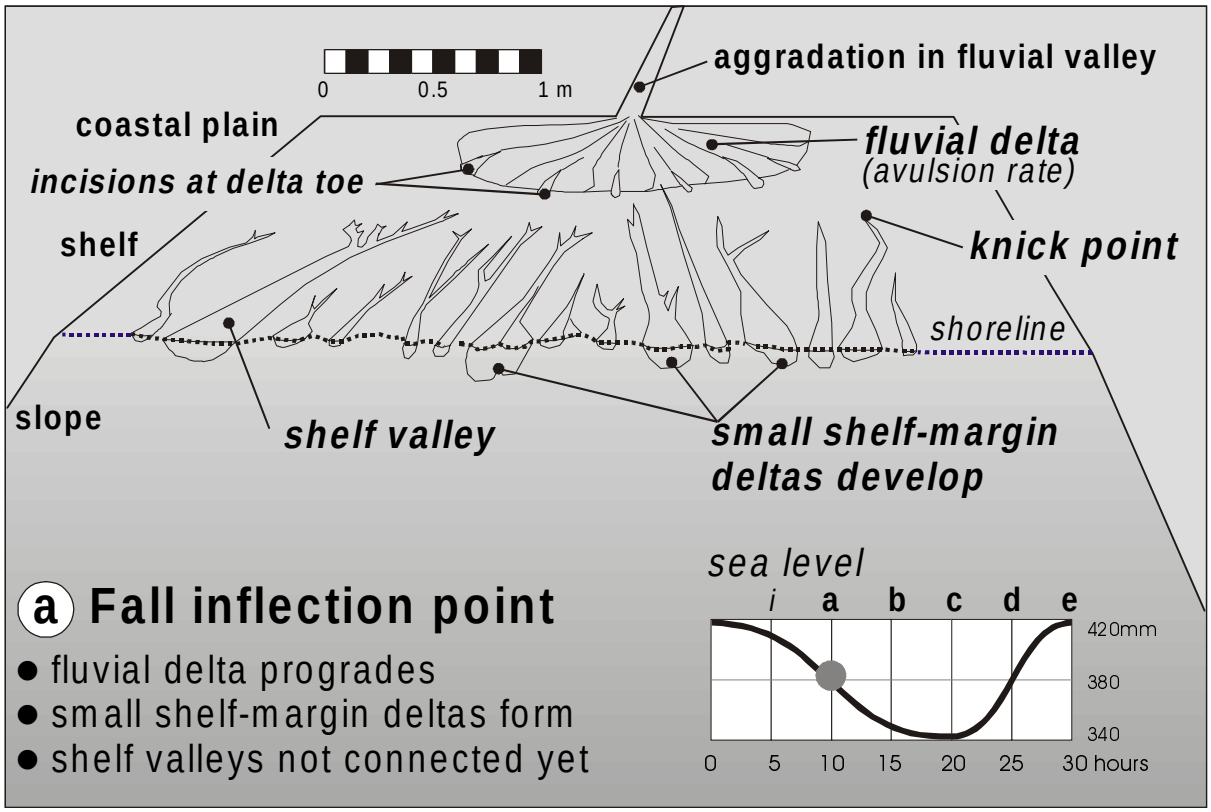

Fig. 2.8—Observations from the experiment at stage a, b, c and d. The labels a to d correspond with Fig. 2.9. (a) The fall inflection point at 10 hours of experiment time.

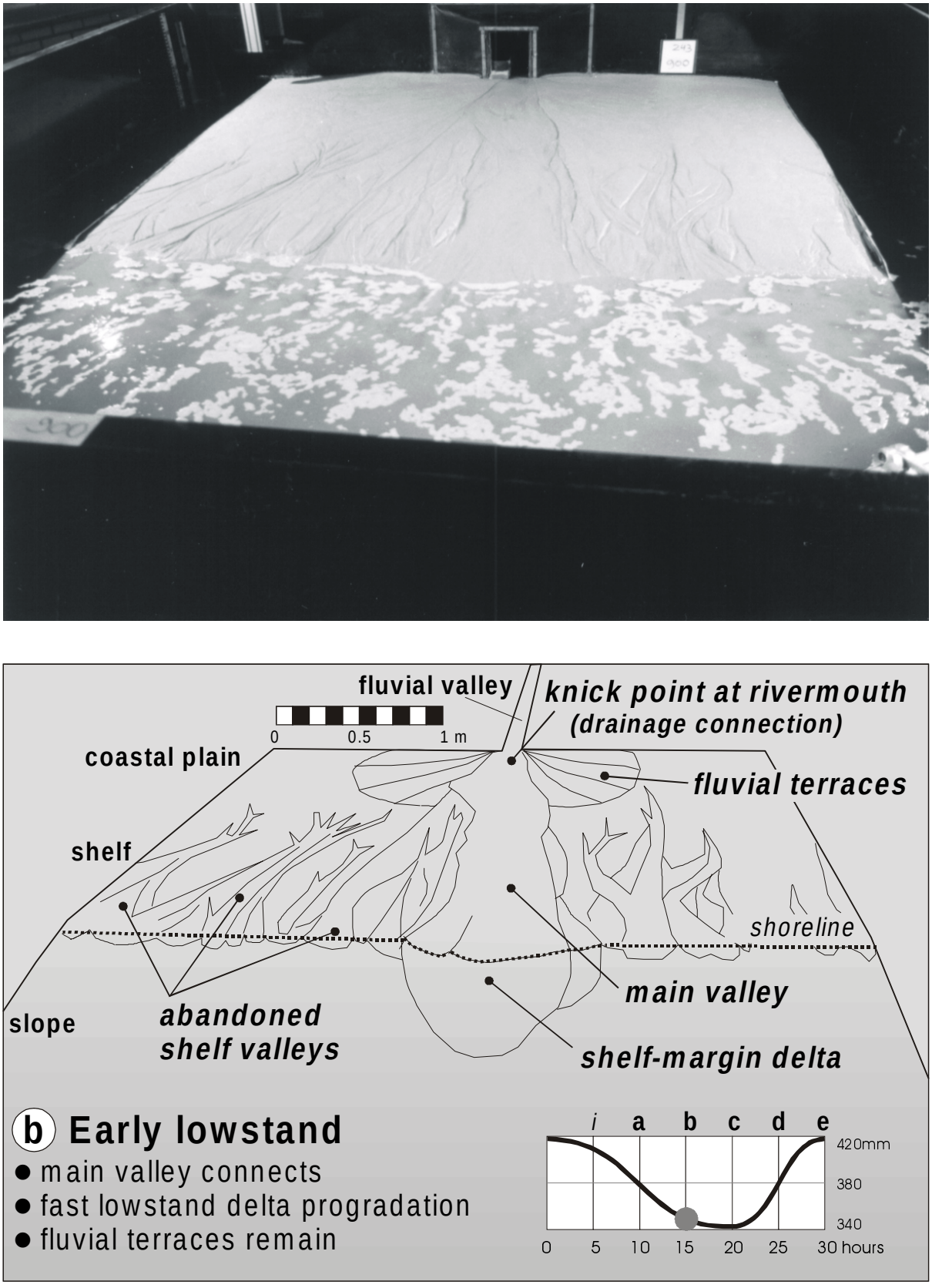

Fig. 2.8—(b) Early lowstand at 15 hours of experiment time.

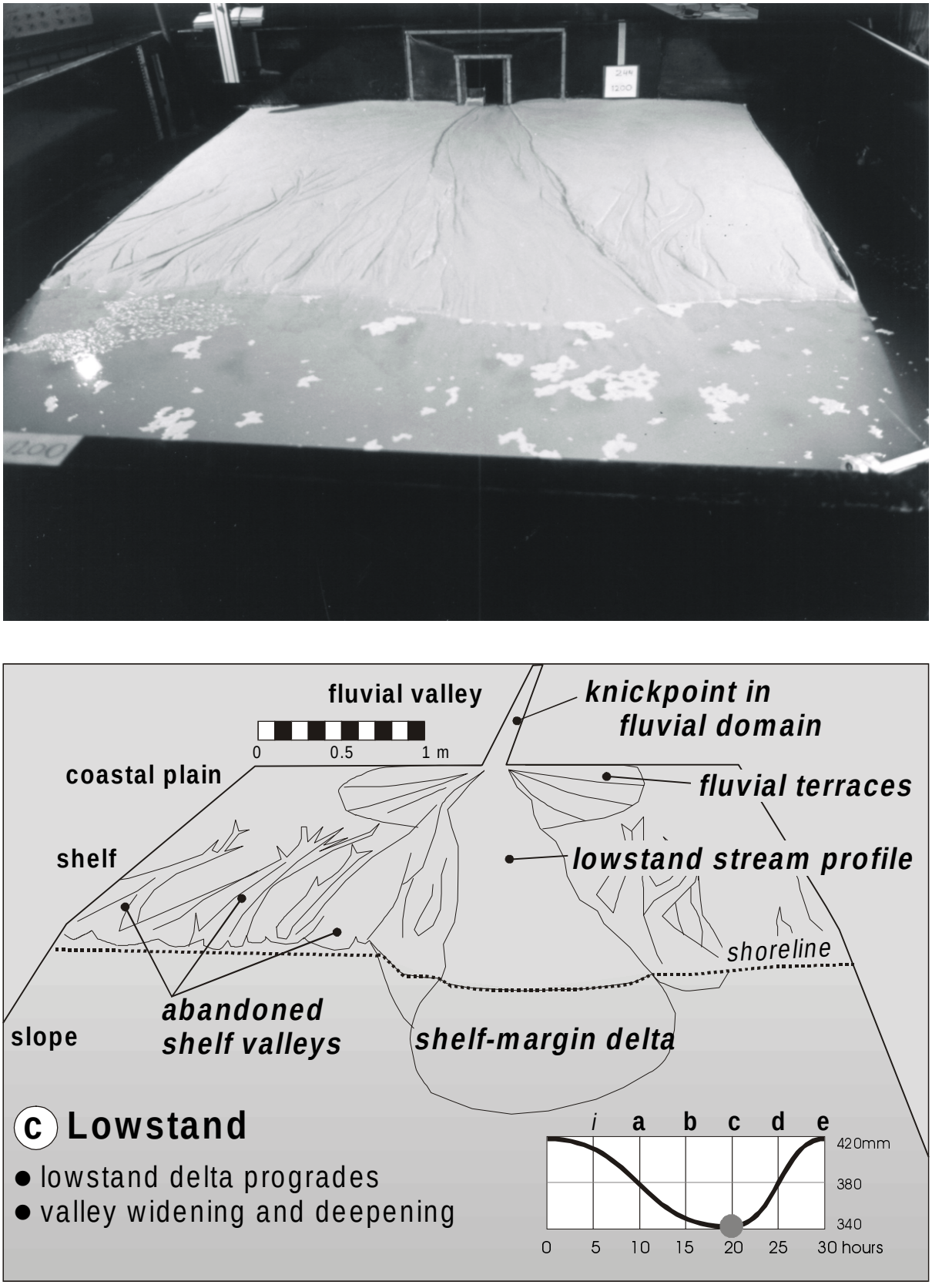

Fig. 2.8—(c) Lowstand at 20 hours of experiment time.

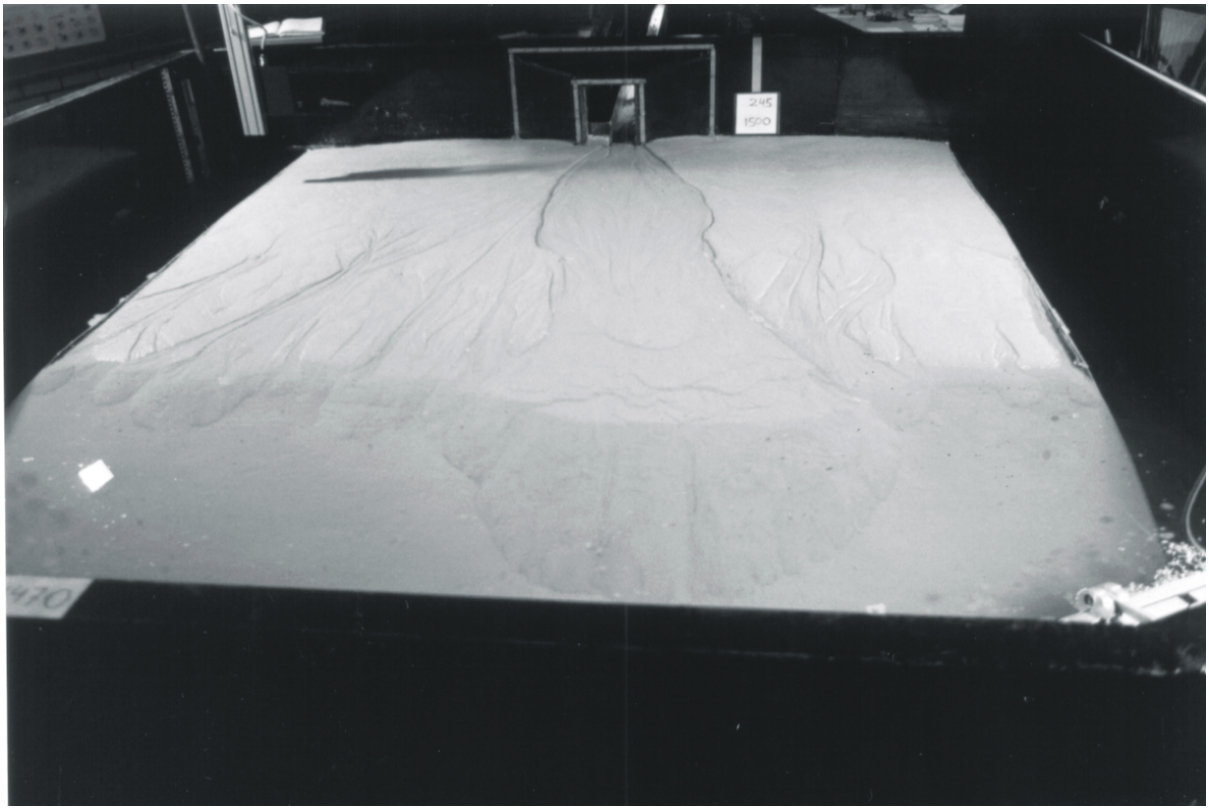

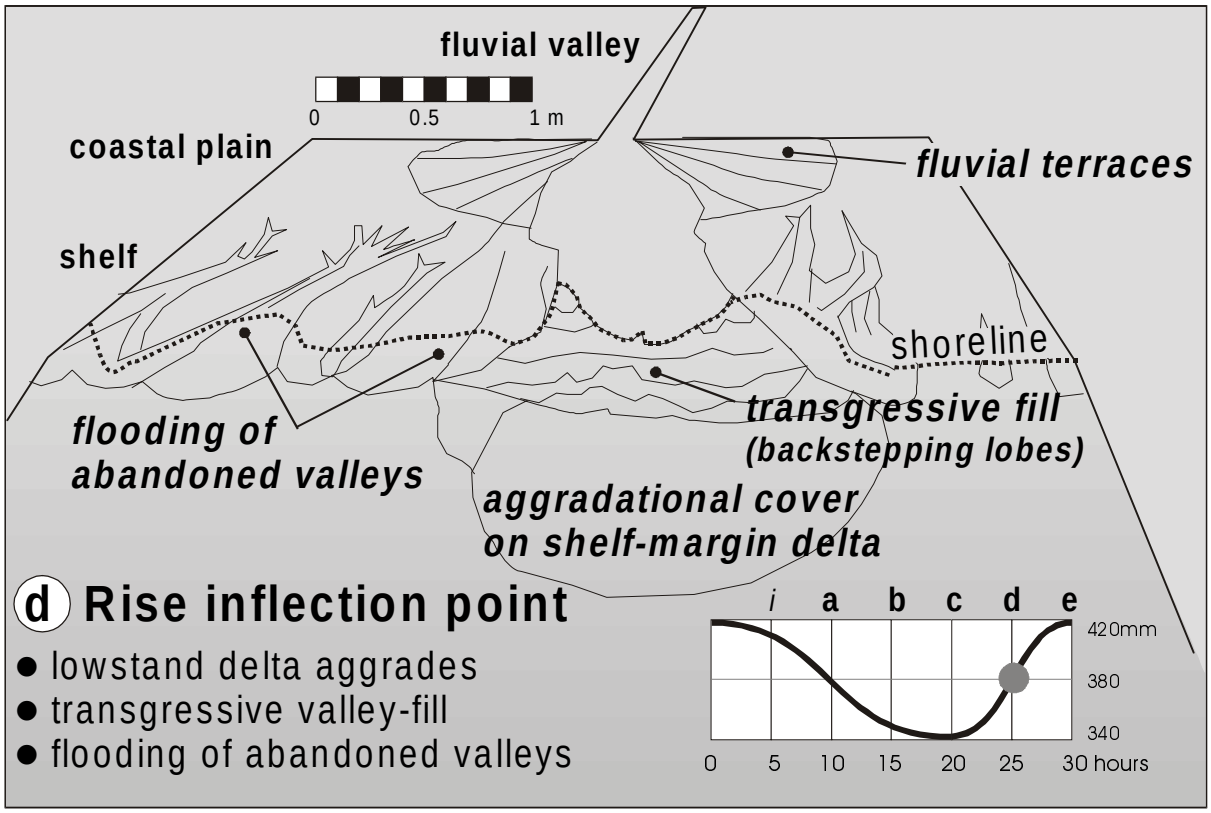

Fig. 2.8—(d) Rise inflection point at 25 hours of experiment time.

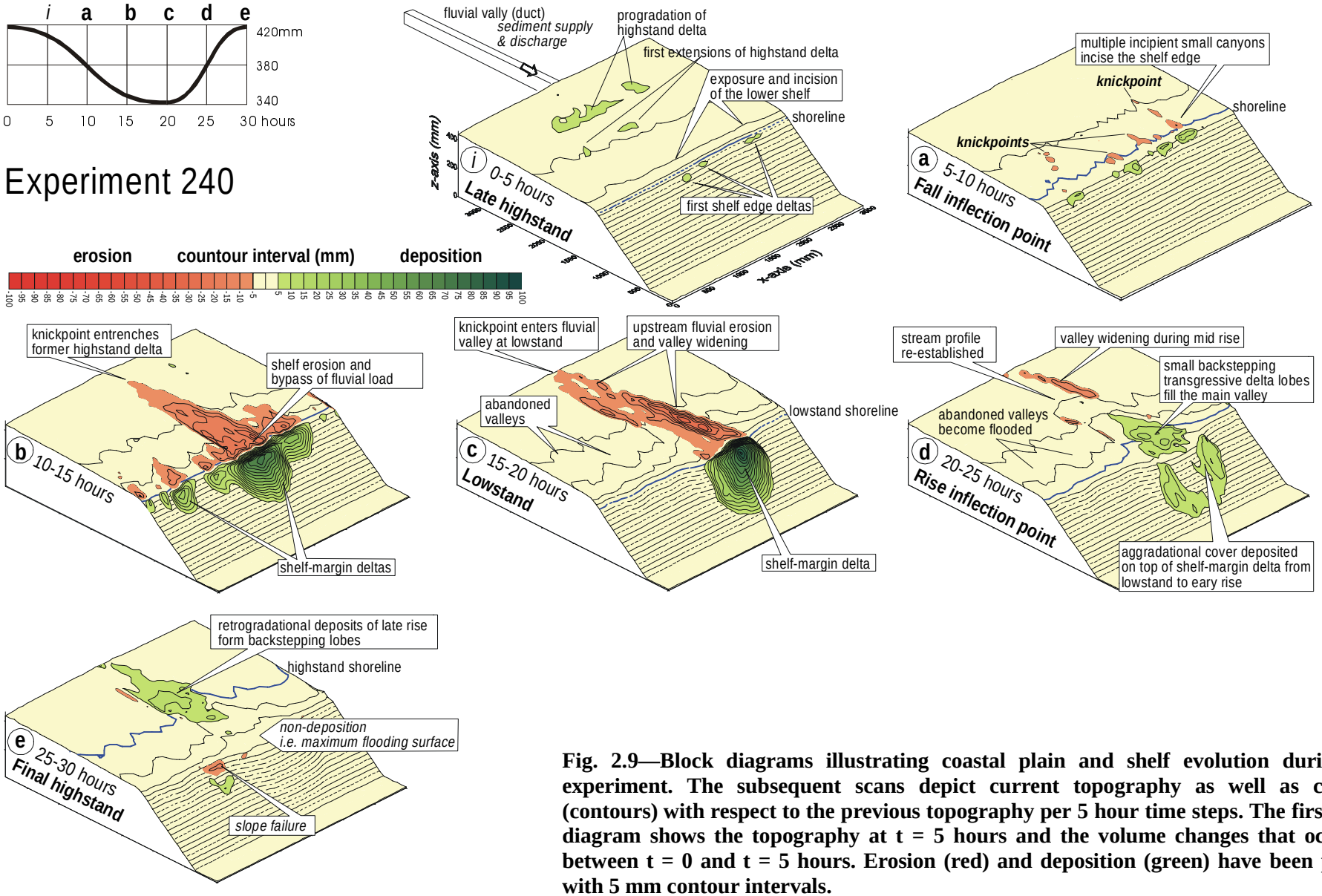

Fig. 2.9—Block diagrams illustrating coastal plain and shelf evolution during the experiment. The subsequent scans depict current topography as well as changes (contours) with respect to the previous topography per 5 hour time steps. The first block diagram shows the topography at t = 5 hours and the volume changes that occurred between t = 0 and t = 5 hours. Erosion (red) and deposition (green) have been plotted with 5 mm contour intervals.

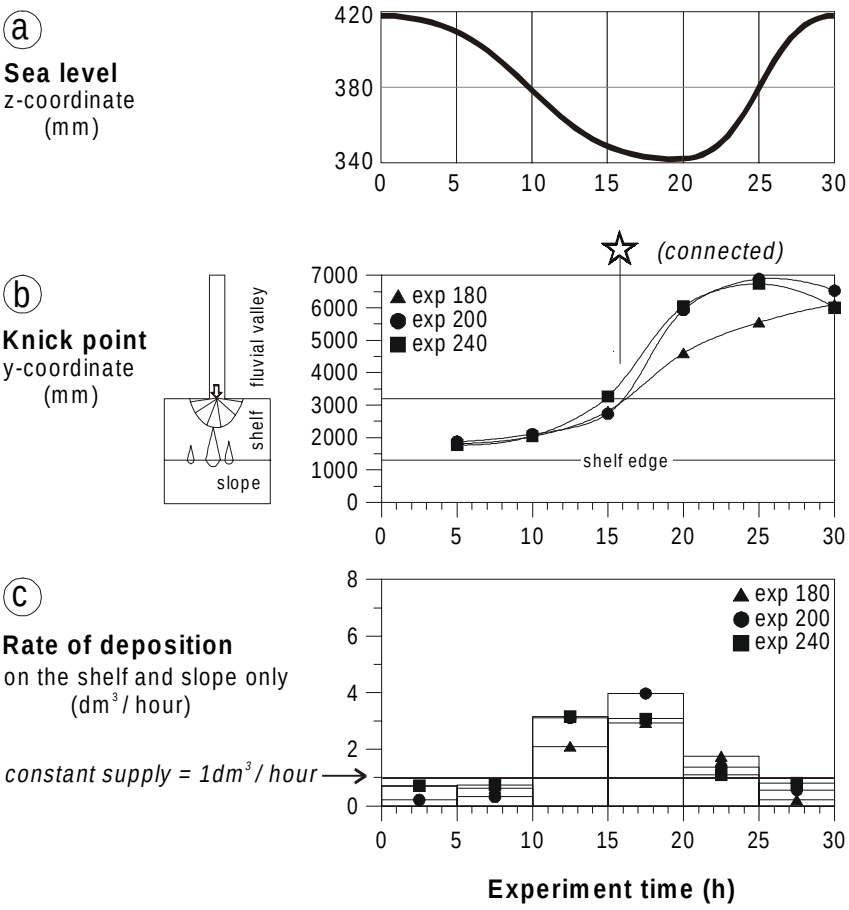

Fig. 2.10—Quantitative comparison of three identical flume experiments. (a) Sea-level curve. (b) Position of the main knickpoint (upstream limit of headward erosion) through time. The head of the main cross-shelf valley makes drainage connection with the fluvial valley between 14 and 17 hours runtime as indicated by the stars below the sea-level cycle. (c) The mean rate of deposition on the shelf shows the effect of a sea-level change on the sediment flux on the coastal plain and shelf and to the lowstand delta (rates were calculated from the green depositional volumes on the scans on Fig. 2.9). Note that for experiment 180 the erosion (knickpoint) did not proceed as far upvalley as in the other two experiments. By way of exception, two cross shelf valleys instead of a single valley were competing for discharge until early lowstand. Overall, the three identical experiments show a good reproducibility.

Model-prototype comparison

Our verification of model and prototype data (Tables 2.2 and 2.5) is shown in Fig. 2.11. The sea-level curves are included for reference (Fig. 2.11a). Figure 2.11b shows the mean rate of deposition on the coastal plain and shelf (i.e., basinward of the rivermouth). The dashed line indicates the fluvial supply rate from the drainage basin. Most apparent is the peak in the rate of sediment supply to the shelf edge during sea-level lowstand for model and prototype. The Basin Fill factor (Bf, Eq. 2.5) is shown in Fig. 2.11c. Bf is negative for a decrease in accommodation space (falling sea level) and positive for an increase. Bf-values for model and prototype show a similar trend.

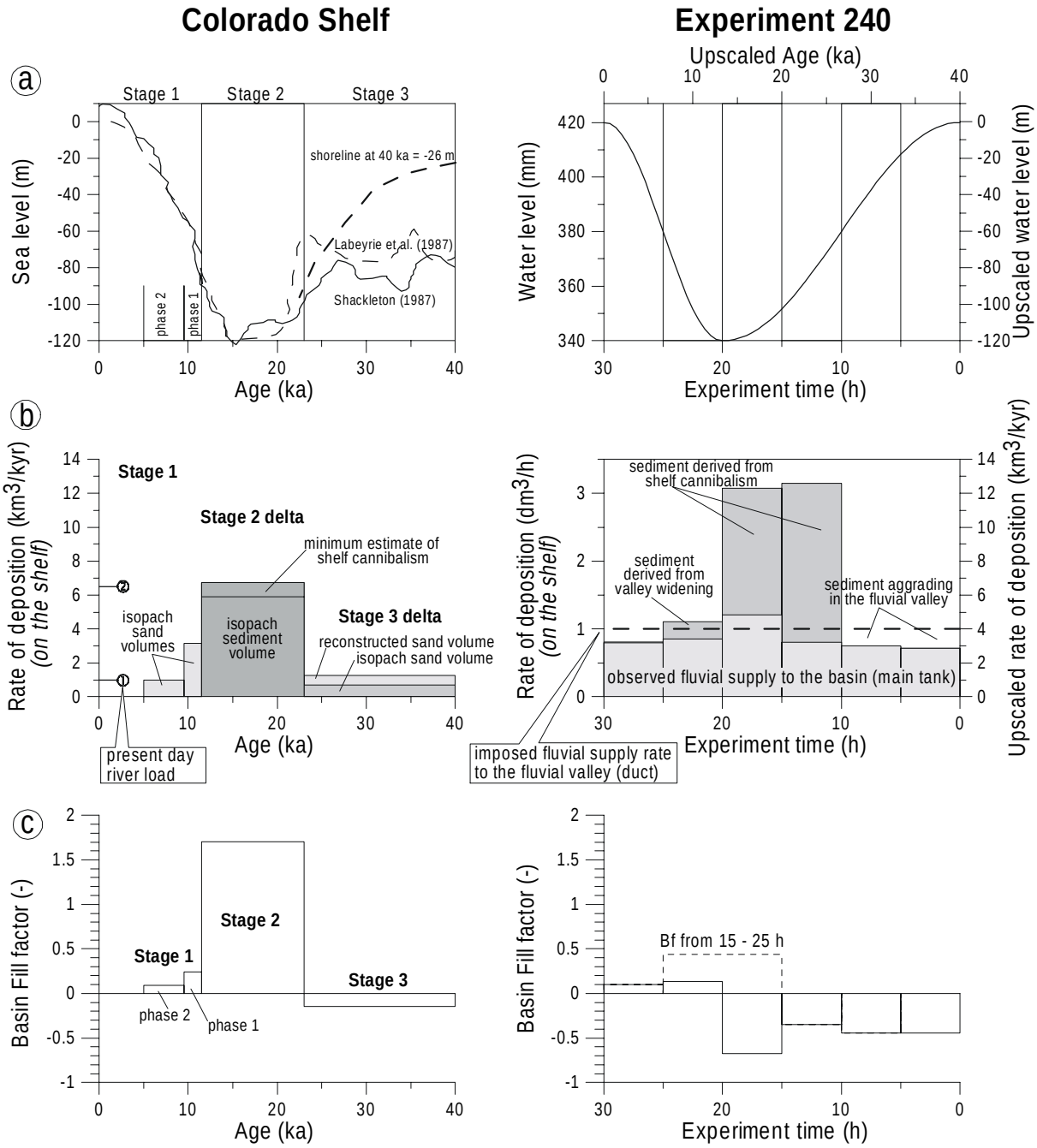

Fig. 2.11—Quantitative results of the Colorado river-shelf evolution (left) compared with the analogue flume experiment (right). The graphs show experimental values and upscaled values by applying the scaling ratios from Table 2.4. (a) Sea-level curves (b) Rate of deposition on the shelf and slope. The deposition rates of stage-3 and stage-1 are based on net sand volumes while the value of stage-2 is based on a total sediment volume. The numbers on the left indicate present-day fluvial bed-load supply rate (1) and total river load (2), both from Burgess & Hovius (1998). The dashed line in the right graph indicates the imposed fluvial-supply rate during the experiment. The grey shading represents the observed fluvial supply to the main tank. (c) Basin Fill factor calculated for model and prototype using Eq. 2.5.

Discussion

Regression

The highstand delta in our experiments develops very similarly to the stage-3 delta on the Colorado shelf. The sandy stage-3 delta suggests proximity of a high gradient fluvial source (Snow, 1998). During the late stage-3 regression, the Colorado River occupied two incised valleys that extended to near the shelf break (Anderson *et al*., 1996). These valleys incised up to 30 m depth and were a few kilometres wide. The structure map of the stage-2 sequence-boundary shows the entrenchment of the Colorado shelf during late stage-3 and stage-2 (Fig. 2.5). The map suggests that the three incised valleys originate from a single point source updip, which legitimates direct comparison with our single feeder model. Most lowstand river systems in the Gulf of Mexico, such as the Rio Grande, Trinity and Sabine rivers, bypassed their sediment to sub-marine canyon systems. In contrast, the fluvial supply dominated Brazos and Colorado rivers both constructed large, shelf-margin deltas. Mass wasting processes only played a role below the upper slope region (Rothwell *et al*., 1991). The Colorado example appears, therefore, suited for comparison with our experimental model that produces Gilbert-type shelf-margin deltas. We were able to reconstruct the net sand volumes of the stage-1 and -3 deltas. However, our estimated volume of the stage-2 shelf-margin delta consists of both mud and sand. We might assume the sand content of the Colorado lowstand delta-phase to be about 50% (cf. Morton & Price, 1987, their fig. 7).

Transgression

The Colorado shelf-margin delta was active throughout the late lowstand well into transgression, which resulted in complex backstepping patterns of aggradation and progradation that are related to 5th-order cycles (Anderson *et al*., 1996). Similarly, our model shows ongoing shelf-margin deposition during early rise followed by deposition of supply dominated backstepping lobes after the first significant rise in sea level. The model shows how shoreline retreat and upstream changes in supply results in a retrogradational valley fill sequence consisting of individual aggradational backstepping lobes that onlap the lowstand channel unconformity (sequence boundary). Similarly to the early transgressive phase in the experiment, the phase-1 delta is restricted to the topographic low created during the stage-2 sequence boundary formation. The phase-1 delta is lobate, fluvially dominated and fed by one trunk system: the ancient Colorado River. The alluvial stratigraphy of the Colorado River suggests that, after a phase of predominant terrace formation between 20ka and 14ka, the river experienced incision between 14 ka and 11 ka (Blum *et al*., 1994). Continuing river-profile adjustment on the inner shelf and coastal plain during early rise may have resulted in additional supply to the phase-1 transgressive delta. At the phase-1 to phase-2 transition, the delta stepped back from –45 to –26 m below present sea level. The phase-2 delta is related to the same, singular distributary system but is elongate and oriented parallel to the coast. It is therefore interpreted as a wave-dominated delta (Snow, 1998). The change in delta regime can be attributed to changes in coastal regime as the sea level rises over the shelf topography. On the other hand, declining supply may be responsible for the change from a fluvially dominated

into a wave-dominated delta system. Although the decrease in supply is believed to be related to a change towards drier climate (Toomey *et al*., 1994), our experimental results indicate that part of the decrease may have been caused by decreasing rates of river-valley cannibalism, which is known to have terminated after 11 ka (Blum *et al*., 1994).

Sea-level fall induced sediment supply

The experimental results show that stream profile adjustment to a sea-level cycle generates a significant peak of sediment supply to the shelf that contributes to the yield from the drainage basin (Fig. 2.10b). The supply rate returns to its initial level as the river valley attains its highstand equilibrium profile towards the end of the experiment. The reconstruction of the volume changes on the Colorado shelf (Fig. 2.11) reveals a comparable peak in supply rate during sea-level lowstand. Schumm (1993, his fig. 13a) found a similar base-level change related pattern of sediment delivery, where a rapid base-level lowering produces a major short term pulse of sediment and a slow base-level drop causes a minor pulse that is also delayed.

Blum & Törnqvist (2000) illustrate such sea-level-fall-induced shelf cannibalisation with the "vacuum cleaner" model. It is contrasted with the "conveyor belt" model, the latter being a metaphor for continuous supply from the drainage basin. The conveyor belt (sediment feeder) in our model supplied 30-40% of the total sediment volume to the lowstand deltas. The rest of the lowstand delta volume was derived from cannibalisation of the shelf and fluvial sediments that previously aggraded during falling and lowstand stage. Blum & Törnqvist (2000, their fig. 11b) estimated the contribution of shelf cannibalisation to the total sediment volume on the Colorado shelf as being one order of magnitude lower than the yield from the drainage basin. Our tentative reconstruction reveals a similar value: the minimum estimate of 9.5 km^3 for the shelf cannibalism during stage-2 contributed to 12% of the total stage-2 shelf-margin delta volume. However, when assuming that the shelf cannibalisation process mainly relocated the sand-rich top of the stage-3 delta, it may contribute to an even larger percentage of the total sand content of the stage-2 lowstand deposits. The total contribution of shelf cannibalism to the volume of the lowstand deposits might be even larger when assuming that the stage-5 sediments from the upper shelf have been eroded during late stage-3 and stage-2 (Rodriguez *et al*., 2000).

Remarks on analogue modelling and scaling

We have established the origin of increased sediment supply to the shelf during a sea-level cycle using laboratory experiments and discussed the results in the light of a case study on the east Texas shelf. By repeating the experiment twice it has been shown that analogue models produce reproducible and consistent results (Fig. 2.10). The experiments used for comparison with the ancient Colorado fluvial/deltaic system are part of a suite of experiments. Therefore, some parameters were generalised for simplification (e.g. shape of the eustatic cycle). This was done to make a general model for river-shelf evolution that was investigated for an array of sea-level cycles (Chapter 3). The rationale behind this is similar to that of Nordlund (1999), that general applicable models are more productive in the development and checking of geologic concepts than a calibration exercise for a single prototype.

We aimed to apply the best possible scaling strategy to be able to verify analogue models on a quantitative basis. The dimensional scaling that determines the relative sediment storage rooms and the scaling of the response time by a Basin Response factor are the most important constraints for modelling sedimentary system's response to allocyclic changes. The scaling factors for spatial dimensions and time are applied to achieve the scaling of the time-averaged sediment transport rates in the model with respect to the prototype (Eq. 2.3). The values of the upscaled time-averaged sediment transport rates of the model are comparable to prototype values (Table 2.4f, Fig. 2.11). However, a full match of the time-averaged sediment transport rate between prototype and the upscaled model is difficult, if not impossible, owing to differences in substrate erodability (depending on grain texture, bed fabric, cohesion, vegetation, non-uniformity of the substrate i.e., geology in Table 2.1) and the transport efficiency that is affected by bank stability, flow properties, etc. In Chapter 3 it is shown how the knickpoint migration rates (rate of headward erosion) in our flume compare with other flume studies (e.g. Brush & Wolman, 1960; Begin *et al*., 1981; Gardner, 1983; Lee & Hwang, 1994), and real world prototypes. The Appendix supports the idea that the model's transport efficiency is constant through time and in accordance with the applied grain size and hydraulic regime. The discrepancy between modelled sediment flux and real world value will increase with the number of tectonic, climate and sea-level cycles that is modelled. Hence, by keeping down the number of cycles that is modelled, we try to prevent progressive divergence of the model from the prototype evolution. In addition, we aimed for an optimum in similarity of the initial relief of model and prototype.

Finally, the Basin Fill factor (Eq. 2.5) is introduced as a geologic scaling "tool" for quantitative comparison of the evolution of sedimentary systems, be it real world or modelled. Although the development of deposition rates is similar for model and prototype, the trend in Bf values differs significantly especially for stage-2. As illustrated by the dashed line in Fig. 2.11c the discrepancy is partly caused by the applied 5 hour sampling interval during the experiment. In retrospect it would be better to base the sampling interval of the model on the available time constraints of the prototype. If such boundaries are not known in advance, it would be recommendable to sample at the smallest possible interval. Overall, we think that the presented model run is not the best representation for the supply dominated (nearly overfilled) Colorado shelf. The contribution of shelf cannibalism to the volume of the lowstand delta in the model is too large compared to the prototype's. In contrast to the incisions on the Colorado shelf that become shallower towards the shelf edge, the shelf canyons in our model becomes deeper and cut down into the shelf edge. This was a simple consequence of sea level falling too far below the shelf edge in our model. The observed difference marks the importance of the initial shelf geometry; a constant gradient was applied in the model while the gradient of the Colorado shelf probably increased towards the shelf edge, like the present day situation. The data from the Colorado shelf suggest that the increase in sediment supply to the shelf during lowstand was predominantly caused by an increased river load. An increase in supply from the Colorado drainage basin may well relate to the wet climate conditions during the Late Pleistocene and early Holocene (Toomey *et al*., 1994; Metcalfe *et al*., 2000). However, our experiments help to demonstrate that the sea-level fall liberates

significant amounts of fluvial, coastal plain and shelfal deposits that must be accounted for when studying the mass balance of a sedimentary system.

A next logical research step would be to expand our “sea-level” model with one that incorporates supply changes and to investigate the effect of temporary sediment storage in the fluvial valley. We did a few pilot studies in which the sediment supply was increased with respect to the value applied here. The effect was that the extra supply was buffered within the fluvial valley system. Imposing higher supply rates would require higher discharges, which clashes with our hydraulic scaling constraints in the present set-up. For the near future we aim to face these problems by combining numerical and analogue modelling efforts. As shown here, the analogue model has to deal with complex scaling issues because of its distorted scaling. Its strong points are that it generates quantitative data of a small sedimentary system that includes parts of the complexity of nature. Numerical studies on the other hand have to deal less with scaling issues since they can be designed on any scale. Once developed, they can produce statistically significant amounts of data for systematic analysis of a sedimentary system. The strength of analogue-numerical model interactions is that the quantitative analogue experiments (known input, data of behaviour) can act as an intermediate between numerical studies and the prototype they share.

Conclusions

This paper dealt with scaling issues for physical models of landscape evolution and stratigraphy. The most essential element in long-term landscape evolution models is the response of the sedimentary system to base-level change invoked by tectonic tilting, sea-level and climate change. We scaled a prototype landscape to the size of a flume tank by:

1) maintaining realistic hydraulic conditions in the model to maintain constancy in bed-load transport;
2) honouring the relative sizes of each of the components of the prototype sedimentary system by maintaining geometric similarity;
3) honouring the ratio of the period of change over the response time of the prototype sedimentary system, which was accounted for by a Basin Response factor, Br;
4) applying the scaling factors for spatial dimensions and time for quantitative comparison of the time-averaged sediment transport rates in the model and prototype;
5) checking the relationship between sedimentation rate and the rate of change in accommodation space in model and prototype, which was done by use of a Basin Fill factor, Bf.

Both qualitative and quantitative aspects of analogue flume models prove to be important for our understanding of the 3D complexity of sedimentary systems. A comparison with the Late Quaternary Colorado shelf system revealed that sea-level fall can cause a significant increase in sand supply to the shelf-margin delta. For reconstruction of climate-forced increase in sediment yield, these numbers are important.

Our analogue studies of the sedimentary system demonstrate a strong need for volumetric data of real world systems. Isopach maps with ages of bounding surfaces are required to facilitate calibration and validation of laboratory models. For landscape studies, a holistic approach is most important, where research in the various parts of the source (drainage basin) as well as the sink (depositional basin) can not be seen as stand alone studies. Very interesting model-prototype comparisons can be expected only if stratigraphic studies of shelf and alluvial deposits have been tied together.

Acknowledgements

This research was funded by Shell International Exploration and Production, Rijswijk, The Netherlands. We thank R. G. de Jongh and G.W.M. de Ruiter for initiating the scientific collaboration with Shell. We acknowledge the permission of Shell to publish this paper. We are grateful to S. Hardy, J. Peakall and J.H. van den Berg for giving their thoughts on the scaling issues. At Utrecht University we acknowledge P.L. de Boer and J. Cleveringa for critical reading of the manuscript. We thank A.C. van der Gon Netcher, J.H. Bliek, P. Anten and M. Reith for technical support.

Chapter 3

Fluvial response to sea-level changes: a quantitative, analogue experimental approach

Max W.I.M. van Heijst & George Postma

Faculty of Earth Sciences, Utrecht University, PO Box 80021, 3508 TA, Utrecht, The Netherlands.

Abstract

Quantitative relationships of fluvial response to allocyclic change are crucial for further progress in understanding the stratigraphic record in terms of processes that have dominant control on landscape evolution. For instance, without quantitative insight into the time lag that is known to exist between a fall in relative sea level and the fluvial response, there is no way to relate fluvial stratigraphy to sea level. It is difficult to put firm constraints on these time-lag relationships on the basis of empirical studies. Therefore we have quantified time-averaged erosion and deposition in the fluvial and offshore realms in response to sea-level change by means of analogue modelling in 4 x 8 m flume-tank model. Sea level was the only independent variable, while other conditions like sediment supply, discharge, and initial geometry were kept constant over 18 experiments.

The experimental results support the idea that neither fall nor rise in sea level does affect the upstream fluvial system instantaneously. An important cause for the delayed fluvial response is that a certain amount of time is required to connect initial incisions on the just emerged shelf (shelf canyons) with the fluvial valley. Base-profile lowering in the fluvial system starts only after the connection of an active shelf canyon with the fluvial valley; until that moment the profile remains steady. We quantified the process of connection through introducing the quantity “connection rate”. The connection rate has a strong bearing on fluvial and shelfal stratigraphy, since it controls: 1) the amount of fluvial aggradation during the sea-level fall; 2) the total sediment volume that bypasses the shelf edge; 3) the percentage of fluvial relative to shelf sediment in the lowstand delta ; 4) the volume of the transgressive systems tract and 5) the amount of diachroneity along the sequence boundary. The experiments demonstrate that the sequence-stratigraphic concept is difficult to apply to continental successions, even when these successions have been deposited within the reach of the influence of sea level.

(Submitted for publication in Basin Research)

Introduction

The original sequence-stratigraphic concept that relates basin-margin architecture to eustatic sea-level changes (Vail *et al*., 1977) was primarily tested for shelf-slope settings and did not include the fluvial system. However, an increasing number of high-resolution shelf studies (e.g. Suter & Berryhill, 1985; Bartek *et al*., 1990; Coleman & Roberts, 1990) have led to the understanding that rivers do play an important role in sediment delivery to the shelf, especially during lowstands. Posamentier & Vail (1988) included some basic constraints on fluvial response to eustatic fluctuations within their sequence-stratigraphic framework. The recognition that the fluvial response to sea-level changes would have significant implications for sediment delivery and depositional geometries on the shelf and slope (Butcher, 1990; Wescott, 1993) explains the increasing interest into the timing of shelfal and adjacent fluvial deposition in relation to the sea-level curve (i.e., attributing systems tracts to alluvial deposits, e.g. Shanley & McCabe, 1991). The special issue on incised valley systems (Zaitlin *et al*., 1994) expressed a strong demand for a consistent sequence-stratigraphic concept for the fluvial domain. Several years later, Ethridge *et al.* (1998) make a strong case not to define systems tracts for the eustatically unaffected, and tectonically and climatically controlled upstream fluvial reach. The problem to which point in the fluvial system the sequence-stratigraphic concepts can still be applied or not is a complex one, so that the question remains how much of the concept of sequence stratigraphy can be applied to continental strata that are beyond the direct influence of sea level (Shanley & McCabe, 1994). The heart of the problem probably lies in our limited understanding of the processes that control base-profile adjustments. The base profile is usually defined as the ideal graded profile at a specific moment relative to a chrono-stratigraphic datum (Quirk, 1996). A graded river (e.g. Mackin, 1948) represents morphological stability (Ethridge *et al*., 1998), where the sediment delivery to the coast equals the supply from the drainage basin. The base profile grades towards base level, which is equal to sea level in coastal regions, although we recognise that rivers can locally erode below sea level (Salter, 1993; Schumm, 1993; Best & Ashworth, 1997). In any case, the position of the base profile is very dynamic: while the river responds to a sea-level change, the base profile changes continuously (Quirk, 1996).

Base-profile adjustment forced by a fall in sea level will start at the coastline and move progressively landward by headward erosion resulting in knickpoint migration (Salter, 1993; Leeder & Stewart, 1996; Quirk, 1996). The adjustment of the valley profile's gradient proceeds by migration of one single knickpoint or by an array of local knickpoints (Gardner, 1983). The point of intersection of the old and new base profile, i.e., the most landward knickpoint, would put an upward limit on the stratigraphic effect of the sea-level fall (cf. Posamentier & Allen, 1993, their fig. 6). Hence, a sea-level fall will not immediately rejuvenate the entire river profile (Leopold & Bull, 1979; Schumm & Ethridge, 1994). Also, slow rates of sea-level fall can be accommodated by a change of channel sinuosity without causing an instantaneous change of the valley-floor gradient (Schumm, 1993).

Table 3.1. Quaternary river-shelf characteristics (extended from Blum & Törnqvist, 2000).

River	Drainage basin (km^2)	river gradient	shelf gradient	Lowstand river extension (km)	Upstream limit of influence from last glacial sea-level lowstand with respect to the present shoreline (km)
Obitsu River	274	0.002	0.006	30	15 (Saito, 1995)
Hawkesbury River	22000	0.0005	0.06	40	140 (Nichol *et al*., 1997)
Colorado (TX)	110000	0.0004	0.0008	100	90 (Blum & Valastro, 1994)
Brazos	118000	0.0002	0.0003	100	70 (Anderson *et al*., 1996)
Mississippi	3344000	0.00002	0.00025	150	300-400 (Saucier, 1996) 1000 (Fisk, 1944)

How far upstream will a sea-level fall be noticed? Paola (1991) regards the fluvial system as a low pass filter for sea-level fluctuations and defines propagation distance of base-level-fall-induced erosion as being proportional to the square root of the period of variation (e.g. a 100 kyr base-level cycle will affect approximately 100 km of fluvial profile). It depends on several factors, how far upstream a river will be rejuvenated. Among these factors, the magnitude and rate of sea-level fall, the river gradient and the supply rate from the catchment area are the most important (Schumm, 1993). The effect of a sea-level fall on fluvial stratigraphy fades upstream in favour of climate and tectonic influence, as well as autocyclic changes such as sediment flux variations and changes in fluvial discharge in the upstream direction (Posamentier & James, 1993). A drop in sea level is felt only several kilometres upstream for small, high-gradient rivers, whereas large, low-gradient rivers with larger drainage basins seem to adjust their profiles 100's of kilometres upstream. For instance, in response to the last glaciation the small Obitsu River incised about 15 km upstream (Saito, 1995), the Colorado River nearly 100 km (Blum, 1993), and the Mississippi 300 km (Saucier, 1996) and possibly even up to 1000 km (Fisk, 1944); see Table 3.1.

The morphologic concept of river-profile adjustment by headward erosion thus implies a time lag between the onset of a sea-level fall and the upstream adjustment of the river's base profile (Butcher, 1990). Our understanding of the time lag is poor (Shanley & McCabe, 1994; Quirk, 1996; Dalrymple *et al*., 1998). The time lag may cause that erosional and depositional cycles in the coastal zone are out-of-phase with the sea-level cycles (Ethridge *et al*., 1998), which illustrates a major difficulty in the application of sequence-stratigraphic concepts to fluvial strata. Application of the concept is also much hindered by the problem of convergence (Schumm, 1991): different allocyclic (climate, tectonics, eustasy) causes and different processes can produce similar results (stratigraphy). For example, any fall in base profile will cause an erosive surface, irrespective whether this bounding surface relates to a fall in sea-level, tectonism or climate change affecting the ratio of discharge over sediment load in the river (Shanley & McCabe, 1994; Quirk, 1996). Reviews on hydrodynamics (Thorne, 1994) and field studies (e.g. Blum & Price, 1998; Törnqvist, 1998) refer to this complex response of the fluvial system. So, even if the coastal and inland fluvial systems seem to be in-phase, it may well be because of different controls involved

(Ethridge *et al*., 1998). Hence, the complexity of the fluvial system does not allow an easy quantification of stratigraphy-controlling parameters through the examination of real-world examples. It probably explains the relative underdevelopment of sequence-stratigraphic models for the alluvial domain with respect to their marine counterparts (Shanley & McCabe, 1998). Only through numerical and physical experimental studies we may be able to resolve some of fluvial complexity by carefully testing the impact of each parameter on stratigraphy (Ethridge *et al*., 1998; Marriott, 1999; Blum & Törnqvist, 2000).

We use an analogue flume model to investigate the response of both the fluvial and the shelfal domain to various rates of sea-level change. The advantage of the analogue approach is that, in contrast to theoretical models (e.g. Burgess & Allen, 1996), the process of knickpoint migration is intrinsically embedded in the flume experiments. Sea-level change is the isolated variable in our study, while initial topography, discharge, sediment supply and tectonic subsidence were held constant. The methodology has been inspired by the analogue experiments of Wood *et al.* (1993) and Koss *et al*. (1994), who produced mainly qualitative results. By making use of high-resolution surface mapping techniques we generate quantitative data on rates of erosion, deposition and knickpoint migration for a wide range of experimental sea-level curves.

Table 3.2. Facts on the set-up and the experimental method.

Experimental set-up	**Properties**
Dimensions	Main tank: 4 x 4 x 1 m, table with shelf-slope configuration 3x3.4 m Fluvial valley, Duct: 4 x 0.5 x 0.11 m
Co-ordinate system	x, y and z axes with values in mm (Fig. 3.1)
Measurements	Main tank: automated bed profiler, accuracy of x, y and z data within 0.4 mm. Applied data point spacing 20 mm. Fluvial valley: manual stream profile measurement with rulers spaced 100 mm apart (accuracy 2 mm).
Discharge	400 dm^3/h
Sediment supply	1 dm^3/h (~1.85 kg of dry sediment per hour)
Sediment properties	Unimodal medium sand used as uniform substrate (bed material) and as supply for the fluvial valley. D_{50}; median grain diameter = 250 μm D_{90}; ninety percentile grain diameter = 700 μm And 40 μm < D < 1000 μm to avoid cohesion problems with clays and to exclude partitional sortening effects of large grains.
Hydraulic conditions	h = 6-10 mm (channel depth) $\overline{u}$ = 0.18 m/s (average flow velocity in the fluvial valley) Fr = 0.77 (Froude number in the fluvial valley) Re = 886 (Reynolds number in the fluvial valley)
Sea level (single variable)	Highstand: z=420 mm Lowstand: z=340 mm or z=260 mm (depending on amplitude)
Length of stream profile (from head to shoreline)	Highstand: 4.7 ± 0.2 m (variation induced by highstand delta size) Lowstand: 6.0 ± 0.2 m (variation induced by amplitude and lowstand delta size)

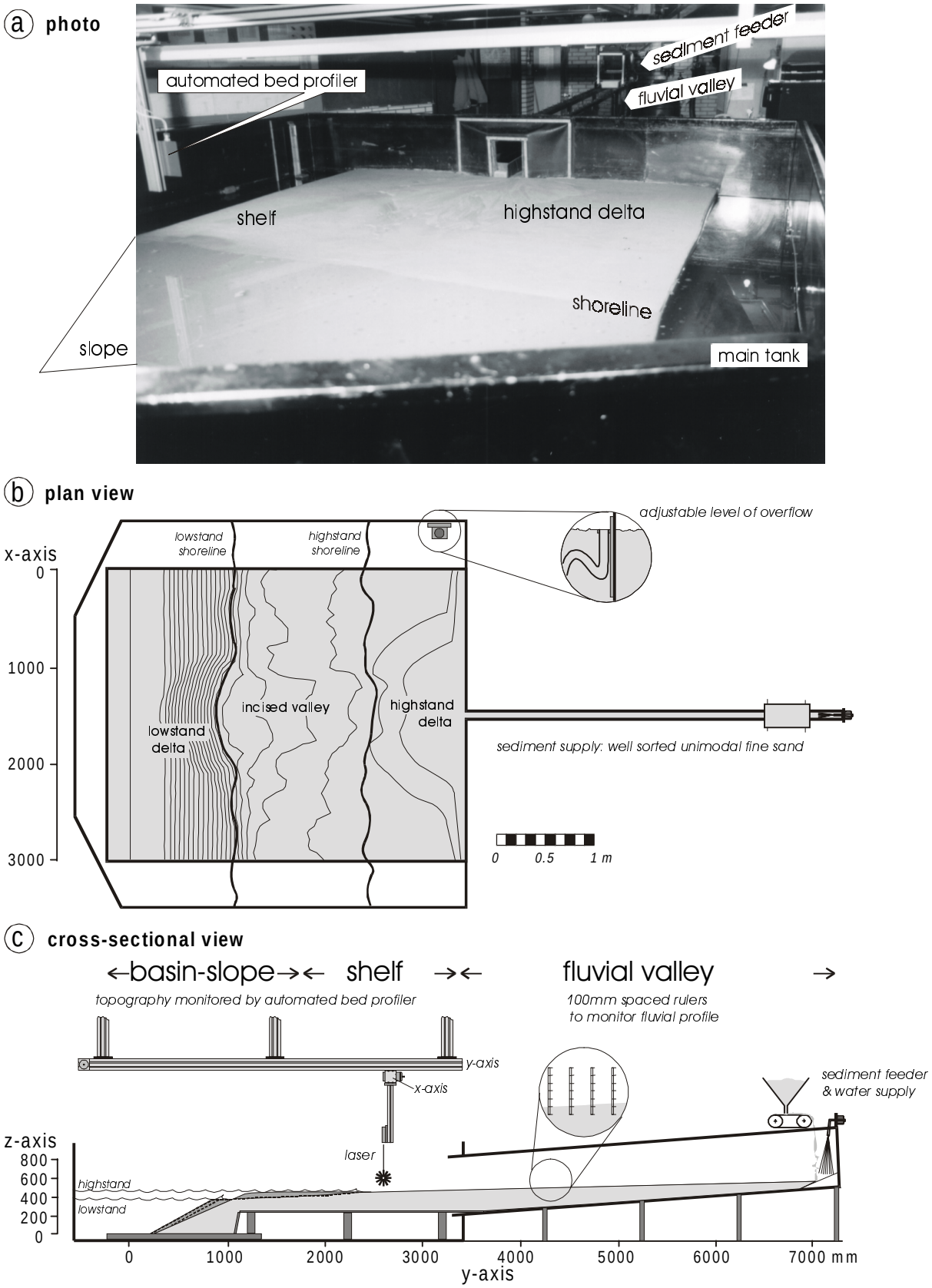

Fig. 3.1—(a) Experimental set-up consisting of a water and sediment filled basin margin (main tank) and a fluvial valley (rectangular duct with the sediment feeder at its up-slope end). An automatic bed profiler (laser) measures the topography of the sedimentary basin. (b) Schematic plan view and (c) cross-section of the experimental set-up showing the x, y and z-axis of the bed profiler that is used as the co-ordinate system.

Methodology

Experiment facility

The set-up consists of an experimental tank of 4 x 4 x 1 m that is connected with a rectangular duct (the fluvial valley) of 4 x 0.11 x 0.5 m (Fig. 3.1, Table 3.2). The tank contains a sediment table with sidewalls that support a sand sheet, which forms the coastal plain, shelf, slope and basin configuration (Table 3.3). A water tap with flow meter provides discharge. A sediment feeder with adjustable conveyor-belt speed controls the sediment supply rate. Both are located at the upstream end of the fluvial valley and act as a surrogate for the drainage basin. The applied sediment is uniform, medium sand (Table 3.2) that is supplied by the feeder and is used as substrate. An adjustable level of overflow controls the water level (sea level) in the main tank. An automatic positioning system, with x and y-axes is attached to the ceiling above the main tank. It carries a Dynavision SPR-2 laser sensor to collect altitude data (z-axis) of the coastal plain-shelf-slope-basin topography. The data are measured according to a 20 x 20-mm grid and has an accuracy of 0.4 mm for all three dimensions. Changes of the fluvial valley's stream profile are measured by means of rulers attached to the valleys glass wall at 10-cm spacing.

Table 3.3. Initial morphology of experiments after the 15 hour preparation run.

Initial model morphology	Inclination ($\Delta y/\Delta x$)	y-co-ordinates (mm)	z-co-ordinates (mm)
Basin	0	0-300	0-10
Slope & shelf edge	0.42	300-1200	10-385
Shelf	0.03	1200-2400	385-420
Coastal plain	0.02	2400-3400	420-440
Fluvial Valley	0.025	3400-7000	440-530

Scaling real-world to experimental time-space dimensions

The relative dimensions of fluvial-valley length versus shelf width and vertical exaggeration is scaled following Hook's (1968) similarity of process approach. This is the only possible way to model landscape evolution, since prototype dimensions are too large to keep up with conventional scale models (Bruun, 1966) and Froude scaling (e.g. Ashworth *et al.*, 1994). We added to the qualitative aspects of analogue modelling by quantifying the time-averaged sediment flux (Q_s) from river to basin over sufficiently long time spans (i.e., graded time of Schumm & Lichty, 1965). However, such quantitative treatment of analogue model results demands an alternative scaling strategy as proposed in Chapter 2. Here we briefly summarise the relevant scaling aspects for analogue experimental studies of fluvial response to sea-level change.

The dimensions in our flume model are designed to represent a common conceptual Quaternary passive margin setting. We have chosen a shelf gradient that is just steeper than the equilibrium profile of the downstream reach of the fluvial valley (see Table 3.3), since most recent natural fluvial-shelf systems do so (e.g. Miall, 1991; Nummedal *et al.*, 1993, see Table 3.1). All gradients of the model are scaled

proportionally to the gradient of the stable equilibrium profile of the fluvial valley, which in turn depended on the bed-load transport of the applied sediment and discharge (Table 3.2). The equilibrium profile of the model's fluvial valley (duct) is 0.025, which is 10-100 times steeper than that of natural rivers (Table 3.1). It is important to note that the coastal plain is chosen less steep than the fluvial and shelf profile which is common for rivers in a passive margin setting (Butcher, 1990; Nummedal *et al.*, 1993). The water-level variations are designed to model glacio-eustatic cycles composed of a slow fall that forces the shoreline below the shelfbreak (cf. Talling, 1998) followed by a rapid rise.

Scaling by similarity of process means that hydraulic scaling conditions are relaxed. However, we kept realistic Froude numbers in the fluvial valley (lower flow regime, see Table 3.2) to avoid bedform formation and, yet, to ensure a constant bed-load transport rate. The fraction smaller than 40 μm was removed to avoid unwanted effects caused by cohesion. All grains larger than 1000 μm were sieved out to avoid any large ratio of particle size over water depth that can lead to partial sorting and bed armouring.

Equilibrium time

In order to investigate the time-lag relationships between sea-level change and fluvial response systematically, the response time of the sedimentary system must be taken into account. The response time compares to the equilibrium time T_{eq} that was defined by Paola *et al.* (1992). They stressed the importance of the ratio between the period of change of a variable and the system's equilibrium time and we agree! For a proper time scaling, we maintain similar values for the ratio of the equilibrium time, T_{eq} over the duration of one cycle of sea-level change, T in both model and prototype by defining a Basin Response factor (Br):

$$Br = \frac{T_{(rw)}}{T_{eq(rw)}} = \frac{T_{(\exp)}}{T_{eq(\exp)}} \qquad [-] \qquad (3.1)$$

To apply above scaling condition we need to establish the equilibrium time of both model and real-world river-shelf systems. The observed equilibrium time is defined as the time that is needed for the fluvial system to regain its equilibrium base profile from the moment that it is disturbed by sea-level or discharge changes. The establishment of an initial equilibrium profile at the beginning of each experiment took 6-10 hours keeping discharge and supply at default values (Table 3.2) and with sea level at highstand.

A few empirical formulae exist to estimate the equilibrium time (T_{eq}) for sedimentary systems. We applied three examples to verify our model's T_{eq}. The predicted values are displayed in Table 3.4. The significance of a response time for a graded river to a downstream change in base level was already recognised by De Vries (1975) who proposed:

$$T_{eq50} = \frac{3 \cdot b \cdot S \cdot (\tfrac{1}{2} L)^2}{\alpha \cdot Q_s} \qquad [T] \quad \textit{if } L > 3h/S \textit{ (=length of backwater curve)} \qquad (3.2)$$

T_{eq50} represents the time required to accommodate 50% of the base-level change and L is the length of the river affected by the change. S is the bed slope; b and h are river width and depth respectively. Q_s is the volumetric bulk sediment transport for the river segment under consideration. We applied the sediment transport formula of Engelmund & Hansen (1967) and found a best fit for $\alpha = 4.6$ for a data set of calibration experiments of the 4 m fluvial valley (see Appendix). Substitution of α in the De Vries (1975) equation yields equilibrium times between 7 and 16 hours, so a little longer than the observed values.

In a review on equilibrium time scales in geomorphology, Howard (1982) proposed:

$$T_{eq} = \frac{L^2 \cdot S}{4 \cdot q_s} \qquad [T] \qquad (3.3)$$

Where q_s is the sediment transport rate per unit width. This formula estimates long equilibrium times (10-20 hours) relative to our observations.

Paola *et al.* (1992) determines the equilibrium time for basins to reach equilibrium by:

$$T_{eq} = \frac{L^2}{k} \qquad [T] \qquad (3.4)$$

The diffusivity constant *k* was derived by Paola *et al*. (1992) from first physical principles, using the bed-load transport formula of Meyer-Peter & Müller (1948) to describe the volumetric sediment transport rate:

$$k = \frac{-8 q_w \cdot A \cdot \sqrt{c_f}}{C_o(s-1)} \qquad [L^2/T] \qquad (3.5)$$

Where q_w is the discharge per unit width (m^2/s) and A is a constant for riverbank stability. C_f is the dimensionless drag coefficient, C_o the sediment concentration of the bed and s the specific density (ρ_s/ρ_w). According to the equation, diffusivity depends mainly on discharge and the constant A for riverbank stability. Parker (1978) found a riverbank stability constant A = 1 for the meandering case and A = 0.15 for the braided case. Similarly we can assume A = 1 for our fluvial valley that is contained between glass walls. The average value of A must be lower than unity downstream the confined fluvial valley, because the stream diverges owing to decrease in bank stability. Therefore, we applied an average value of A=0.8, which yields values for T_{eq} that compare well with the observations (Table 3.4). Hence, we find a diffusivity of $1.17q_w$ for the experiments. Based on empirical data Paola *et al*. (1992) used $0.1q_w$, which furthermore suggest that the real-time values for sediment transport rates in our flume diverge about a factor ten from these real-world values.

All formulae predict T_{eq} within the range of observations for the 4 m fluvial valley length (Table 3.4). However, for lowstand conditions (L~6m) the estimates lie further apart. During the experiments we observed that the gradient and the actual

sediment-supply rate increased as an experiment progressed towards lowstand. This is not accounted for in the calculations. Therefore, the calculated values for T_{eq} might be overestimated for L > 5m conditions (Table 3.4).

Based on observations and above calculations we assume the model's T_{eq}~10 hours and have set out a suite of experiments that explores the fluvial response to sea-level changes systematically for 0.4<Br<4 (Fig. 3.2). The Br>1 condition (i.e., $T>T_{eq}$) that we have chosen for the majority of our experiments (Table 3.5) compares nicely with moderately-sized Quaternary river systems issuing on 100 km wide shelf margins during the Quaternary.

Table 3.4. Estimates of the equilibrium time, T_{eq} of the model. Note that L depends on the shoreline position and progradation.

L, Length (m)	T_{eq} (h) (De Vries, 1975) Eq. 3.2 with α=4.6	T_{eq} (h) (Howard, 1982) Eq. 3.3	T_{eq} (h) (Paola *et al.*, 1992) Eq. 3.4&3.5 with A=0.8	T_{eq} (h) Observed
4 (~fluvial valley)	7	11	5	6-10
5	11	17	7	~10
6 (~shelf exposed)	16	24	10	~12

Applied values: channel width: b=0.11 m, h=0.0056 m, S=0.025, Q_w=0.4 m^3/h, Q_s=0.001 m^3/h, Cf=0.027, Co=0.68, and ρ=1000 kg/m^3 and ρ_s=2650 kg/m^3.

Experimental procedure

All experiments started with an identical coastal plain-shelf-slope topography (Table 3.3). The sediment in the fluvial valley was levelled according to an inclined marker line on the valley wall prior to each experiment. The sidewalls of the table in the main tank were used as standard levels to assure similar sediment-surface height before the start of each experiment. The sand bed was submerged two times to improve its packing. The water level was raised to highstand level at the beginning of each experiment. A 15-hour preparation run with sea level held at highstand level and sediment supply and discharge at their default values preceded each experiment in order to establish a stable fluvial profile as uniform starting condition. Thus, we started each experiment with a graded stream where the sediment supply rate at the valley outlet is constant and equals the constant supply rate of the feeder at its upstream end. Discharge and rate of sediment supply were monitored throughout the experiments. Table 3.5 gives an overview of the 18 experiments. Sea-level variations consisted of 160 or 80 mm amplitude sinusoidal curves (Fig. 3.2). Four sea-level curves have been repeated two or three times to test the reproducibility of the analogue-model results.

The subsequent morphological changes were monitored, photographed and recorded on time-lapse video. The fluvial stream profile was measured every hour and twice hourly for short experiments. The topography of the entire sand bed in the main tank was scanned every 5 hours, and more frequently for very short experiments (Table 3.5). Laser scans were done subaerially. Therefore, prior to each scan the tank was drained slowly to avoid disturbances in the grain fabric. Water level, discharge and sediment supply were checked before the experiment was resumed.

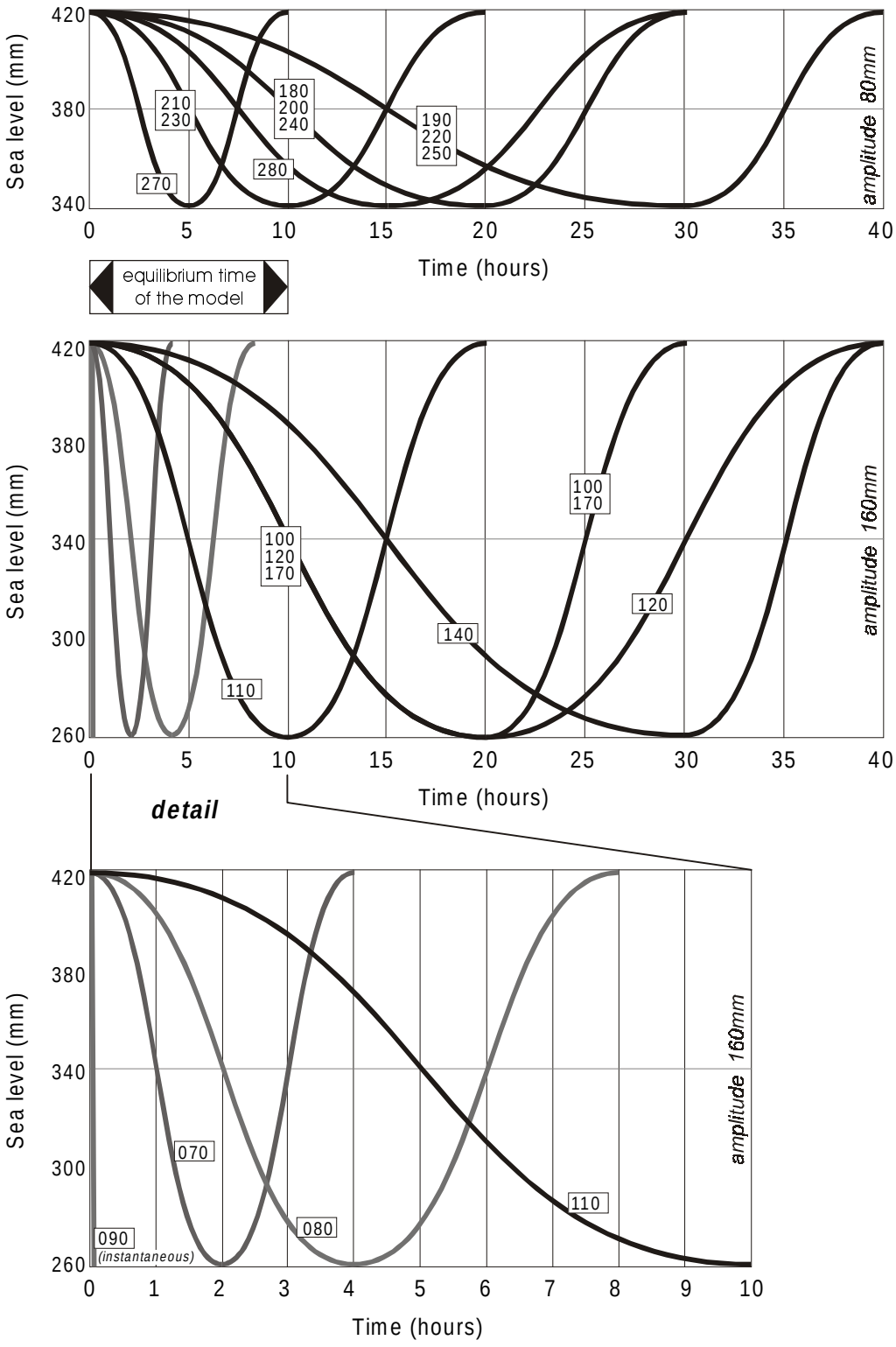

Fig. 3.2—Applied sinusoidal sea-level curves with 80 mm and 160 mm amplitude. The labels indicate experiment numbers corresponding to Table 3.5. The majority of the experimental sea-level cycles took two to four times longer than the model's equilibrium time of approximately ten hours.

Table 3.5. Overview of the experiments.

Experiment number (Fig. 3.2)	**Sea-level amplitude** (mm)	**Duration of sea-level fall** (h)	**Rate of sea-level fall** (mm/h)	**Duration of sea-level rise** (h)	**Rate of sea-level rise** (mm/h)	**Time between scans** (h)
90	160	0,1	1000	0	-	5
70	160	2	80	2	80	1
80	160	4	40	4	40	2
100*	160	20	8	10	16	5
110*	160	10	16	10	16	5
120*	160	20	8	20	8	5
140*	160	30	5,33	10	16	5
170	160	20	8	10	16	5
180	80	20	4	10	8	5
190	80	30	2,67	10	8	5
200	80	20	4	10	8	5
210	80	10	8	10	8	5
220	80	30	2,67	10	8	5
230	80	10	8	10	8	5
240	80	20	4	10	8	5
250	80	30	2,67	10	8	5
270	80	5	16	5	16	2.5
280	80	15	5,33	15	5,33	5

** Fluvial valley width is 220 mm instead of the 110 mm during other experiments*

Results

In each experiment, a stable fluvial profile was established between the 6th and 10th hour of the 15 hour preparation run. The equilibrium slope of the fluvial valley varied between 0.024 and 0.026. Meanwhile, a highstand delta developed on the coastal plain. Although the highstand delta deposits are very thin (~ 1 cm), they caused the coastal plain to be less steep than the fluvial valley and the shelf (Table 3.3). This section focuses on the results of two extremes of the 80 mm amplitude experiments; a fast rate of sea-level fall and a very slow rate of sea-level fall relative to the model's equilibrium time. The comparison is based on two experiments for each extreme, both showing good mutual reproducibility. After the comparison, the quantitative data of the full range of experiments are presented.

>>>The following pages show the results of a comparison between an experiment with a fast rate of sea-level fall and one with a slow rate of sea-level fall.

Figures 3.3 and 3.4 show block diagrams that depict the evolution of the coastal plain and shelf.

Figure 3.5 shows a medial cross-section of experiment 210 with a fast rate of sea-level fall. The stages a to d correspond to Fig. 3.3. The successive diagrams illustrate the balance between the deposition of newly introduced sediment from the feeder and redeposited sediment from cannibalisation of the shelf and fluvial valley. The successive profiles show the delay in upstream propagation of the headward erosion in the fluvial domain. The knickpoint reaches the fluvial valley at lowstand (10 h) and the sea-level-fall-induced erosion continues until late rise.

Figure 3.6 shows a medial cross-section of experiment 250 with a slow sea-level fall. The stages a to d correspond to Fig. 3.4. The experiment shows significant fluvial aggradation during stages a and b. Erosion on the shelf and within the fluvial valley resulting from a slow sea-level fall is much more in phase than for the fast-fall experiment (cf. Fig. 3.5). The knickpoint reaches the fluvial valley at early lowstand (18 h) and fluvial erosion ceases at early rise.

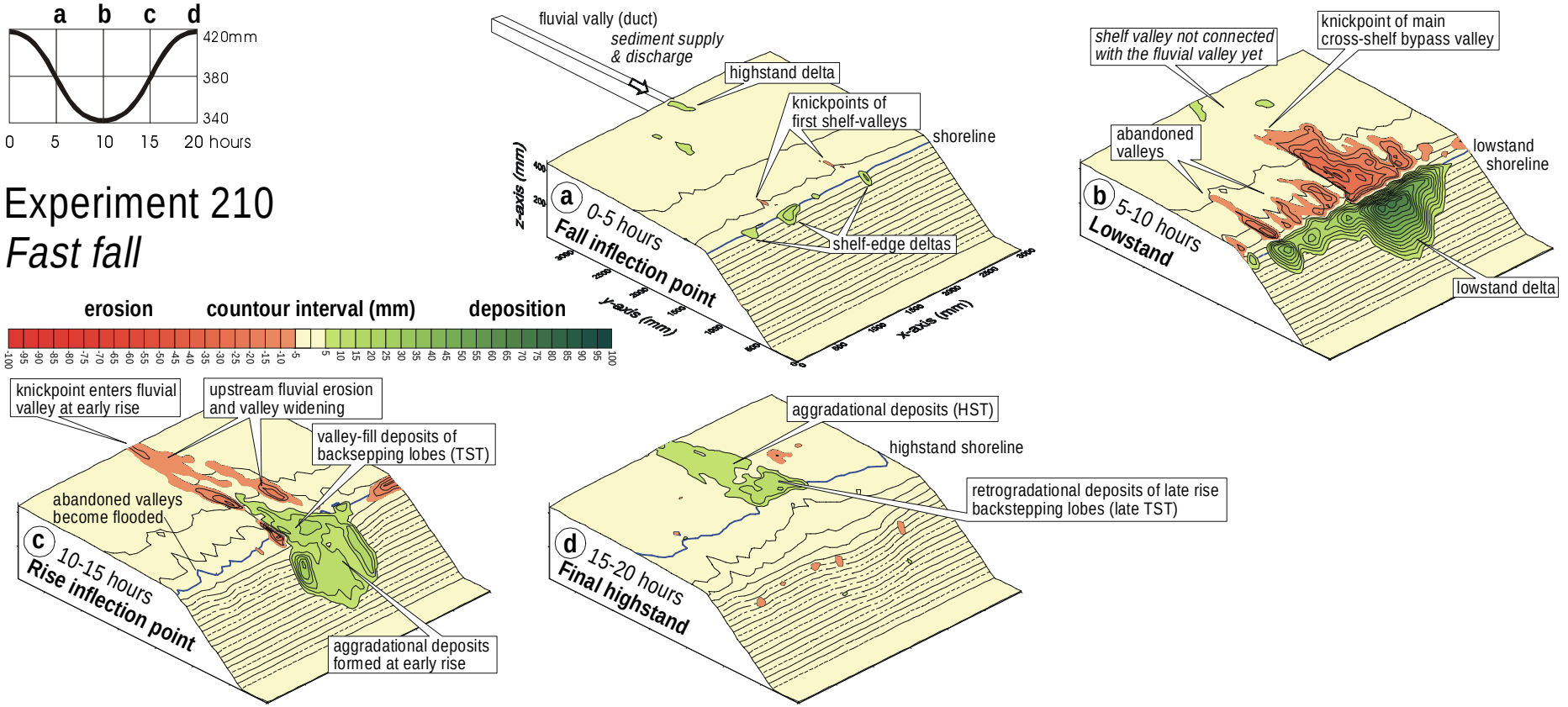

Fig. 3.3—Block diagrams illustrating coastal plain and shelf evolution during experiment 210 with a fast sea-level fall. The subsequent scans depict current topography as well as changes (contours) with respect to the previous topography for 5 hour time steps. The first block diagram shows the topography at t=5 hours and the volume changes that occurred between t=0 and t=5 hours. Erosion (red) and deposition (green) have been plotted with 5-mm contour intervals.

>>> next page: Fig. 3.4—Similar block diagrams illustrating coastal plain and shelf evolution during experiment 250 with a slow sea-level fall.

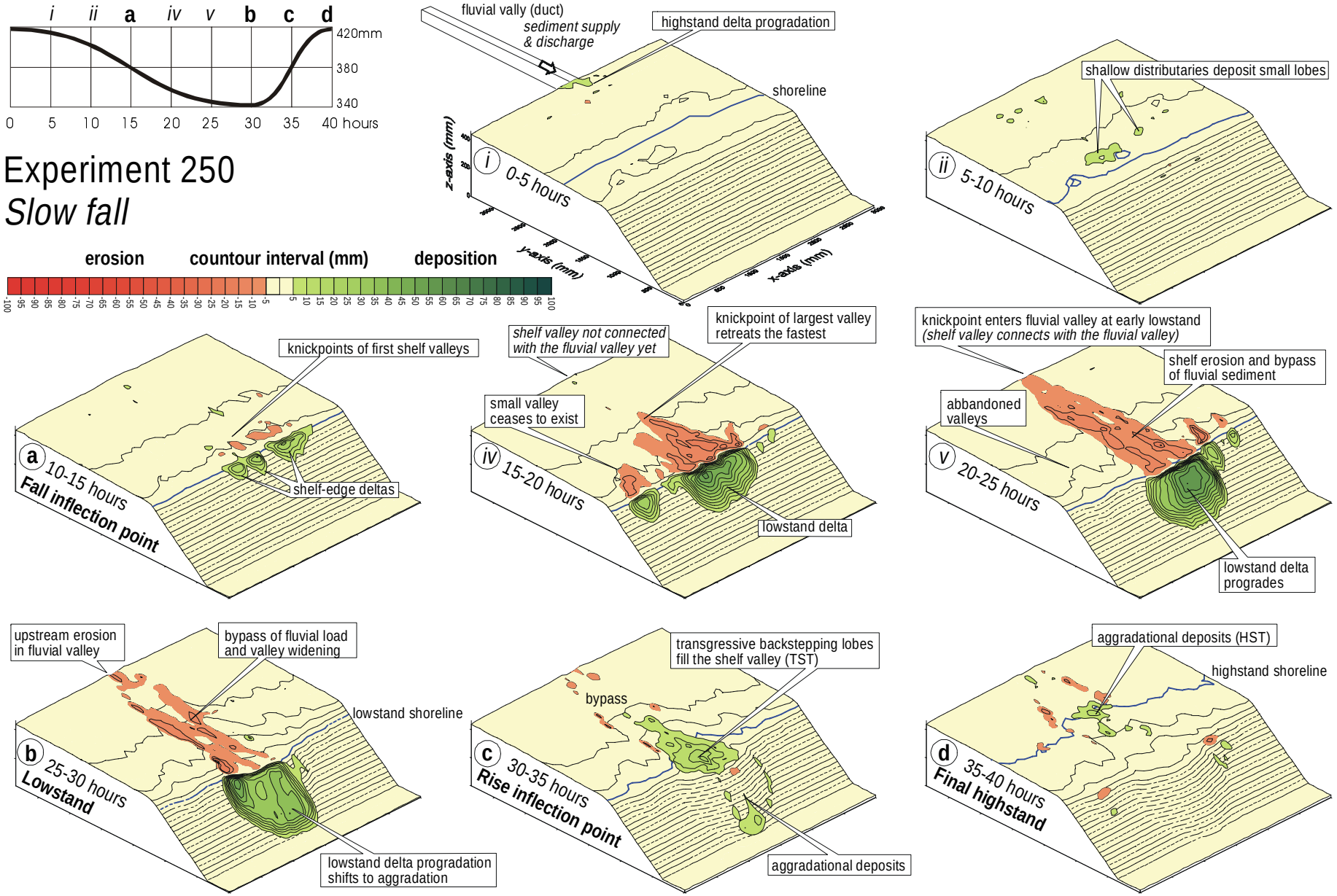
i ii a iv v b c d
420mm
380
340
0 5 10 15 20 25 30 35 40 hours
Experiment 250
Slow fall
erosion
countour interval (mm)
deposition
fluvial vally (duct)
sediment supply & discharge
highstand delta progradation
shoreline
z-axis (mm)
y-axis (mm)
x-axis (mm)
i 0-5 hours
ii 5-10 hours
shallow distributaries deposit small lobes
knickpoints of first shelf valleys
a 10-15 hours
Fall inflection point
shelf-edge deltas
shelf valley not connected with the fluvial valley yet
knickpoint of largest valley retreats the fastest
small valley ceases to exist
iv 15-20 hours
lowstand delta
knickpoint enters fluvial valley at early lowstand
(shelf valley connects with the fluvial valley)
shelf erosion and bypass of fluvial sediment
abbandoned valleys
v 20-25 hours
lowstand delta progrades
upstream erosion in fluvial valley
bypass of fluvial load and valley widening
lowstand shoreline
b 25-30 hours
Lowstand
lowstand delta progradation shifts to aggradation
transgressive backstepping lobes fill the shelf valley (TST)
bypass
c 30-35 hours
Rise inflection point
aggradational deposits
aggradational deposits (HST)
highstand shoreline
d 35-40 hours
Final highstand

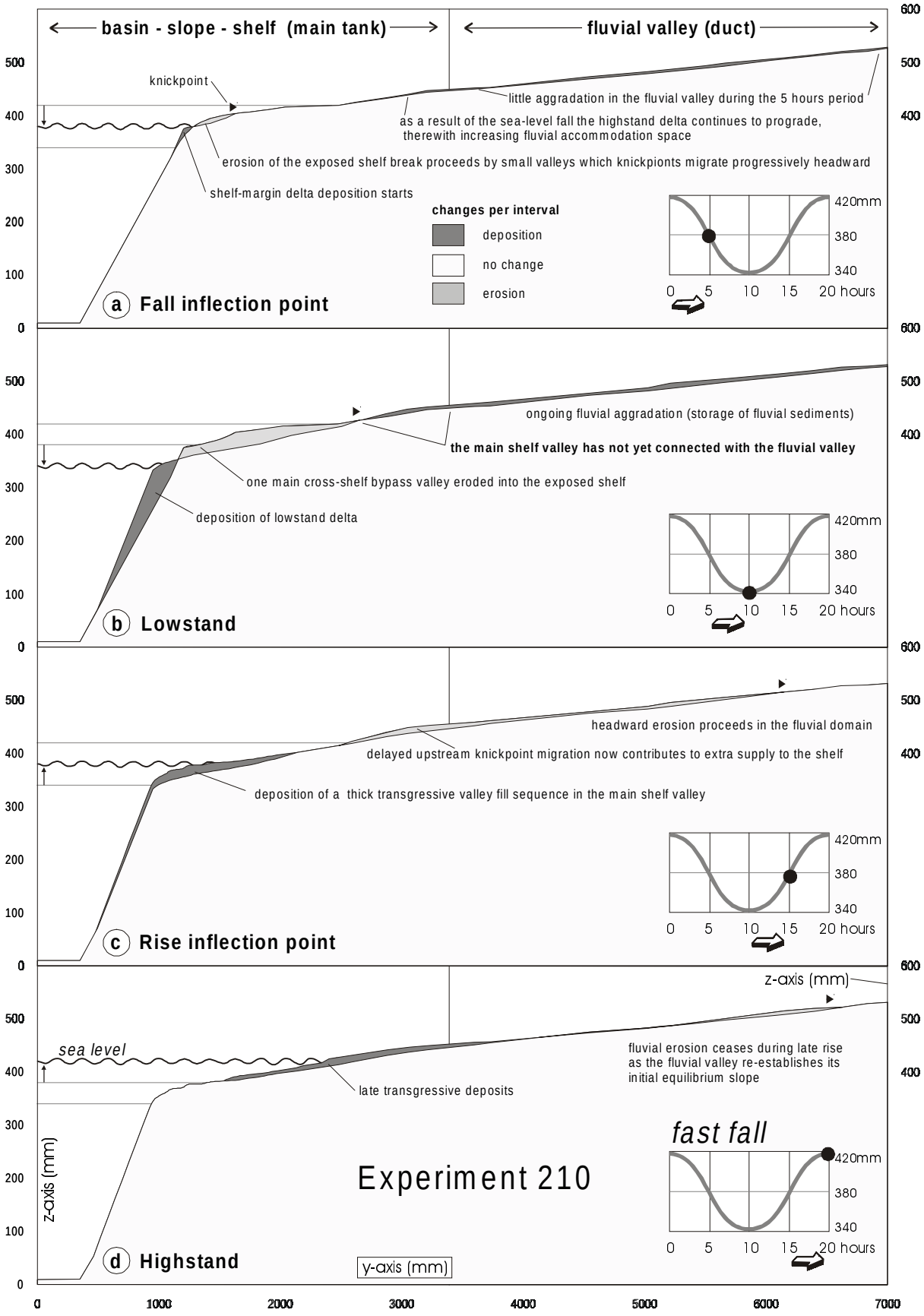

Fig. 3.5—Medial cross-sections (x=1500 mm) illustrating experiment 210 with a fast rate of sea-level fall. The sea-level curve is divided into stages a to d that correspond to Fig. 3.3.

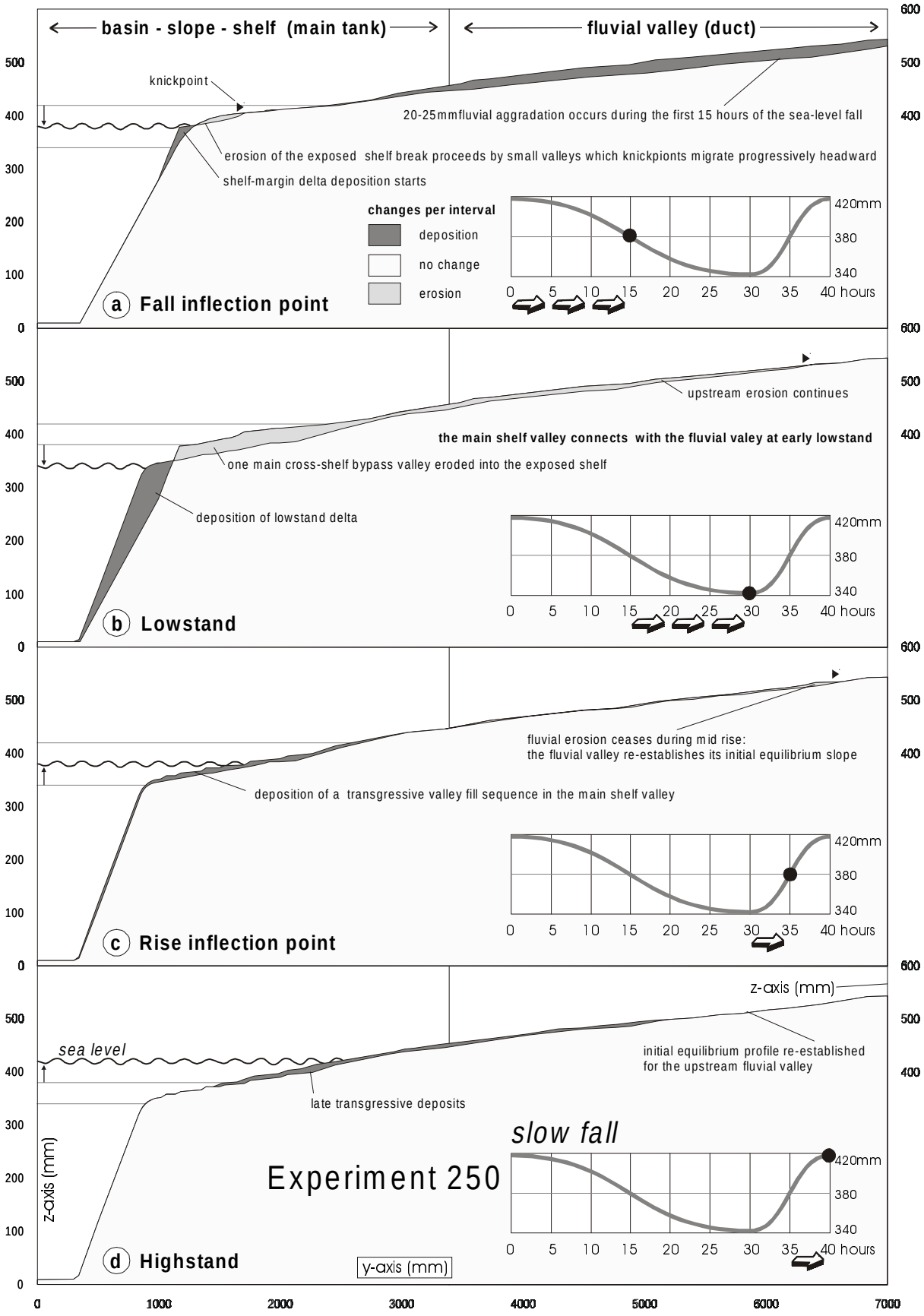

Fig. 3.6—Medial cross-sections illustrating experiment 250 with a slow rate of sea-level fall. The stages a to d correspond to Fig. 3.4

Shelfal response to sea-level changes

Figures 3.3 and 3.4 show the topographic changes on the coastal plain-shelf-slope setting for Experiment 210 (fast fall) and 250 (slow fall). Both experiments show many similarities in shelf evolution in response to one full cycle of sea-level fall and rise. As the shoreline drops over the outer shelf and shelf edge, small canyons develop along that part of the lower shelf that receives the discharge. Multiple, small, V-shaped canyons simultaneously incise the outer shelf and deposit small shelf-edge deltas (Figs 3.3a and 3.4a). The shelf canyons compete for the available discharge from the fluvial valley that is distributed through stream avulsion on the apex of the delta. Canyon cutting proceeds by knickpoints migrating up the shelf. The valley that captures most of the discharge has the most proximal knickpoint i.e., the upstream limb of the red coloured central shelf valley in Fig. 3.3b. By cutting off smaller valleys, this valley starts monopolising all available discharge as its knickpoint reaches the middle shelf. The dominating valley progressively deposits the largest lowstand delta while the smaller systems become starved of discharge and sediment. Finally, the dominant valley connects with the fluvial valley and becomes a single, shelf bypass valley that feeds one large, lowstand delta (Figs 3.3c and 3.4v). During the subsequent sea-level rise, which is of similar duration for both groups of experiments, lowstand delta progradation shifts to aggradation. As the rate of rise increases towards the rise inflection point, the main shelf-bypass valley becomes flooded and filled by small backstepping lobes (Figs 3.3c and 3.4c). During late transgression, the upper part of the incised valley is backfilled.

Fluvial response to sea-level changes

Although the drainage development on the shelf is similar for both the slow and the fast fall in sea level, the timing at which the main valley erodes into fluvial strata differs significantly. The differences in timing of deposition and erosion on the coastal plain and fluvial domain for both cases are illustrated by their medial cross sections in Figs 3.5 and 3.6 for experiments 210 and 250, respectively. Both experiments start with a graded fluvial profile in equilibrium with a highstand delta on the coastal plain. Near the fall inflection point, and earlier with increasing rate of fall, the stream incises into the highstand delta. The incision is forming the apex for a new delta lobe that aggrades and progrades at a lower level on the shelf. Simultaneously, aggradation continues in the fluvial system (cf. Figs 3.5a and 3.6a). The volume of fluvial aggradation, however, is largest for the slow fall (Fig. 3.6a) because of the longer time span available. The knickpoint positions on the exposed shelf are still fairly similar for both cases (cf. Figs 3.5a and 3.6a). At lowstand, the dominating shelf canyon has not connected with the fluvial valley, as yet, in case of the fast sea-level fall. In contrast, connection occurs before lowstand during the slow-fall experiment (cf. Figs 3.3b and 4v). Remarkably, the early transgression of the shelf is still accompanied by upstream erosion in the fluvial valley resulting in extra sediment delivery to the shelf edge in both experiments. Erosion in the fluvial domain continues until the rise inflection point during the slow sea-level fall experiment (Fig. 3.6d), and until late rise during the fast sea-level fall experiment (Fig. 3.5d). Finally, the fluvial valley re-establishes its initial equilibrium slope towards the new highstand shoreline before highstand in both examples.

Effect of sea-level amplitude

The above results show that the connection time, the time at which the dominant shelf valley connects with the fluvial valley, differs for the fast-fall and slow-fall experiment. A star below the sea-level curves in Fig. 3.7a indicates the connection time (i.e., the first appearance of the knickpoint in the fluvial valley). The knickpoint paths over the shelf are shown in Fig. 3.7b and illustrate that the knickpoint of the dominant shelf canyon migrated much faster upstream during the fast fall than the slow-fall experiment. Figure 3.7c shows the rate of deposition on the shelf (deposition rate of the green patches in Figs 3.3 and 3.4).

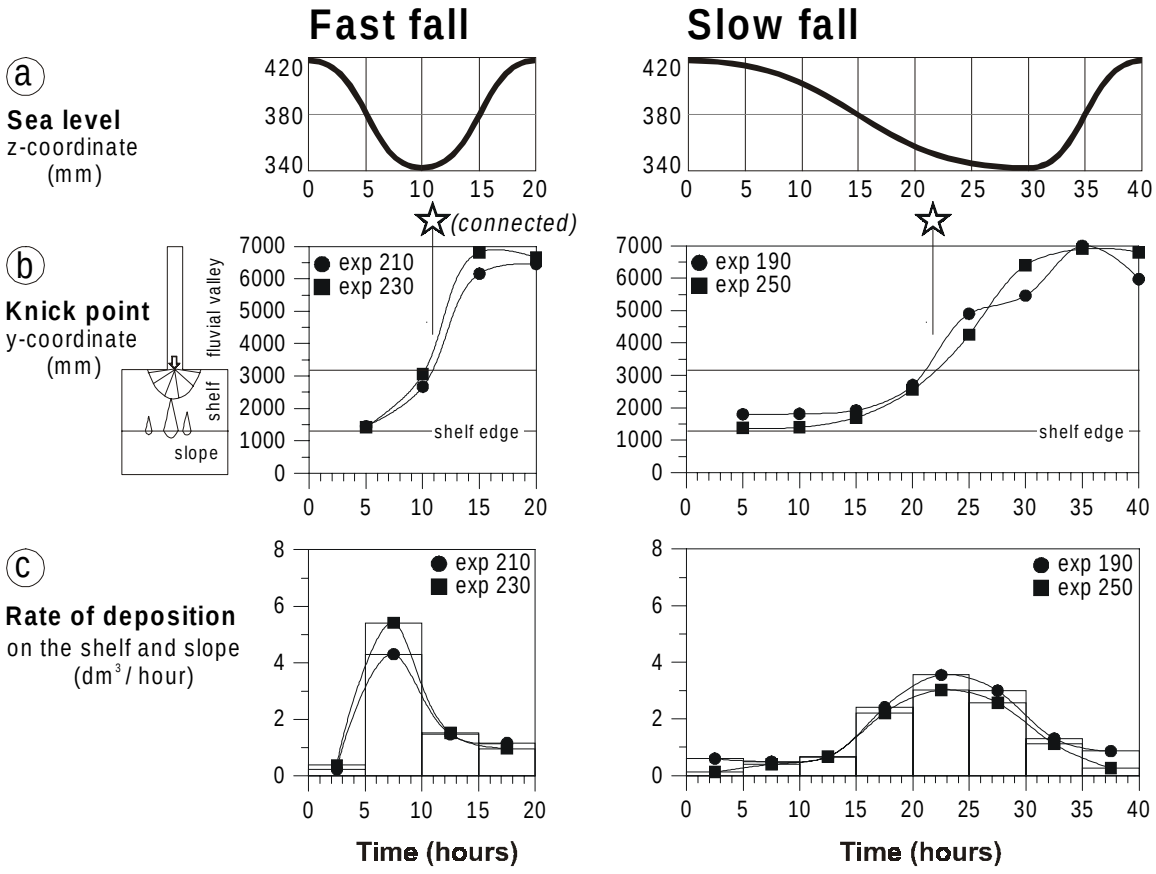

Fig. 3.7—Quantitative comparison of two fast and two slow sea-level fall experiments with 80 mm amplitude. (a) Sea-level curve. (b) Knickpoint migration paths show that shelf valleys connect at or just after lowstand for the fast-fall experiments while the slow-fall experiments show connection already at early lowstand as indicated by the stars below the sea-level cycle. (c) The measured mean rate of deposition downstream of the fluvial valley shows the effect of a sea-level change on the sediment flux to the coastal plain, shelf and lowstand delta. (Fluxes were calculated from the green depositional volumes on the scans).

Similar trends in knickpoint migration and the rate of deposition on the shelf were found for experiments with large amplitude (Fig. 3.8). Obviously, the 160 mm amplitude experiments connected sooner than the 80 mm amplitude experiments (cf. Figs 3.7 and 3.8). It must be noted at this point that during the high, 160 mm, amplitude experiments the sea level dropped further below the shelf break and resulted in a steeper lowstand stream gradient. The results show a difference in timing of connection relative to the sea-level cycle for the 80 mm and 160 mm amplitude experiments (Fig. 3.9). Generally, experiments of both amplitudes show that the sequences on the shelf and the fluvial system become progressively more out-of-phase as the rate of sea-level fall increases.

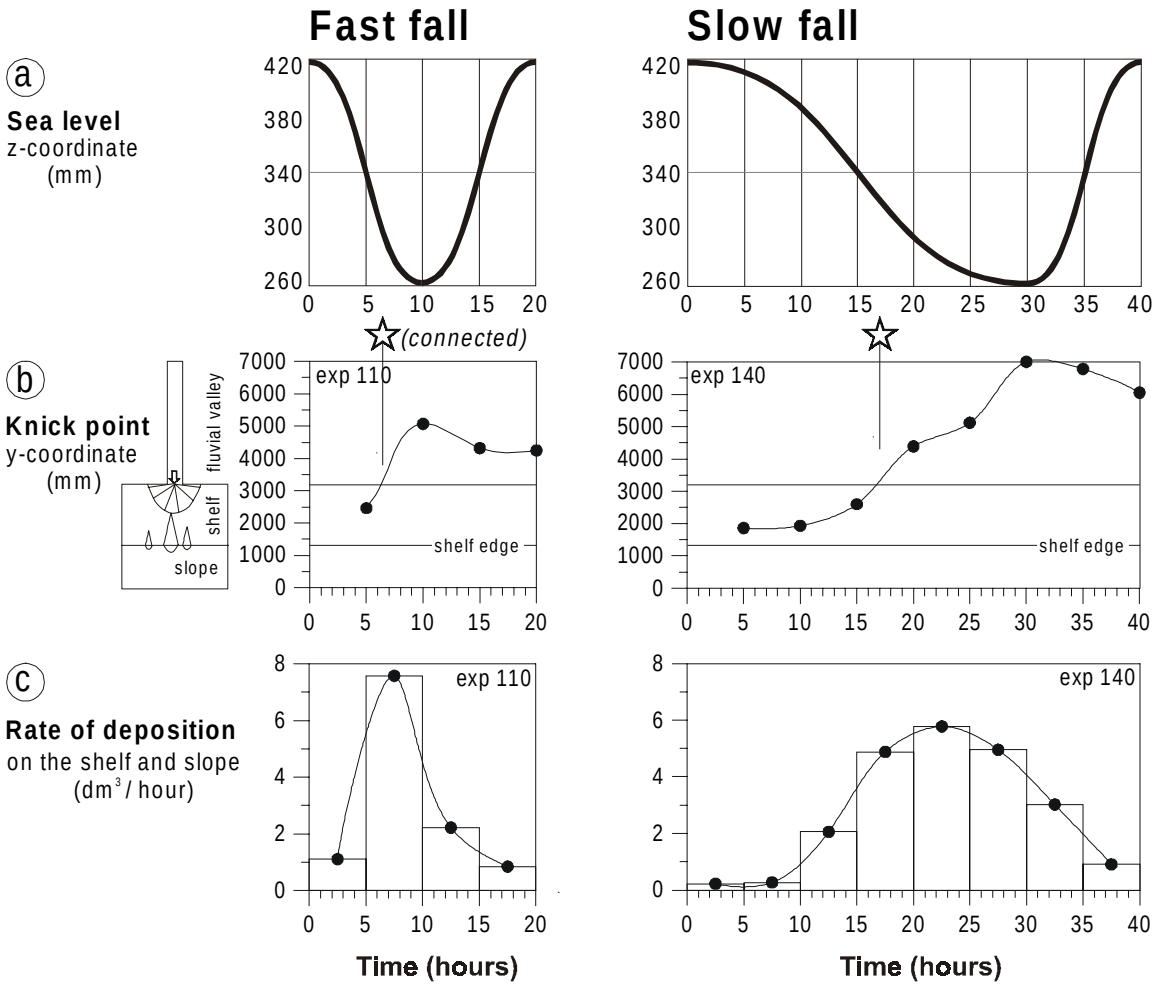

Fig. 3.8—Quantitative comparison of a fast and a slow sea-level fall experiment with 160 mm amplitude. (a) Sea-level cycle. (b) Knickpoint migration paths show that the main shelf valley connects at early lowstand in both experiments (indicated by the star below the sea-level curve). The 160 mm amplitude experiments show much faster knickpoint migration rates on the shelf and consequently higher fluxes were measured downstream of the fluvial valley (c) than for the 80 mm amplitude experiments (cf. Fig. 3.7).

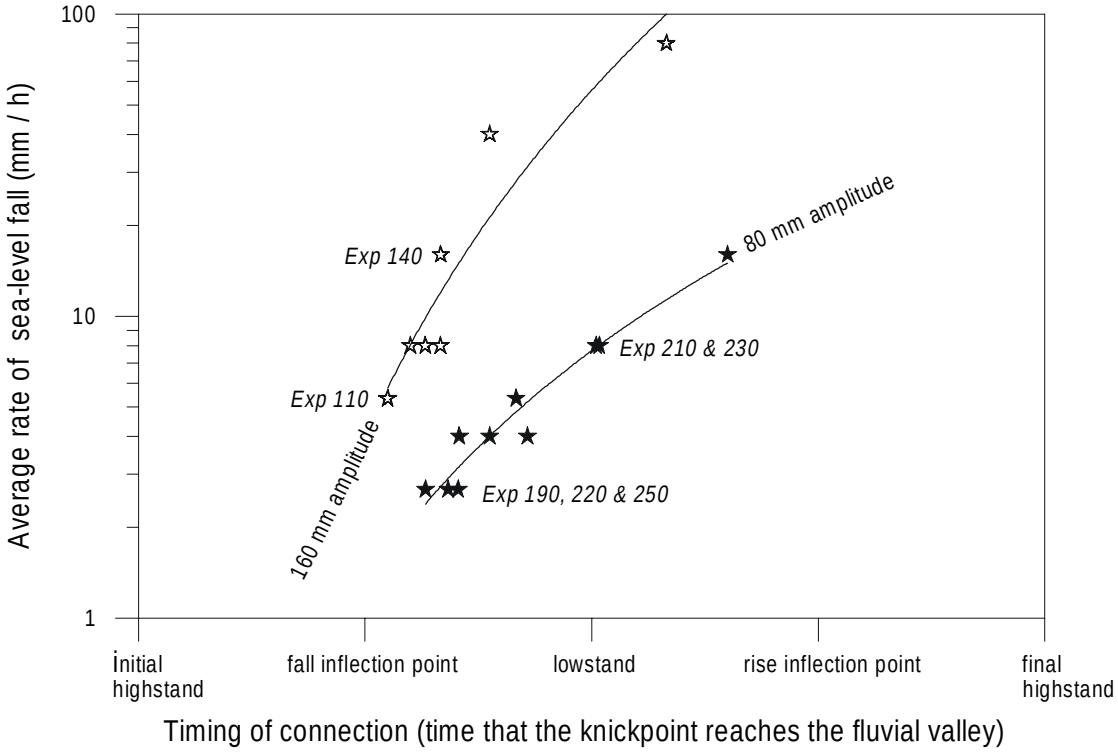

Fig. 3.9—The timing of connection, the onset of fluvial erosion, relative to the sea-level cycle. Experiments with a fast rate of sea-level fall develop a shelf valley that connects closer to lowstand than experiments with a slow rate of sea-level fall. High-amplitude and low-amplitude experiments are marked by open and closed symbols, respectively.

Connection Rate

All experiments show a delay in response between a fall in sea level and the first features of erosion in the fluvial domain. This delay relates to the time required to propagate the headward erosion process up the shelf towards the fluvial valley. It can be more generally quantified as connection rate, R_c:

$$R_c = \frac{L_s}{T_c - T_i} \qquad [\mathrm{L/T}] \qquad (3.6)$$

Where L_s is the shelf width under lowstand conditions, T_c-T_i represents the connection delay defined as the period between the moment that the shelf break becomes exposed and the first shelf canyons develop (T_i) and the connection time (T_c), when a shelf canyon connects with the fluvial valley. The experimental results show that connection time depends on the rate of sea-level fall (Fig. 3.10a). High rates of sea-level fall relate to minor connection delays. However, even for an instantaneous sea-level fall (Experiment 90), it took at least an hour before a shelf canyon connected with the fluvial valley and up to 12 hours before a lowstand equilibrium profile was established. The connection rate correlates well with the average rate of sea-level fall (Fig. 3.10b). For the homogenous substrate in our set-up, the connection rate compares also with the average rate of knickpoint migration on the shelf associated with the headward cutting shelf valleys. Consequently, both the rate of shelf erosion (Fig. 3.11)

and the connection rate (Fig. 3.10b) show a similar strong correlation with the rate of sea-level fall. The observed rates of erosion and deposition on the shelf are entirely reproducible and show a consistent trend over the full range of experiments (cf. Figs 3.7, 3.8 and 3.11).

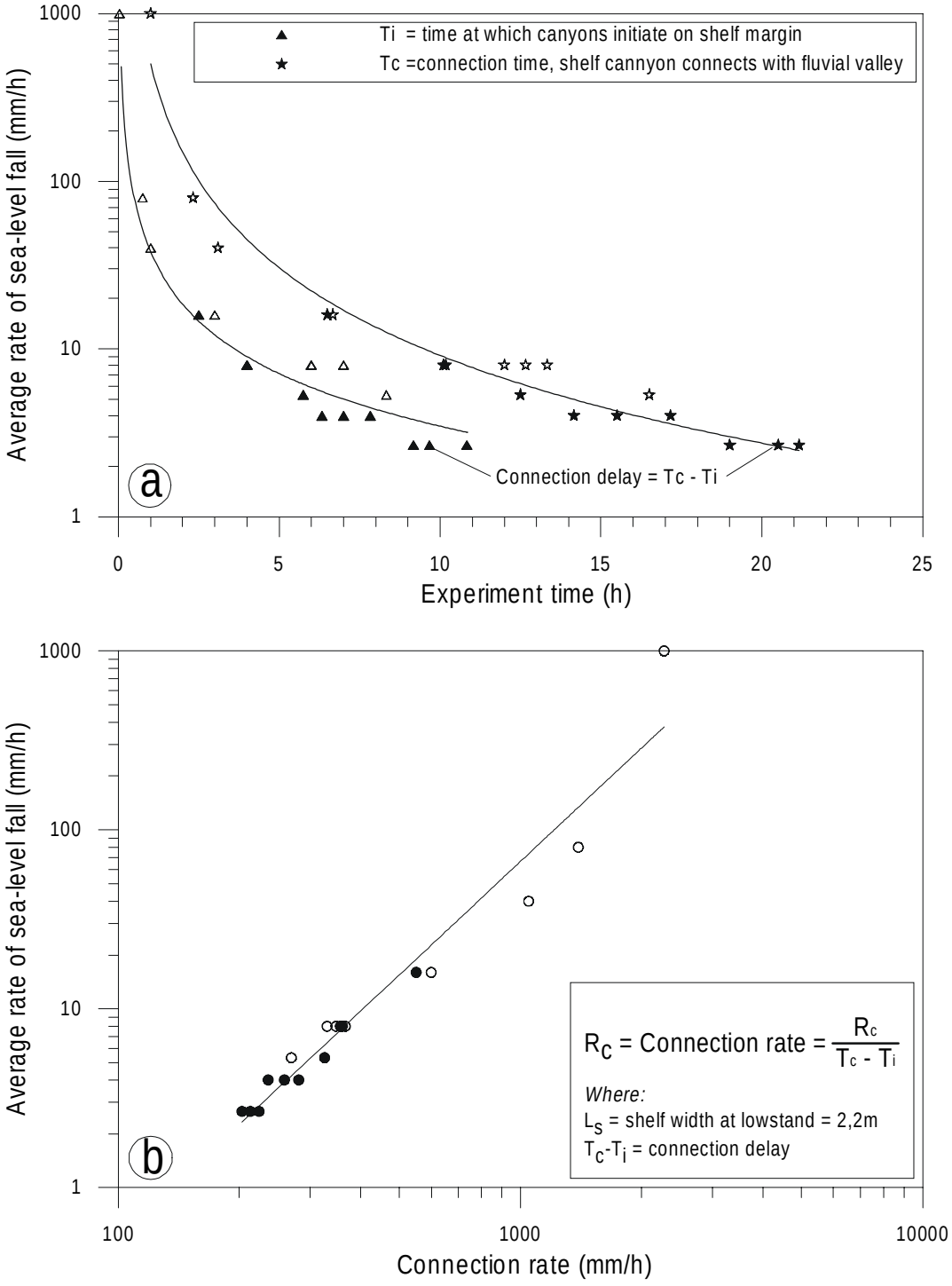

Fig. 3.10—(a) The connection delay is defined as the time span between the first signs of headward erosion on the shelf edge (triangles) and connection time, the moment that the dominating shelf valley connects with the fluvial valley (stars). (b) The connection rate (Eq. 3.6) correlates well with the rate of sea-level fall. High-amplitude and low-amplitude experiments are marked by open and closed symbols, respectively.

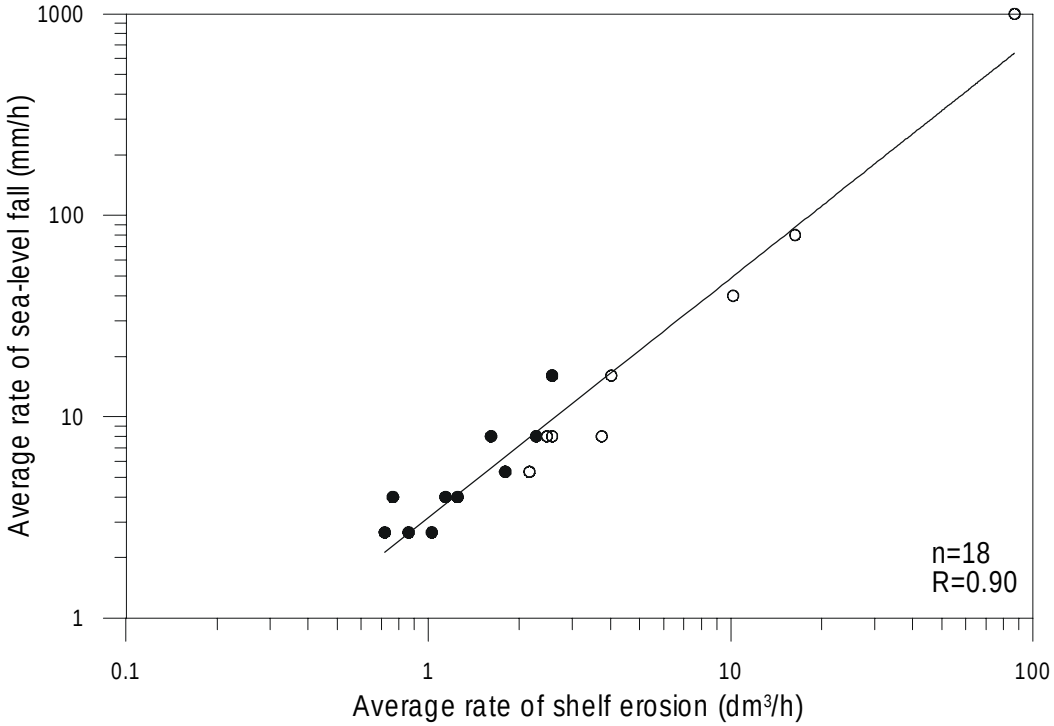

Fig. 3.11—The rate of erosion on the shelf correlates well with the rate of sea-level fall. High-amplitude and low-amplitude experiments are marked by open and closed symbols, respectively.

The effect of connection time on shelf and fluvial stratigraphy

Figure 3.12 compares the composite stratigraphic sections for the fast-fall and slow-fall experiment (Figs 3.5 and 3.6). It illustrates the degree of diachroneity of the lowstand bounding unconformity (i.e., sequence boundary) on the shelf and fluvial domain. The formation of the sequence boundary on the outer shelf is completed at lowstand, irrespective of the rate of sea-level fall. The surface is thus synchronous with the lowstand. However, further upstream the unconformity was still being formed by continued fluvial erosion during the sea-level rise, which illustrates a clear diachroneity. The amount of diachroneity along the unconformity is much higher for the fast-fall than for the slow-fall experiment, which is reflected in the fluvial and shelf stratigraphy. Thus, the age of the sequence boundary becomes younger upsection and correlates with the rise-inflection point for the slow fall and with the highstand for the fast-fall experiment (Fig. 3.12).

The timing of the connection of one of the shelf canyons with the fluvial valley has a strong bearing on the final volume of the slope fan and lowstand delta, because it determines the change of aggradation to degradation of the fluvial valley. Low rates of sea-level fall produce large lowstand deltas and high rates of sea-level fall produce small ones (Fig. 3.13). The volume of the lowstand delta relates to the time period available for lowstand deposition. The fluvial erosion starts after the peak in deposition of the lowstand delta on the shelf in case of the fast fall (Fig. 3.7c, left). This illustrates that the timing of connection relative to the sea-level cycle not only controls the lowstand-delta volume, but also affects its composition, i.e., the percentage of fluvial over redeposited shelf sediment. As a result, lowstand deltas that are formed during high rates of sea-level fall consist largely of cannibalised shelf material and for only 20-30% of fluvial sediment (Fig. 3.14). In contrast, the lowstand deltas of the slow-fall experiments (shelf valley connected during early fall) contain up to 50% fluvial sediment. Obviously, the percentage of fluvial relative to shelf sediment in the lowstand delta drastically increases after connection.

The rate of sea-level fall has also implications for the rate of deposition on the shelf and in the fluvial valley during the subsequent rise. Experiments with fast rates of sea-level fall show connection close to or just after lowstand, while connection proceeds much earlier for slower rates of sea-level fall (Fig. 3.9). Connection accompanies fluvial degradation and points to the moment that the fluvial valley starts to release previously aggraded sediments. Consequently, the transgressive valley-fill sequence in the fast-fall experiments shows a larger volume than in the slow-fall experiments, as is evidenced by the difference in geometry of the stage-c deposits in Figs 3.12 and 3.13. The full range of experiments shows that the total volume of the transgressive systems tract increases with increasing rates of the preceding sea-level fall (Fig. 3.15).

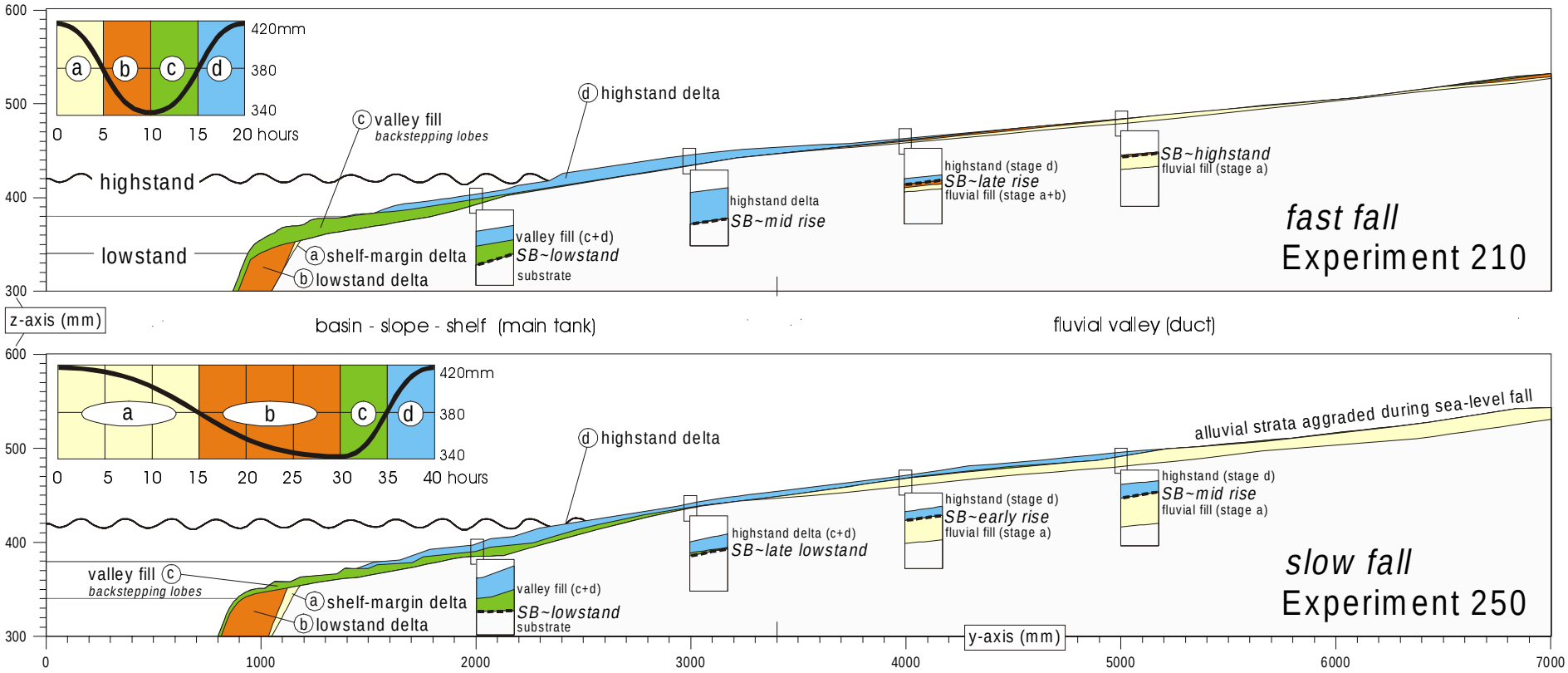

Fig. 3.12—Composite stratigraphic sections compiled from Experiment 210 and 250. The stages a to d marked in the sea-level curves correspond with the sediments and with the stages of Figs 3.3 to 3.6. The stratigraphic columns on the shelf, coastal plain and river show that the diachroneity of the sequence boundary is largest for the fast-fall experiment. With increasing diachroneity of the sequence boundary it becomes less straightforward to apply systems tracts terminology to upstream alluvial strata. The fluvial deposits overlying the sequence boundary lag half a sea-level cycle behind the sediments overlying the (lowstand) unconformity on the shelf. The comparison between the two experiments is a conceptual test that reveals the problems related to attributing systems tract terminology to alluvial strata (vertical exaggeration 2.25 times).

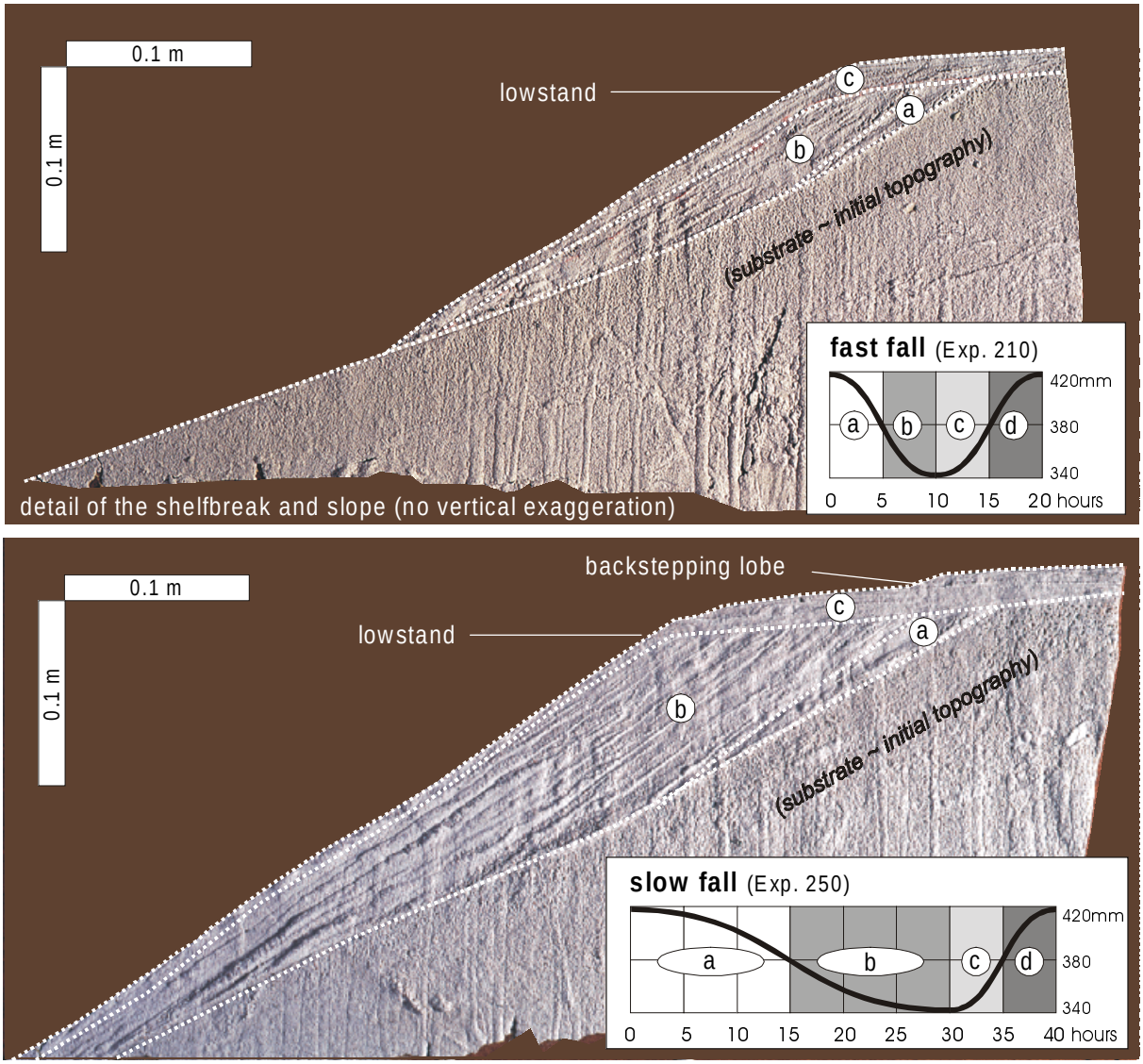

Fig. 3.13—Lacquer peels of experiments 210 and 250 illustrating the lowstand delta on the shelf break of Fig. 3.12. The stages a to d are delineated on the experimental stratigraphy and show that the fast fall resulted in a smaller lowstand delta (b) but in a thicker transgressive systems tract (c) compared to the slow fall.

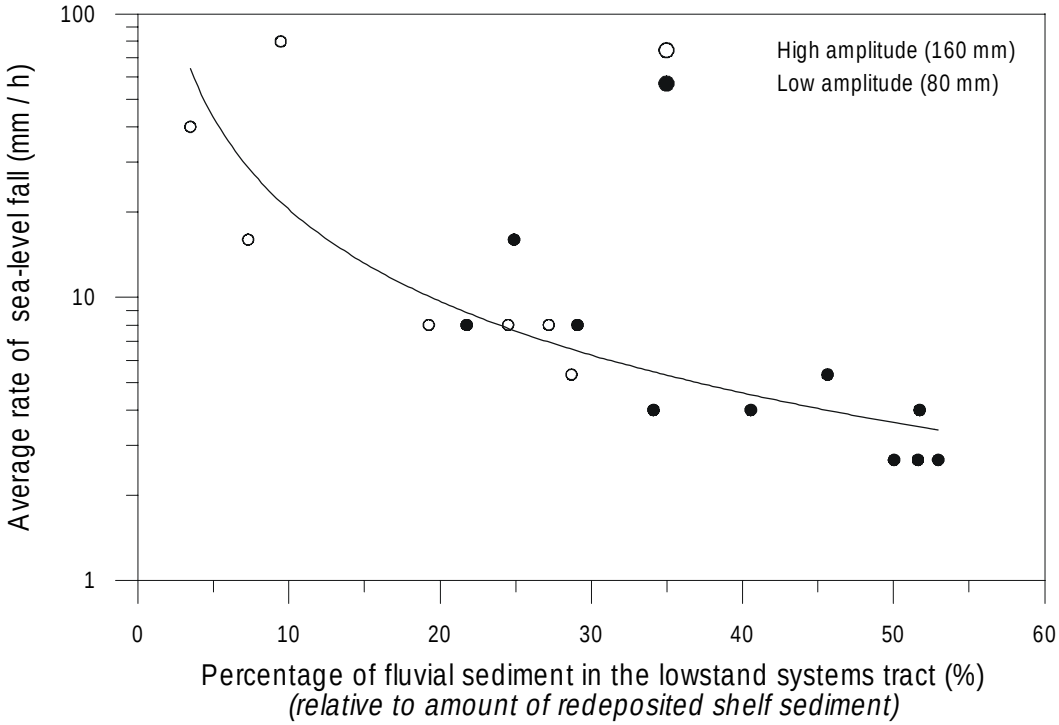

Fig. 3.14—Composition of the lowstand systems tract (lowstand delta) related to the rate of sea-level fall. Low rates of sea-level fall relate to a high content of fluvial sediment in the lowstand delta. The content of fluvial sediments in the lowstand delta depends on the rate at which sediments are released by the fluvial valley and bypasses over the shelf. The rest of the lowstand-delta volume is cannibalised and redeposited shelf sediment.

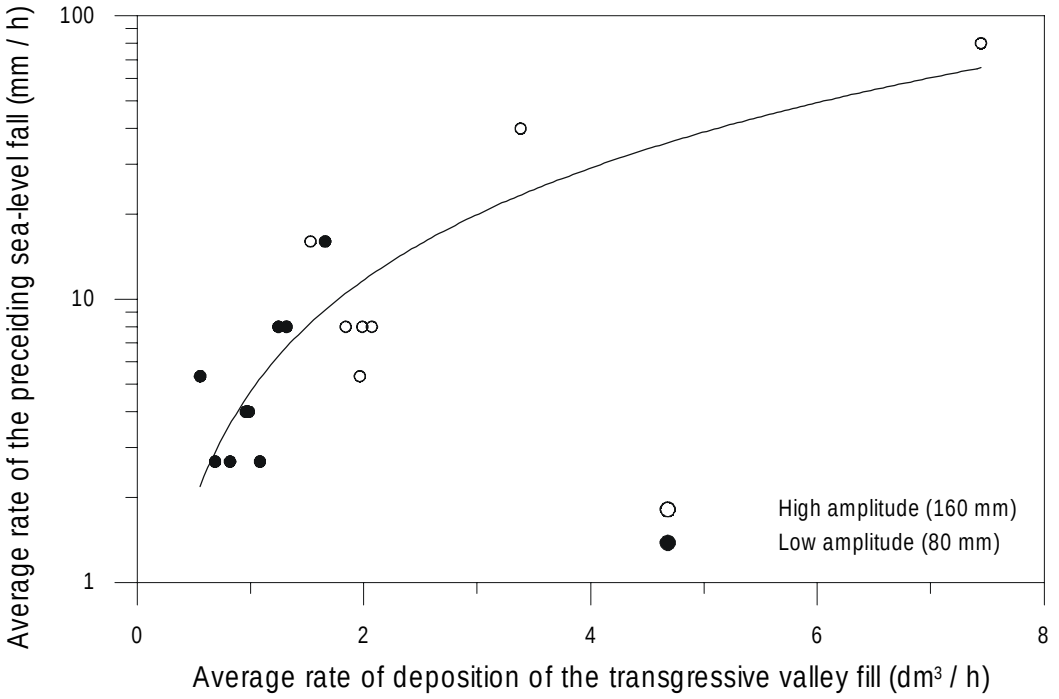

Fig. 3.15—The rate of deposition of the transgressive-valley-fill sequence related to the rate of the preceding sea-level fall. The faster the preceding fall, the higher the rate of deposition of the valley fill during the subsequent transgression. The connection delay causes fluvial degradation to occur during early rise in case of a fast sea-level fall with as consequence higher fluxes to the coastal plain and shelf as compared to the case of a slow rate of fall.

Discussion

Analogue models according to Hooke's (1968) similarity of process approach, are small dynamic sedimentary systems that, perhaps better than existing numerical models, incorporate simplified versions (analogues) of the fundamental processes (Paola, 2000). Analogue models, in comparison with numerical models, have at least one strong point in favour: They allow only a limited control by the experimentalist and are, therefore, less susceptible to purposeful matching. Our experiments show to be reproducible and to give deterministic results for a range of rates in sea-level fall (see Figs 3.7, 3.10 and 3.11). Hence, the approach is suitable for sensitivity analysis of isolated variables. However, we regard on the one hand a model as heuristic (see Oreskes *et al*., 1994); it can support a hypothesis, but being only a model it is unable to prove it. On the other hand, it is unlikely that the complex feedback between allocyclic changes can be unravelled from ancient stratigraphy alone (e.g. Blum & Price, 1998).

The first part of the discussion concerns the question which aspects of the model can be applied to real-world river and shelf settings and how the observed rates of knickpoint migration and connection rates in our flume model relate to values for Quaternary shelf evolution. The second part discusses the analogue experimental results in the light of existing stratigraphic concepts for both the fluvial and shelfal realms exemplified by empirical studies. Finally, we discuss what parts of the sequence-stratigraphic concepts need modification in the light of our experimental results to apply for fluvial successions.

Scalability of headward erosion process

A base profile responds to a drop in base level by the process of upstream knickpoint migration. Here we point to the possibility to use the process of knickpoint migration and the average rate of knickpoint retreat as an independent scaling tool. The knickpoints in our flume tank migrated according to the inclination model of Gardner (1983), which is a realistic process for the applied uniform, non-resistant bed material. The average rate of knickpoint migration on the shelf rapidly declines with increasing time from the onset of sea-level fall (Fig. 3.16a). According to Begin (1988), the distance over which the knickpoint travels is proportional to the square root of the time since the beginning of the sea-level fall. Consequently, the rate of knickpoint migration must be inversely proportional to the square root of the time since base level was lowered (see also Quirk, 1996). In our 18 experiments, knickpoint migration rates for the shelf fit close to this relation as shown in Fig. 3.16b. The question is how do the flume values relate to knickpoint migration rates on an emerged Quaternary alluvial plain and shelf?

The magnitude of knickpoint migration rates in various flume studies and the real world on different time scales is given in Fig. 3.17. Substrate properties, slope and bankfull discharge are not included in the comparison because it is not intended to give a functional relationship for knickpoint migration rates here, but rather to display the range of variation. Knickpoint migration rates in small-scale systems like flume models are presumably higher than on real-world shelves owing to differences in slope and substrate. Sediment transport is proportional to the slope of the channel bed (following any diffusive approach e.g. Begin *et al*., 1981; Salter, 1993; Leeder & Stewart, 1996) and real-world alluvial plain and shelves have a typically non-uniform

morphology and geology. All experimental studies, except for the one that had very resistant bed material, show values for knickpoint retreat rates within a close range, their variation being related mainly to the duration of an experiment. The lower-right hand side of Fig. 3.17 shows retreat rates for bedrock rivers that vary between 0.001 to 0.1 m/yr., which is in close agreement with model estimates of Whipple & Tucker (1999). Rivers that incise sediments show high knickpoint migration rates for flashflood dominated streams observed over decades. Based on the data in Fig. 3.17 we infer that knickpoint migration rates over sandy and muddy Quaternary shelves and alluvial plains range between 1 and 70 m/yr. However, it must be noted that the data set will include the effect of the measured time interval; a 10^4 to 10^5 year change may include a one order of magnitude decrease in erosion rate (Gardner *et al*., 1987). Thus, the expected values for knickpoint migration on Quaternary shelves may actually be more concentrated in the high part of the range, between 10 and 70 m/yr. Diffusion models support similar numbers for the Mississippi River in response to the 100 m sea-level fall during the Wisconsin glaciation (Salter, 1993; Leeder & Stewart, 1996). Both models assume that sea-level-fall-induced incision occurred as far as 350 km inland of the Mississippi outlet (shelf edge), thus up to Baton Rouge (Saucier, 1996). Salter (1993) calculates that more than 6600 years are required for the knickpoint to reach that position. This would implicate a maximum average rate of knickpoint migration of 50 m/yr (A in Fig. 3.17). In contrast, the model of Leeder & Stewart (1996, their fig. 6) implies a lower value, around 3 m/yr for knickpoint migration up to Baton Rouge (B in Fig. 3.17). Although it is clear that estimates for knickpoint migration rates show a large spreading, field observations and diffusion models support the existence of several kyr response time between 4th order glacio-eustatic sea-level fall and the related fluvial response.

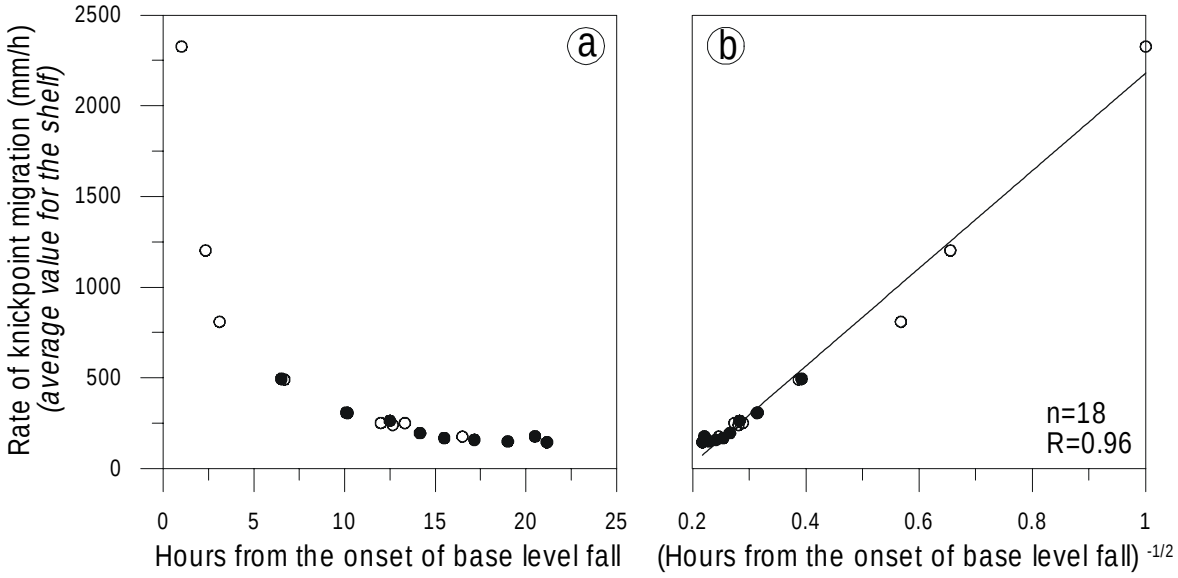

Fig. 3.16—(a) Average knickpoint migration rate shows a rapid decline when plotted against the time span over which sea level was lowered. (b) The same data show a linear correlation with the reciprocal of the square root of the time since base level was lowered.

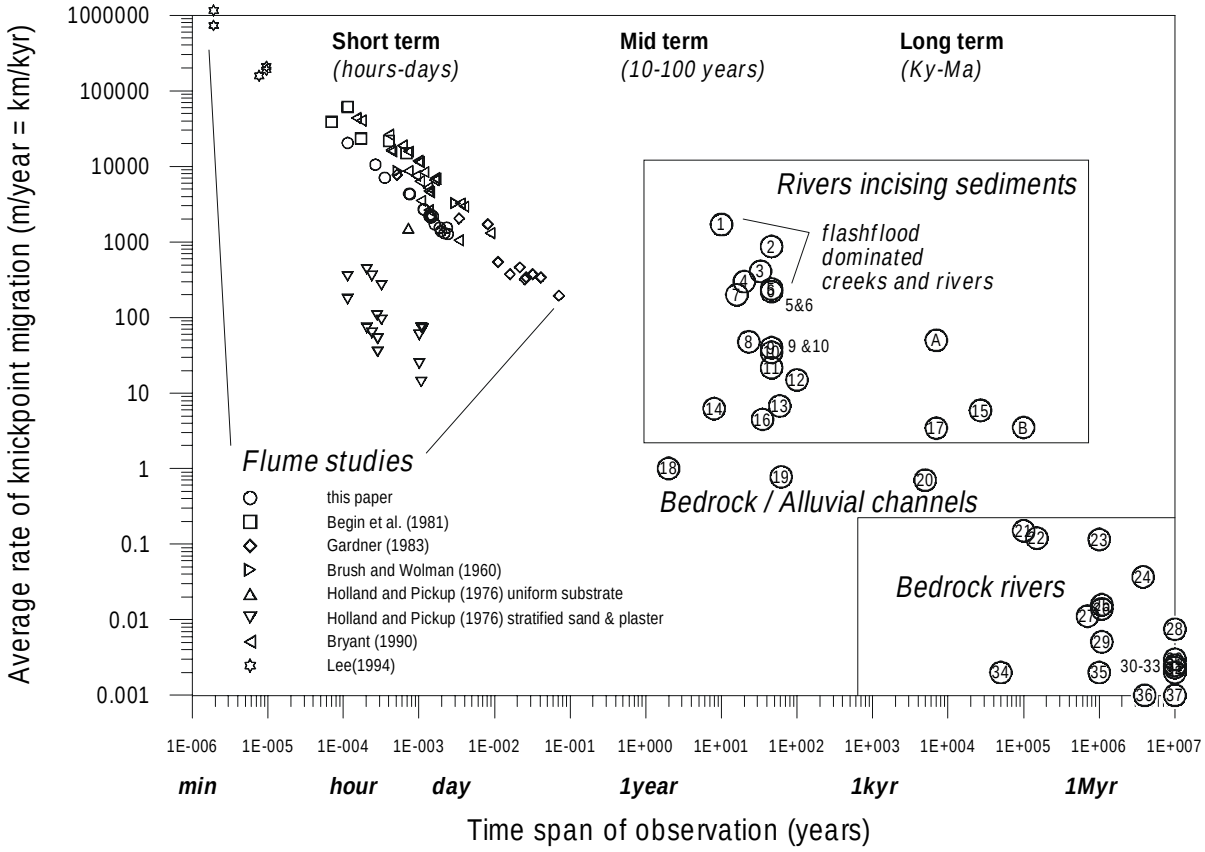

Fig. 3.17—Average knickpoint migration rates plotted against the time scale of their occurrence (observation). The graph does not intend to show a numerical relation, but wants to illustrate the order of magnitude of knickpoint migration rates in flumes and various rivers. In the graph we plotted average retreat rates, although it is known (Gardner, 1983; Leeder & Stewart, 1996) and also observed from our flume experiments that knickpoint migration rates decrease from an initially high value. Bedrock rivers typically adjust their profiles with knickpoint migration rates between 0.001-0.1 m/yr while short term river adjustment indicates values between 100-1000 m/yr. Knickpoint migration rates on alluvial plain and shelves that accommodate 100 kyr glacio-eustatic sea-level changes are inferred to range from 1-70 m/kyr. The symbols represent data of flume studies (Brush & Wolman, 1960; Holland & Pickup, 1976; Begin *et al.*, 1981; Gardner, 1983; Bryan, 1990; Lee & Hwang, 1994). A and B are model estimates for knickpoint migration during the Wisconsin glaciation of the Mississippi River from Salter (1993) and Leeder & Stewart (1996) respectively. The numbers represent river data from: 1 West Tennessee channels (Simon, 1991); 2 Homochitto River (Yodis & Kesel, 1993); 3 Dry Creek (Begin, 1988); 4 Deep Creek (Schumm *et al.*, 1996); 5 St. Catharine Creek (Yodis & Kesel, 1993); 6 Homochitto tributaries (Yodis & Kesel, 1993); 7 Pechahalee Creek (Begin, 1988); 8 Crawfords Creek (Begin *et al.*, 1981); 9 St. Catharine Creek tributaries (Yodis & Kesel, 1993); 10 Harding Bayou (Yodis & Kesel, 1993); 11 Spanish Bayou (Yodis & Kesel, 1993); 12 Saikawa River (Begin, 1988); 13 Pleasant Valley, Nevada (Begin, 1988); 14 Oaklimiter Creek (Begin, 1988); 15 Indus (Leland *et al.*, 1998); 16 Wolf Creek (Eaton, 1991); 17 Mattole River (Pazzaglia *et al.*, 1998); 18 Blue Hills channels (Dick *et al.*, 1997); 19 Gully near Imlay, Nevada (Begin, 1988); 20 Niagara Falls (Wohl, 1998); 21 South River (Bank & Harbor, 1998); 22 Rio Jemez (Pazzaglia *et al.*, 1998); 23 Rappahannock River (Howard *et al.*, 1994); 24 Susquehanna (Pazzaglia *et al.*, 1998); 25 Swede (Stock & Montgomery, 1999); 26 French (Stock & Montgomery, 1999); 27 Amargosa River (Butler, 1984); 28 Tumut River (Young & McDougall, 1993); 29 Cowlet (Stock & Montgomery, 1999); 30 Tumbarumba Creek (Young & McDougall, 1993); 31 Wheeo Creek (Stock & Montgomery, 1999); 32 Shoalhaven River (Nott *et al.*, 1996); 33 Paddys River (Young & McDougall, 1993); 34 Dabang River (Yang & Li, 1988); 35 Maclean River (Weissel & Seidl, 1997); 36 Hawaiian channels (Seidl *et al.*, 1994); 37 Boggy Creek (Young & McDougall, 1993).

Fluvial and shelf response to sea-level fall

Posamentier & Vail (1988) launched the sequence-stratigraphic concept that widespread fluvial deposition would occur during early stages of eustatic fall, followed by progressive valley incision and sediment bypass during late stages of fall. According to this view the first significant river incision commences when the bayline moves basinward from the equilibrium point, i.e., when the shoreline is forced basinward as a result of a relative sea-level fall (forced regression e.g. Posamentier *et al*., 1992).

In our experiments we observed a quite different sequence of events. The fluvial valley that was aggrading during the highstand progradation continued to aggrade during the fall in sea level until one of the shelf canyons was connected with the fluvial valley. It confirms the ideas of Quirk, (1996), that alluviation during a sea-level fall must be placed in the context of different processes that can occur simultaneously downstream and upstream of the migrating knickpoint. During the fall we observed in every experiment (Figs 3.3 to 3.6): 1) continued aggradation in the river valley and on the highstand-delta plain; 2) continued avulsion at the apex of the original highstand-delta plain; 3) incision by headward erosion at local negative changes in gradient (e.g. highstand delta front); 4) avulsion- controlled change in discharge and activity of middle shelf distributaries and development of inner-shelf down-stepping delta lobes; 5) canyon formation by headward erosion on the outer shelf. Observations 1-4 are similar to the findings of Törnqvist *et al.* (in press) who described both deposition and erosion in the coastal prism of the Rhine-Meuse system (see also below) during the last glacio-eustatic sea-level fall.

Until connection, the experimental fluvial profile continued to grade to local base level: i.e., the extended highstand-delta front and not to the actual shoreline at the shelf edge. This explains why all experiments showed continuing aggradation in the fluvial valley on the coastal plain and inner shelf during the early phase of sea-level fall. As the sea-level fall proceeded, the aggradation was observed to diminish in the river valley and on the shelf as the knickpoint of the dominant shelf canyon approached the fluvial valley. Aggradation stopped completely after connection. At this point in time, migration of the knickpoint accelerated once it was in the confinement of the valley (e.g. Fig. 3.7b). Erosion in the valley continued until a new equilibrium profile was established (Fig. 3.5c and 6d). The rate at which the equilibrium was established depended on the amount of erosion during the preceding sea-level fall, which in our experiments was related to the rate of fall. The results are conform Schumm's (1993) assumptions that high rates of sea-level fall will cause significant channel erosion upstream, even after sea-level has returned to its original position.

The observations above support Nummedal's (1993) concept of alluviation during early sea-level fall for the common river-shelf setting, where the gradient of the fluvial valley is greater than that of the coastal plain. Such deposits are equivalent to the falling stage systems tract (Hunt & Tucker, 1992; Plint & Nummedal, 2000). We add to this concept by pointing out the importance of connection time, which marks the onset of degradation in the fluvial realm. The connection rate is an intrinsic variable of the fluvial system that relates connection time to the sea-level curve (Eq. 3.6). The connection rate illustrates that the rate of sea-level fall not only has

implications for the rate and volume of erosion on the shelf, but also for the volume of aggradational deposits in the fluvial domain, as shown by our experimental results. Consequently, a slow sea-level fall produces thicker falling-stage deposits in the fluvial valley than a fast sea-level fall (Fig. 3.12).

The connection rate depends on the geology of the substrate; the topography (including shelf width), the amplitude and period of sea-level change, and the sediment supply rate by the fluvial system. The connection rate, however, will have a lower value than locally observed knickpoint migration rates, because avulsions of distributaries determine the amount of supply and discharge to the multiple canyon heads. Therefore, in our experiments with a uniform, non-cohesive substrate, the connection rate was observed basically similar to the average knickpoint migration rate of the connecting shelf canyon. In contrast with our experiments that started with identical smooth shelf topography, real-world shelf evolution occurs less predictable, because of the effect of antecedent relief (e.g. Talling, 1998; Ricketts & Evenchick, 1999), a heterogeneous substrate, etc. (e.g. Woolfe *et al*., 1998).

Fluvial and shelfal response to sea-level rise

The experimental valley-fill sediments deposited from lowstand to early rise are composed of small, backstepping delta lobes that onlap on the main unconformity. The backstepping geometry of the transgressive valley fill and its coastal onlap are in high agreement with the general sequence stratigraphic concepts (Posamentier & Vail, 1988). It was successfully modelled in previous analogue experiments (Koss *et al*., 1994). The backstepping results from coastal retreat that forces the new base profile to intersect its former profile progressively closer to the hinterland (Quirk, 1996). In our experiments, backstepping of the shoreline and subsequent progradation of small delta lobes appears to be an autonomous process, forced by distributary shift and local supply changes within the flooded river valley and not by higher order changes in the sea-level curve. Thus, the stacked delta lobes can be designated as parasequences.

The slow-fall experiments show significant aggradation in the middle part of the fluvial valley during late rise (Fig. 3.6d). This contrasts with the model of Nummedal *et al.* (1993) that allows aggradation in the lower flooded estuary of the river close to the shoreline only. However, in our view some effects of a sea-level rise further upstream seem likely, since backfilling during a transgression of a formerly incised lower reach of a river involves re-grading of at least a part of its upstream profile (Schumm, 1993). Overall, the experimental results support the notion that the average depth of incision and the length over which the valley floor rejuvenates due to base-level fall largely exceed the average thickness and longitudinal extent of the deposits formed during the subsequent rise (Ethridge *et al*., 1998).

Examples from the Quaternary

How do we attribute river-valley stratigraphy to features like connection rate, and can this concept improve our understanding of fluvial valley stratigraphy in relation to the sea-level curve? A recent review by Blum & Törnqvist (2000) illustrates how the Quaternary alluvial plains of the Colorado and Rhine-Meuse Rivers were controlled by a complex interaction of climate and sea-level changes. Both examples are governed predominantly by sea level and climate controls, because subsidence rates on the alluvial plains were low, about 12 cm/kyr for the Holocene Rhine-Meuse (Törnqvist, 1998) and 3-4 cm/kyr for the Colorado (Blum & Price, 1998). Very analogous to our experimental results, the Colorado and Rhine-Meuse system demonstrate that aggradation occurred in the river valley during the falling stage of the last glacial lowstand, and that incision of fluvial strata occurred during the sea-level rise (Blum & Törnqvist, 2000).

The upper Colorado alluvial plain shows high gradient fluvial terraces, deposited during the falling stage, lowstand and early rise (20-14 ka), that are intersected by less steep, younger (<11 ka) terraces 80 kilometres upslope from the present shoreline (Blum, 1993). Deposition during falling stage and lowstand has been attributed to high sediment yield enabling the river to form fluvial terraces during multiple episodes of aggradation, degradation and abandonment of flood plains (Blum & Valastro, 1994; Blum & Price, 1998). A comparable reconstruction of two intersecting fluvial terraces on the Rhine-Meuse alluvial plain revealed that a high-yield, braided system resulted in predominant aggradation during the last glacial lowstand until the early rise (Törnqvist, 1998). Similar deposits are found to be preserved in the Texas Gulf Coast River systems and in the Po coastal plain (Törnqvist *et al.*, in press, and references therein). Although Blum & Törnqvist (2000) point to climate control as being primarily responsible for alluviation during relative sea-level fall, our model results suggest that forced regression can produce down-stepping fluvial terraces (alluviation) on the emerged inner shelf in conjunction with aggradation on the highstand delta plain.

A phase of aggradation on the Colorado floodplain during the sea-level rise from 20-14 ka was followed by incision, while the sea-level rise continued. Blum *et al.* (1994) suggested that the incision occurred due to diminished river loads with respect to stream capacity during early to mid-rise from 14-11 ka. The Colorado coastal plain sediments are underlain by a composite basal unconformity that corresponds in part to the lowstand systems tract and in part to the transgressive systems tract (Blum & Valastro, 1994). The same coastal prism is truncated by an erosive surface (14-11 ka) that merges with the basal unconformity upstream, which shows that the unconformity is strongly time transgressive (Blum & Price, 1998). The diachroneity along the sequence boundary complicates the correlation of fluvial strata within the influence of sea-level changes with the relative sea-level curve (Blum, 1993). Note that the diachroneity in the sequence boundary of the model stratigraphy causes similar ambiguities (Fig. 3.12). The model results thus support the notion of Blum & Price (1998) that falling stage and lowstand does not instantly result in complete bypass of the floodplain as proposed in earlier sequence models (e.g. Posamentier & Vail, 1988). However, Blum & Price (1998) regard the time lag between sea-level fall and its related incision upstream the alluvial plain as insignificant compared to the rate and

duration of the base-level fall itself. Our modelling shows how fluvial incision continues during early to mid sea-level rise (e.g. Fig. 3.5). From this perspective we suggest that incision of the Colorado alluvial plain during rise (14-12 ka) might have been promoted both by delayed headward erosion originating from the sea-level fall in combination with an increase of the river load relative to stream capacity related to climate change.

What do the analogue experiments tell us?

On a common level, the experimental results support the hypothesis that a sea-level fall does not instantly lower the downstream reach of the fluvial system (Butcher, 1990; Blum & Price, 1998; Dalrymple *et al*., 1998; Ethridge *et al*., 1998). The model clearly shows a delay between exposure of the shelf and the moment that sea-level fall induced erosion advanced to the fluvial domain. Connection time in relation to the sea-level curve is most important for understanding fluvial and basin stratigraphy in terms of genetically related sequences (cf. Butcher, 1990; Quirk, 1996).

The strong impact of the Basin response factor, Br (Eq. 3.1) on the analogue model results support the notion of Paola *et al.* (1992) that the ratio of the period of change (T) over the model's equilibrium time (T_{eq}) is extremely important. A few equations exist to estimate equilibrium times from real-world rivers. Application of present-day values for large river systems yields equilibrium times of the order of 1 to 10 kyr, but it is not straightforward to derive input values from ancient stratigraphy. However, we feel that the Basin response factor needs further exploration and refinement for the coupling among basin models themselves and with their prototypes. The strong bearing of the Basin response factor on the final analogue model stratigraphy supports the notion that comparison of Quaternary 4th order glacio-eustatic sequences with longer term eustatic sequences must be done with caution (cf. Boyd *et al*., 1989; Poag, 1992; Talling, 1998, with Blum, 1993 page 277).

A remaining question is how the sequence-stratigraphic concept applies to the fluvial valley sediments within the knickpoint reach. Delineation of our experimental stratigraphy allows a precise reconstruction of the timing of unconformity formation relative to the imposed sea-level cycle. The exercise shows that it is not straightforward to put systems tract terminology on the fluvial and even shelfal deposits that were only affected by a single sea-level cycle (Figs 3.12 and 3.13). Apparently, there are some obvious pitfalls as misinterpretation of aggradational strata that formed in the fluvial valley during the early sea-level fall. It becomes preserved as a fluvial valley-fill that seems out of phase with the sea-level change. The experiments make clear that with increasing diachroneity of the sequence boundary it is increasingly difficult to attribute systems tracts to fluvial strata. Under such conditions correlation between sediment body and position in the sea-level cycle remains speculative, despite their very suggestive names. The degree of complexity of our experimental stratigraphy demonstrates that there cannot be a simple and common rule that can correct for these out-of-phase relationships. Only absolute time-constrained stratigraphy, which is implicit in analogue model studies can elucidate on time-lag relationship in stratigraphic successions.

Conclusions

The analogue experiments with sea-level change as the only independent variable proved to be reproducible and produced statistically significant quantitative data for various rates of sea-level change. The results support the notion that neither a fall nor rise in sea level does instantly affect the upstream fluvial reaches. We have quantified this lag in system's development by the term connection delay that represents the time required to connect incipient shelf canyons on the just emerged shelf with the fluvial valley by the process of headward erosion. In order to study such delays more generally, we introduced the quantity connection rate: the ratio between shelf width and the connection delay. The Connection rate is a function of the rate of headward erosion induced by the sea-level fall. It showed a strong bearing on fluvial and shelfal stratigraphy by controlling:

1) the amount and duration of initial fluvial aggradation during sea-level fall;
2) the percentage of fluvial sediment versus eroded shelf material in the lowstand delta;
3) the volume of the lowstand delta;
4) the volume of the transgressive systems tract;
5) the amount of diachroneity along the sequence boundary.

The results support the idea that designating systems tract terminology to fluvial strata is appropriate up to the upstream limit of sea-level-fall-induced erosion (i.e., knickpoint) for small connection delays. Only absolute time-constrained stratigraphy can elucidate on time-lag relationships in stratigraphic successions.

Acknowledgements

Shell International Exploration and Production, Rijswijk, The Netherlands funded the research. We thank R. G. de Jongh and G.W.M. de Ruiter for initiating the scientific collaboration with Shell. We acknowledge the permission of Shell to publish this paper. P.L. de Boer, J. Cleveringa, W.P. van Kesteren, X.D. Meijer, T.E. Törnqvist and W. Schlager are thanked for their critical reading of an earlier version of the manuscript. At Utrecht University we are grateful to A.C. van der Gon Netcher, J.H. Bliek, P. Anten and M. Reith for their technical support and M. de Kleine for his assistance during the first series of experiments.

Chapter 4

Control of syn-depositional faulting on systems tract evolution across growth-faulted shelf margins: an analogue experimental model of the Miocene Imo River Field, Nigeria

Max W.I.M. van Heijst[1], George Postma[1], Wessel P. van Kesteren[1] and Ruud G. de Jongh[2]

1) Faculty of Earth Sciences, Utrecht University, PO Box 80021, 3508 TA, Utrecht, The Netherlands.
2) Shell Production and Development Company-Eastern Division, Port Harcourt, Nigeria.

Abstract

Syn-sedimentary growth faults on shelf-margin deltas complicate the sequence-stratigraphic interpretation of deltaic successions. Therefore, the combined effect of growth faulting, regional subsidence and eustasy on depositional architecture on a systems tract scale was studied for both hangingwall and footwall blocks by analogue flume experiment. Values for the governing variables were based on the seismic and well data of the Imo River Field in the Niger Delta, which was used as a prototype to calibrate the experimental results. The flume model was spatially scaled, with a tenfold vertical exaggeration to reconcile the different slope angles in the flume model and those of the prototype. Realistic values for time-averaged sediment transport rates with respect to the prototype were maintained. The sediment supply rate was kept constant and was scaled proportional to the gain in accommodation space due to subsidence. The spatial scale in conjunction with the supply rate results in a time scaling that allows to model basin fill processes that operated over more than 5 Million years in 90 hours of experiment. Digital topography scans were made of the model at preset time intervals to determine the bulk sediment transport.

The resultant experimental sedimentary succession at both sides of the growth-faulted shelf margin were sliced and correlated across the fault. The results were compared to the Imo River Field prototype first and subsequently to examples from the Gulf coast and from extensional basin settings. This comparison led to the formulation of a conceptual sequence model for growth-faulted margins that focuses on the systems tract distribution on each side of the fault and how it is related to eustasy. The hangingwall succession is built-up by falling stage- and lowstand, and by early-transgressive deposits. The footwall succession, in contrast, is characterised by late-transgressive, incised valley-fill and highstand deposits. The hydrocarbon trapping potential of the observed stratigraphic features in the experimental sequence model and their field analogues are discussed.

(Submitted for publication in the American Association of Petroleum Geologists Bulletin)

Introduction

Growth faulting is a common feature on shelf-margin deltas (Doust & Omatsola, 1990) and their adjacent slope and offshore regions (Damuth, 1994), where differential loading of prodelta muds and high excess pore pressures trigger the faulting process (Crans *et al*., 1980; Mandl & Crans, 1981). The faulting will cause different deformation features (e.g. rollover anticlines in the hanging-wall block) and different accommodation space histories across the growth fault, which complicates correlation and sequence-stratigraphic interpretations. For instance, onlap patterns in the hanging wall succession may be completely absent in the footwall block succession (Tobias, 1990). Similarly, the geometry of systems tracts may deviate significantly from those established for simple passive margin systems (cf. Posamentier & Vail, 1988).

Although some empirical models have helped to evaluate the problems encountered in correlation exercises of hangingwall and footwall strata (Mitchum *et al*., 1990; Howell & Flint, 1996), no common predictive model for systems tract organisation in growth-faulted, shelf-margin deltas has been developed, as yet. Sandbox models have contributed much to understanding growth-fault kinematics (McClay & Ellis, 1987; Mauduit *et al*., 1997; Mauduit & Brun, 1998; McClay *et al*., 1998), but are not suitable for the study of related depositional architecture as governed by both faulting and eustatic sea-level changes.

We studied the combined effect of growth faulting and sea-level change on the depositional architecture of shelf-edge deltas in a flume experiment. The experiment is calibrated with the Imo River Field, a well-documented, Miocene growth-faulted delta succession of the Niger delta complex. The approach is directed towards application and testing of sequence-stratigraphic principles in growth-faulted settings and the ability to evaluate the stratal patterns in terms of hydrocarbon trapping potential.

Stratigraphy of the prototype

The prototype taken is the oil-producing, Imo River Field, which shows all the common features characteristic of growth faulting (Fig. 4.1a) and has a relatively simple architecture with a major growth fault on its northern and an antithetic, counter-regional fault on its southern margin (Fig. 4.1b). Both faults enclose a hangingwall anticline as shown in Fig. 4.1c. The growth faulting coincided with deposition of the middle Burdigalian, paralic sequence and with the late Burdigalian and early Langhian paralic to continental successions. Marine, prodelta shales that form the base of the succession formed the zone of décollement (Doust & Omatsola, 1990). Subsidence rates in the Imo River Field decreased in late Langhian. The interplay of delta progradation and growth faulting typically resulted in a step-wise progradation (Knox & Omatsola, 1989), where the paralic succession becomes progressively continental, and where the prograding delta front triggers a new growth fault more basinward of the former one.

A seismic dip section through the centre of the growth fault (maximum throw) is shown in Fig. 4.2. The seismic line partly overlaps the cross-section in Fig. 4.1c. The paralic and continental successions were divided into 5 third-order sequences, numbered 1-5. The sequence boundaries have been identified by using both seismic and well data. The ages of the sequence boundaries were derived from the existing chrono-stratigraphic framework of the field shown in Fig. 4.3.

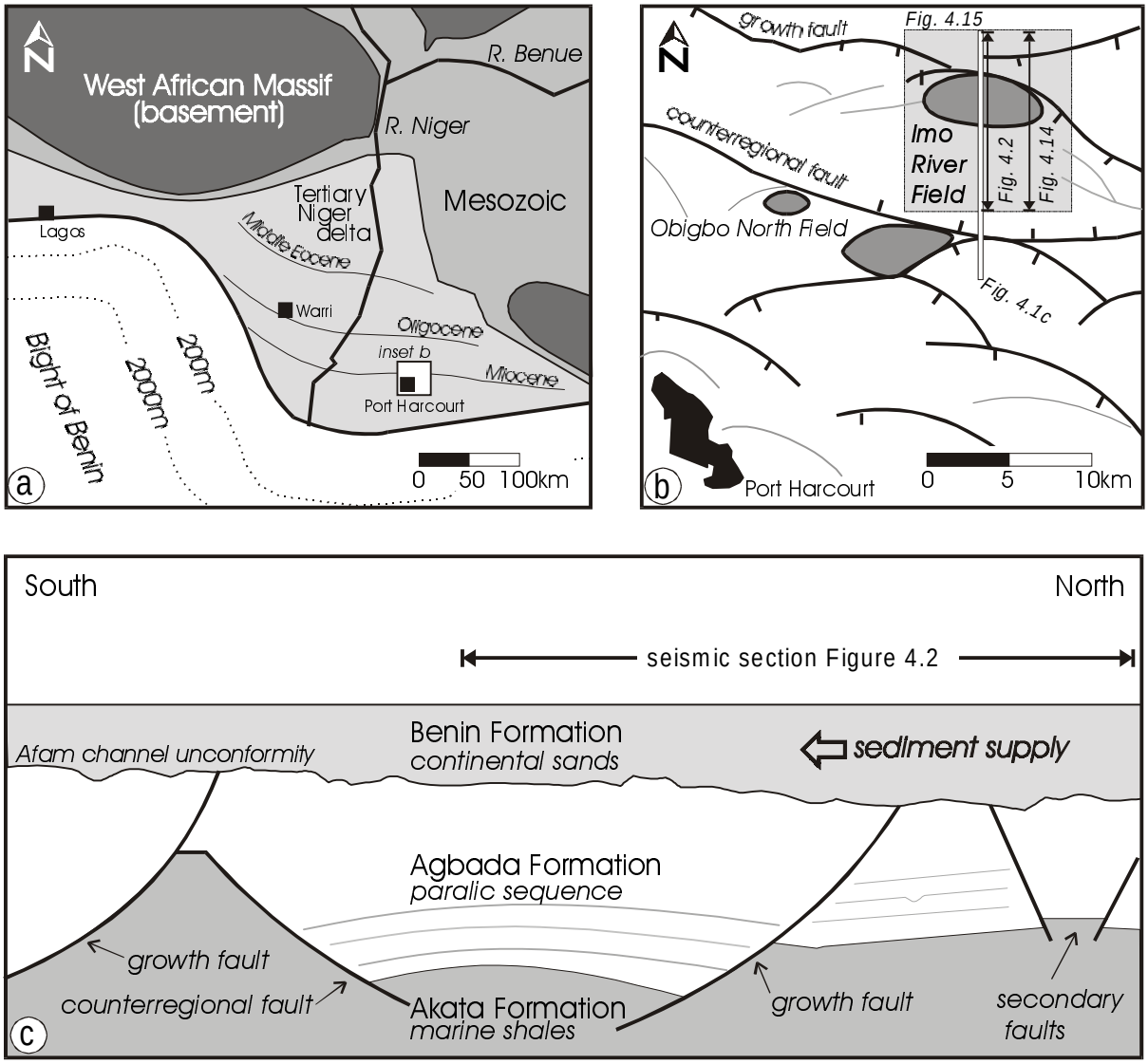

Fig. 4.1—Geologic setting of the Niger delta. (a) The delta has been progressively prograded southward since Mesozoic times, here illustrated by paleoshorelines (after Short & Stauble, 1967). The Imo River Field is located within Miocene sediments. (b) Structural setting around the field at approximately 1500 m depth. It shows the typical style of growth faulting for the Tertiary Niger Delta. (c) Schematic cross-section through the Imo River Field indicates the main stratigraphical units and primary and secondary syn-sedimentary growth faults (partly after Doust & Omatsola, 1990). Fig. 4.1b shows the position of the cross section in Fig. 4.1c and the seismic lines in Figs 4.2 and 4.14.

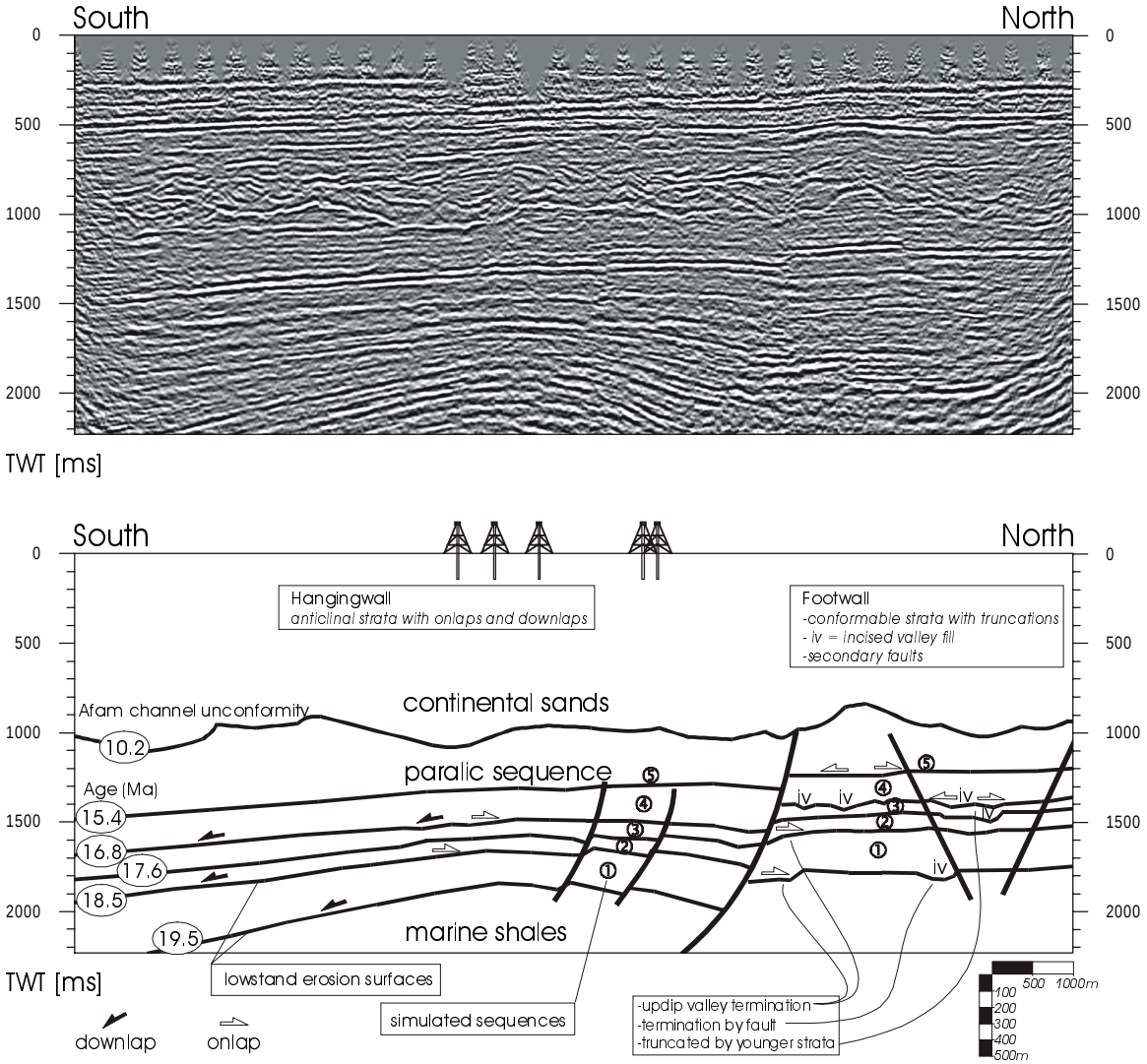

Fig. 4.2—Dip section through the centre of the growth-fault block showing paralic sequences 1 to 5 stacked in the rollover anticline of the hangingwall. The sequence boundaries were identified on the basis of well data from 5 wells indicated at the top of the interpreted line. Fig. 4.1b shows the position of the seismic line. Section courtesy of SPDC.

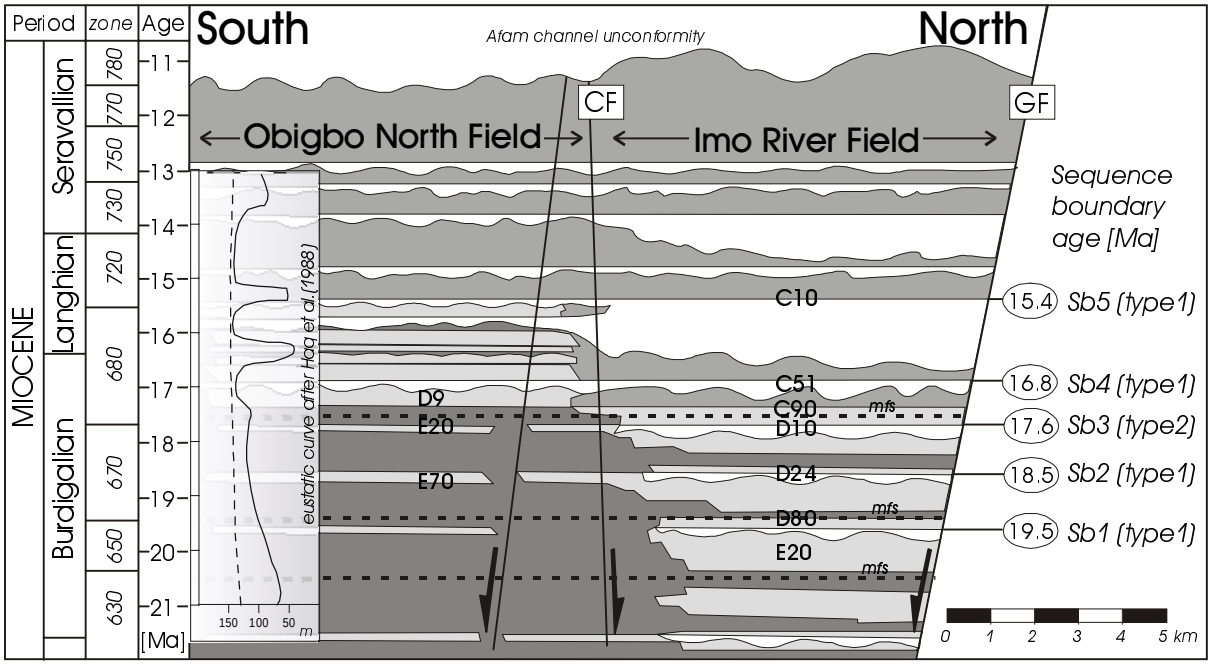

Fig. 4.3—Chrono-stratigraphic chart of the Imo River Field and the adjacent Obigbo North Field to the south. The growth fault and counterregional fault are indicated with GF and CF respectively. The chart shows the timing of the subsequent paralic (light grey) and continental successions (grey) that were deposited before, during and after the activity of the growth fault in the Imo River Field spanning the period from 21 to 11 Ma. Hiatuses are indicated in white and turbiditic basin floor sediments by dark grey shading. The graph on the left-hand side shows the eustatic curve of Haq *et al.* (1988). Chronostratigraphy courtesy of SPDC.

Experimental approach

Important boundary conditions

To simulate the Imo River Field stratigraphy in a flume tank, we have established the values for all the important parameters that control depositional architecture on both sides of the growth fault (cf. Posamentier *et al.*, 1988; Posamentier & Allen, 1993; Schlager, 1993). Since we aim to scale accommodation space and supply, the important parameters include eustatic sea-level change, regional subsidence, local subsidence by fault growth, and rate of sediment supply. For practical purposes, we define in this paper local subsidence as the subsidence of the hangingwall block produced solely by the growth faulting. For the stable footwall block, we define regional sea level that includes an amount of regional subsidence, i.e., the effects of compaction and isostatic compensation. In contrast to the footwall, the hangingwall experiences local sea-level changes that are the sum of regional sea-level changes and local subsidence of the hangingwall.

The required data (listed in Table 4.1) have been inferred from several dip sections of the seismic survey (e.g. Fig. 4.2). The model is based on the compacted thickness of the five sandy paralic and continental sequences, since compaction and isostatic compensation of the sediment and water load affect the development of depositional sequences (Embry, 1990; Steckler *et al.*, 1993). The obtained values for local subsidence are based on the amount of throw of subsequent sequence boundaries

measured in the dip sections. The values for the counter-regional fault were based on data from the adjacent field. The local sea-level curve has been designed to reproduce both the relative thickness of each sequence proportional to the hangingwall of the field stratigraphy and the type of sequence boundary (type-1 or type-2). The local sea-level variation is established by the relative position of the shoreline, which was derived from field studies (Knox & Omatsola, 1989). Subtraction of the local sea-level curve from the local subsidence curve gives the regional sea-level curve, which includes regional subsidence and thus is different from the *Haq et al.* (1988) eustasy curve (see inset of Fig. 4.3).

We used a constant sediment yield throughout the experiment. The rate of supply is chosen to just maintain paralic conditions, the amount being based on the average gain in accommodation space due to the growth faulting over all five sequences that were simulated. A constant sediment yield is not unreasonable, since the model simulated a 10x10 km area on the Niger Delta, where autocyclic (e.g. avulsions, lobe shifting) and allocyclic climatic cycles are extremely short compared to the few million years needed to fill one growth-faulted delta segment (Knox & Omatsola, 1989). Of course, the assumption of constant sediment yield is a simplification, but by reducing the number of variables we are able to determine the amount of cannibalism that is induced by the relative sea-level change.

Table 4.1. Field data derived from seismic and well-data of the hangingwall shown in Fig. 4.2.

Sequence		**Sequence boundary**			
Seq. Number	Thickness (m) on the central hangingwall	Age (Ma)	Unconformity type	Marker (Fig. 4.3)	Throw along the growth fault (m)
(1)	270	19.5	Type 1	E20	225
(2)	70	18.5	Type 1	D24	190
(3)	130	16.6	Type 2	D10	170
(4)	230	16.8	Type 1	C51	145
(5)	80	15.4 (base) 14.4 (top)	Type 1	C10 -	110 100
(1)-(5)	780m (centre) 700m (average)	19.5-14.4 Ma		Base E20 Top above C10	125m of throw during period

Experiment set-up

The experiment set-up consists of a rectangular duct (the fluvial valley) and a main tank (the basin) as shown in Fig. 4.4. On a table in the main tank a coastal plain, shelf and slope topography has been pre-moulded. One type of moderately sorted, unimodal sand with a median grain size of 250 μm was applied in the experiment. The table contained a 1x1.5 m fault window, which was lowered by a spindle construction. A rubber sheet overlying the fault window ensured containment of the sediment. A water pump re-circulated water from the main tank through the upstream end of the fluvial valley, where it entrained sediment with 10% coal dust fed by an adjustable sediment feeder. The water level in the tank was controlled by a manually adjustable overflow. The bed height in the fluvial valley was measured by using rulers spaced 10 cm apart. A laser probe with a 0.4-mm vertical accuracy scanned the bed topography in the main tank according to a 2x2-cm grid.

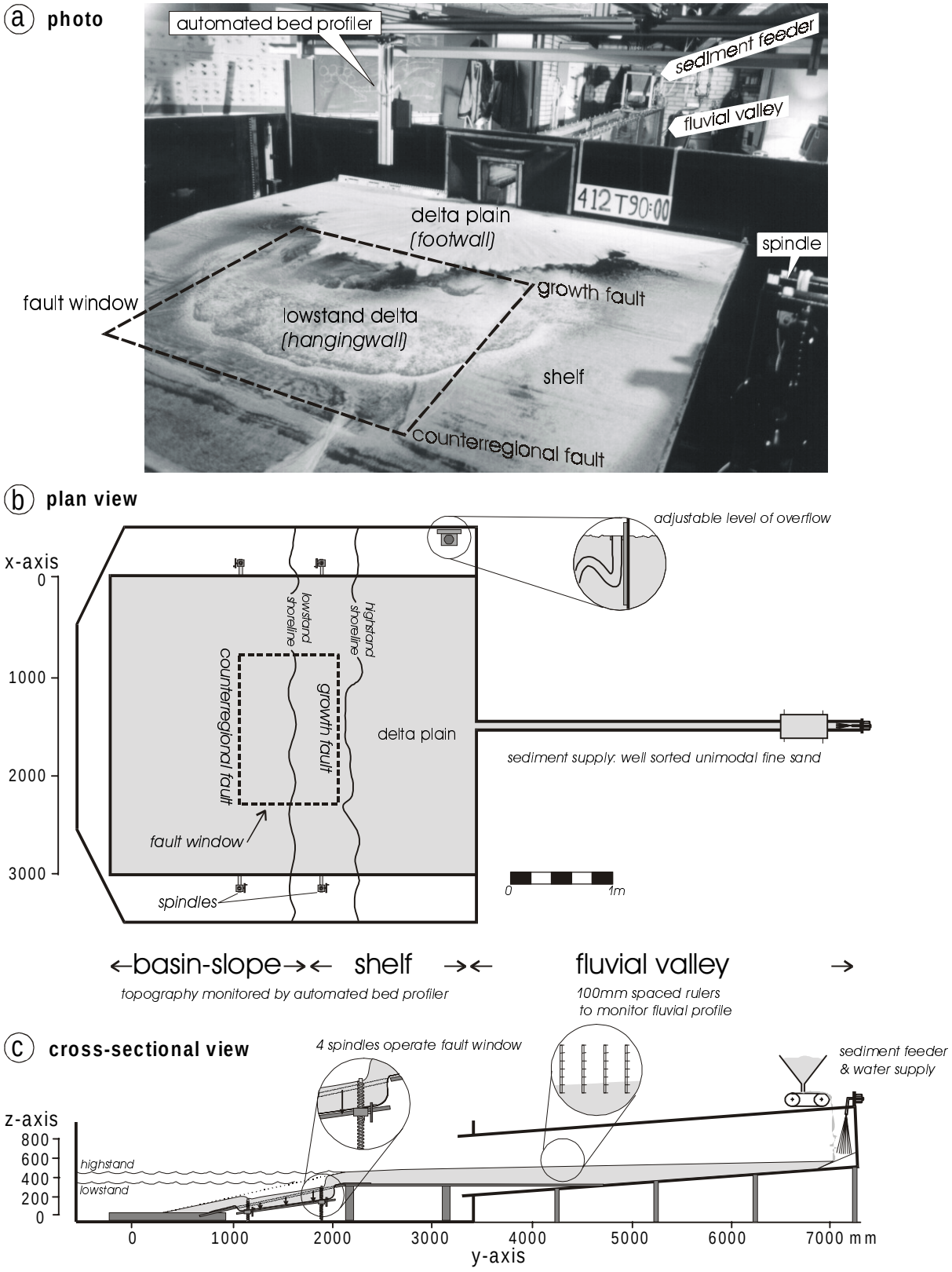

Fig. 4.4—(a) Photograph of the experimental set-up showing a water and sediment-filled basin (main tank with growth-fault window operated by 4 spindles) and a fluvial valley (rectangular duct with the sediment feeder at its up-slope end). An automated scanning device (laser) measures the topography of the sedimentary basin. (b) Schematic plan view and (c) cross-section of the experimental set-up showing the x, y and z-axis as are used as coordinate system by the automated bed profiler.

Scaling

Physical models of large-scale landscape evolution cannot be scaled according to conventional or distorted, Froude scale-modelling (Peakall *et al*., 1996). Wood *et al.* (1993) and Koss *et al.* (1994) addressed the scaling issue of large-scale, physical models and regard these as analogue models rather than true-scaled models. We aimed at adding quantitative aspects to the analogue modelling of landscape evolution and its resultant stratigraphy. Quantitative treatment of analogue models requires an alternative scaling strategy as exemplified for analogue modelling of the Quaternary Colorado river-delta evolution in Chapter 2. For this study a similar scaling approach was followed but here primarily directed towards maintaining mass balance. We maintained a constant time-averaged sediment transport rate throughout the experiment that was related to the time-averaged change in accommodation space. This means that the rate of infill (Qs) over the rate of change in the available accommodation space (Acc.) was scaled from the real world prototype (rw) to the model (exp):

$$\frac{Qs_{(rw)}}{Acc._{(rw)}} \sim \frac{Qs_{(\exp)}}{Acc._{(\exp)}} \qquad [-] \qquad (4.1)$$

Where Qs is the time-averaged volumetric sediment transport rate determined by a volume of displaced sediment ΔV over a time span ΔT:

$$Q_s = \frac{\Delta V_{(rw)}}{\Delta T_{(rw)}} = \frac{\Delta V_{(\exp)} \cdot \left(\lambda_x \cdot \lambda_y \cdot \lambda_z\right)}{\Delta T_{(\exp)} \cdot \left(\lambda_t\right)} \qquad [L^3/T] \qquad (4.2)$$

The scaling factors λ operate on the spatial dimensions (x-y-z) and the time (t). The appointed values for the scaling factors are listed in Table 4.2.

Horizontal dimensions of sediment storage rooms (i.e., fluvial valley, delta plain, shelf and slope) are scaled according to a ratio $\lambda=10^4$ (Table 4.2a). For applied discharge and sediment supply we obtained an equilibrium profile in the flume valley of 0.025, about ten times steeper than that of the Niger River (Table 4.2b). The slope gradient in the flume is about ten times steeper, which implies ten times vertical exaggeration and a scaling ratio of $\lambda=10^3$ for the vertical dimension (Table 4.2c). The accommodation space resulting from growth faulting must be balanced by sufficient sediment supply to maintain paralic environmental conditions as inferred from the field data (i.e., honouring Eq. 4.1). From the known constant sediment supply rate at the outlet of the fluvial valley it follows that 90 hours runtime is required to compensate for the 0.1 m^3 gain in accommodation space by growth faulting (Table 4.2d-2f). Hence, 6.1 Ma of depositional history (paralic sequences 1 to 5) scaled by 90 hours means a time-scaling ratio of 5.9×10^8. The time scaling implies that the model's equilibrium time (~10 hours see Chapter 2) is less than the duration of an imposed sea-level cycle. This approximately matches the prototype conditions of a Miocene shelf margin delta of tens of kilometres in size with an equilibrium time of about 0.1 Ma controlled by third order eustatic changes and local subsidence.

Table 4.2. Characteristics of the prototype and the model over the modelled period.

a) Horizontal scaling / dimensions $\lambda_x=\lambda_y=1 \times 10^4$	**Imo river Field**	**Model**
Length of coastal plain	12 km	1200 mm
Spacing between both faults	10 km	1000 mm
Size of the hangingwall block	10 x 15 km	1000 x 1500 mm
Shelf width	20 km	2000 mm
Unit width of modelled area	30 km	3000 mm
b) Slopes $\lambda_s=10$	**Imo River Field**	**Model**
Gradient of the outlet of the fluvial valley	S=0.002 (~0.01°)	S=0.025 (~1.5°)
Paleodip of coastal plain/shelf	S=0.004 (~0.2°)	S=0.04 (~2°)
Paleodip of the delta slope	S=0.02 (~1°)	S=0.2 (~10°)
c) Vertical scaling $\lambda_z=1 \times 10^3$	**Imo River Field**	**Model**
Amplitude of sea-level changes	80 m (Haq *et al*., 1988)	80 mm
Overall sea level rise (2nd order transgression)	40 m	40 mm
Total throw of growth fault	120 m	120 mm
Total throw of counter regional fault	80 m	80 mm
d) Sediment supply and discharge	**Present Niger Delta**	**Model**
Sediment load of the fluvial system	1015 kg/s (Allen, 1997)	sand: 1.80 kg/h~1.0 dm^3/h coal: 0.05 kg/h~0.15 dm^3/h
Sediment transport rate	0.58 m^3/s	total load = 1.15 dm^3/h (~3.19 x 10^{-7} m^3/s)
D50; median grain diameter	250 µm (Allen, 1965) mouthbar sands	sand 250 µm coal 400 µm
D90; ninety percentile grain diameter	500µm (Allen, 1965) mouthbar sands	sand 700 µm coal 670 µm
Discharge	6020 m^3/s (Allen, 1997)	400 dm^3/h (~1.1 x 10^{-4} m^3/s)
Channel depth	2-20 m	6-10 mm
H/D90 for bed-load transported sand		6 / 0.7 mm > 8
e) Accommodation space on hangingwall	**Imo River Field**	**Model**
Estimated volume of sequences 1-5 on hangingwall	1.05x10^{11} m^3 (= 105 km^3) (700 x 10000 x 15000 m) *average thickness of 700 m for seq. 1-5 on the hanging-wall is based on Table 4.1*	0.10 m^3 *volume of fault window*
f) Time scaling $\lambda_t=5.9 \times 10^8$	**Imo River Field**	**Model**
Middle Burdigalian – Langhian (Pollen zones P670 and 680)	19.4-13.4 Ma *time span of 6.1 Ma*	0-90 hours
g) Time averaged sediment-flux per unit width	**Imo River Field**	**Model**
$Q_s = \frac{\Delta V_{(rw)}}{\Delta T_{(rw)}} = \frac{\Delta V_{(\exp)} \cdot (\lambda_x \cdot \lambda_y \cdot \lambda_z)}{\Delta T_{(\exp)} \cdot (\lambda_t)}$	$= \frac{1.05 \times 10^{11}\, m^3}{6.1 Ma}$	$= \frac{0.10\, m^3}{90 h} \cdot \frac{\lambda_x \cdot \lambda_y \cdot \lambda_z}{\lambda_t}$
Note that there is near a factor ten difference between the total flux divided by the total time for prototype and experiment (see discussion section).	$Qs_{(rw)}$ = 5.46 x 10^{-4} m^3/s	$Qs_{(exp)}$ = 5.23 x 10^{-5} m^3/s
h) Wave regime	**Present Niger delta**	**Model**
Wave period	5-12 s (Allen, 1965)	1 s
Wave length	40-225 m (Allen, 1965)	100-300 mm
Wave height	0.9-1.8 m (Allen, 1965)	8-12 mm
Sediment transport rate by waves	-	1.3±0.3 x 10^{-7} m^3/s

We modelled time-averaged sediment flux by bed-load transport over a uniform substrate. By scaling the dimensions and time, we assume that the time-averaged sediment flux in model and prototype are about of the same order. However, the time-averaged sediment flux in model and real world are expected to deviate owing to differences in substrate erodability and transport efficiency. The actual value differed nearly by a factor ten as shown by the calculation in Table 4.2g. It must be noted that this is an overall value for the full duration of the experiment; the discrepancy for the first two cycles of the experiment is actually less as will be discussed later.
While scaling time by the amount of volume displacement over a given period of time and while relaxing the hydraulic scaling conditions (Peakall *et al*., 1996), it is still important to maintain realistic Froude numbers. Bedforms are undesired because these change the apparent bed roughness and effect the sediment flux. We applied low current velocities (lower flow regime, $Fr < 0.8$) to avoid bedform formation in the flume, but yet sufficiently high to transport the unimodal, moderately sorted medium sand. The ratio of the ninety percentile grain diameter over water depth was approximately 7-10 (see Table 4.2d), which kept partial sorting of coarse size grades to a minimum (e.g. Middleton & Southard, 1984).

Shelf erosion by waves is an important process, which results in planing of the shelf during transgression. Planing by waves may wipe out antecedent valleys and cause a change of feeder conduits to the hangingwall block. Therefore, waves may not only have a strong control on the development of the transgressive systems tracts, but also on the architectural development of subsequent sequences and their internal organisation (i.e., stacking and volume of systems tracts). To incorporate the shelf planing process, we used a wave generator that produced small waves during the sea-level rise. Instead of scaling the physical properties of waves, we scaled the wave-induced sediment transport to values lying between half and one third of the fluvial transport (Table 4.2h).

Experimental procedure

The values of the imposed variables in the experiment are shown in Fig. 4.5. The reconstructed throw of the growth fault in the Imo River Field (dashed line in Fig. 4.5a) is modelled by lowering the fault window according to the solid lines in the same graph. Fig. 4.5b shows two sea-level curves: one local sea-level curve for the hangingwall that includes the fault throw (local subsidence) and one regional sea-level curve for the footwall block The water-level change in the basin was imposed according to the sinusoidal regional sea-level curve of Fig. 4.5b by adjustment of the overflow pipe every 15 minutes. The sediment feeder was adjusted to supply a dry volume of one litre of sand and 0.15 litre of coal powder per hour runtime (properties in Table 4.2d). The much lower density of the coal powder makes it a surrogate for suspension load, which settles only in very low-energy environments. The sand is transported as bed load. Subsidence of the fault window was invoked by adjustment of the spindles in 1-mm steps according to the local subsidence curve (see Fig. 4.5a).

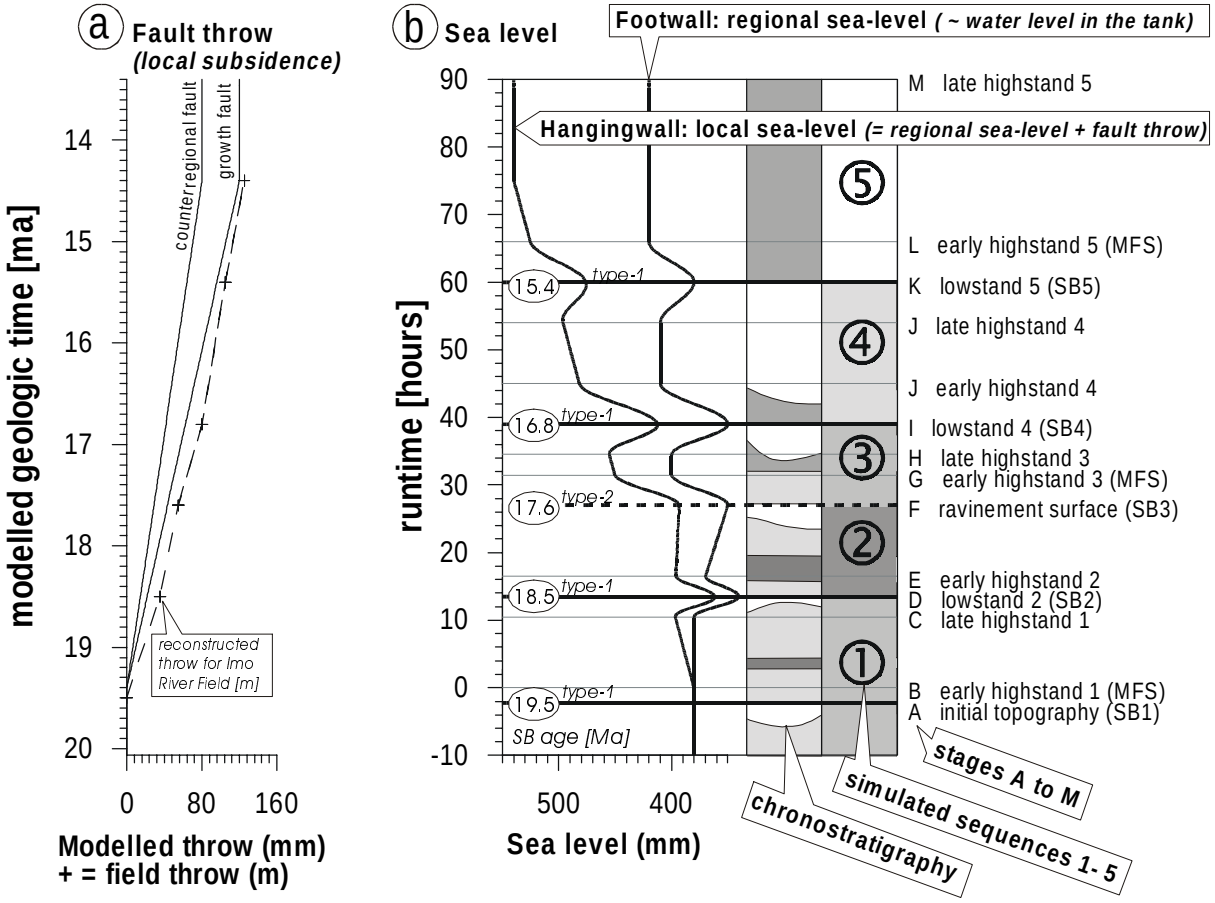

Figure 4.5—The experimental scenarios of fault throw, regional and local sea level. The left axis in geologic time (Ma) corresponds to the right axis in runtime (hours). (a) Graphs of the applied throw rates of the experimental fault window (solid lines). The dashed line shows the reconstructed throw of the main growth fault of the Imo River Field for comparison. (b) Graph of imposed sea-level changes. The right curve shows the water-level changes in the main tank (regional sea level) and applies to the footwall block. Note that the curve includes an overall rise to account for regional subsidence. The left curve is the sum of regional sea level and local subsidence of the fault window and thus shows the local sea-level changes as experienced by the hangingwall.

In accordance with the Imo River Field conditions at around 19.5 Ma, the experiment was started with the shoreline positioned at the shelf break. Under equilibrium conditions, the sediment supply rate at the downstream end of the fluvial valley equalled the applied constant sediment supply rate of the feeder. Therefore, an initial ten-hour run with constant water level was conducted prior to stage A to establish an equilibrium stream profile in the fluvial valley. The experiment was paused at each stage A to M depicted in Fig. 4.5 to allow the laser probe to scan the sediment surface. Before each scan the water table was lowered. Tracers were evenly spread over the topography after each scan and the water level was subsequently raised carefully to avoid disturbance of the bed. Both faults reached their respective maximum amount of throw after 75 hours runtime. The experiment continued for another 15 hours in order to preserve the most recent incised valley sequence and to finish the succession with a highstand systems tract.

Results

Table 4.3 summarises the large-scale sedimentary development of each systems tract as found by the experiment. The left column indicates the various development stages denoted by the capitals A to M in Fig. 4.5. The same stages are also indicated in Figs 4.6 to 4.8. A selection of photographs of the experiment is shown in Fig. 4.6. A sequence of topographic scans in Fig. 4.7 illustrates the progressive, volumetric and morphological evolution of the modelled, growth-faulted margin for each stage.

The experiment consists of four sea-level cycles. Each cycle shows a similar timing of drainage evolution on the experimental shelf-margin delta. All highstand episodes result in delta progradation. Stream avulsions at the delta apex cause a steady progradation of the entire delta front. During the subsequent sea-level fall, a number of incisions (canyons) initiate on the exposed delta front and start to erode headward towards the apex of the highstand delta (Stages C and K in Figs 4.6 and 4.7). The canyons cut down progressively up to base profile and funnel the fluvial load plus the freshly eroded shelf sediment to the lowstand wedges. Near lowstand, one of the shelf canyons connects with the fluvial valley while the others cease to be used. During sea-level rise, small back-stepping lobes are deposited inside the antecedent lowstand drainage network (incised valleys), while the abandoned valleys shows only wave reworking (see Stage D and L in Fig. 4.6). Note that stage F, which was intended to model a type-2 unconformity differs from the other eustatic lowstands: no distinct incised valleys developed during stage E and the subsequently formed transgressive systems tract covered the entire delta (Stage F in Figs 4.6 and 4.7). Generally, the deposition of the transgressive systems tract follows the retreating shoreline. At late rise to highstand, the retrogradation changes into aggradation resulting in restoration of the incised highstand delta on the footwall. During late highstand the delta progrades, down-lapping on the previous late transgressive deposits on the footwall.

Table 4.3. Experiment observations. The stages A to M apply to Figs 4.5, 4.6, 4.7 and 4.8.

Time span, h (stage)	Observations	Systems tract	Sequence
(-10 - 0) **(A)**	Preparation run establishes fluvial equilibrium profile after 6 hours	HST 1 (highstand)	
0 - 10.5 **(B)**	The fluvial equilibrium profile extends due to highstand progradation and develops a large radial delta with graded plain profile.		Seq. 1 *(prog.)*
10.5 - 13.5 **(C)**	Two hours before lowstand, two channels incise the delta plain and develop two lowstand deltas (stage C in Figs 4.6 and 4.7).	FSST 1 (falling stage)	
13.5 - 16.5 **(D)**	A thin aggradational sediment pile covers the lowstand delta at early rise. After one hour of rise, small backstepping lobes fill the main channel. Waves form a ravinement surface on the right part of the delta (stage D in Figs 4.6 and 4.7). At 16 hours runtime the delta shifts from retrogradation to highstand progradation (first downlap).	LST2 (lowstand) & TST 2 (transgressive)	Seq. 2
16.5 - 27 **(E)**	Highstand progradation widens the delta plain. Local erosion and wave reworking flattens the lower delta plain because relative sea level on the hangingwall was kept constant during this stage. A shelf margin systems tract is deposited at the delta toe (stage E in Figs 4.6 and 4.7).	SMST 2 (shelf margin)	*(prog.)*
27 - 31.5 **(F)**	Small backstepping delta lobes overlie the wave ravinement surface. The transgressive systems tract covers the entire delta plain over its full width, in contrast to the previous transgression (stage F in Figs 4.6 and 4.7).	TST 3 (transgressive)	
31.5 - 34.5 **(G)**	Highstand progradation proceeds at slow rate on footwall block while a condensed sequence forms on hangingwall (Stage G in Fig. 4.7).	HST 3 (highstand)	Seq. 3 *(aggr.)*
34.5 - 39 **(H)**	The progradation rate increases, as the sea level lowers again. The right and middle part of the delta plain is progressively being incised (stage H in Fig. 4.7). Two lowstand deltas initiate at the middle and right part of the delta toe. *Note that incision now takes place on the right part of the delta plain which was unaffected during cycle 1.*	FSST 3 (falling stage)	
39 - 45 **(I)**	After a short period of aggradation, backstepping delta lobes form in the previous lowstand channel. Transgressive systems tract covers nearly 60% of the delta, mainly the middle and right part (stage I in Fig. 4.7).	LST4 (lowstand) & TST 4 (transgressive)	
45 - 54 **(J)**	A phase of highstand progradation fills the antecedent valleys on the footwall block. The delta radius increases. The hangingwall is sediment starved (Stage J in Fig. 4.7).	HST 4 (highstand)	Seq. 4 *(retrogr.)*
54 - 60 **(K)**	At 55 hours runtime highstand progradation changes into incision of the delta plain (footwall). Two valleys on the middle-left part and right part of the delta supply two lowstand wedges on the hangingwall (stage K in Figs 4.6 and 4.7). *Note that the incisions on the delta plain are located adjacent to the previous lowstand channel and transgressive valley-fill sequence.*	FSST 4 (falling stage)	
60 - 66 **(L)**	Small backstepping delta lobes fill both lowstand channels. Waves rework the right hand side of the delta front, (stage L in Figs 4.6 and 4.7).	LST5 (lowstand) & TST 5 (transgressive)	Seq. 5
66 - 90 **(M)**	Highstand progradation proceeds very slowly; it takes until 73 hours runtime before the toe of the highstand delta downlaps on the hangingwall sediments. At 75 hours runtime subsidence stops. Ultimately the toes of the highstand delta progrades over the head of the previous lowstand delta on the hangingwall (stage M in Fig. 4.7).	HST 5 (highstand)	*(retrogr.)*

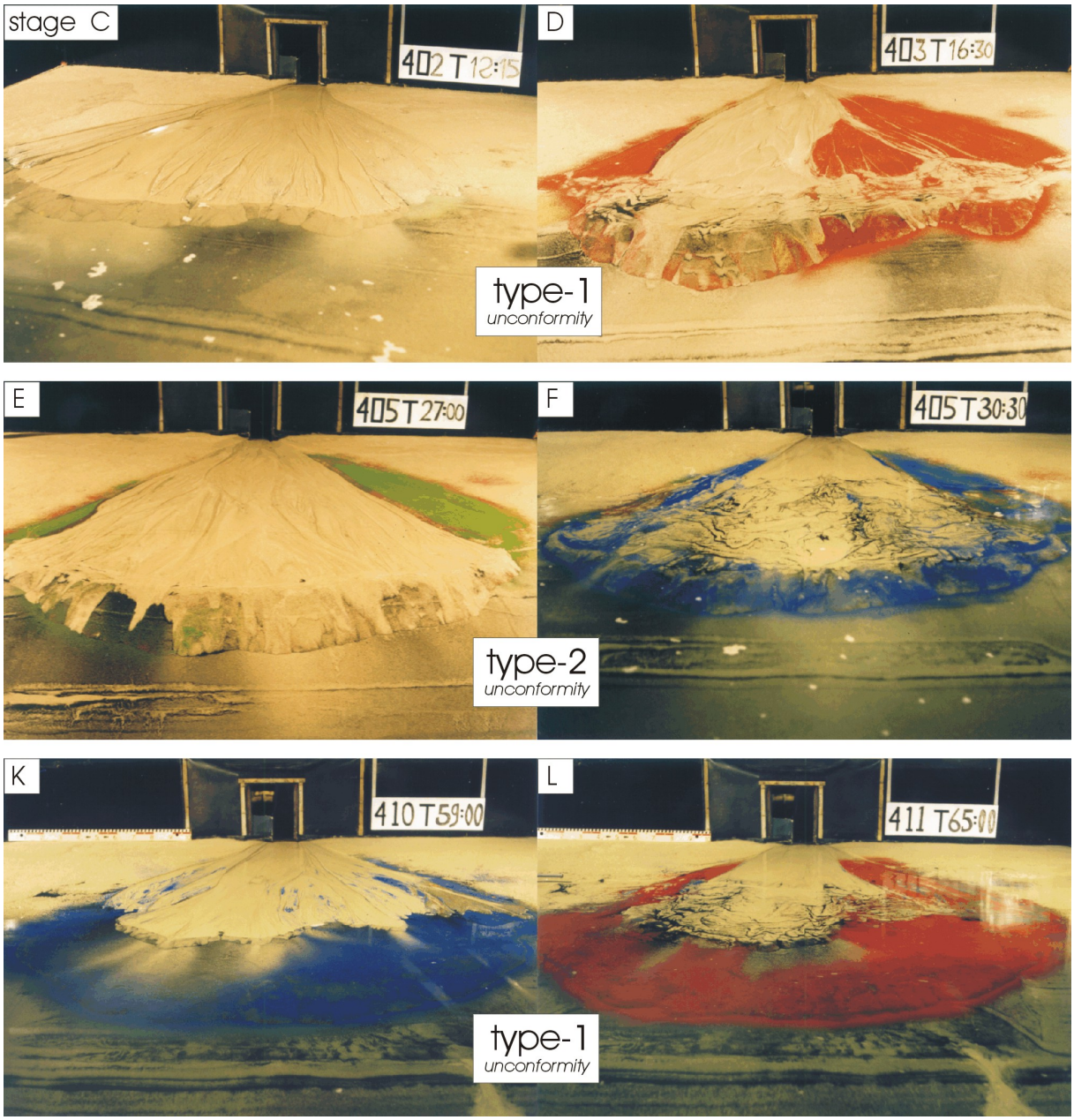

Fig. 4.6—Photographs of successive experiment stages taken from the distal part of the experimental tank, looking in the direction of the downstream end of the fluvial valley. The runtime (T hours: min) is indicated on the upper right. A 1m-scale bar is shown at stages K and L. The layers of tracers that mark each stage are coloured. Coal dust, supplied together with the sand, enhances the sedimentary structures and acts as a surrogate for fines that are carried in suspension. Note that the slope becomes progressively darker throughout the experiment owing to the suspension load of the coal dust. Observations of the experiment per stage are listed in Table 4.3. Stages D to E and stages K to L show the formation of a type-1 unconformity: incision of a single valley on the delta that is subsequently filled with backstepping delta lobes during transgression. During stage E a type-2 sequence boundary with a wave ravinement surface formed. Note that no distinct incision took place and that the subsequent transgressive systems tract covered the entire delta in absence of antecedent valleys.

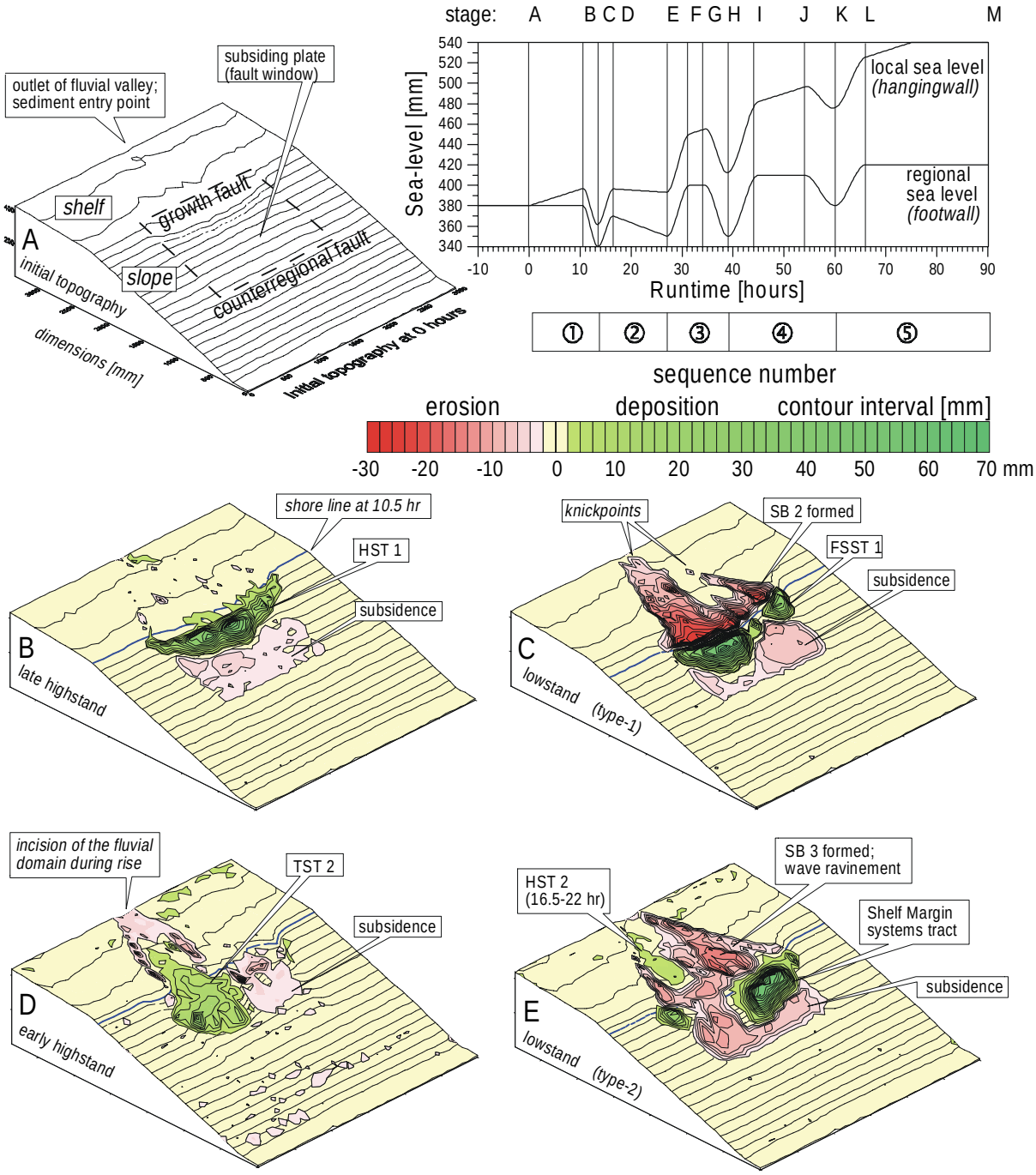

Fig. 4.7—Block diagrams of topographical scans showing the volumetrical and morphological evolution of the analogue delta complex monitored at each time step A to M. The sequence of block diagrams starts with the initial topography at time A (upper left). Diagram B shows topography at stage B with a graded colours-contour map of erosion and deposition plotted on top (here for the time span from stage A to B). The depositional (green) geometries represent the distribution and thickness of systems tracts. Red contour intervals represent negative deposition caused by erosion or subsidence of the fault window. The blue line indicates the shoreline position. SB = sequence boundary; FSST1 = falling stage systems tract of sequence 1; TST = transgressive systems tract; HST = highstand systems tract.

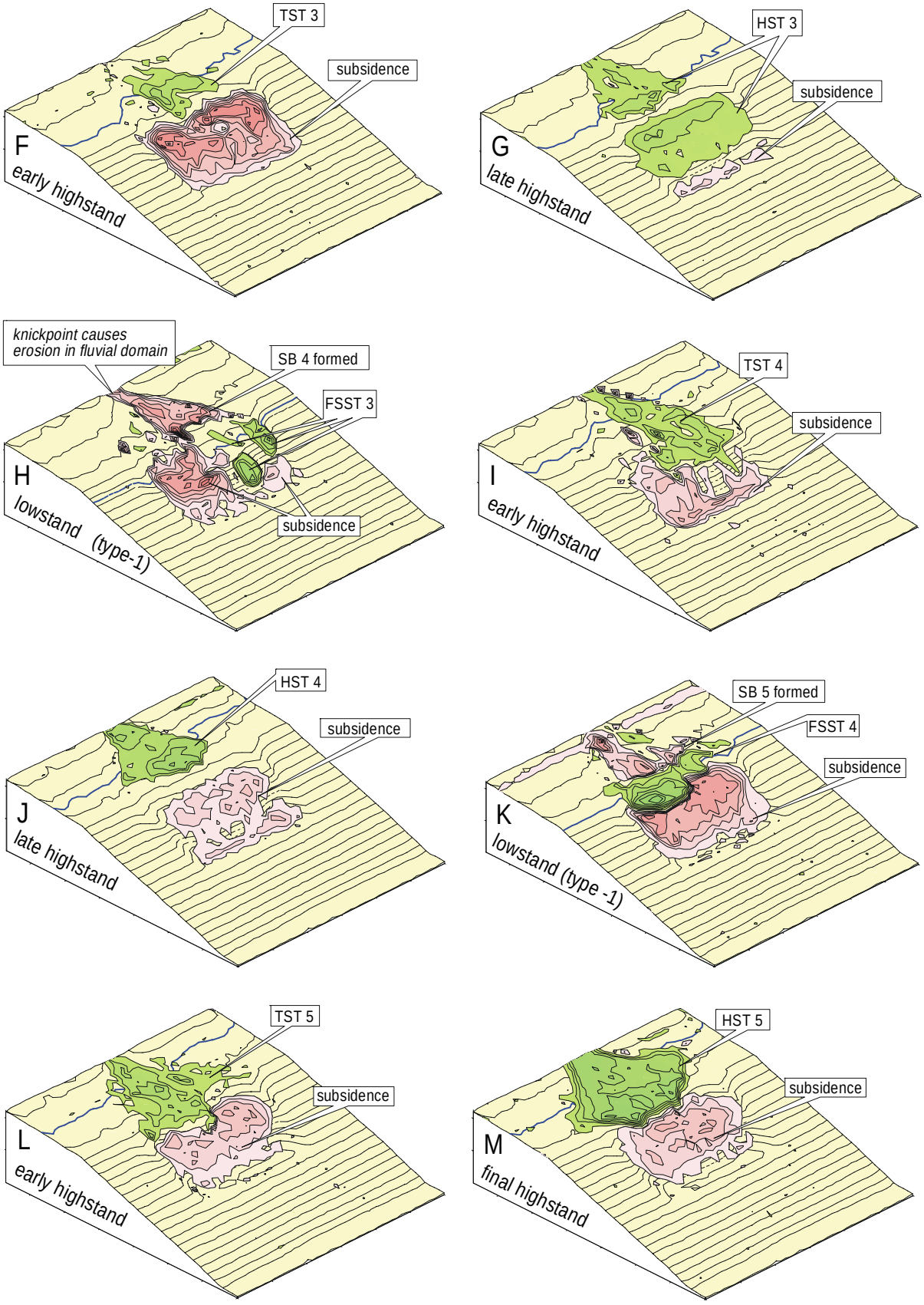

Fig. 4.7—Continued.

Figure 4.8 depicts curves of the applied variables (graphs a and b) against the timing of sediment supply to the hangingwall (c) and shoreline changes (d). Figure 4.8e evaluates the total amount of sediment introduced by the fluvial valley to the main tank and the total amount of increase of accommodation space caused by the growth faulting. Both volumes were calculated from the scans. Note that during stages E to H, accommodation space by subsidence increased rapidly, even though the fault window was lowered at a constant rate. Both curves in Fig. 4.8e show that halfway through the experiment, supply temporally lagged behind the increase in accommodation space. Figure 4.8f quantifies measured sediment fluxes. The fluvial sediment flux to the main tank varied during the first stages of the experiment, probably owing to temporal aggradation and erosion in the lower fluvial reach (cf. Stage B and D in Fig. 4.7). However, fluvial supply became constant at a value of 1.15 dm^3/h after stage E. Footwall erosion coincided with each lowstand in sea level and, therefore, appears to be eustatically driven. The modelled type-2 sequence boundary (stage E) showed no significant footwall erosion. Footwall cannibalism during type-1 unconformity formation contributes to a temporal increase in sediment flux to the hangingwall of 1.5 to 2 times the average fluvial sediment supply rate (Fig. 4.8f). The peaks of footwall deposition in Fig. 4.8f are contemporaneous with stages of highstand progradation and are, consequently, out of phase with the peaks of footwall erosion.

>>> next page: Fig. 4.8—Experiment observations compared with the imposed fault throw and relative sea-level changes. (a) Imposed subsidence curve of the growth fault and the counter-regional fault. (b) Applied regional sea-level curve (water level) that applies to the stable footwall block. The local sea-level curve is the sum of fault throw (local subsidence) and regional sea-level change and applies to the hangingwall. (c) Episodes when the down-thrown block received sediment. (d) Observed changes in shoreline migration. (e) The total volume of accommodation space added by subsidence (grey) and the observed sediment supply from the fluvial valley to the basin (dark grey). Both curves were calculated from the scans and illustrate in retrospect to what degree the hangingwall subsidence was compensated by the sediment supply. Note that in spite of lowering the experimental fault window at a constant rate, the observed rate of accommodation space increase is not constant, but shows a rapid positive increase from stage A to H. (f) Quantification of sediment fluxes. The fluvial sediment supply varies during the first part of the experiment and lingers around 1.15 dm^3/hour since stage E. Peaks of footwall erosion seem related to sea-level lowstands that created type-1 unconformities. Footwall cannibalism contributes a 150 to 200% increase of sediment flux to the hangingwall with respect to the average fluvial supply rate. Footwall deposition shows maximum values during episodes of highstand progradation.

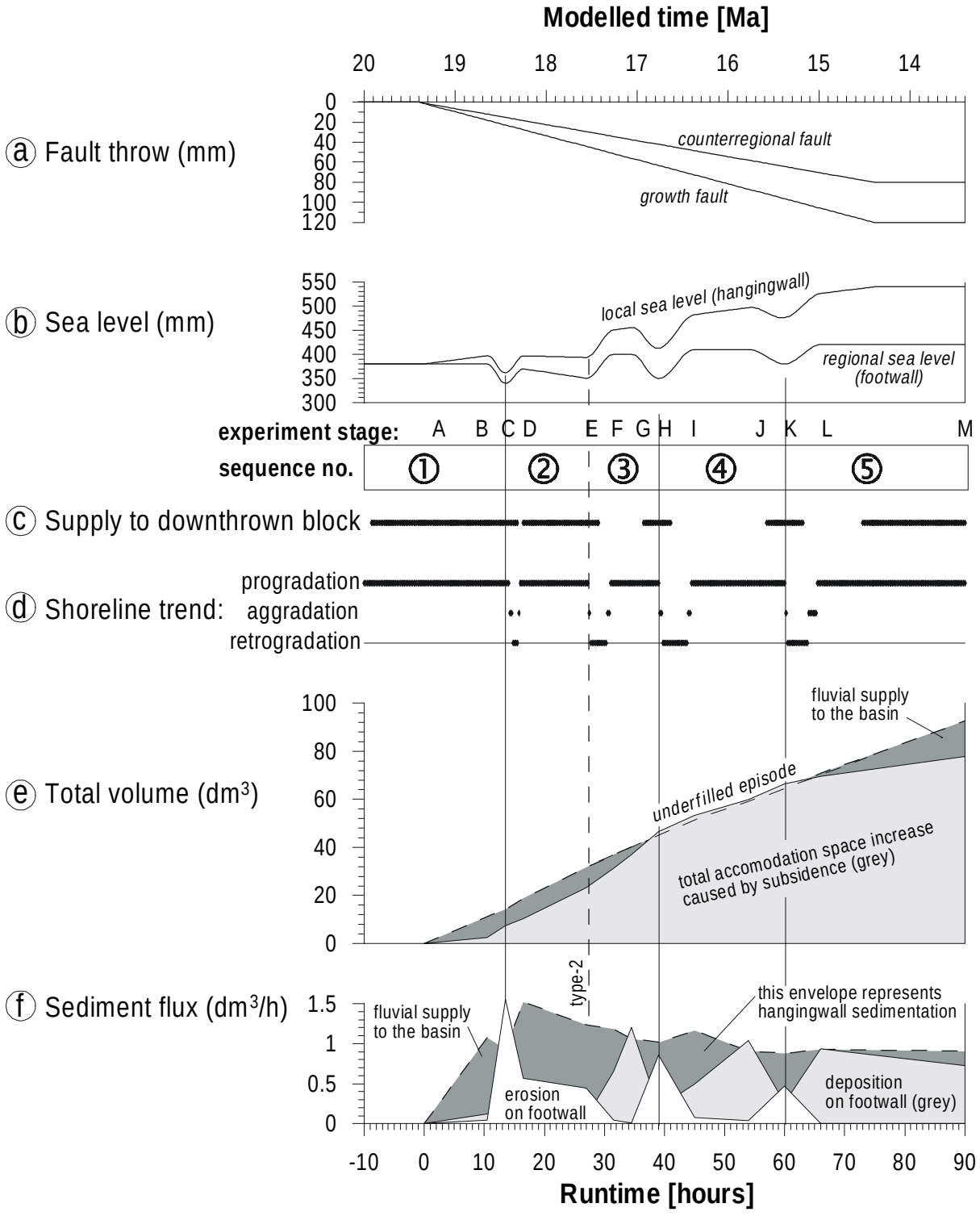

Fig. 4.8—Quantification of the experiment results (see previous page).

The resultant stratigraphy was sampled by means of lacquer peels, of which the locations are shown in Fig. 4.9. Peels A1 to A11 are radial sections that run from the valley outlet (apex) towards the basin. Peels F and H run shore parallel over the footwall and hangingwall respectively. The applied tracers and the coal powder aided in unravelling the complex stratigraphy and sedimentation patterns across the growth-fault zone on all lacquer peels. A selection of lacquer peels and their interpretations are shown in Figs 4.10-4.13. Comparison of the footwall with the hangingwall stratigraphy shows that the model comprises a high degree of spatial variability and suggests that both the location and dimension of incised valleys on the footwall correlate with both location and thickness of the lowstand fan in the hangingwall section (Fig. 4.13).

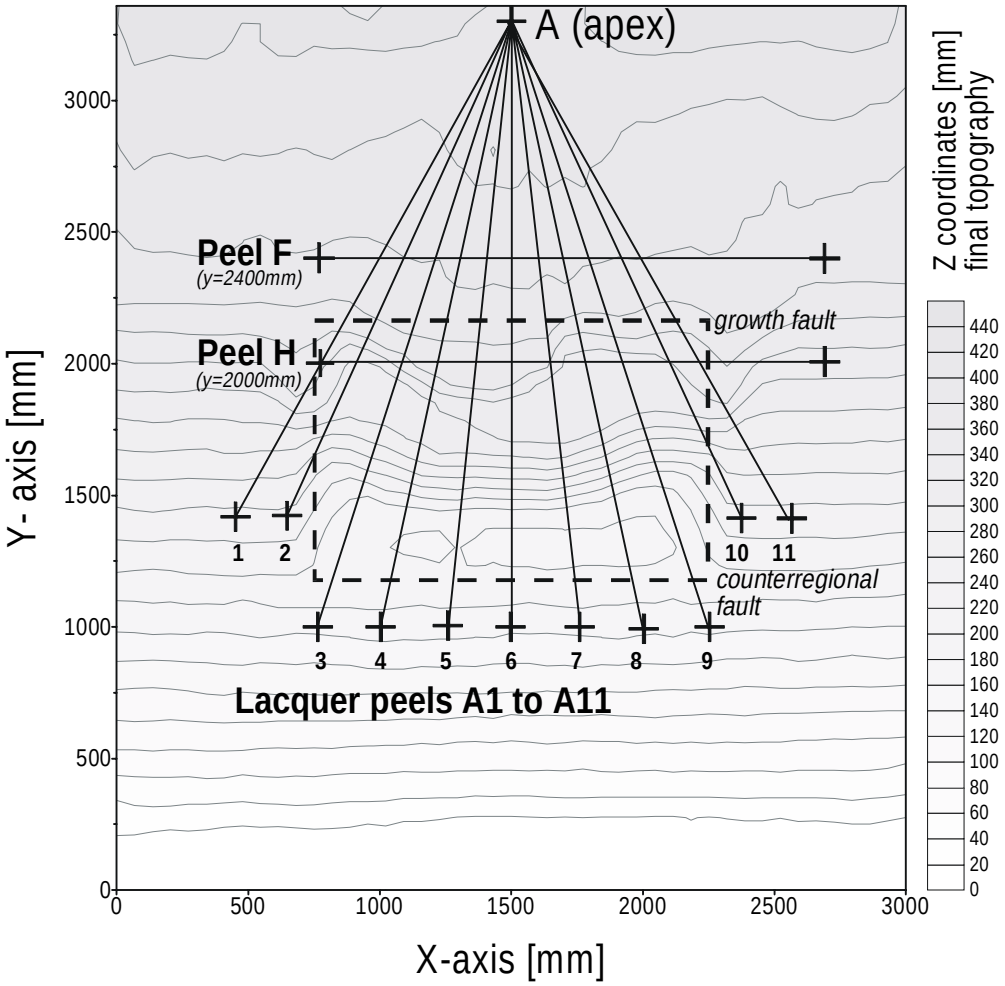

Fig. 4.9—Contour map of the experiments final topography with the locations of 11 lacquer peels (radial cross sections A1 to A11). Two parallel strike lacquer peels F (footwall block) and H (hanging wall block) are positioned at coordinates Y=2000mm and Y=2400mm, respectively.

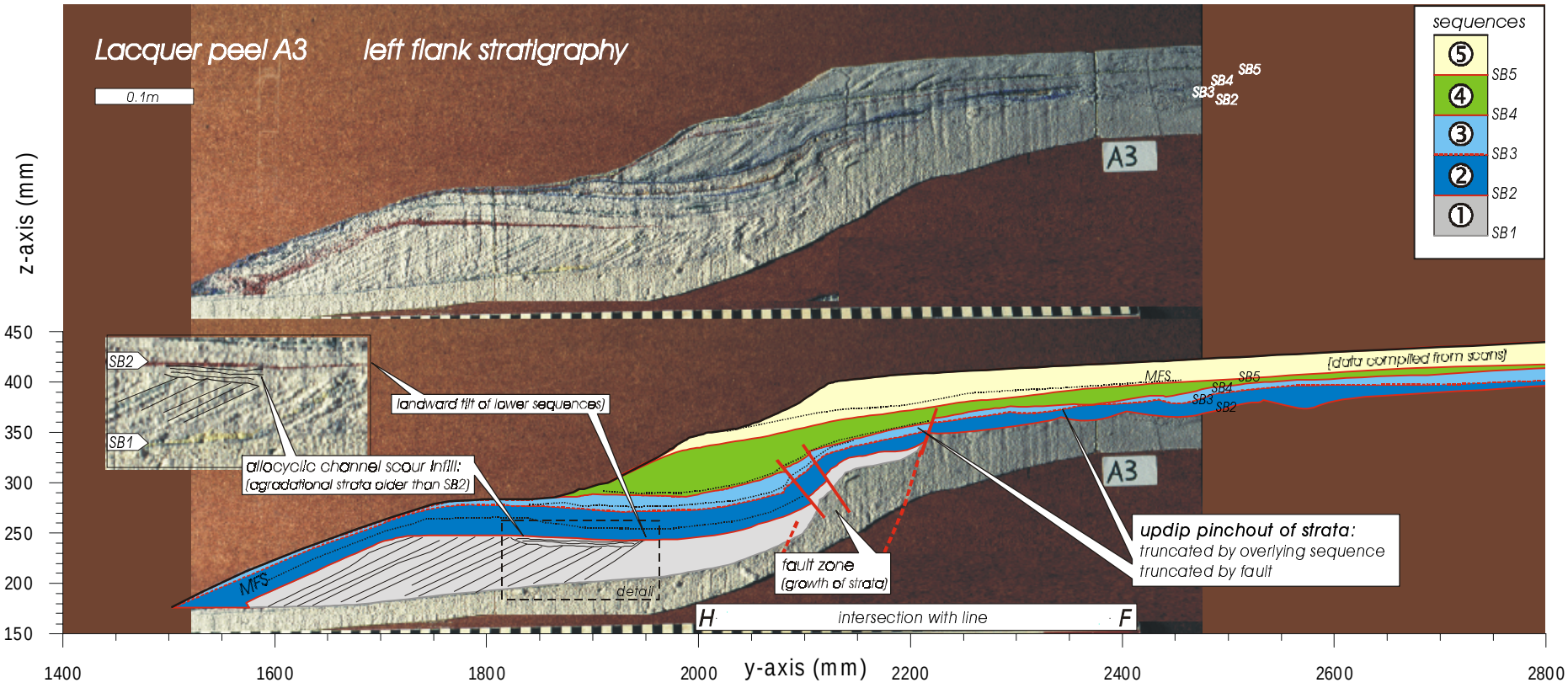

along y and z-axes refer to the basin location (compare block diagrams in Fig. 4.7). The lower interpreted section shows both the fault zone, the landward tilting of hangingwall strata and the preservation of incised valley fills on the footwall. Note that sequence 2 is best preserved along this section. The aggradational strata just below SB2 on the hangingwall are interpreted as allocyclic channel scours formed at lowstand.

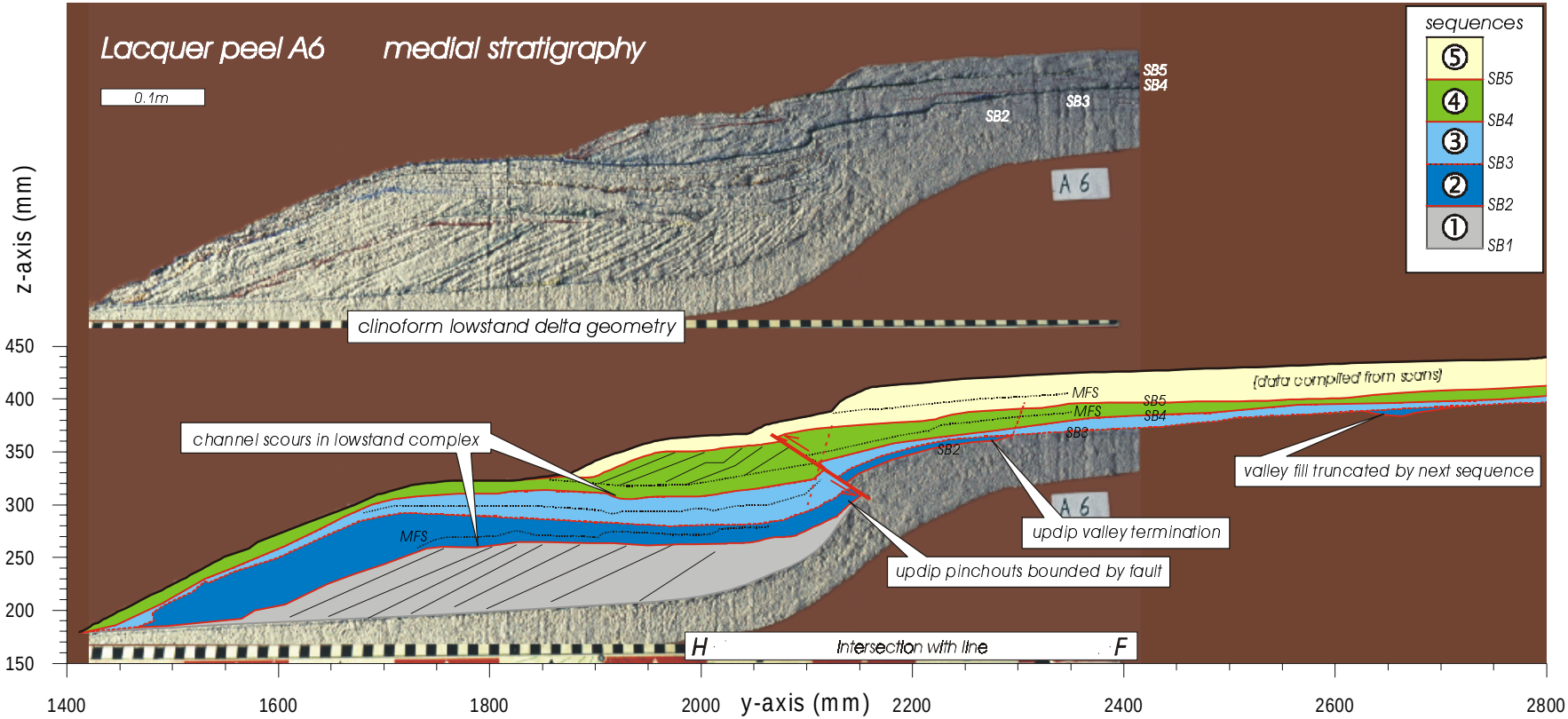

]
]

footwall shows poor preservation of sequences 2 and 3 compared to the flank stratigraphy (cf. Fig. 4.10).

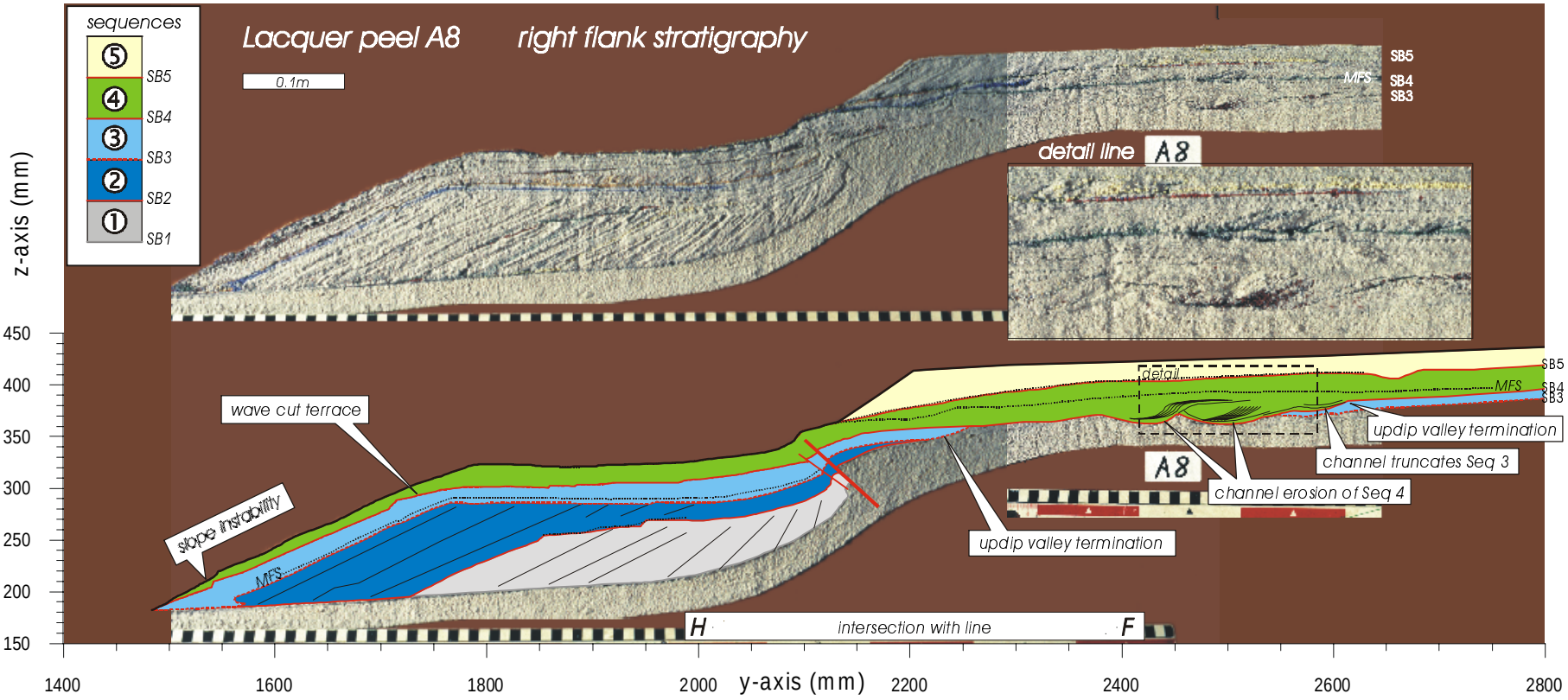
sequences
⑤ SB5
④ SB4
③ SB3
② SB2
① SB1
Lacquer peel A8 right flank stratigraphy
0.1m
SB5
MFS
SB4
SB3
detail line A8
z-axis (mm)
450
400
350
300
250
200
150
wave cut terrace
slope instability
MFS
detail
SB5
MFS
SB4
SB3
updip valley termination
channel truncates Seq 3
A8
channel erosion of Seq 4
updip valley termination
H
intersection with line
F
1400
1600
1800
2000
y-axis (mm)
2200
2400
2600
2800

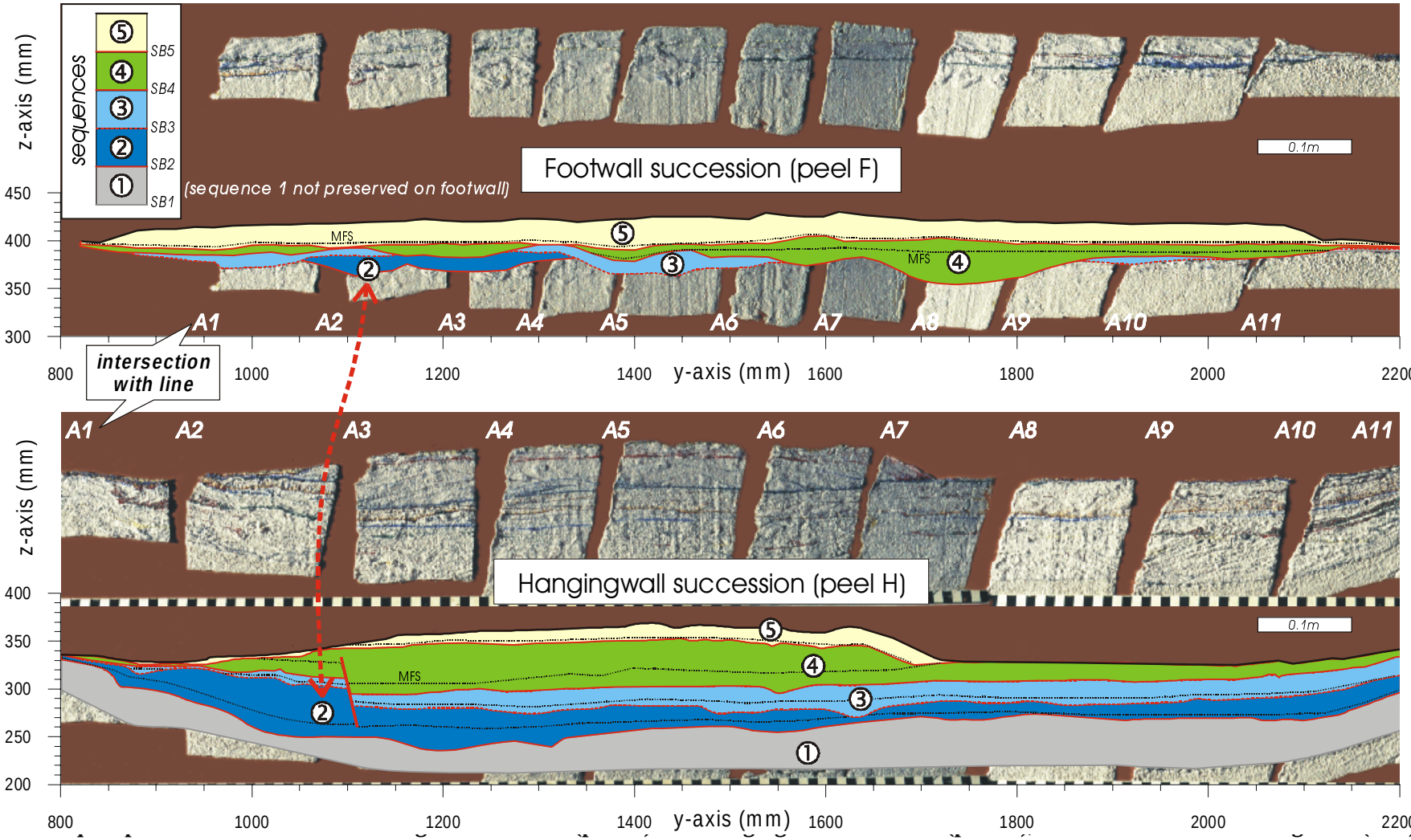

The footwall shows a high lateral variability of the incised valley fill successions. Comparison of both peels reveals that the footwall-topography (delta plain) controls the hangingwall-stratigraphy. Incised valleys on the footwall generally correlate to largest thickness of both the falling stage and lowstand systems tracts on the hangingwall (the dashed arrow indicates an example in sequence 2).

Discussion

The sequence-stratigraphic interpretation of our model stratigraphy reveals the common problems with stratigraphic correlation across a growth-fault margin. We focus our discussion on pitfalls in recognition and correlation of bounding surfaces as experienced under controlled modelling conditions. Our approach is here to point out the similarities between model, prototype and other examples of growth-faulted margins. Subsequently, we discuss the role of type of sediment routing in the delta plain and shelf area as observed in our model and in the light of systems tracts evolution in extensional basins. Finally, the hydrocarbon trapping potential of stratigraphic features of the experimental sequence model and their field analogues are reviewed.

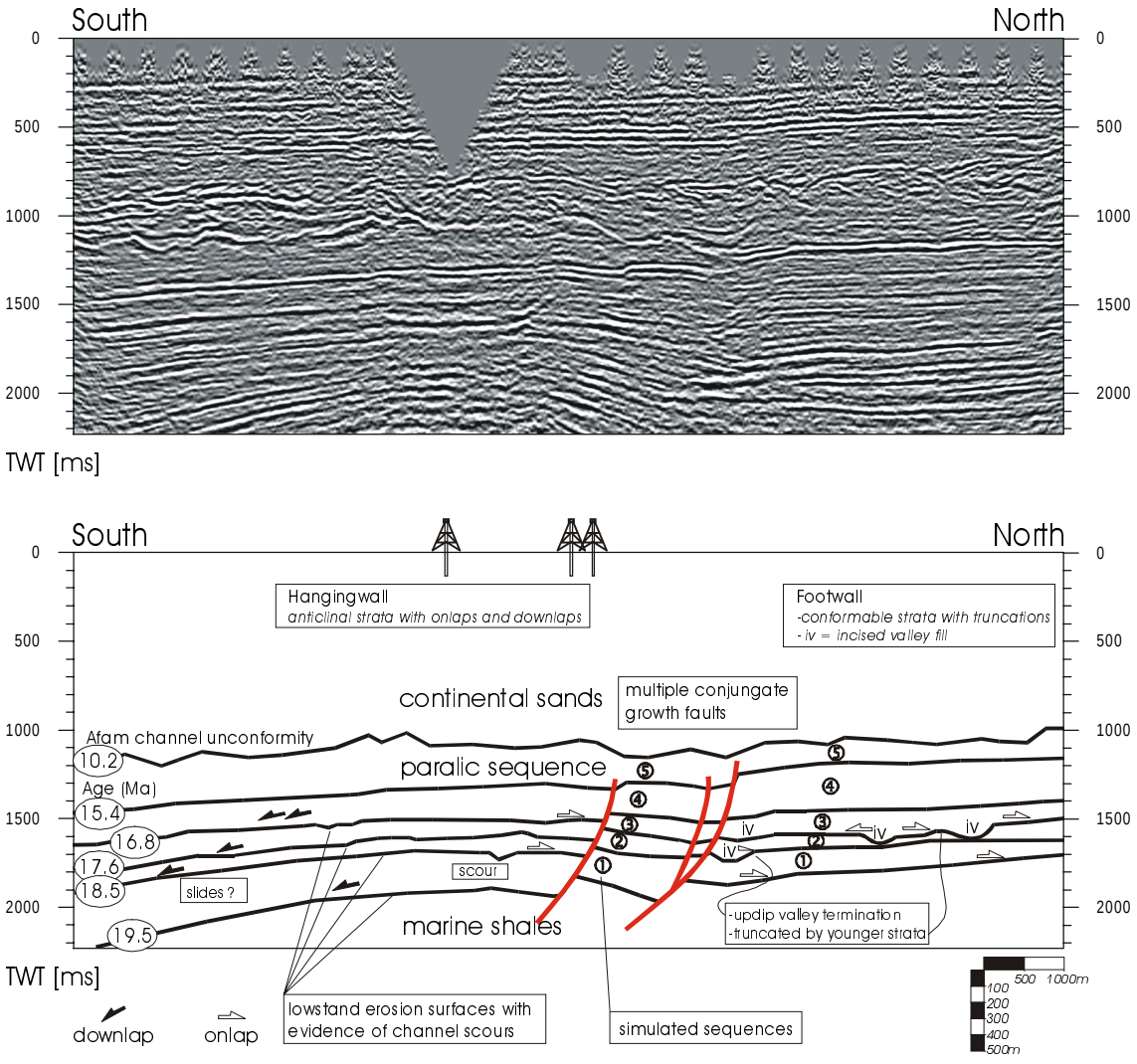

Fig. 4.14—Dip section trough the flank of the Imo River Field. The simulated sequences are marked 1 to 5. The ages of the five sequence boundaries are given in Ma. The position of the line is indicated in Figs 4.1 and 4.15. Section courtesy of SPDC.

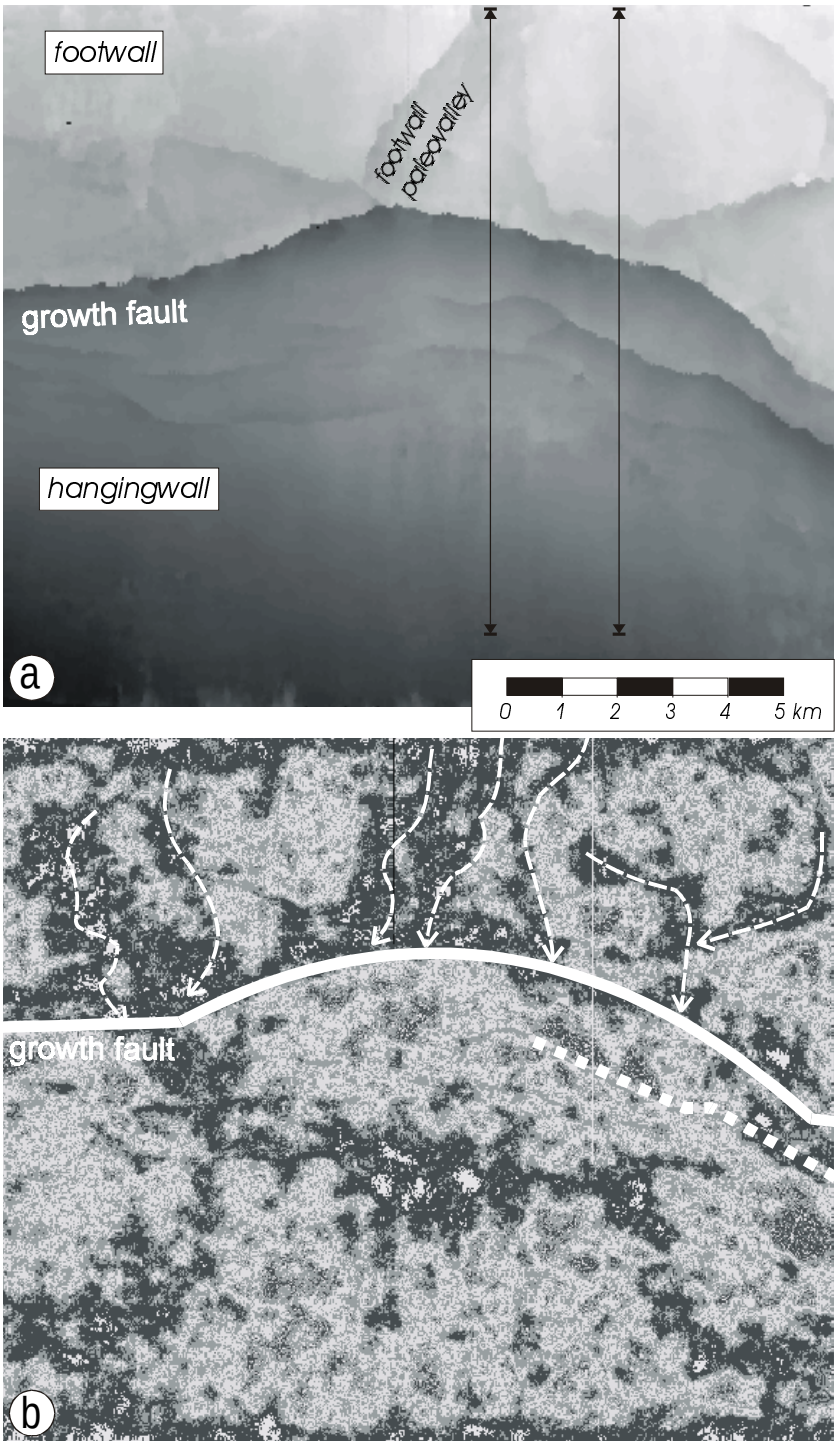

Fig. 4.15—Maps of the 18.5 Ma sequence boundary in the Imo River Field derived from the 3D seismic survey. The area covered by the map is shown in Fig. 4.1b. (a) Topographic map (altitude in TWT, milliseconds) showing a paleovalley topography on the footwall which dimensions compare well with the model equivalent, stage C in Figs 4.6 and 4.7. Two lines indicate the position of seismic sections on Figs 4.2 and 4.14. (b) Map of seismic amplitude of the same area. We infer incised valleys for the N-S running black and dark grey (high amplitude) patterns on the footwall on basis of erosional features on the seismic lines. The E-W running black and dark grey patches on the hangingwall coincide with the axis of the rollover anticline, which is characterised by the lowest local subsidence rate and therefore, likely exposed to erosion. Maps courtesy of SPDC.

Prototype-model comparison

Comparison of radial cross-sections of the model with seismic dip sections of the Imo River Field shows a high degree of similarity for relative thickness of strata and type of unconformity on the hangingwall section. Similar to the Imo River Field, the model developed a thickened hangingwall succession due to syn-sedimentary faulting. The tilting of strata within the rollover anticline in the Imo river Field fades up-section and towards the flank as illustrated by comparison of seismic dip sections across the central hangingwall and the flank of the field (e.g. Figs 4.2 and 4.14). Although the model did not produce a real rollover anticline, landward tilting of hangingwall strata did occur in the central part of the delta. Similar as in the Imo River Field, the angle of tilting decreases up-section and towards the edges of the experimental fault window (compare Figs 4.10 and 4.11).

The model shows incised valleys on the footwall block that funnelled sediments to the hanging wall lowstand fan at times of sea-level fall and lowstands. The seismic data of the Imo River Field suggest the presence of similar incised valleys on the footwall block in the Middle to upper Miocene succession (Fig. 4.14). The modelled incised valley of stage C (see Figs 4.6 and 4.7) compares well with the morphology and dimension of the Imo River Field 18.5 Ma valley equivalent shown in Fig. 4.15a. Figure 4.15b shows an amplitude map of this 18.5 Ma unconformity and reveals the drainage pattern of the incised valleys on the footwall that acted as point sources for lowstand wedges on the hangingwall.

Although the geometrical model-results satisfy the scaling constraints for the hangingwall, the thickness of the modelled footwall stratigraphy developed a sequence which is about 50% thinner than one of the Imo river Field. The footwall preservation potential was presumably low because it was kept static following the regional sea-level curve. As a result, the modelled increase in accommodation space was insufficient to preserve the early transgressive systems tracts on the footwall. Close to the fault, our model stratigraphy differs from the real world because of the different fault behaviour. The reverse faulting in our model is in part due to the fact that the required horizontal extension could not be accomplished with the subsiding hatch.

The last two sea-level cycles show a significant difference in supply rate between the flume model and the prototype. Throughout the Burdigalian and Langhian, the Imo River Field sequences show significant basinward shoreline migration with facies becoming progressively more continental (Fig. 4.3). In contrast, the last two sequences in our analogue model show evidence of undersupply. Although the experimental fault window was lowered at a constant rate, the rate of accommodation space increase was not constant as evidenced by the rapid increase from stage A to H in Fig. 4.8e. The inconsistency was probably introduced by extension of the rubber sheeting of the experimental fault window. A positive change in the rate of increase of basin volume is, however, not unusual for natural growth-fault systems (Schlische, 1991). Taking into account that the Imo River field became progressively continental during the middle to late stage of growth-fault activity, means that supply rates must have increased during the last two cycles of the Imo River prototype. In retrospect, the sediment flux for the first two cycles seems well scaled. However undersupply during the last two cycles resulted that the sediment flux over the entire experiment was lower than in the prototype as shown by the calculation

in Table 4.2g. Hence, our assumption of constant sediment supply seems not to be a good model condition for the last two cycles. However, an increase in regional sediment supply for the Imo River Field is supported by the regional Miocene development of the Niger delta, which is characterised by increased rates of sedimentation and subsidence in progressively younger sequences (Doust & Omatsola, 1990). Knox & Omatsola (1989) attribute the increase in sediment supply during Early to Middle Miocene time to uplift within the African craton, (e.g. Cameroon uplift). It is interesting to note that the inferred supply increase coincides with the two lowstands on the Haq *et al.* (1988) curve, which is illustrated by the inset of Fig. 4.3.

Thus, the experimentally produced stratigraphy deviates at some points with that of the Imo River Field. Main points of deviation include: 1) the amount of footwall preservation is underestimated with respect to the Imo River Field, with consequences for sequence-stratigraphic comparisons, 2) strata close to the experimental fault are not representative for natural growth-fault settings and are excluded from further consideration, and 3) the last two sequences maintain paralic conditions while the Imo River Field becomes progressively continental owing to strong increase in sediment supply. However, the strong geometrical similarity of the model with the Imo River Field sequences indicates reasonable scaling of sediment flux relative to the desired subsidence and associated gain in accommodation space (cf. Fig. 4.8e). Simulation of delta and fluvial architecture (systems tracts) in both the up-thrown and down-thrown block was the focus of this study rather than creating a dynamically correct faulting model.

Experimental sequence stratigraphy of growth-faulted shelf deltas

In order to test the results on sequence-stratigraphic principles, the model stratigraphy was subdivided into systems tracts according to seismic-stratigraphic conventions (Figs 4.10 to 4.13). The medial cross-section of Fig. 4.16a is a representative example of the distribution of systems tracts across the fault. The systems tract distribution of the model shares many similarities with the Imo River Field. The model shows that the hangingwall preserves all tracts, with coarse-grained deposits formed during the eustatic fall, lowstand and early rise. The footwall succession represents a stack of late transgressive and highstand deposits, which was repeatedly subject to erosion and sediment bypass as the shoreline moved seaward of the fault during lowstands (Table 4.4).

The sequence boundaries in Fig. 4.16a separate the falling stage systems tract (FSST cf. Hunt & Tucker, 1992; Hunt & Tucker, 1995; Kolla *et al*., 1995; Plint & Nummedal, 2000) from a thin, progradational to aggradational lowstand systems tract, which was formed during the eustatic minimum and early transgression. In contrast to the Imo River Field stratigraphy, the lowstand prograding wedge in the model is a very thin systems tract that relates to the brief period of time that the sea-level lowstand was maintained. It is a thin layer between the falling stage and transgressive systems tract. Therefore, we have not separately marked the lowstand systems tract on the interpreted cross-sections in Figs 4.10-4.13. The transgressive systems tracts are characterised by small, back-stepping lobes (parasequences), which overlie the lowstand wedge. The lobes are produced by shifting of the main stream and are thus supply controlled.

Table 4.4. Variation in systems tract development in the model on either side of the growth fault.

Sequence-Stratigraphic Units	**Footwall block** Accommodation creation only by regional sea-level rise	**Hangingwall block** Accommodation creation by: regional sea-level rise and local subsidence
Highstand systems tract (HST)	highstand progradation (downlap) highstand delta; fluvial and deltaic deposits	condensed section *(incidental: toe of highstand delta)*
Falling stage systems tract (FSST)	erosion/bypass by incised valleys on delta plain (type-1)	type-1 sequence: lowstand delta progradational wedge
	bypass by braided fluvial system on whole delta plain (type-2)	type-2 sequence: shelf margin delta systems tract (SMST)
Lowstand systems tract (LST)	bypass	thin progradational to aggradational wedge
Early Transgressive systems tract (TST)	bypass	backstepping lobes that cover lowstand wedge and valleys on lower delta plain
Mid to late Transgressive systems tract (TST)	incised valley-fill with backstepping geometries	condensed section

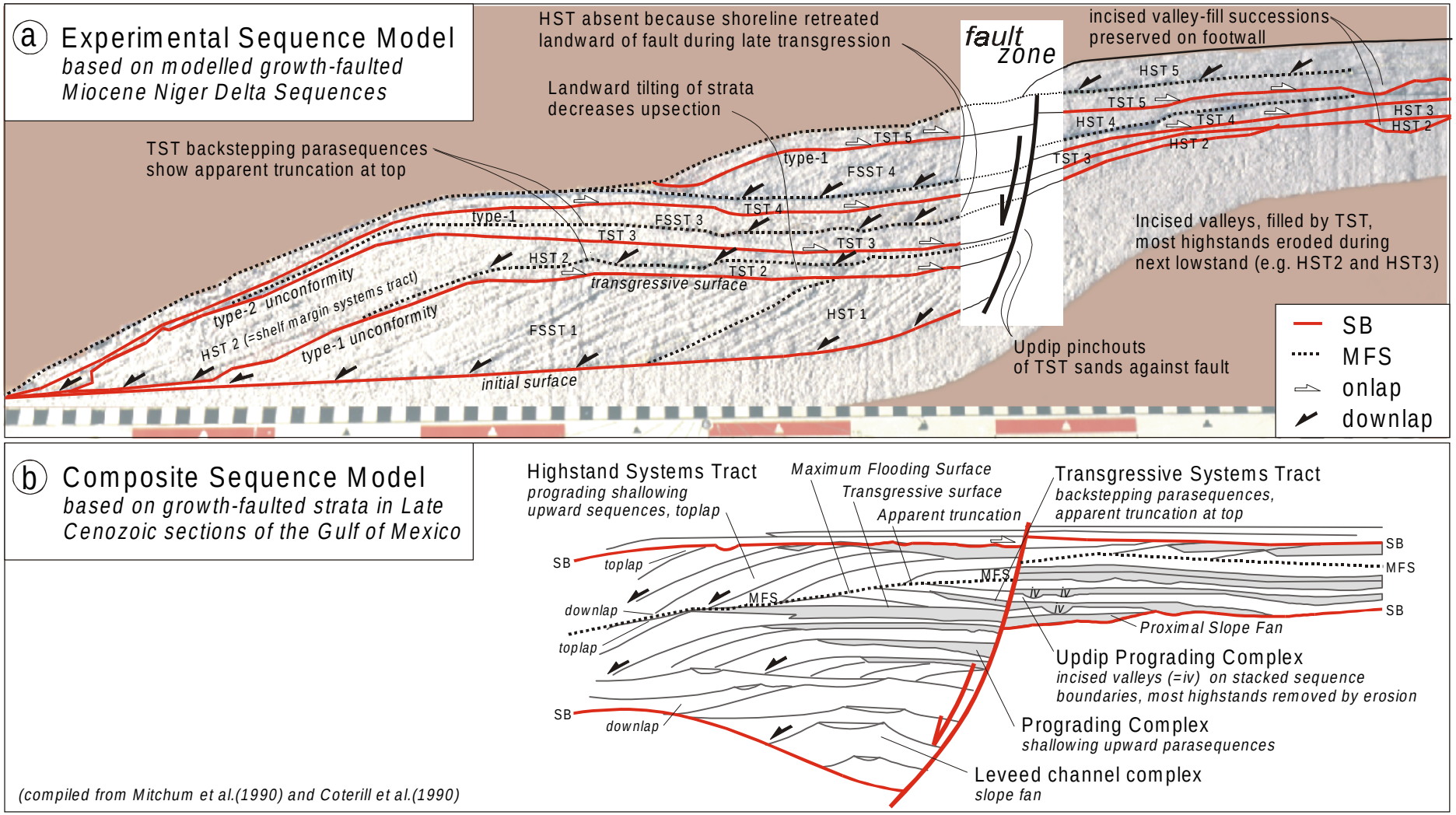

Fig. 4.16—(a) Sequence model based on the across fault correlation of the medial stratigraphy of the completed model (Lacquer peel A6 in Fig. 4.11). The strata close to the experimental fault are not representative for natural settings and have been excluded from the sequence model. (b) Conceptual systems tract model for Cenozoic 4th order sequences along growth faults of the Gulf of Mexico after Mitchum *et al.* (1990) and Coterill *et al.* (1990).

Recognition of sequence boundaries and maximum flooding surfaces

Unconformities (sequence boundaries) could be more easily identified in the experiments than maximum flooding surfaces. Pitfalls and common problems, such as encountered by Galloway (1989); Thorne & Swift (1991) when trying to identify and to correlate subaerial erosion surfaces across a basin can be simply resolved in a model by marking important bounding surfaces with a tracer. The method showed, for instance, diachronous erosion and deposition along the stream profile as a consequence of the sea-level change (see also Chapter 3, Fig. 3.12). The stream profile at maximal sea-level lowstand would be analogous to the type-1 unconformity. During the subsequent rise, we observe a strong diachronous development, with deposition commencing on the shelf and delta plain and with erosion continuing in landward direction. This diachroneity will be enhanced in growth-fault settings. For instance, stage D on Fig. 4.7 shows how the incision on the upper delta and in the fluvial domain continued during early rise and coincided with deposition of the transgressive systems tract on the hangingwall. Thus, the upstream part of the unconformity on the footwall does not record the lowstand hiatus but originates from early rise and becomes progressively younger updip.

Maximum flooding surfaces are characterised by downlap of clinoforms. In field settings, the faunal abundance makes the maximum flooding surface often a much better time-stratigraphic interval to tie shelf to slope sediments than the unconformity (Mitchum *et al*., 1990). In fact, the “surface” represents a continuum of deposition of fine basinal sediments (Posamentier & James, 1993). The conformable part of the sequence boundary would be a more synchronous surface than the maximum flooding surface, because it is less subject to local variations in subsidence and sediment flux (Wehr, 1993). In our model, maximum flooding surfaces are best preserved in the hangingwall succession, where the clinoforms downlap on condensed sequences of coal dust deposited at times of basin starvation (see Fig. 4.8c). However, their preservation in the shallow marine strata of the footwall block is minimal (see Fig. 4.16a). Hence for correlation across the fault one has to rely on sequence boundaries, in spite of these showing strong diachroneity.

We note that in some lacquer-peel sections, aggradation can be observed just below the sequence boundary on the lowstand delta (see inset in Fig. 4.10). We can ascribe the aggradation to rapid back-filling of channel scours that formed just before lowstand. Without the tracers one could easily put the sequence boundary too low. The example is very analogous to the allocyclic channel scours of Best & Ashworth (1997).

Role of type of unconformity on delta plain and shelf morphology and sediment routing

According to the concept of Posamentier & Allen (1993), the interplay of eustatic sea-level change and local subsidence determines the type of unconformity and lowstand basin physiography, which would control, in turn, the morphology of the following transgressive systems tract. Not only is this view further substantiated by our experiment, but also some other, new growth-fault related morphological features became apparent. The role of the type of unconformity on shelf morphology and sediment routing to lowstand fans becomes clear from a comparison of the products of the two unconformities in our model. The interplay between both regional and local subsidence and eustasy in the Imo River Field resulted in three type-1 unconformities and one type-2 unconformity for the hangingwall and four type–1 unconformities for the footwall block.

The *type-1 unconformity* (stage C, H and K) is characterised by a few, cross-shelf bypass valleys that form a point source for lowstand fans (Fig. 4.17a). These valleys transfer significant volumes of freshly eroded footwall sediment to the lowstand fans on the hangingwall (Fig. 4.8f). The cross-shelf bypass valleys in our model (Fig. 4.7c) are representative for the Imo river Field (Fig. 4.15) and agree with the notion that deposition of channel sands in the Miocene lowstand wedges of the Niger delta complex occurred largely from point sources (Pacht, 1996). Both position and depth of the valleys in the footwall correlate roughly with the position and volume of lowstand fans in the hangingwall (Fig. 4.13). At lowstand, the shelf physiography consists of one or two main cross-shelf valleys, which capture most of the sediment deposited during the subsequent rise (Fig. 4.17a). Wave-induced sediment transport was only partly capable to erase former valley topography (Stage D in Fig. 4.6)

The *type-2 unconformity* (stage E) is characterised by little to no incision of river valleys into the delta plain and shelf, so that the feeder system of the delta can potentially behave as a line source (Fig. 4.17b). A drainage network of braided channels develops on the delta plain that acts as a line source and feeds the delta along the entire shelf-margin during Stage E in Fig. 4.7). As a consequence, the subsequent transgressive systems tract consists of a sand sheet that covers the entire delta plain and is not confined by antecedent valleys (compare stage D and F in Figs 4.6 and 4.7). In addition, the lowstand braid plain was further planed by wave-induced sediment transport during the subsequent rise. The development of a type-2 drainage morphology means for real world situations that there would be potential for frequent avulsion of rivers and equal distribution of the sediment over the entire delta plain area. This is for a great part depended on the inherited relief as is exemplified by stages H to K in Fig. 4.7: Stage H shows an incised valley in the right hand side of the footwall, which is back-filled during the late rise and highstand (Stage I). The footwall-edge and the hanging-wall block become sediment starved (Stage J). Only, the complete filling of the valleys allowed the development of a braid plain with local and minor incision. Evidence for the line source in the Imo River example should come from the even distribution of lowstand fan material in the form of slope-apron systems.

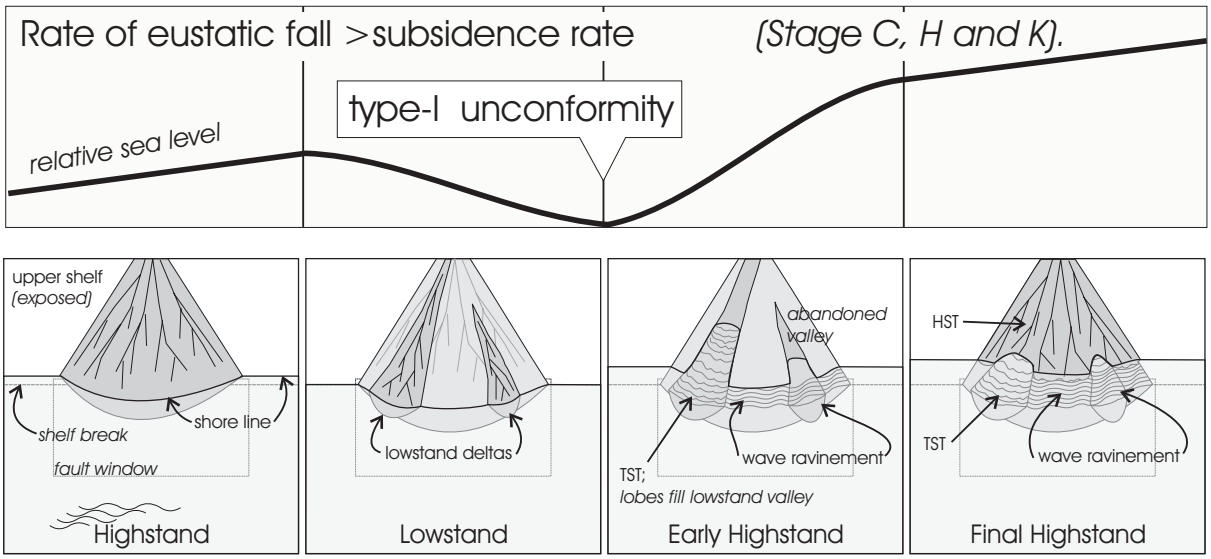

Type-1 sequence:

ⓐ

-incisions develop on the delta plain and feed sediments to lowstand deltas
-basinward shift of facies
-TST deposited in previously incised valleys only

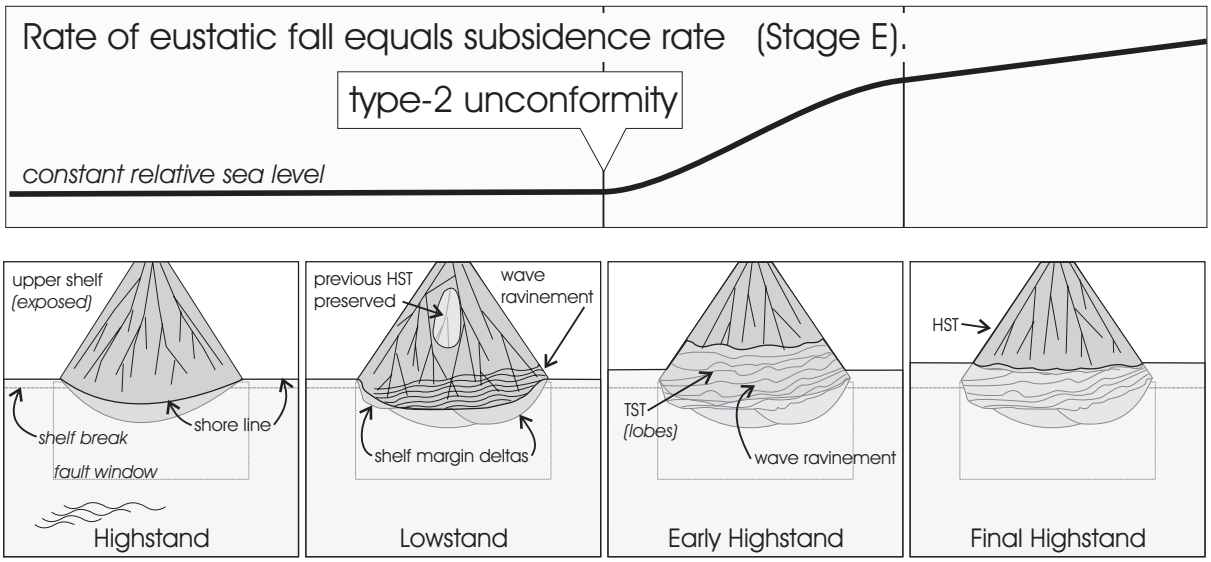

Type-2 sequence:

ⓑ

-absence of incised valleys during lowstand, flow on entire delta plain
-shelf margin systems tract deposited (no basinward shift of facies)
-TST deposited on whole delta

Fig. 4.17—Main differences in delta evolution as observed for our experimental type-1 and type-2 sequences. (a) A type-1 sequence results in valley incision, which migrates progressively upslope until one of the valleys reaches the fluvial valley and captures all discharge. The subsequent TST is only present in this main valley. (b) A type-2 sequence develops a braided system on the entire delta plain and consequently the subsequent TST covers the entire delta-shelf system.

Model comparison with Gulf Coast prototypes

Sequence-stratigraphic models have been developed for Cenozoic growth-faulted margins in the Gulf Coast (Coterill *et al*., 1990; Mitchum *et al*., 1990; Pacht, 1990; Mitchum *et al*., 1993). The models are based on composite characteristics of 4th-order sequences by superimposing the high-order eustatic imprint on the lower-frequency tectonic control. Although our experimental sequence model was calibrated for 3rd order sea-level cycles, its sequence stratigraphy is very similar to the 4th-order frequency cycles of the Gulf Coast prototypes in terms of systems tract distribution (Fig. 4.16). In the Gulf Coast prototypes, the basin-floor and slope fans occur predominantly on the down-thrown side of the fault while the lowstand wedge, transgressive and highstand tracts occur on both sides of the fault (Mitchum *et al*., 1990). Incised valley-fill sequences are most common on the footwall and their sediments relate to late stages of formation of the lowstand prograding wedge (Mitchum *et al*., 1990; Pacht, 1990). Both the Gulf Coast prototype (Coterill *et al*., 1990) and the experiment model show back-stepping features in the transgressive systems tract in conjunction with an overall vertical fining into a condensed shale interval (coal dust layer in the model). The highstand deposits on the footwall are frequently eroded in both models (Fig. 4.16).

Model comparison with sequence-stratigraphic development in extensional tectonic settings

Growth faulting in extensional basins shows similarities with fault growth in delta systems, although the origin of the faulting process is different (Schlische, 1991). Hence, both sedimentary systems must have similarities in their basin fill architecture. If we wish to apply our model results to syn-rift strata, at least two boundary conditions should be met: 1) the location of the fault has to coincide approximately with the depositional shelf-break, and 2) supply and creation of accommodation space by local subsidence must be balanced (i.e., similar to our model conditions). Both the boundary conditions control shoreline changes and thus the stratigraphy of the footwall and hangingwall blocks. The topographic ramp of the syn-depositional fault actively controls the location of the depositional shelf break in half-graben settings (Leeder & Gawthorpe, 1987, their figure 5; Gawthorpe *et al*., 1994). Similarly, a listric growth fault in ramp settings coincides with the shelf-slope transition because the gravitational gliding is induced by high sediment loading at the delta front (Mitchum *et al*., 1990; Pacht, 1990). Although our discussion focuses here essentially on the 2D architecture along the centre-line across the fault, we are aware of the three-dimensionality of extensional syn-rift strata in half-graben settings (Dart *et al*., 1994; Gawthorpe *et al*., 1994; Collier & Gawthorpe, 1995; Howell & Flint, 1996; Gupta *et al*., 1999) and in growth faulted shelf deltas (Coterill *et al*., 1990; Mitchum *et al*., 1990; Reijers *et al*., 1997).

A half-graben prototype that meets our boundary conditions is the Puffin terrace of the Jurassic North-Sea Central Graben. The creation of accommodation space was proportional to supply, since local subsidence was driven by sediment flux (Howell & Flint, 1996, their figure 1, case 6). The example shares many similarities with our experimental sequence model and the Gulf Coast models for growth-faulted shelf-margin deltas (Fig. 4.16). Similar to these models the eustatically driven shoreline fluctuations on the footwall resulted in valley formation on the emerged Puffin Terrace (Underhill & Partington, 1993, their figure 8). During early lowstand, sand that bypassed the footwall shelf was deposited in the lowstand fans on the hangingwall. Therefore, the nature of these lowstand deposits on the hangingwall was found to be controlled by both topography of the footwall (shelf canyons) and the effects of eustatic fall across the footwall and not by the subsidence of the hangingwall itself (Howell & Flint, 1996). Theoretically, high subsidence rates will reduce or may even cancel out the effect of the eustatic fall on the hangingwall succession (Steckler *et al*., 1993; Gawthorpe *et al*., 1994), although not in those cases, where our boundary conditions have been met. Both model and prototype examples from the Imo River Field, Gulf Coast and Puffin Terrace show that the eustatic signal will be recorded in the hanging wall succession irrespective of the rate of hangingwall subsidence. The eustatic signatures include an extra supply to the lowstand fan through shelf cannibalism (cf. Postma *et al*., 1993).

Stratigraphic and economic significance of experimental analogues

On the basis of similarities of large-scale systems tract development in our model and the above mentioned prototypes, we propose an idealised depositional model for growth-faulted shelf margins (Fig. 4.16b), which can act as a template for better reservoir prediction (Mitchum *et al*., 1990). Table 4.5 lists a series of analogue features found in experimental and prototype examples. The right column discusses the possibility of the presence of viable stratigraphic traps in such deposits.

Rollover anticlines are the conventional hydrocarbon trapping geometry in growth-faulted shelf deltas (Weber & Daukoru, 1975; Doust, 1989). Condensed sequences below and at the maximum flooding surface may form possible seals that overlie clinoform lowstand wedges and transgressive sands. Other common trapping configurations are fault-bound traps and stratigraphic traps, among them truncation traps and channel-fills (Stacher, 1995).

Incised valley-fill sequences can be preserved on the footwall, and were discovered on the footwall of the growth-faulted shelf deltas of the Gulf Coast (Pacht, 1990). Incision results from the eustatic fall over the footwall. These footwall channels act as point sources that funnel delta plain sands to the lowstand wedges improving their reservoir quality. The experimental-results relate 3 types of up-dip pinch-out structures to incised valley-fills on the footwall: 1) up-dip valley termination, 2) truncation by younger strata and 3) truncation by faults. Their field examples and experimental analogues are listed in Table 4.5. The duration of the late TST and the HS stage and the amount of suspension load control the thickness and the lateral continuity of the sealing muds (Mitchum *et al*., 1990; Muntingh & Brown, 1993).

Table 4.5. Experimental analogues compared with the Imo River Field and other examples.

Stratigraphic feature description	Experimental analogue	Field example	Possible hydrocarbon trapping configuration
Hangingwall anticline Clinoform strata in hangingwall block	Medial peels: Peel A3 in Fig. 4.10 Peel A6 in Fig. 4.11	Figs 4.2 & 4.14	Conventional play type: lowstand wedges and transgressive deposits sealed by MFS.
Incised valley-fill sequences preserved on the footwall	Peel F in Fig. 4.13	Figs 4.2 & 4.14 Fig. 4.15 Gulf coast; (Pacht, 1990)	Incised valley-fill sequences on the footwall formed during transgression. They consist of coastal and estuarine sands. Flooding at highstand may form a seal of estuarine muds.
Updip pinchout structures related with incised valley-fills:			The origin of the pinchout implies various seal potential:
-updip valley termination	-Peel A6 in Fig. 4.11	-Fig. 4.14	-lateral seal
-truncated by younger strata	-Peel A8 in Fig. 4.12	-Fig. 4.2	-problematic; channel lag
-truncated by faults	-Peel A3 in Fig. 4.10	-Fig. 4.2	-lateral seal

Conclusions

For the first time an analogue flume experiment was used to study the combined effect of growth faulting and sea-level change on the depositional architecture of shelf-edge deltas. The experimental model was calibrated with the Miocene stratigraphy of the Imo River Field of the Niger Delta complex. From our discussion it is apparent that sequence-stratigraphic models that have been developed for stable passive margins (Posamentier & Vail, 1988) do apply to other settings, but not without modifications.

The model results indicate that the amplitude of sea-level fall (i.e., the shoreline position relative to the growth fault on a shelf-margin delta) determines the potential amount of shelf cannibalism on the relatively stable footwall. The cutting of canyons in the footwall thus results in a supply signal and a systems architecture on the hanging-wall that are driven by regional sea-level changes, and that are independent of the rate and total amount of local subsidence in the hangingwall.

The sequence stratigraphy of the model emphasises the strong relationship between depositional architecture and rate of subsidence, which varies along and perpendicular to the fault strike. The systems-tract distribution of the modelled, growth-faulted, shelf-margin delta shows that the expanded hangingwall section preserves all tracts formed during eustatic fall, lowstand and early rise. The footwall section, in contrast, only records a thin succession of late transgressive and highstand deposits which is repeatedly reworked by erosion at times of eustatic fall, at lowstands and even during the rise. Volumes and locations of lowstand wedges on the hangingwall correlate to the geometry and locations of cross-shelf bypass valleys on the footwall. These valleys are characteristic for a type-1 sequence. They act as point sources during episodes of eustatic fall, lowstand and early rise and may do so during subsequent cycles as antecedent valleys. The relief inherited from lowstand morphology formed by type-1 sequences was also found to govern the lateral variability of the transgressive and highstand systems tract and even the architecture of the next sequence. In contrast, a type-2 unconformity planed the exposed shelf by erasing antecedent valleys and thus favoured the development of new drainage morphology. The preservation of maximal flooding surface in the shallow marine strata of the footwall block is minimal (see Fig. 4.16a). Hence for correlation across the fault one has to rely on sequence boundaries, in spite of these showing strong diachroneity.

This paper illustrates how analogue models have a potential to investigate quantitatively the control of syn-sedimentary faulting and eustatic sea-level changes in three dimensions. Flume models, unlike sandbox models, do allow investigation of the effects that sedimentary processes as controlled by changes in subsidence and eustasy have on the final stratigraphic architecture. It is a new type of forward modelling that is largely unexplored, and with at least one advantage above a numerical model that is that the operator can hardly influence the outcome. The ability to study, even in considerable detail, the lateral variability within and between the simulated sequences is an additional advantage, which will be a guide for stratigraphers that wish to expand their insights in cause and effects.

Acknowledgements

This research was funded by Shell International Exploration and Production, Rijswijk, The Netherlands under contract wc/56809. We acknowledge the permission of the Nigerian Department of Petroleum Resources (DPR) and Shell Production and Development Company of Nigeria (SPDC), operator on behalf of the NNPC joint venture, for publication of this paper. We thank T. Cortis, W.C. Lee and L.D. Meckel (Shell, Rijswijk) for their assistance with the seismic interpretation and their contributions to discussions in early stages of the manuscript. At Utrecht University we acknowledge A.C. van der Gon Netcher, J.H. Bliek, P. Anten and M. Reith for technical support and B.J.M. Benders for the assistance with photography. Drafts of this paper benefited from extensive reviews by P.L. de Boer, X.D. Meijer, W. Nijman and W. Schlager.

Appendix

Grain properties and sediment transport

Applied sediment

Unimodal medium sand was used as substrate and as feeder material during all experiments (Fig. A.1). The clay fraction (<40 μm) was washed out to avoid cohesion effects. All grains larger than 1000 μm were sieved out to avoid any large ratio of particle size over water depth that can lead to partial sorting.

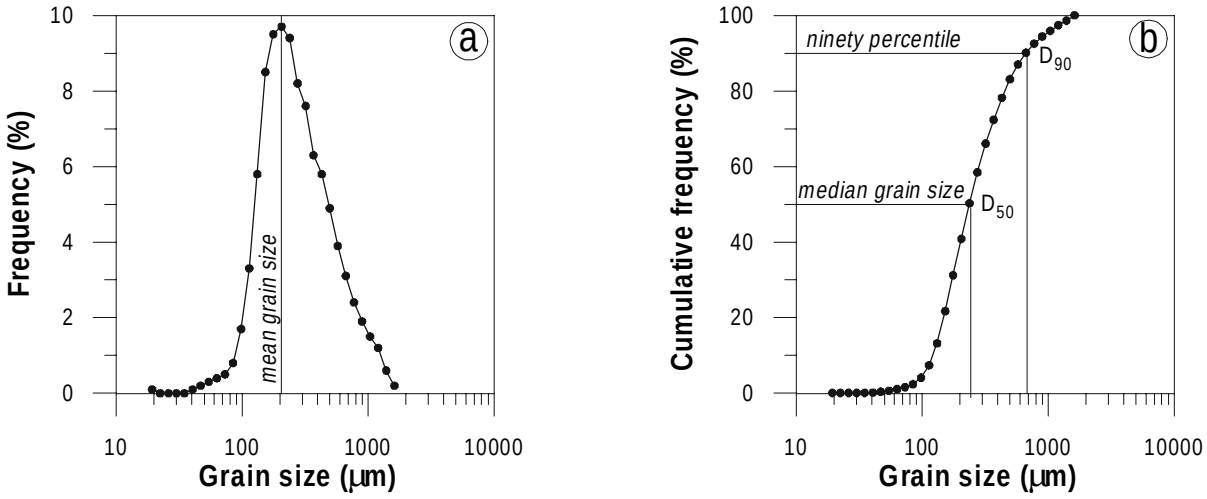

Fig. A.1—(a) Grain-size distribution of the applied unimodal medium sand obtained from a Malvern laser particle sizer. The cumulative frequency diagram (b) shows the median and ninety percentile grain diameter.

Observed and calculated sediment transport

We applied the empirical sediment transport equations of Meyer-Peter & Müller (1948), Bagnold (1966), Van Rijn (1984) and Engelmund & Hansen (1967) to verify whether the bed-load transport in the fluvial valley of our model has realistic values for the applied conditions. The verification was done for 5 different discharge regimes ranging from 200 to 600 dm^3/h. The feeder at the upstream end of the fluvial valley was adjusted to a constant sediment supply of $1dm^3/h$ (default). A dam fixed the base level at the downstream end. Each test established a graded (equilibrium) stream profile in the fluvial valley. Under graded conditions the sediment transport rate at each position along the equilibrium profile equals the supply rate of 1 dm^3/h at the feeder. The observed value was compared with the calculated values using the four empirical transport formulae (Table A.1). We tested four approaches, because each deterministic bed-load equation emphasises different variables, as will be discussed.

Meyer-Peter & Müller (1948) define the volumetric bed-load transport rate as:

$$q_b = 8 \cdot (\mu \cdot \theta - 0.047)^{1.5} \cdot (s-1)^{0.5} \cdot g^{0.5} \cdot D_m{}^{1.5} \qquad \text{(A.1)}$$

Where:

q_b		volumetric bed-load transport rate (m^2/s)
μ	$= (C/C')^{1.5}$	bed form or efficiency factor (-)
θ	$= \frac{\tau_b}{(\rho_s - \rho) \cdot g \cdot d_m}$	dimensionless particle mobility parameter (-)
s	$= \rho_s/\rho$	relative density (-)
ρ		density of the fluid (kg/m^3)
ρ_s		density of the sediment (kg/m^3)
g	$= 9.81$	acceleration of gravity (m^2/s)
D_m		mean particle diameter (equals $1.3 \cdot D_{50}$) (m)
C	$= \bar{u}/(h \cdot S)^{0.5}$	overall Chézy-coefficient ($m^{0.5}/s$)
C'	$= 18\log(12h/d_{90})$	grain related Chézy-coefficient ($m^{0.5}/s$)
τ_b	$= \rho \cdot g \cdot h \cdot S$	bed-shear stress (N/m_2)
$\bar{u}$		depth-averaged velocity (m/s)
h		water depth (m)
S		energy gradient or slope (-)

The equation directly depends on the particle diameter D_m in the equation, but also on the grain roughness accounted for in the grain related Chézy coefficient.

Bagnold (1966) reduces the bed-load prediction problem by relating only a few kinetic parameters to the transport rate. The bed-load transport is independent of the particle diameter and bed roughness by bedforms. The transport depends on the overall bed-shear stress and not on the effective stress:

$$q_b = \frac{e_b \cdot \tau_b \cdot \bar{u}}{(\rho_s - \rho) \cdot g \cdot \cos\beta \cdot (\tan\phi - \tan\beta)} \qquad \text{(A.2)}$$

Where:

q_b		volumetric bed-load transport rate (m^2/s)
e_b	$= 0.1$	efficiency factor (-)
τ_b	$= \rho \cdot g \cdot h \cdot S$	bed-shear stress (N/m^2)
$\bar{u}$		depth-averaged velocity (m/s)
$\tan\beta$	$= S$	energy gradient or slope (-)
$\tan\phi$	$= 0.6$	dynamic friction coefficient (-)

Van Rijn (1984) defines the bed-load transport rate as a product of particle velocity, saltation height, and bed-load concentration. This equation incorporates bedform effects by using the dimensionless bed-shear parameter T*:

$$q_b = 0.053 \cdot (s-1)^{0.5} \cdot g^{0.5} \cdot D_{50}{}^{1.5} \cdot D_*{}^{-0.3} \cdot T_*{}^{1.5} \qquad \text{(A.3)}$$

Where:

q_b		volumetric bed-load transport rate (m^2/s)
s	= ρ_s/ρ	relative density (-)
g	= 9.81	gravity (m^2/s)
D_{50}		median grain size (m)
D_*	= $d_{50}((s-1)g/\nu^2)^{1/3}$	dimensionless particle diameter (-)
ν		kinematic viscosity coefficient (m^2/s)
T*	= $(\tau'b - \tau b,cr) / \tau b,cr$	dimensionless bed-shear parameter (-)
τ'_b	= $\rho g(\bar{u}/C')^2$	effective bed-shear stress (N/m^2)
$\tau_{b,cr}$		critical bed-shear stress acc. to Shields (N/m^2)
$\bar{u}$		depth-averaged velocity (m/s)
C'	= $18\log(12h/d_{90})$	grain related Chézy-coefficient ($m^{0.5}/s$)

Engelmund & Hansen (1967) propose a formula that predicts total transport based on an energy-balance concept:

$$q_{t,c} = \frac{0.05 \cdot (\bar{u})^{\alpha}}{(s-1)^2 \cdot g^{0.5} \cdot D_{50} \cdot C^3} \qquad \text{(A.4)}$$

Where:

$q_{t,c}$		volumetric current related total load transport (m^2/s)
$\bar{u}$		depth-averaged velocity (m/s)
α	=	exponent of sediment transport equation (-)
s	= ρ_s/ρ	relative density (-)
D_{50}		median grain size (m)
C	= $\bar{u}/(h \cdot S)^{0.5}$	overall Chézy-coefficient ($m^{0.5}/s$)

The problem is to obtain a reliable value for the exponent α, which is usually assumed to vary between 3 (bed load) and 5 (suspension load). A best-fit value was obtained for $\alpha = 4.6$ by iteration for the observed bed-load transport rate.

The deterministic sediment transport formulae mentioned above are known to predict the bed-load sediment transport in natural river systems within a factor of two in about 70% of the cases (Van Rijn, 1984; Reid & Frostick, 1994). The fluvial valley of our set-up shows a better fit between predictions and observations of the bed-load transport. All formulae predict sediment bed-load transport within a factor 0.6 to 1.3 of the observed value. The equation of Van Rijn (1984) underestimates the bed-load transport rate because the calculated values of the apparent bed roughness are too high. T* was found to be in the order of 2 or 3 which is an apparent bed roughness that relates to small-scale ripples. However, ripples were not observed for a discharge lower than 600 dm^3/h. The Meyer-Peter & Müller (1948) equation also slightly underestimates the actual sediment transport rate of the flume. The Bagnold equation does not depend on grain size or bedforms but shows good results despite its simplicity. Note that the equation of Bagnold (1966) and of Engelmund & Hansen (1967) with $\alpha = 4.6$ show good agreement.

Table A.1. Observed (right) and calculated sediment transport rate in the 4 m fluvial valley for various discharge regimes. The calculated values can be read as the ratio of the predicted over the observed transport rate since the observed value equals unity.

Q_w discharge (dm^3/h)	**h** depth (m)	$\overline{u}$ velocity (m/s)	**S** Gradient (-)	**Q_s, sediment transport rate (dm^3/h)**				
				(Meyer-Peter & Müller, 1948)	(Bagnold, 1966)	(Van Rijn, 1984)	(Engelmund & Hansen, 1967) with $\alpha = 4.6$	***Observed Transport***
200	0.0033	0.153	0.052	0.80	1.15	0.63	1.036	1.0±0.1
300	0.0045	0.168	0.039	0.84	1.26	0.61	1.248	1.0±0.1
400*	0.0056	0.180	0.025	0.77	1.10	0.62	1.053	1.0±0.1
500	0.0065	0.194	0.021	0.86	1.10	0.73	1.076	1.0±0.1
600	0.0076	0.200	0.018	0.82	1.12	0.67	1.126	1.0±0.1

** default discharge during flume experiments. Applied values: channel width: b = 0.11 m, $\rho = 1000\ kg/m^3$, $\rho_s = 2650\ kg/m^3$, $D_{50} = 0.00025$ m, $D_{90} = 0.00070$ m, $\tau_{b,cr} = 0.18\ N/m^2$ and $\nu = 1.14x10^{-6}\ m^2/s$.*

References

Allen, J. R. L. (1965) Coastal geomorphology of Eastern Nigeria: beach-ridge barrier islands and vegetated tidal flats. *Geologie en Mijnbouw*, **44**, 1-21.

Allen, P. A. (1997) *Earth Surface Processes*. Blackwell Science, Oxford, 404 pp.

Anderson, J. B., Abdulah, K. C., Sarzaleojo, S., Siringan, F. P. & Thomas, M. A. (1996) Late Quaternary sedimentation and high-resolution sequence stratigraphy of the east Texas shelf. In: *Geology of Siliciclastic Shelf Seas* (Ed. by M. De Batist and P. Jacobs), *Geological Society of London Special Publication*, ***117***, 95-124.

Ashworth, P. J., Best, J. L., Leddy, J. O. & Geehan, G. W. (1994) The physical modelling of braided rivers and deposition of fine-grained sediment. In: *Process models and theoretical geomorphology* (Ed. by M. J. Kirkby), 115-139.

Bagnold, R. A. (1966) An Approach to the sediment transport problem from general physics. *Geological Survey Professional Paper*, **422-I**.

Bank, G. C. & Harbor, D. J. (1998) Headward advance of the James River basin by the capture of St. Marys River from the Shenandoah River basin, Virginia. *Geological Society of America Abstracts with Programs*, **30**, 140.

Bartek, L. R., Anderson, J. B. & Abdulah, K. C. (1990) The importance of overstepped deltas and "interfluvial " sedimentation in the transgressive systems tract of high sediment yield depositional systems, brazos-colorado deltas, Texas. In: *Sequence Stratigraphy as an exploration tool: concepts and practices from the Gulf Coast: Programs and Abstracts, 11th Annual Research Conference, Gulf Coast Section of Society of Economic Paleontologists and Mineralogists, Houston, Texas*, 59-70.

Begin, Z. B. (1988) Application of a diffusion-erosion model to alluvial channels which degrade due to base-level lowering. *Earth Surface Processes and Landforms*, **13**, 487-500.

Begin, Z. B., Meyer, D. F. & Schumm, S. A. (1981) Development of longitudinal profiles of alluvial channels in response to base-level lowering. *Earth Surface Processes and Landforms*, **6**, 49-68.

Berryhill, H. L. (1987) The Continental Shelf off South Texas. In: *Late Quaternary facies and structure, Northern gulf of Mexico* (Ed. by H. L. Berryhill, J. R. Suter and N. S. Hardin), *AAPG Studies in Geology*, ***23***, 11-80.

Best, J. L. & Ashworth, P. J. (1997) Scour in large braided rivers and the recognition of sequence stratigraphic boundaries. *Nature*, **387**, 275-277.

Blum, M. D. (1993) Genesis and Architecture of Incised Valley Fill Sequences: A Late Quaternary Example from the Colorado River, Gulf Coastal Plain of Texas. In: *Siliciclastic Sequence Stratigraphy, Recent Developments and Applications* (Ed. by P. Weimer and H. W. Posamentier), *American Association of Petroleum Geologists Memoir*, ***58***, 259-283.

Blum, M. D. & Price, D. M. (1998) Quaternary alluvial plain construction in response to glacio-eustatic and climatic controls, Texas Gulf coastal plain. In: *Relative Role of Eustasy, Climate, and Tectonism in Continental Rocks* (Ed. by K. W. Shanley and P. J. McCabe), *Society of Economic Paleontologists and Mineralogists Special Publication*, ***59***, 31-48.

Blum, M. D., Toomey, R. S. & Valastro, S. (1994) Fluvial response to Late Quaternary climatic and environmental change, Edwards Plateau, Texas. *Palaeogeography, Palaeoclimatology, Palaeoecology*, **108**, 1-21.

Blum, M. D. & Törnqvist, T. E. (2000) Fluvial response to climate and sea-level change: a review and a look forward. *Supplement to Sedimentology*, **47**, 2-48.

Blum, M. D. & Valastro, S. (1994) Late Quaternary sedimentation, lower Colorado River, Gulf Coastal Plain of Texas. *Geological Society of America Bulletin*, **106**, 1002-1016.

Boyd, R., Suter, J. R. & Penland, S. (1989) Relation of sequence stratigraphy to modern sedimentary environments. *Geology*, **17**, 926-929.

Brush, L. M. & Wolman, M. G. (1960) Knickpoint behaviour in noncohesive material: a laboratory study. *Geological Society of America Bulletin*, **71**, 59-74.

Bruun, P. (1966) Model Geology: Prototype and Laboratory Streams. *Geological Society of America Bulletin*, **77**, 959-974.

Bryan, R. B. (1990) Knickpoint evolution in Rillwash. *Catena Supplement*, **17**, 111-132.

Bryant, M., Falk, P. & Paola, C. (1995) Experimental study of avulsion frequency and rate of deposition. *Geology*, **23**, 365-368.

Bull, W. B. (1979) Threshold of critical power in streams. *Geological Society of America Bulletin*, **90**, 453-464.

Burgess, P. M. & Allen, P. A. (1996) A forward-modelling analysis of the controls on sequence stratigraphical geometries. In: *Sequence Stratigraphy in British Geology* (Ed. by S. P. Hesselbo and D. N. Parkinson), *Geological Society of London Special Publication, **103***, 9-24.

Burgess, P. M. & Hovius, N. (1998) Rates of delta progradation during highstands: consequences for timing of deposition in deep-marine systems. *Journal of the Geological Society, London*, **155**, 217-222.

Butcher, S. W. (1990) The Nickpoint Concept and its Implications Regarding Onlap to the Stratigraphic Record. In: *Quantitative Dynamic Stratigraphy* (Ed. by T. A. Cross), 375-385.

Butler, P. R. (1984) Fluvial response to on-going tectonism and base-level changes, Lower Amargosa River, Southern Death Valley, California. *Sedimentary Geology*, **38**, 107-125.

Coleman, J. M. & Roberts, H. H. (1990) Cyclic Sedimentation of the Northern Gulf of Mexico Shelf. In: *Sequence Stratigraphy as an exploration tool: concepts and practices from the Gulf Coast: Programs and Abstracts, 11th Annual Research Conference, Gulf Coast Section of Society of Economic Paleontologists and Mineralogists, Houston, Texas*, 113-134.

Collier, R. E. & Gawthorpe, R. L. (1995) Neotectonics, drainage and sedimentation in central Greece: insights into coastal reservoir geometries in syn-rift sequences. In: *Hydrocarbon Habitat in Rift Basins* (Ed. by J. J. Lambiase), *Geological Society of London Special Publication, **80***, 165-181.

Coterill, K., Allen, S., De Tagle, F., Soto, A., Liu, C., Perez-Cruz, G., Wornardt, W. W. & Vail, P. R. (1990) Well log/seismic sequence stratigraphy of Miocene-Pleistocene, depositional sequences, High Island area, offshore Texas. In: *Sequence Stratigraphy as an exploration tool: concepts and practices from the Gulf Coast: Programs and Abstracts, 11th Annual Research Conference, Gulf Coast Section of Society of Economic Paleontologists and Mineralogists, Houston, Texas*, 135-138.

Crans, W., Mandl, G. & Haremboure, J. (1980) On the theory of growth faulting: a geomechanical delta model based on gravity sliding. *Journal of Petroleum Geology*, **2**, 265-307.

Curray, J. R. (1964) Transgressions and regressions. In: *Papers in Marine Geology, Shepard commemorative volume* (Ed. by R. L. Miller), 175-203.

Dalrymple, M., Prosser, D. J. & Williams, B. (1998) A Dynamic Systems Approach to the Regional Controls on Deposition and Architecture of Alluvial Sequences, Illustrated in the Statfjord Formation (United Kingdom, Northern North Sea). In: *Relative Role of Eustasy, Climate, and Tectonism in Continental Rocks* (Ed. by K. W. Shanley and P. J. McCabe), *Society of Economic Paleontologists and Mineralogists Special Publication, **59***, 65-82.

Damuth, J. E. (1994) Neogene gravity tectonics and depositional processes on the deep Niger Delta continental margin. *Marine Petroleum Geology*, **11**, 320-346.

Dart, C. J., Collier, R. E., Gawthorpe, R. L., Keller, J. V. A. & Nichols, G. (1994) Sequence stratigraphy of (?) Pliocene-Quaternary synrift, Gilbert-type fan deltas, northern Peloponesos, Greece. *Marine and Petroleum Geology*, **11**, 545-560.

De Vries, M. (1975) A morphological time-scale for rivers. In: *Proceedings of the XVIth IAHR Congress, Delft Hydraulics publication, **147***, 1-7.

De Vries, M. (1983) *Hydraulic Scale Models*. International Institute for Hydraulic and Environmental Engeneering, Delft, The Netherlands, 93 pp.

Dick, G. S., Anderson, R. S. & Sampson, D. E. (1997) Flash floods and channel evolution in the Blue Hills badlands, Caineville. *Geological Society of America Abstracts with Programs*, **29**, 139.

Doust, H. (1989) The Niger Delta: hydrocarbon potential of a major Tertiary delta province. In: *KNGMG Symposium Coastal Lowlands, Geology and Geotechnology* (Ed. by W. J. M. Van der Linden, S. A. P. Cloetingh, J. P. K. Kaasschieter, W. J. E. Van der Graaf, J. Vandenberghe and J. A. M. Van der Gun), 203-212.

Doust, H. & Omatsola, E. M. (1990) Niger Delta. In: *Divergent/Passive margin basins* (Ed. by J. D. Edwards and P. A. Santogrossi), *American Association of Petroleum Geologists Memoir, **48***, 201-238.

Driscoll, N. W. & Karner, G. D. (1999) Three-dimensional quantitative modelling of clinoform development. *Marine Geology,* **154**, 383-398.

Eaton, L. S. (1991) *Fluvial-geomorphic analysis of Wolf Creek Basin, Alexander Country, Ilinois, Master's thesis, Southern Illinois University,* Carbondale, IL, 73 pp.

Embry, A. F. (1990) A Tectonic Origin for Third Order Depositional Sequences in Extensional Basins - Implications for Basin Modeling. In: *Quantitative Dynamic Stratigraphy* (Ed. by T. A. Cross), pp. 491-501. Prentice Hall, Englewood Cliffs NJ.

Endo, N., Masuda, F. & Yokokawa, M. (1996) Grain-size distributions of sediment carried by single transportation models in an experimental microdelta system. *Sedimentary Geology,* **102**, 297-304.

Engelmund, F. & Hansen, E. (1967) *A monograph on sediment transport in alluvial streams.* Teknisk Forlag, Copenhagen, Denmark.

Ethridge, F. G., Wood, L. J. & Schumm, S. A. (1998) Cyclic Variables controlling fluvial sequence development: problems and perspectives. In: *Relative Role of Eustasy, Climate, and Tectonism in Continental Rocks* (Ed. by K. W. Shanley and P. J. McCabe), *Society of Economic Paleontologists and Mineralogists Special Publication, **59***, 17-30.

Fisk, H. N. (1944) *Geological investigation of the alluvial valley of the Lower Mississippi River.* Mississippi River Commission, Vicksburg.

Galloway, W. E. (1989) Genetic Stratigraphic Sequences in Basin Analysis I: Architecture and Genesis of Flooding-Surface Bounded Depositional Units. *American Association of Petroleum Geologists Bulletin,* **73**, 125-142.

Gardner, T. W. (1983) Experimental study of knickpoint and longitudinal profile evolution in cohesive, homogeneous material. *Geological Society of America Bulletin,* **94**, 664-672.

Gardner, T. W., Jorgensen, D. W., Shuman, C. & Lemieux, C. R. (1987) Geomorphic and tectonic process rates: effects of measured time interval. *Geology,* **15**, 259-261.

Gawthorpe, R. L., Fraser, A. J. & Collier, R. E. (1994) Sequence stratigraphy in active extensional basins: implications for the interpretation of ancient basin-fills. *Marine Petroleum Geology,* **11**, 642-658.

Germanowski, D. & Schumm, S. A. (1993) Changes in braided river morphology resulting from aggradation and degradation. *Journal of Geology,* **101**, 451-466.

Gupta, S., Underhill, J. R., Sharp, I. R. & Gawthorpe, R. L. (1999) Role of fault interactions in controlling synrift sediment dispersal patterns: Miocene, Abu Alaga Group, Suez Rift, Sinai, Egypt. *Basin Research,* **11**, 167-189.

Haq, B. U., Hardenbol, J. & Vail, P. R. (1988) Mezozoic and Cenozoic chronostratigraphy and cycles of sea-level change. In: *Sea-level changes: an integrated approach* (Ed. by C. K. Wilgus, B. S. Hastings, C. G. St Kendall, H. W. Posamentier, C. A. Ross and J. C. Van Wagoner), *Society of Economic Paleontologists and Mineralogists Special Publication, **42***, 71-108.

Hardin, N. S. (1987) Mass Transport Deposits of the Upper Continental Slope, Northwestern Gulf of Mexico. In: *Late Quaternary facies and structure, Northern gulf of Mexico* (Ed. by H. L. Berryhill, J. R. Suter and N. S. Hardin), *AAPG Studies in Geology, **23***, 241-284.

Hernandez-Molina, F. J., Somoza, L., Rey, J. & Pomar, R. L. (1994) Late Pleistocene-Holocene sediments on the Spanish continental shelves: Model for very high resolution sequence stratigraphy. *Marine Geology,* **120**, 129-174.

Holland, W. N. & Pickup, G. (1976) Flume study of knickpoint development in stratified sediment. *Geological Society of America Bulletin,* **87**, 76-82.

Hooke, R. L. (1968) Model Geology: Prototype and Laboratory Streams: Discussion. *Geological Society of America Bulletin,* **79**, 391-394.

Howard, A. D. (1982) Equilibrium and time scales in geomorphology: application to sand-bed alluvial streams. *Earth Surface Processes and Landforms,* **7**, 303-325.

Howard, A. D., Dietrich, W. E. & Seidl, M. A. (1994) Modeling fluvial erosion on regional to continental scales. *Journal of Geophysical Research,* **99**, 13971-13986.

Howell, J. A. & Flint, S. S. (1996) A Model for high resolution sequence stratigraphy within extensional basins. In: *High resolution sequence stratigraphy: Innovations and applications* (Ed. by J. A. Howell and J. F. Aitken), *Geological. Society of London Special Publication, **104***, 129-137.

Hubbert, M. K. (1937) Theory of scale models as applied to the study of geologic structures. *Geological Society of America Bulletin*, **48**, 1459-1520.

Hunt, D. & Tucker, M. E. (1992) Stranded Parasequences and the forced regressive wedge systems tract: deposition during base-level fall. *Sedimentary Geology*, **95**, 147-160.

Hunt, D. & Tucker, M. E. (1995) Stranded parasequences and the forced regressive wedge systems tract: deposition during base-level fall - reply. *Sedimentary Geology*, **95**, 147-160.

Jervey, M. T. (1988) Quantitative geological modelling of siliciclastic rock sequences and their seismic expression. In: *Sea-level changes: an integrated approach* (Ed. by C. K. Wilgus, B. S. Hastings, C. G. St Kendall, H. W. Posamentier, C. A. Ross and J. C. Van Wagoner), *Society of Economic Paleontologists and Mineralogists Special Publication, **42***, 47-69.

Jopling, A. V. (1963) Hydraulic studies on the origin of bedding. *Sedimentology*, **2**, 115-121.

Knox, G. J. & Omatsola, E. M. (1989) Development of the Cenozoic Niger delta in terms of the "Escalator Regression" model and impact on hydrocarbon distribution. In: *KNGMG Symposium Coastal Lowlands, Geology and Geotechnology* (Ed. by W. J. M. Van der Linden, S. A. P. Cloetingh, J. P. K. Kaasschieter, W. J. E. Van der Graaf, J. Vandenberghe and J. A. M. Van der Gun), 181-202.

Kolla, V., Posamentier, H. W. & Eichenseer, H. (1995) Stranded parasequences and the forced regressive wedge systems tract: deposition during base-level fall - discussion. *Sedimentary Geology*, **95**, 139-145.

Kooi, H. & Beaumont, C. (1996) Large-scale geomorphology: Classical concepts reconciled and integrated with contemporary ideas via a surface processes model. *Journal of Geophysical Research*, **101**, 3361-3386.

Koss, J. E., Ethridge, F. G. & Schumm, S. A. (1994) An experimental study of the effects of base-level change on fluvial, coastal plain and shelf systems. *Journal of Sedimentary Research*, **B64**, 90-98.

Labeyrie, L. D., Duplessy, J. C. & Blanc, P. L. (1987) Variations in mode of formation and temperature of oceanic deep waters over the past 125,000 years. *Nature*, **327**, 477-482.

Lawrence, D. S. L. (1996) Physical modelling in fluvial geomorphology: principles, applications and unresolved issues. In: *Proceedings of the 27th Binghamton Symposium in Geomorphology* (Ed. by B. L. Rhoads and C. E. Thorn), pp. 273-288. John Wiley & Sons, Chichester.

Leddy, J. O., Ashworth, P. J. & Best, J. L. (1993) Mechanisms of anabranch avulsion within gravel-bed braided rivers: observations from a scaled physical model. In: *Braided Rivers* (Ed. by J. L. Best and C. S. Bristow), *Geological Society of London Special Publication, **75***, 119-127.

Lee, H. Y. & Hwang, S. T. (1994) Migration of backward-facing step. *Journal of Hydraulic Engineering*, **120**, 693-705.

Leeder, M. R. & Gawthorpe, R. L. (1987) Sedimentary models for extensional tilt-block/half-graben basins. In: *Continental Extensional Tectonics* (Ed. by M. P. Coward, J. F. Dewey and P. L. Hancock), *Geological. Society of London Special Publication, **28***, 139-152.

Leeder, M. R. & Stewart, M. D. (1996) Fluvial incision and sequence stratigraphy: alluvial response to relative sea-level fall and their detection in the geological record. In: *Sequence Stratigraphy in British Geology* (Ed. by S. P. Hesselbo and D. N. Parkinson), *Geological Society of London Special Publication, **103***, 25-39.

Lehner, P. (1969) Salt Tectonics and Pleistocene stratigraphy on the continental slope of Northern Gulf of Mexico. *American Association of Petroleum Geologists Bulletin*, **53**, 2431-2479.

Leland, J., Reid, M. R., Burbank, D. W., Finkel, R. & Caffee, M. (1998) Incision and differential bedrock uplift along the Indus River near Nanga Parbat, Pakistan Himalaya, from 10Be and 26Al exposure age dating of bedrock straths. *Earth and Planetary Science Letters*, **154**, 93-107.

Leopold, L. B. & Bull, W. B. (1979) Base level, aggradation and grade. *Proceedings of the American Philosophical Society*, **123**, 168-202.

Ludwick, J. C. (1964) Sediment in the Northeastern Gulf of Mexico. In: *Papers in Marine Geology, Shepard commemorative volume* (Ed. by R. L. Miller), 204-240.

Mackin, J. H. (1948) Concept of the graded river. *Bulletin of the Geological Society of America*, **59**, 463-511.

Mandl, G. & Crans, W. (1981) Gravitational gliding in deltas. In: *Thrust and Nappe Tectonics* (Ed. by K. R. McClay and N. J. Price), *Geological Society of London Special Publication, **9***, 41-54.

Marriott, S. B. (1999) The use of models in the interpretation of the effects of base-level change on alluvial architecture. In: *Fluvial sedimentology VI* (Ed. by N. D. Smith and J. Rogers), *International Association of Sedimentologists Special Publication, **28***, 271-281.

Martinez, P. A. & Harbaugh, J. W. (1993) *Simulating nearshore environments*. Pergamon Press, Oxford, 265 pp.

Mauduit, T. & Brun, J.-P. (1998) Growth fault/rollover systems: Birth, growth and decay. *Journal of Geophysical Research*, **103-(B)**, 18,119-18,136.

Mauduit, T., Guerin, G., Brun, J.-P. & Lecanu, H. (1997) Raft tectonics: the effects of basal slope angle and sedimentation rate on progressive extension. *Journal of Structural Geology*, **19**, 1219-1230.

McClay, K. R., Dooley, T. & Lewis, G. (1998) Analog modeling of progradational delta systems. *Geology*, **26**, 771-774.

McClay, K. R. & Ellis, P. G. (1987) Analogue models of extensional fault geometries. In: *Continental Extensional Tectonics* (Ed. by M. P. Coward, J. F. Dewey and P. L. Hancock), *Geological. Society of London Special Publication, **28***, 109-125.

Metcalfe, S. E., O'Hara, S. L., Margarita, C. & Davies, S. J. (2000) Records of Late Pleistocene-Holocene climatic change in Mexico: a review. *Quaternary Science Reviews*, **19**, 699-721.

Meyer-Peter, E. & Müller, R. (1948) Formulas for Bed-Load transport. In: *Sec. Int. IAHR congress*, pp. 39-64, Stockholm, Sweden.

Miall, A. D. (1991) Stratigraphic Sequences and their Chronostratigraphic Correlation. *Journal of Sedimentary Petrology*, **61**, 494-505.

Miall, A. D. (1992) Exxon global cycle chart: An event for every occasion? *Geology*, **20**, 787-790.

Middleton, G. V. & Southard, J. B. (1984) *Mechanics of Sediment Movement*, 401 pp.

Milana, J. P. (1998) Sequence stratigraphy in alluvial settings: a flume based model with applications to outcrop and seismic data. *American Association of Petroleum Geologists Bulletin*, **82**, 1736-1753.

Mitchum, R. M., Sangree, J. B., Vail, P. R. & Wornardt, W. W. (1990) Sequence stratigraphy in late Cenozoic expanded sections, Gulf of Mexico. In: *Sequence Stratigraphy as an exploration tool: concepts and practices from the Gulf Coast: Programs and Abstracts, 11th Annual Research Conference, Gulf Coast Section of Society of Economic Paleontologists and Mineralogists, Houston, Texas*, 237-256.

Mitchum, R. M., Sangree, J. B., Vail, P. R. & Wornardt, W. W. (1993) Recognizing Sequences and Systems Tracts from Well Logs, Seismic Data, and Biostratigraphy: Examples from the Late Cenozoic of the Gulf of Mexico. In: *Siliciclastic Sequence Stratigraphy, Recent Developments and Applications* (Ed. by P. Weimer and H. W. Posamentier), *American Association of Petroleum Geologists Memoir, **58***, 163-197.

Mix, A. C. & Ruddiman, W. F. (1984) Oxigen-isotope analysis and Pleistocene ice volumes. *Quaternary Research*, **21**, 1-20.

Morton, R. A. & Price, A. W. (1987) Late Quaternary sea-level fluctuations and sedimentary phases of the Texas coastal plain and shelf. In: *Sea-level fluctuation and coastal evolution* (Ed. by D. Nummedal, O. H. Pilkey and J. D. Howard), *Society of Economic Paleontologists and Mineralogists Special Publication, **41***, 181-189.

Mulder, T. & Syvitski, J. P. M. (1996) Climatic and Morphologic Relationships of Rivers: Implications of Sea-level fluctuations on river loads. *Journal of Geology*, **104**, 509-523.

Muntingh, A. & Brown, L. F. (1993) Sequence Stratigraphy of Petroleum Plays, Post-Rift Cretaceous Rocks (Lower Aptian to Upper Maastrichtian), Orange Basin, Western Offshore, South Africa. In: *Siliciclastic Sequence Stratigraphy, Recent Developments and Applications* (Ed. by P. Weimer and H. W. Posamentier), *American Association of Petroleum Geologists Memoir, **58***, 71-97.

Nichol, S. L., Zaitlin, B. A. & Thom, B. G. (1997) The upper Hawkesbury River, New South Wales, Australia: a Holocene example of an estuarine bayhead delta. *Sedimentology,* **44**, 263-286.

Niedoroda, A. W., Reed, C. W., Swift, D. J. P., Arato, H. & Hoyanagi, K. (1995) Modelling shore-normal large-scale coastal evolution. *Marine Geology,* **126**, 181-199.

Nordlund, U. (1999) Stratigraphic modelling using common-sense rules. In: *Numerical experiments in stratigraphy: recent advances in stratigraphic and sedimentologic computer simulations* (Ed. by J. W. Harbaugh, W. L. Watney, E. C. Rankey, R. L. Slingerland, R. H. Goldstein and E. K. Franseen), *Society of Economic Paleontologists and Mineralogists Special Publication, **62***, 245-251.

Nott, J., Young, R. & McDougall, I. (1996) Wearing down, wearing back, and gorge extension in the long term denudation of a highland mass: quantitative evidence from the Shoalhaven catchment, Southeast Australia. *Journal of Geology,* **104**, 224-232.

Nummedal, D., Riley, G. W. & Templet, P. L. (1993) High-resolution sequence architecture: a chronostratigraphic model based on equilibrium profile studies. In: *Sequence Stratigraphy and Facies Associations* (Ed. by H. W. Posamentier, C. P. Summerhayes, B. U. Haq and G. P. Allen), *International Association of Sedimentologists Special Publication, **18***, 55-68.

Nummedal, D. & Swift, D. J. P. (1987) Transgressive stratigraphy at sequence-bounding unconformities: some principles derived from Holocene and Cretaceous examples. In: *Sea-level fluctuation and coastal evolution* (Ed. by D. Nummedal, O. H. Pilkey and J. D. Howard), *Society of Economic Paleontologists and Mineralogists Special Publication, **41***, 129-143.

Oreskes, N., Schrader-Frechette, K. & Belitz, K. (1994) Verification, Validation, and Confirmation of Numerical Models in the Earth Sciences. *Science,* **263**, 641-646.

Pacht, J. A. (1990) Sequence stratigraphy of Plio-Pleistocene strata in the offshore Louisiana Gulf Coast: applications to hydrocarbon exploration. In: *Sequence Stratigraphy as an exploration tool: concepts and practices from the Gulf Coast: Programs and Abstracts, 11th Annual Research Conference, Gulf Coast Section of Society of Economic Paleontologists and Mineralogists, Houston, Texas*, pp. 269-285.

Pacht, J. A. (1996) Sequence Stratigraphic framework of Neogene strata in off-shore Nigeria. *American Association of Petroleum Geologists Bulletin,* **80**, 1321.

Paola, C. (1991) The response distance of river systems to variations in sea level. *Geological Society of America Abstracts with Programs,* **23**, A170-171.

Paola, C. (2000) Quantitative models of sedimentary basin filling. *Supplement to Sedimentology,* **47**, 121-178.

Paola, C., Heller, P. L. & Angevine, C. L. (1992) The large-scale dynamics of grain-size variation in alluvial basins, 1: Theory. *Basin Research,* **4**, 73-90.

Parker, G. (1978) Self-formed straight rivers with equilibrium banks and mobile bed. Part 2: The gravel river. *Journal of Fluid Mechanics,* **89**, 127-146.

Pazzaglia, F. P., Gardner, T. W. & Merritts, D. J. (1998) Bedrock Fluvial incision and longitidinal profile development over geologic time scales determined by fluvial terraces. In: *Rivers over rock; fluvial processes in bedrock channels* (Ed. by K. J. Tinkler and E. E. Wohl), *Geophysical Monograph, **107***, 207-235.

Peakall, J., Ashworth, P. J. & Best, J. L. (1996) Physical modelling in fluvial geomorphology: principles, applications and unresolved issues. In: *Proceedings of the 27th Binghamton Symposium in Geomorphology* (Ed. by B. L. Rhoads and C. E. Thorn), 221-254.

Plint, A. G. & Nummedal, D. (2000) The falling stage systems tract: recognition and importance in sequence stratigraphic analysis. In: *Sedimentary Responses to Forced Regressions* (Ed. by D. Hunt and R. L. Gawthorpe), *Geological Society of London Special Publication, **172***, 1-17.

Poag, C. W. (1992) U.S. Middle Atlantic continental rise: Provenance, dispersal, and deposition of Jurassic to Quaternary Sediments. In: *Geologic evolution of Atlantic continental rises* (Ed. by C. W. Poag and P. C. de Graciansky), 100-156.

Posamentier, H. W. & Allen, G. P. (1993) Variability of the sequence stratigraphic model: effects of local basin factors. *Sedimentary Geology,* **86**, 91-109.

Posamentier, H. W., Allen, G. P. & James, D. P. (1992) High resolution sequence stratigraphy-the East Coulee Delta, Alberta. *Journal of Sedimentary Petrology,* **62**, 310-317.

Posamentier, H. W., Allen, G. P., James, D. P. & Tesson, M. (1992) Forced Regressions in a Sequence Stratigraphic Framework: Concepts, Examples, and Exploration Significance. *American Association of Petroleum Geologists Bulletin,* **76**, 1687-1709.

Posamentier, H. W. & James, D. P. (1993) An overview of sequence-stratigraphic concepts: uses and abuses. In: *Sequence Stratigraphy and Facies Associations* (Ed. by H. W. Posamentier, C. P. Summerhayes, B. U. Haq and G. P. Allen), *International Association of Sedimentologists Special Publication, **18***, 3-18.

Posamentier, H. W., Jervey, M. T. & Vail, P. R. (1988) Eustatic controls on clastic deposition I - Conceptual framework. In: *Sea-level changes: an integrated approach* (Ed. by C. K. Wilgus, B. S. Hastings, C. G. St Kendall, H. W. Posamentier, C. A. Ross and J. C. Van Wagoner), *Society of Economic Paleontologists and Mineralogists Special Publication, **42***, 109-124.

Posamentier, H. W. & Vail, P. R. (1988) Eustatic controls on clastic deposition II - Sequence and Systems Tract Models. In: *Sea-level changes: an integrated approach* (Ed. by C. K. Wilgus, B. S. Hastings, C. G. St Kendall, H. W. Posamentier, C. A. Ross and J. C. Van Wagoner), *Society of Economic Paleontologists and Mineralogists Special Publication, **42***, 125-154.

Postma, G. (1990) Depositional architecture and facies of river and fan deltas: a synthesis. In: *Coarse Grained Deltas* (Ed. by A. Collela and D. B. Prior), *International Association of Sedimentologists Special Publication, **10***, 13-27.

Postma, G., Hilgen, F. J. & Zachariasse, W. J. (1993) Precession punctuated growth of a late Miocene submarine-fan lobe on Gavdos (Greece). *Terra Nova,* **5**, 438-444.

Quirk, D. G. (1996) Base profile: a unifying concept in alluvial sequence stratigraphy. In: *High resolution sequence stratigraphy: Innovations and applications* (Ed. by J. A. Howell and J. F. Aitken), *Geological Society of London Special Publication, **104***, 37-49.

Reid, I. & Frostick, L. E. (1994) Fluvial sediment transport and deposition. In: *Sediment transport and depositional processes* (Ed. by K. Pye), 421.

Reijers, T. J. A., Petters, S. W. & Nwajide, C. S. (1997) The Niger Delta Basin. In: *African Basins* (Ed. by R. C. Selley), *Sedimentary Basins of the World, **3***, 151-172.

Ricketts, B. D. & Evenchick, C. A. (1999) Shelfbreak gullies: products of sea-level lowstand and sediment failure: examples from browser basin, Northern British Columbia. *Journal of Sedimentary Research,* **69**, 1232-1240.

Rodriguez, A. B., Anderson, J. B., Banfield, L. A., Taviani, M., Abdulah, K. C. & Snow, J. N. (2000) Identification of a -15m middle Wisconsin shoreline on the Texas inner continental shelf. *Palaeogeography, Palaeoclimatology, Palaeoecology,* **158**, 25-43.

Rothwell, R. G., Kenyon, N. H. & McGregor, B. A. (1991) Sedimentary features of the south Texas continental slope as revealed by side-scan sonar and high-resolution seismic data. *American Association of Petroleum Geologists Bulletin,* **75**, 298-312.

Saito, Y. (1995) High-resolution sequence stratigraphy of an incised-valley fill in a wave- and fluvial dominated setting: latest Pleistocene-Holocene examples from the Kanto Plain of central Japan. In: *Sequence Stratigraphy - Toward a new dynamic stratigraphy* (Ed. by Y. Saito, K. Hoyanagi and M. Ito), *Memoirs of the geological Society of Japan, **45***, 76-99.

Salter, T. (1993) Fluvial scour and incision: models for their influence on the development of realistic reservoir geometries. In: *Characterization of fluvial and eaolian reservoirs* (Ed. by C. P. North and D. J. Prosser), *Geological Society of London Special Publication, **73***, 33-51.

Saucier, R. T. (1996) A contemporary appraisal of some key Fiskian concepts with emphasis on Holocene meanderbelt formation and morphology. *Engineering Geology,* **45**, 67-86.

Schlager, W. (1993) Sediment supply and accommodation: a dual control. *Sedimentary Geology,* **86**, 111-137.

Schlager, W. (2000) The future of applied sedimentary geology. *Journal of Sedimentary Research,* **70**, 2-9.

Schlische, R. W. (1991) Half-graben basin filling models: new constraints on continental extensional basin development. *Basin Research,* **3**, 123-141.

Schumm, S. A. (1977) *The Fluvial System*. John Willey & Sons, New York, 338 pp.

Schumm, S. A. (1991) *To interpret the earth: Ten Ways to be Wrong*. Cambridge University Press, Cambridge, 131 pp.

Schumm, S. A. (1993) River Response to Baselevel Change: Implications for sequence Stratigraphy. *Journal of Geology*, **101**, 279-294.

Schumm, S. A., Erskine, W. D. & Tilleard, J. W. (1996) Morphology, hydrology, and evolution of the anastomosing Ovens and King Rivers, Victoria, Australia. *Geological Society of America Bulletin*, **108**, 1212-1224.

Schumm, S. A. & Ethridge, F. G. (1994) Origin, Evolution and Morphology of Fluvial Valleys. In: *Incised-valley systems: origin and sedimentary sequences* (Ed. by R. W. Dalrymple, R. Boyd and B. A. Zaitlin), *Society of Economic Paleontologists and Mineralogists Special Publication*, ***51***, 11-28.

Schumm, S. A. & Khan, H. R. (1972) Experimental Study of Channel Patterns. *Geological Society of America Bulletin*, **83**, 1755-1770.

Schumm, S. A. & Lichty, R. W. (1965) Time, space, and causality in geomorphology. *American Journal of Science*, **263**, 110-119.

Schumm, S. A., Mosley, P. M. & Weaver, W. E. (1987) *Experimental fluvial geomorphology*. John Wiley & Sons, New York, 413 pp.

Seidl, M. A., Dietrich, W. E. & Kirchner, J. W. (1994) Longitudinal profile development into Bedrock: an analysis of Hawaiian Channels. *Journal of Geology*, **102**, 457-474.

Shackleton, N. J. (1987) Oxygen isotopes, ice volume and sea level. *Quaternary Science Reviews*, **6**, 183-190.

Shanley, K. W. & McCabe, P. J. (1991) Predicting facies architecture through sequence stratigraphy-An example from the Kaiparowits Plateau, Utah. *Geology*, **19**, 742-745.

Shanley, K. W. & McCabe, P. J. (1993) Alluvial architecture in a sequence stratigraphic framework: a case history from the Upper Cretaceous of southern Utah, USA. In: *The geological modelling of hydrocarbon reservoirs and outcrop analogues* (Ed. by S. S. Flint and M. Bryant), *International Association of Sedimentologists Special Publication*, ***15***, 21-56.

Shanley, K. W. & McCabe, P. J. (1994) Perspectives of the Sequence Stratigraphy of Continental Strata. *American Association of Petroleum Geologists Bulletin*, **78**, 544-568.

Shanley, K. W. & McCabe, P. J. (1998) Relative Role of Eustasy, Climate, and Tectonism in Continental Rocks: An Introduction. In: *Relative Role of Eustasy, Climate, and Tectonism in Continental Rocks* (Ed. by K. W. Shanley and P. J. McCabe), *Society of Economic Paleontologists and Mineralogists Special Publication*, ***59***, iii-iv.

Short, K. C. & Stauble, A. J. (1967) Outline of Geology of Niger Delta. *American Association of Petroleum Geologists Bulletin*, **51**, 761-779.

Simon, A. (1991) *Morphology and dynamics of incised alluvial channels, West Tennessee, Master's thesis, Colorado State University*, Fort Collins, CO, 273 pp.

Skene, K. I., Piper, D. J. W., Aksu, A. E. & Syvitski, J. P. M. (1998) Evaluation of the global oxigen isotope curve as a proxy for Quaternary sea level by modeling delta progradation. *Journal of Sedimentary Research*, **68**, 1077-1092.

Snow, J. N. (1998) *Late Quaternary highstand and transgressive deltas of the ancestral Colorado River: eustatic and climatic controls on deposition, unpublished Ph.D. thesis, Rice University, Houston, Texas*, 138 pp.

Stacher, P. (1995) Present understanding of the Niger Delta Hydrocarbon habitat. In: *Geology of Deltas* (Ed. by M. N. Oti and G. Postma), 257-267.

Steckler, M. S., Reynolds, D. J., Coakley, B. J., Swift, B. A. & Jarrard, R. (1993) Modelling passive margin sequence stratigraphy. In: *Sequence Stratigraphy and Facies Associations* (Ed. by H. W. Posamentier, C. P. Summerhayes, B. U. Haq and G. P. Allen), *International Association of Sedimentologists Special Publication*, ***18***, 19-41.

Stock, J. D. & Montgomery, D. R. (1999) Geologic constraints on bedrock river incision using the stream power law. *Journal of Geophysical Research*, **104**, 4983-4993.

Suter, J. R. & Berryhill, H. L. (1985) Late Quaternary shelf-margin deltas, Northwest Gulf of Mexico. *American Association of Petroleum Geologists Bulletin*, **69**, 77-91.

Suter, J. R., Berryhill, H. L. & Penland, S. (1987) Late Quaternary sea-level fluctuations and depositional sequences, Southwest Louisiana continental shelf. In: *Sea-level fluctuation and coastal evolution* (Ed. by D. Nummedal, O. H. Pilkey and J. D. Howard), *Society of Economic Paleontologists and Mineralogists Special Publication*, ***41***, 199-219.

Talling, P. J. (1998) How and where do incised valleys form if sea-level remains above the shelf edge? *Geology*, **26**, 87-90.

Tesson, M., Gensous, B., Allen, G. P. & Ravenne, C. (1990) Late Quaternary Deltaic Lowstand Wedges on the Rhône Continental Shelf, France. *Marine Geology*, **91**, 325-332.

Thorne, J. A. (1994) Constraints on riverine valley incision and the response to sea-level change based on fluid mechanics. In: *Incised-valley systems: origin and sedimentary sequences* (Ed. by R. W. Dalrymple, R. Boyd and B. A. Zaitlin), *Society of Economic Paleontologists and Mineralogists Special Publication*, ***51***.

Thorne, J. A. & Swift, D. J. P. (1991) Sedimentation on continental margins, VI: a regime model for depositional sequences, their component systems tracts, and bounding surfaces. In: *Shelf sand and sandstone bodies* (Ed. by D. J. P. Swift, G. F. Oertel, R. W. Tillman and J. A. Thorne), *International Association of Sedimentologists Special Publication*, ***14***, 189-255.

Tobias, S. (1990) Expansion profiles and sequence stratigraphy: a new way to identify system tracts, sequence boundaries and eustatic histories. In: *Sequence Stratigraphy as an exploration tool: concepts and practices from the Gulf Coast: Programs and Abstracts, 11th Annual Research Conference, Gulf Coast Section of Society of Economic Paleontologists and Mineralogists, Houston, Texas*, 351-361.

Toomey, R. S., Blum, M. D. & Valastro, S. (1994) Late Quaternary climates and environments of the Edwards Plateau, Texas. *Global and Planetary Change*, **7**, 299-320.

Törnqvist, T. E. (1998) Longitudional profile evolution of the Rhine-Meuse system during the last deglaciation: interplay of climate change and glacio-eustacy? *Terra Nova*, **10**, 11-15.

Törnqvist, T. E., Wallinga, J., Murray, A. S., De Wolf, H., Cleveringa, P. & De Gans, W. (in press) Response of the Rhine-Meuse system (west-central Netherlands) to the Last Quaternary glacio-eustatic cycles: a first assessment. *Global and Planetary Change*.

Underhill, J. R. & Partington, M. A. (1993) Use of sequence stratigraphy in defining and determining a regional tectonic control on the Mid-Cimmerian Unconformity; Implications for North Sea basin development and the global sea-level chart. In: *Siliciclastic Sequence Stratigraphy: Recent Developments and Applications* (Ed. by P. Weimer and H. W. Posamentier), *American Association of Petroleum Geologists Memoir*, ***58***, 449-484.

Vail, P. R., Mitchum, R. M., Todd, R. G., Widmier, J. M., Thompson, S. I., Sangree, J. B., Bubb, J. N. & Hatelid, W. G. (1977) Seismic Stratigraphy - applications to hydrocarbon exploration. In: *Seismic Stratigraphy - applications to hydrocarbon exploration* (Ed. by C. E. Payton), *American Association of Petroleum Geologists Memoir*, ***26***, 49-212.

Van Rijn, L. C. (1984) Sediment Transport, Part I: Bed-Load Transport. *Journal of Hydraulic Engineering, ASCE*, **110**.

Van Wagoner, J. C., Posamentier, H. W., Mitchum, R. M., Vail, P. R., Sarg, J. F., Loutit, T. S. & Hardenbol, J. (1988) An overview of the fundamentals of Sequence Stratigraphy and key definitions. In: *Sea-level changes: an integrated approach* (Ed. by C. K. Wilgus, B. S. Hastings, C. G. St Kendall, H. W. Posamentier, C. A. Ross and J. C. van Wagoner), *Society of Economic Paleontologists and Mineralogists Special Publication*, ***42***, 39-45.

Wang, Z. & Kron, W. (1991) Time distortion in large scale sediment model tests. *Journal of Hydraulic Research*, **29**, 161-178.

Weber, K. J. & Daukoru, E. (1975) Petroleum geology of the Niger Delta. In: *Ninth World Petroleum Congress Proceedings, Vol. 2*, pp. 209-221. Applied Science publishers, London.

Wehr, E. L. (1993) Effects of variations in subsidence and sediment supply on parasequence stacking patterns. In: *Siliciclastic Sequence Stratigraphy: Recent Developments and Applications* (Ed. by P. Weimer and H. W. Posamentier), *American Association of Petroleum Geologists Memoir*, ***58***, 369-380.

Weissel, J. K. & Seidl, M. A. (1997) Influence of rock strength properties on escarpment retreat across passive continental margins. *Geology*, **25**, 631-634.

Wescott, W. A. (1993) Geomorphic Thresholds and Complex Response of Fluvial Systems-Some Implications for Sequence Stratigraphy. *American Association of Petroleum Geologists Bulletin*, **77**, 1208-1218.

Wetzel, A. (1993) The transfer of River load to deep-sea fans: a quantitative approach. *American Association of Petroleum Geologists Bulletin*, **77**, 1679-1692.

Whipple, K. X. & Tucker, G. E. (1999) Dynamics of the stream-power river incision model: Implications for height limits of mountain ranges, landscape response timescales, and research needs. *Journal of Geophysical Research*, **104**, 17661-17674.

Willgoose, G., Bras, R. L. & Rodriquez-Iturbe, I. (1990) Results from a new model of river basin evolution. *Earth Surface Processes and Landforms*, **16**, 237-254.

Wohl, E. E. (1998) Bedrock channel morphology in relation to erosional processes. In: *Rivers over rock; fluvial processes in bedrock channels* (Ed. by K. J. Tinkler and E. E. Wohl), *Geophysical Monograph 107*, 113-151.

Wood, L. J., Ethridge, F. G. & Schumm, S. A. (1993) The effects of rate of base-level fluctuation on coastal-plain, shelf, and slope depositional systems: an experimental approach. In: *Sequence Stratigraphy and Facies Associations* (Ed. by H. W. Posamentier, C. P. Summerhayes, B. U. Haq and G. P. Allen), *International Association of Sedimentologists Special Publication*, ***18***, 43-54.

Wood, L. J., Ethridge, F. G. & Schumm, S. A. (1993) An Experimental Study of the Influence of Subaquous Shelf Angles on Coastal Plain and Shelf Deposits. In: *Siliciclastic Sequence Stratigraphy: Recent Developments and Applications* (Ed. by P. Weimer and H. W. Posamentier), *American Association of Petroleum Geologists Memoir*, ***58***, 381-391.

Woodbury, H. O., Spotts, J. H. & Akkers, W. H. (1978) Gulf of Mexico continental-slope sediments and sedimentation. In: *Framework, facies and oil-trapping characteristics of the upper continental margin* (Ed. by A. H. Bouma, G. T. Moore and J. M. Coleman), *AAPG Studies in Geology*, ***7***, 117-137.

Woolfe, K. J., Larcombe, P., Naish, T. & Purdon, R. G. (1998) Lowstand rivers need not to incise the shelf: an example from Great Barrier Reef, Australia, with implications for sequence stratigraphic models. *Geology*, **26**, 75-78.

Yalin, M. S. (1971) *Theory of Hydraulic Models*. Macmillan, London, 266 pp.

Yang, H. & Li, P. (1988) The evolution of a knick-point belt in a river section in Huangguoshu. *IAHS Publication*, **176**, 225-232.

Yodis, E. G. & Kesel, R. H. (1993) The effects and implications of base -level changes to Mississippi River Tributaries. *Zeitschrift zur Geomorphologie*, **37**, 385-402.

Young, R. & McDougall, I. (1993) Long-term landscape evolution: Early Miocene and Modern rivers in Southern New South Wales, Australia. *Journal of Geology*, **101**, 35-49.

Zaitlin, B. A., Dalrymple, R. W. & Boyd, R. (1994) The stratigraphic organization of incised valley systems associated with relative sea-level change. In: *Incised-valley systems: origin and sedimentary sequences* (Ed. by R. W. Dalrymple, R. Boyd and B. A. Zaitlin), *Society of Economic Paleontologists and Mineralogists Special Publication*, ***51***, 45-60.

Zhang, Y., Swift, D. J. P., Niedoroda, A. W., Reed, C. W. & Thorne, J. A. (1997) Simulation of sedimentary facies on the Northern California Shelf. *Geology*, **25**, 635-638.

Samenvatting voor de leek

(Simplified summary in Dutch based on Chapter 1)

Inleiding

Is het u wel eens opgevallen dat de grillig vertakte stroompjes op het strand verrassend veel lijken op luchtfoto's van rivieren en delta's? Deze stroompjes zijn te beschouwen als een analoog voor rivieren op een veel grotere schaal (Figuur 1a). Dit is het principe achter het onderzoek van dit proefschrift. Daarbij is met een analoog model gewerkt om meer inzicht te krijgen in de geologische geschiedenis (de vorming) van rivieren en delta's. Bij een stroompje op het strand of bij een echte rivierdelta zijn niet alle omstandigheden en variabelen bekend en controleerbaar. Bij de gebruikte laboratoriumopstelling met een waterbassin is dit wel het geval.

Deze samenvatting behandelt allereerst de probleemstelling, het doel en de praktische toepasbaarheid van dit onderzoek. Daarna volgt een samenvatting per hoofdstuk gevolgd door de conclusies.

Probleemstelling

Er zijn drie belangrijke variabelen die de vorming van afzettingen in rivierbeddingen, delta's en kustvlakten beïnvloeden in de loop van duizenden tot miljoenen jaren. Dit zijn zeespiegelvariaties, klimaat en tektoniek (verticale bodembewegingen). Zo varieerde het zeeniveau maximaal 150 m tijdens het Kwartair (de afgelopen 1.7 miljoen jaar). Achttienduizend jaar geleden bijvoorbeeld, tijdens de recente ijstijd, stond de zeespiegel 120 m lager dan nu. Tijdens een periode met een lage zeespiegelstand komt de shelf, dat is het ondiepe deel van de zeebodem ofwel continentaal plat, boven water. De shelf vormt dan een verlenging van de kust waarover rivieren zich zeewaarts kunnen verleggen. Daarom wordt in deze studie het traject van de riviervallei, de kust en de shelf als één geheel beschouwd: het rivier-shelf sedimentaire systeem (Figuur 1a). Klimaatsveranderingen, bijvoorbeeld die de ijstijden in het Kwartair veroorzaakten, hebben tevens invloed op de hoeveelheid sedimenttransport van de rivier naar de zee (neerslag, vegetatie, bodemsamenstelling). Tektoniek in de vorm van bodemdaling van de riviervallei of de delta, geeft extra ruimte om sedimenten op te slaan. Daarentegen veroorzaakt opheffing van de bodem afbraak (erosie) van eerder neergelegde sedimenten.

De gevormde opeenstapeling van de sedimentlagen (afzettingen) in het rivier-shelf sedimentaire systeem is dus het resultaat van veranderingen in zeespiegel, klimaat en tektoniek tijdens de geologische geschiedenis (Figuur 1b). Geologen proberen op basis van de fossiele afzettingen de invloed te bepalen van elke variabele. Het praktische probleem hierbij is dat de sedimentlagen in de bodem maar beperkt toegankelijk zijn voor studie. Daarnaast kan een verticale opeenvolging van sedimentlagen hiaten bevatten (perioden waarin geen afzetting plaats vond of een bestaande laag weer is verdwenen door erosie). Tevens laten zeespiegelvariaties, klimaatschommelingen en tektoniek geen uniek spoor achter in de ondergrond. Verschillende combinaties van deze drie factoren kunnen een identiek patroon van sedimentlagen opleveren. Bijvoorbeeld: een zeespiegelverlaging maakt dat de kustlijn en ook de riviermonding zeewaarts verschuiven. Daardoor wordt de benedenloop van de rivier langer en zal de gradiënt (helling) van de rivier zich aanpassen. Maar ook

klimaat (water- en sedimentafvoer) en tektoniek (bodembeweging) kunnen veranderingen in de riviergradiënt veroorzaken die leiden tot een zeewaartse uitbouw van de delta.
Het is meestal onmogelijk om achteraf te bepalen in welke verhouding de variabelen een rol hebben gespeeld. De geoloog die de opbouw van de verschillende sedimentlagen in rivieren en delta's onderzoekt kijkt terug in de tijd bij het maken van zijn reconstructie. Modelstudies als deze bieden de mogelijkheid om het ontstaan van deze afzettingen na te bootsen (voorwaarts te modelleren).

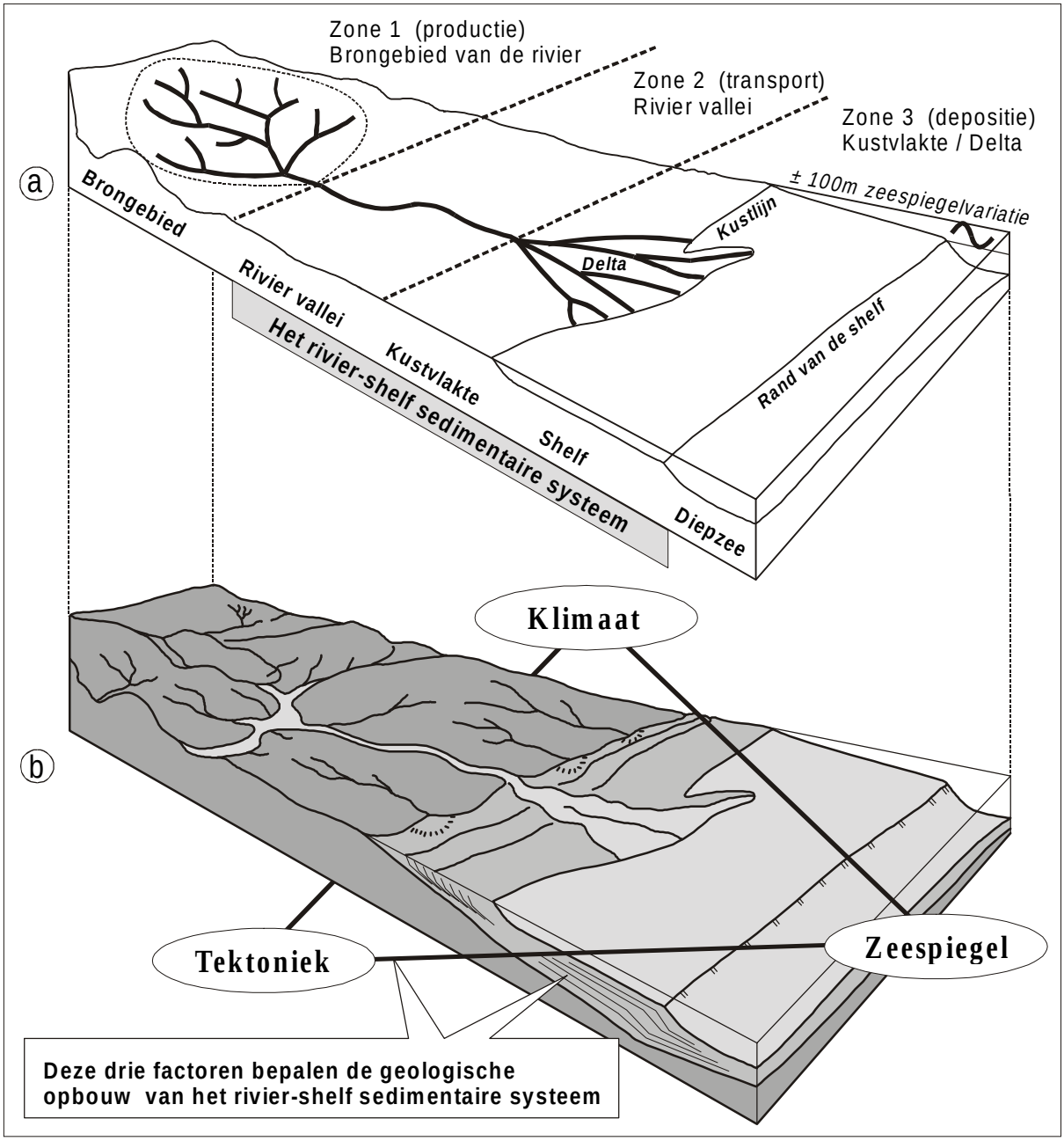

Figuur 1—(a) De loop van een rivier vanaf het brongebied (zone 1: sediment productie) via de riviervallei (zone 2: sedimenttransport) naar zone 3: afzetting van sedimenten op de delta en de kust. Indeling volgens Schumm, (1977). Deze studie modelleert het rivier-shelf sedimentaire systeem. Dit omvat de riviervallei, de kustvlakte en de shelf. (b) Het afzettingspatroon van het rivier-shelf sedimentaire systeem wordt op een geologische tijdschaal bepaald door zeespiegelvariaties, klimaat en tektoniek.

Doel

Hoofddoel van dit onderzoek is het bepalen van de rol van zeespiegelvariaties, tektoniek en klimaat op de ontwikkeling van het rivier-shelf sedimentaire systeem. Hiertoe is in een waterbassin met behulp van een analoog model de ontwikkeling van de riviervallei, de kustvlakte en de shelf over geologische perioden van duizenden tot enkele miljoenen jaren nagebootst. Op deze manier kunnen veldhypothesen worden getest. Daarnaast kunnen in een model zeespiegelvariaties, tektoniek en klimaat systematisch worden gevarieerd om zo de gevoeligheid van de rivierdelta voor deze factoren te testen.

De onderzoeksmethode is geïnspireerd op soortgelijke modelstudies aan de Colorado State University. (Wood *et al*., 1993; Koss *et al*., 1994). Momenteel is deze toepassing van analoge modellen in de geologie vrijwel uniek. Alleen aan de University of Minnesota loopt een vergelijkbaar programma (Paola, 2000). Inmiddels wordt steeds vaker de computer ingezet om dergelijke onderzoeken te doen. Het blijft echter moeilijk, zoniet onmogelijk, om alle processen van het sedimenttransport in rivieren en delta's in één computermodel onder te brengen.

Een voordeel van analoge modellen, zoals hier toegepast, is dat ze gebaseerd zijn op realistisch sedimenttransport, weliswaar op een veel kleinere schaal. Sedimenttransport-processen zijn er dus op natuurlijke wijze in verwerkt. Een nadeel van de bestaande analoge model studies was dat ze slechts beschrijvend waren (kwalitatief). Er waren dus enkel grove schattingen van de sedimentverplaatsingen mogelijk. Daardoor was het onmogelijk de resultaten naar de werkelijkheid op te schalen. Dit onderzoek heeft zich er allereerst op gericht om een meetbrug te ontwikkelingen waarmee de resultaten van analoge modellen kwantitatief gemaakt kunnen worden.

In 1995 is de projectgroep Sedimentologie van de Faculteit Aardwetenschappen van de Universiteit Utrecht in samenwerking met Shell begonnen met de ontwikkeling van deze meetbrug. Hiermee wordt sedimentoppervlak van een analoog model nauwkeurig opgemeten. Deze studie kreeg een vervolg in dit door Shell gefinancierde promotieonderzoek waarbij de meetbrug is verbeterd. De nieuwe bijdrage van dit onderzoek is dat de gemodelleerde rivieren en delta’s en hun sedimentverplaatsingen op 0.4 mm nauwkeurig zijn opgemeten. Deze uitkomsten zijn gekwantificeerd voor reeksen experimenten. Door de sedimentverplaatsingen in het model te meten kunnen de modeluitkomsten beter met die van een echte rivierdelta worden vergeleken. Daarnaast is er naar een manier gezocht om het analoge model zo goed mogelijk te schalen naar echte rivier-shelf systemen. Op deze manier dragen analoge modellen op een kwantitatieve manier bij aan een beter begrip van de geologische ontwikkeling het rivier-shelf sedimentaire systeem.

Praktische toepasbaarheid

De resultaten van dit onderzoek laten de invloed zien van zeespiegelvariaties, klimaatveranderingen en bodembewegingen op rivierdelta’s op een geologische tijdschaal van duizenden tot enkele miljoenen jaren. Dit onderzoek richt zich ook op het testen van een veel toegepast geologisch concept: de sequentie stratigrafie. Bij sequentie stratigrafie reconstrueert men de omstandigheden waaronder sedimenten zijn afgezet op basis van de aard en de driedimensionale vorm van de afzettingen

(geometrie). Door het bestuderen van de sedimenten, die tijdens een experiment met bekende variabelen zijn afgezet, kunnen de sterke en zwakke punten van het sequentie stratigrafisch concept worden bepaald. Door het analoge model te beschouwen als een klein rivier-shelf sedimentair systeem waarvan wel alle parameters bekend zijn kunnen de resultaten tevens worden gebruikt om computermodellen te testen. (Fig. 1.3 op pag. 14). Tenslotte kunnen de onderzoeksresultaten helpen bij het voorspellen van mogelijke locaties van olie en gas reservoirs in fossiele rivier-shelf systemen.

Leeswijzer en samenvatting per hoofdstuk

Dit Engelstalige proefschrift bestaat uit een inleiding (hoofdstuk 1) gevolgd door drie artikelen (de hoofdstukken 2 t/m 4). ***Hoofdstuk 1*** is een uitgebreide inleiding en samenvatting van het gehele proefschrift.

Hoofdstuk 2 begint met een inventarisatie van alle aspecten en variabelen die van belang zijn voor het analoog modelleren van sedimentaire systemen. Bij het modelleren over geologische tijdspannen van duizenden tot miljoenen jaren zijn de conventionele schalingsmethoden niet meer bruikbaar. In dit onderzoek is gekozen voor de best mogelijke schalings strategie. De gebruikte schalingsmethode komt er in het kort op neer dat een hoeveelheid verplaatst sediment in een bepaalde periode in het analoge model kan worden vergeleken met verplaatste sediment volumes over een geologisch tijdsbestek in een echte rivierdelta. Hierbij is de schaling van de korrelgrootte van het sediment buiten beschouwing gelaten. Het zand in het model is enkel het medium waaraan het sedimenttransport is gemeten.

Daarnaast zijn er drie randvoorwaarden gesteld. De dynamica van het sedimenttransport moet realistisch zijn. Ten tweede moeten de dimensies (lengte, breedte en hoogte) zijn geschaald voor model en werkelijkheid. Ten derde moet de reactietijd van het model (bijvoorbeeld op een zeespiegelverlaging), gerelateerd worden aan de reactietijd van een reëel sedimentair systeem. Hierbij wordt gelet op de verhouding tussen de reactietijd en totale tijdsduur waarover wordt gemodelleerd. Deze verhouding moet ongeveer gelijk zijn voor het model en de werkelijkheid.

De methode wordt uitgelegd en verantwoord met een vergelijking tussen een experiment en de ontwikkeling van de Colorado Delta. Tijdens de afgelopen veertigduizend jaar vonden hier een daling en stijging van de zeespiegel plaats die verband hielden met de laatste ijstijd. De sedimentlobben die de Colorado Rivier hierbij heeft achtergelaten op de kust en op de zeebodem worden vergeleken met de delta ontwikkeling in een experiment dat zoveel mogelijk dezelfde zeespiegelverandering nabootst. Het experiment is twee maal herhaald om de reproduceerbaarheid ervan na te gaan. Vergelijking van het experiment met de Colorado Delta laat zien dat een zeespiegelverlaging bijdraagt tot erosie van de kustvlakte en de blootgelegde zeebodem. De erosie veroorzaakt een extra puls van sediment naar de zeewaarts verschoven kustlijn waar zich, op de rand van de shelf, een delta vormt. De experimenten ondersteunen het eerder geopperde idee dat de hogere sedimentafvoer gedurende een periode met een lager zeeniveau (ijstijd) niet enkel moet worden toegeschreven aan klimaat maar dat het deels ook wordt veroorzaakt door toename van erosie als gevolg van de zeespiegelverlaging zelf.

Hoofdstuk 3 beschrijft de resultaten van een reeks van 18 experimenten waarbij enkel de snelheid van zeespiegelverandering is gevarieerd en alle andere

omstandigheden gelijk zijn gehouden. Op deze manier is de gevoeligheid van het analoge model van het rivier-shelf systeem voor zeespiegelveranderingen onderzocht. Hierbij is voornamelijk gelet op de manier waarop de rivier zich aanpast wanneer de shelf tijdens een zeespiegelverlaging bloot komt te liggen. In het geologische concept van de sequentie stratigrafie leidt een zeespiegelverlaging tot erosie van de rivierbedding (verlaging van het rivierprofiel). Een zeespiegelstijging leidt tot depositie (opvulling van het rivierprofiel). De aanpassing van de rivier aan zeespiegelvariaties zou volgens de gangbare gepubliceerde theorieën vrijwel direct plaatsvinden (zie bijv. Posamentier & Vail, 1988). Of die aanpassing van de rivier inderdaad zo snel verloopt wordt echter steeds meer betwijfeld (Shanley & McCabe, 1994; Dalrymple *et al*., 1998; Ethridge *et al*., 1998).

De resultaten van de experimenten ondersteunen de gedachte dat een rivier niet direct reageert op een zeespiegelverlaging. Erosie van de shelf door een zeespiegelverlaging start vanaf de nieuwe, meer zeewaarts gelegen kustlijn en heeft tijd nodig om in landwaartse richting de benedenloop van de rivier te bereiken en daar verlaging van het rivierprofiel te veroorzaken. Ondertussen blijft in de riviervallei de sedimentatie doorgaan. Er is dus na een daling van de zeespiegel een vertraging, ofwel reactie tijd, van het moment waarop het erosieproces de voormalige kustvlakte bereikt. Omgekeerd leidt een stijging van de zeespiegel niet meteen tot depositie in de riviervallei. De experimenten laten zien dat tijdens zeespiegelstijging eerst alleen depositie plaatsvindt op de shelf terwijl deze onder water komt te staan. Ondertussen gaat de erosie bovenstrooms (in de rivier) nog door. Pas wanneer de zeespiegelstijging goed heeft doorgezet treedt ook weer sedimentatie in de rivier op.

Deze vertraagde reactie van een rivier op zeespiegelfluctuaties bleek statistisch goed aantoonbaar voor de gehele reeks experimenten. Het optreden van deze vertraging heeft gevolgen voor de samenstelling en de vorm van de afzettingen in de rivier en op de shelf. Deze vertraging in de aanpassing van rivieren op zeespiegelvariaties leidt ertoe dat een erosievlak dat wordt gevormd op de shelf tijdens het laagste zeespiegelniveau, stroomopwaarts steeds jonger wordt. Op de shelf kan dat erosievlak dus worden gerelateerd aan het laagste zeeniveau. Het benoemen en dateren van sedimenten met episodes uit de zeespiegelcurve aan de hand van deze erosievlakken, zoals gebruikelijk in de sequentie stratigrafie, is dus goed toepasbaar voor de shelf. Echter, omdat dit erosievlak in landwaartse richting steeds jonger wordt, dient deze werkwijze stroomopwaarts bij riviersedimenten met grote voorzichtigheid te gebeuren. Hoofdstuk 3 geeft tevens voorbeelden van studies aan rivierafzettingen van de Rijn-Maas en Colorado Rivier die zijn gevormd tijdens de laatste ijstijd. Zeer vergelijkbaar met deze geologische voorbeelden, laten de experimenten zien dat depositie in de rivier nog doorgaat tijdens een zeespiegeldaling en dat erosie nog plaatsvindt tijdens het eerste gedeelte van de zeespiegelstijging.

Hoofdstuk 4 behandelt een modelstudie naar de effecten van locale tektoniek —in combinatie met zeespiegelvariaties— op delta ontwikkeling. Het model is gebaseerd op het Imo River olieveld in Nigeria. Deze delta werd gevormd tijdens het Mioceen (19 tot 13 miljoen jaar geleden). Hierbij daalde de kustzone instantaan omdat de ondergrond van slappe zeebodemsedimenten het gewicht van de uitbouwende delta niet kon dragen. Er ontstond een lepelvormige (listrische) afschuivingsbreuk. Dit type breuk wordt groeibreuk ofwel syn-sedimentaire breuk genoemd omdat deze zich

tijdens de vorming van de delta steeds verder ontwikkelt. Doordat deze breuk tijdens afzetting van de delta wordt gevormd verschillen de laagdikte en eigenschappen van afzettingen aan beide zijde van de breuk. Hierdoor is het moeilijk om achteraf te bepalen welke sedimentlagen aan beide zijden van de breuk oorspronkelijk verbonden waren. Een analoog model biedt de mogelijkheid om hiervan een complete reconstructie te maken. Met behulp van markers (gekleurd zand) zijn ter controle tijdens het experiment tijdlijnen aangebracht. Het resultaat van het experiment wordt gepresenteerd als een algemeen stratigrafisch model voor delta afzettingen die worden doorsneden door een groeibreuk. Dit model vertoont veel overeenkomsten met het bestudeerde prototype in de Niger Delta en met vergelijkbare groeibreuk-delta-afzettingen in de Golf van Mexico. Tevens blijkt het model van toepassing op delta's die tijdens afzetting worden doorsneden door normale rechte breuken. Tenslotte wordt het modelresultaat gebruikt om de voorkomende sedimentaire structuren te beoordelen op hun mogelijke geschiktheid als olie en gas reservoirs.

Conclusies

Dit onderzoek bewijst dat analoge modellen, mits goed geschaald, op een kwantitatieve manier inzicht kunnen geven in de ontwikkeling van sedimentaire systemen. Hierbij is de schaling van de responsetijd van het systeem essentieel omdat deze bepalend is voor de gevormde afzettingen. Rivierafvoer en sedimentaanvoer zijn zoveel mogelijk constant gehouden om het effect van zeespiegel en tektoniek goed te onderzoeken. Het effect van klimaat op de rivierafvoer is in deze studie beperkt aan bod gekomen. Het zou interessant zijn om het effect van deze variabele ook met dit model te onderzoeken met een serie vergelijkbare experimenten.

De experimenten ondersteunen de toepasbaarheid van het concept van de sequentie stratigrafie voor de shelf. De resultaten laten zien dat de riviervallei zich niet direct aanpast aan zeespiegelvariaties. Daardoor kan het relateren van afzettingen aan bepaalde episodes uit de zeespiegelcurve zoals gebruikelijk in de sequentie stratigrafie tot onjuiste conclusies leiden wanneer dit wordt toegepast op riviersedimenten.

Deze modelstudie heeft geleid tot het inzicht dat een zeespiegelverlaging een belangrijke toename van de sediment aanvoer geeft vanuit het land en de kustvlakte naar de shelf. Deze puls staat dus los van klimatologische veranderingen, zoals bijvoorbeeld tijdens een ijstijd, en wordt puur veroorzaakt door de zeespiegelverlaging zelf. Zelfs in tektonisch actieve gebieden waar de tektonische daling de zeespiegeldaling bijhoudt, is door deze verhoogde sedimenttoevoer het effect van een zeespiegelverlaging nog duidelijk waarneembaar in de gevormde afzettingen.

Dit onderzoek heeft een nieuw kwantitatief aspect toegevoegd aan de bestaande methode van het analoog modelleren van sedimentaire systemen. Daarbij is een zo goed mogelijke schaling van dimensies, sedimenttransport en tijd nagestreefd. Met deze werkwijze kunnen de resultaten van analoge modellen beter en objectiever worden vergeleken met echte geologische voorbeelden. Kwantitatieve analoge modelstudies als deze zijn geschikt voor het toetsen en ontwikkelen van geologische concepten en het kalibreren van computermodellen. Bovenal zijn analoge modellen een goed hulpmiddel om geologen meer inzicht te geven in de ruimtelijke ontwikkeling van sedimentaire systemen, omdat de experimenten “live” te volgen zijn.

Acknowledgements

Specific contributions to the project are briefly acknowledged at the end of each chapter. In the daily practice of research there is a much larger group of people involved, each contributing in their own way. I take this opportunity to express my thanks more explicitly.

I am indebted to the staff of the Sedimentology group for their guidance. In the first place, I thank George Postma my co-promotor and project initiator for his daily supervision. Due to his enthusiasm, George was very committed to the project and has spent much time with me in the laboratory looking at the experiments and sharing ideas and knowledge. In the writing phase he has put an enormous effort into revising the manuscripts. I am grateful to Poppe de Boer, my promotor, for reviewing the manuscript at several stages. Wout Nijman gave valuable feedback on the experimental growth structures by reviewing Chapter 4. I acknowledge the members of the dissertation committee (page 6) for their contributions to the thesis.

The research reported in this thesis is a scientific collaboration between Utrecht University and Shell Exploration and Production BV, Rijswijk, the Netherlands. I thank Shell for full financial support of the project. The project started with a pilot study to investigate the feasibility of the analogue modelling approach. Meindert de Ruiter and Ruud de Jongh from Shell, together with George Postma initiated the analogue modelling project at Utrecht University at the end of 1994. I am very grateful that I had the opportunity to step into the project at this stage for my M.Sc. research. I am indebted to all those people of the first hour who helped to make the pilot study a success. Most of them also assisted with the experiment work of this thesis and I mention them below. Here I express my thanks to Peter van de Wouw for assisting with the pilot experiments during the summer of 1995.

I greatly appreciated the continuous in-house technical assistance, which was provided by Tony van der Gon Netcher and Hans Bliek. Paul Anten and Marjan Reith from the Sedimentology Laboratory are thanked for logistic support and for providing grain-size analyses. Joseph Kiraly programmed the software of the measurement system. Marco de Kleine assisted with 6 experiments as part of his M.Sc. programme.

At Shell I wish to thank Meindert de Ruiter, Ruud de Jongh, John Barwis, Trey Meckel, Wong Chung Lee, Tony Cortis and Kees van der Zwan for their interest in the project, feedback on presentations and for providing facilities at Shell Rijswijk. After he moved to Nigeria, Ruud de Jongh initiated the modelling study of the Imo River Field. He invited us for a very productive and pleasant visit to make us familiar with the data set and the geology of Nigeria.

John Anderson, Rice University, Houston, Texas, introduced me to siliciclastic sequence stratigraphy on a field course in Mallorca, Spain in 1993. This has initiated my interest in the geology of siliciclastic shelves. We met again on a workshop in 1998, where he was immediately willing to start up a comparison study between the analogue model and deposits on the Quaternary Colorado shelf. I gratefully acknowledge John and his former Ph.D. student Jennifer Snow for providing their field data and the always quick feedback on questions and manuscripts.

The project has much common ground with the discipline of Physical Geography. It was a pleasure to exchange ideas with people from Physical Geography department of Utrecht University. I thank Leo van Rijn for his courses on hydraulics and the dynamics of sediment transport in rivers and seas. Janrik van den Berg and Maarten Kleinhans aided with suggestions on the scaling rationale. Discussions with Torbjörn Törnqvist helped me to realise the research questions of fluvial stratigraphers in the field. Torbjörn also reviewed Chapter 3.

I am grateful to the supporting staff of the Faculty. I thank the library personnel, Marnella van der Tol, Pien van Minnen and Marjolein van Wijk from the administration office and Boubker Kaouass and Boudewijn ‘t Hart from the financial department. Paul van Oudenallen, Isaak Santoe, Fred Trappenburg, Jaco Bergenhegouwen and Birgit Benders kindly assisted with the artwork for poster presentations and prepared the cover. In addition I acknowledge all people within the Faculty of Earth Sciences that participated in discussions on the experimental results, co-operated with the courses for second and third year geology students, or simply passed by in the laboratory asking questions when looking at the flowing water. I appreciated the company of many people from other disciplines from the institute and I hope that I mention them all: Natasja Jannink, Tanja van Kouwenhoven, Michiel van der Meulen, Joris Steenbrink, Hayfaa Abul Azis, Hendrik-Jan Bosch, Bart Bos, Jan ter Heege, Froukje Brouwer, Armelle Kloppenburg, Rene de Kloe, Marga Zuiderwijk, Andor Lips, Marleen Nyst, Annemarie Bos, Edith Hafkensheid, Jeroen van Hunnen, Gert-Jan Reichart, Hans de Bruin, Jan van Dam, Albert van der Meulen, Jan-Willem Zachariasse, Bert van der Zwaan, Bernard de Jong, Hans de Bresser, Martin Drury and Herman van Roermund.

It was a pleasure to work with the enthusiastic group of colleges in the sedimentology department of the Faculty of Earth Sciences at Utrecht University. I thank Albert Oost, Johan ten Veen, Maarten Prins, Jelmer Cleveringa, Jan-Berend Stuut, Quintijn Clevis, Xander Meijer, Wessel van Kesteren en Sjoukje de Vries for their collegiality. All of them have improved the thesis by participation in tutorials and discussions. Some of them were particularly helpful by doing peer reviews. Xander Meijer and Wessel van Kesteren have greatly contributed to Chapters 2 and 4 respectively.

I express my thanks to my friends who joined me in social activities and sports like sailing, biking and field hockey to escape from the laboratory in the basement of the institute. Some friends provided particularly encouraging comments: “so every time-consuming experiment reduces to one datum point on a chart”. I very much appreciated those conversations that put science in another perspective. In this respect I mention my former housemate Kaspar van Everdingen and my “paranimfen” Felix van der Kooij and Pieter van Heiningen.

Finally I thank Jetske Hielkema, my parents and my sister Stance for their patience and their continuous interest and support that encouraged me to undertake this research project. Jetske verified each chapter on readability for a broad geologic audience. Stance clarified the summary in Dutch for the non-geologist.

Curriculum Vitae

Born (1971) and educated (till 1990) in Breda, the author started his study in Geology at the Faculty of Earth Sciences of the Utrecht University. He specialised in Sedimentology and Basin Analysis and finished his study in 1996 with extracurricular courses in Management and Organisation. He wrote a Master's Thesis on the pilot study "Experimental Sequence Stratigraphy" that was conducted at the Sedimentology Group of the faculty. The research was continued as a Ph.D. project from 1996 to 2000, which is reported in this thesis. Since October 2000 he is employed as a project manager at the Raw Materials Department of the Road and Hydraulic Engineering Division of the Directorate General of Public Works and Water Management, Delft, The Netherlands.